AD-A173 229 STRENGTH DESIGN OF REINFORCED CONCRETE HYDRAULIC STRUCTURES REPORT 4 LOAD.. (U) ARMY ENGINEER WATERWAYS EXPERIMENT STATION VICKSBURG MS STRUC.. 1/2

UNCLASSIFIED V P CHIARITO ET AL. AUG 86 WES/TR/SL-80-4-4 F/G 13/13 NL

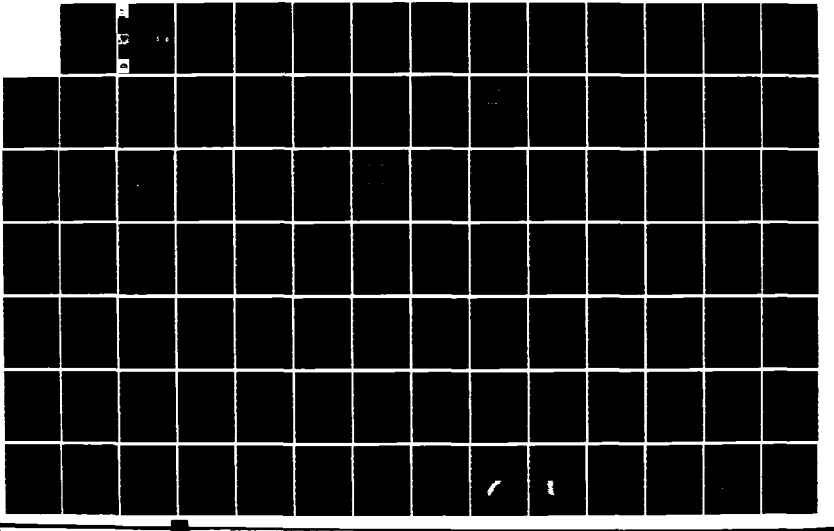

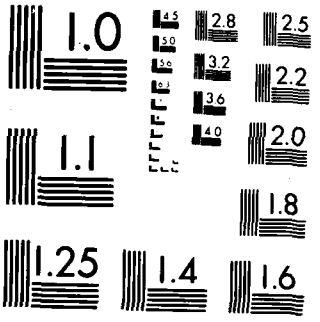

US Army Corps of Engineers

TECHNICAL REPORT SL-80-4

STRENGTH DESIGN OF REINFORCED CONCRETE HYDRAULIC STRUCTURES

Report 4
LOAD-MOMENT CHARACTERISTICS OF REINFORCED CONCRETE CIRCULAR CONDUITS

by

Vincent P. Chiarito, Paul F. Mlakar

Structures Laboratory

DEPARTMENT OF THE ARMY
Waterways Experiment Station, Corps of Engineers
PO Box 631, Vicksburg, Mississippi 39180-0631

August 1986
Report 4 of a Series

Prepared for

DEPARTMENT OF THE ARMY
US Army Corps of Engineers
Washington, DC 20314-1000

STRUCTURES LABORATORY

Unclassified

SECURITY CLASSIFICATION OF THIS PAGE (When Data Entered)

REPORT DOCUMENTATION PAGE		READ INSTRUCTIONS BEFORE COMPLETING FORM
1. REPORT NUMBER Technical Report SL-80-4	2. GOVT ACCESSION NO AD-A173	3. RECIPIENT'S CATALOG NUMBER 229
4. TITLE (and Subtitle) STRENGTH DESIGN OF REINFORCED CONCRETE HYDRAULIC STRUCTURES; Report 4, LOAD-MOMENT CHARACTERISTICS OF REINFORCED CONCRETE CIRCULAR CONDUITS		5. TYPE OF REPORT & PERIOD COVERED Report 4 of a series 6. PERFORMING ORG. REPORT NUMBER
7. AUTHOR(s) Vincent P. Chiarito Paul F. Mlakar		8. CONTRACT OR GRANT NUMBER(s)
9. PERFORMING ORGANIZATION NAME AND ADDRESS US Army Engineer Waterways Experiment Station Structures Laboratory PO Box 631, Vicksburg, Mississippi 39180-0631		10. PROGRAM ELEMENT, PROJECT, TASK AREA & WORK UNIT NUMBERS
11. CONTROLLING OFFICE NAME AND ADDRESS DEPARTMENT OF THE ARMY US Army Corps of Engineers Washington, DC 20314-1000		12. REPORT DATE August 1986 13. NUMBER OF PAGES 169
14. MONITORING AGENCY NAME & ADDRESS(if different from Controlling Office)		15. SECURITY CLASS. (of this report) Unclassified 15a. DECLASSIFICATION/DOWNGRADING SCHEDULE

16. DISTRIBUTION STATEMENT (of this Report)

Approved for public release; distribution unlimited.

17. DISTRIBUTION STATEMENT (of the abstract entered in Block 20, if different from Report)

18. SUPPLEMENTARY NOTES

Available from National Technical Information Service, 5285 Port Royal Road, Springfield, Virginia 22161.

19. KEY WORDS (Continue on reverse side if necessary and identify by block number)

Curvature
Hydraulic structures
Reinforced concrete

20. ABSTRACT (Continue on reverse side if necessary and identify by block number)

The effect of initial curvature on the thrust-moment characteristics of reinforced concrete circular conduit sections was investigated. This study was undertaken since conduit sections built by the Corps of Engineers are often so sharply curved relative to their thicknesses that initial curvature effects might be significant.

(Continued)

DD FORM 1 JAN 73 1473 EDITION OF 1 NOV 65 IS OBSOLETE

Unclassified

SECURITY CLASSIFICATION OF THIS PAGE (When Data Entered)

20. ABSTRACT (Continued).

The effect of initial curvature was investigated through curved beam, Airy stress function, and nonlinear finite element analyses. In addition, three model conduits representative of Corps construction were instrumented and simultaneously loaded on eight equally spaced diameters.

For the range of design variables investigated, the analytical and experimental results indicate that initial curvature has no statistical significant effect. Further testing will be needed to obtain a larger statistical sample and evaluate the effects of more extreme curvatures than studied in this report.

PREFACE

This study was conducted during the period September 1980 through September 1983 by the US Army Engineer Waterways Experiment Station (WES) under the sponsorship of the Office, Chief of Engineers (OCE), US Army, and the US Army Engineer District, Savannah. The Technical Monitor was Mr. Don Dressler, OCE.

This work was conducted under the supervision of Messrs. Bryant Mather, Chief, Structures Laboratory (SL), and James T. Ballard, Assistant Chief, SL, and Dr. Jimmy P. Balsara, Chief, Structural Mechanics Division (SMD), SL. Dr. Paul F. Mlakar, formerly of SMD, was involved in the planning and directing phases of the work. Instrumentation support was provided by personnel of the Instrumentation Services Division, WES. Engineering and Construction Services Division personnel fabricated the unusual testing system used to load the conduit models. Messrs. Robert E. Walker, C. Dean Norman, and R. Stephen Wright, SL, provided technical guidance. Mmes. Linda S. Marble and Frances M. Warren, SL, processed the test data. This report was prepared by Dr. Mlakar and Mr. Vincent P. Chiarito, SMD. The report was edited by Ms. Janean C. Shirley, Information Products Division, Information Technology Laboratory, WES.

The previous Director of WES was COL Allen F. Grum, USA; the present Commander and Director is COL Dwayne G. Lee, CE. Dr. Robert W. Whalin is Technical Director.

CONTENTS

CONVERSION FACTORS, NON-SI TO SI (METRIC)
UNITS OF MEASUREMENT

Non-SI units of measurement used in this report can be converted to SI (metric) units as follows:

Multiply	By	To Obtain
Fahrenheit degrees	5/9	Celsius degrees or Kelvins*
feet	0.3048	metres
inches	2.54	centimetres
inch-pounds (force)	0.1129848	metre-newtons
kips (force)	4.448222	kilonewtons
kips (force) per square inch	6.894757	megapascals
pounds (force)	4.448222	newtons
pounds (force) per square inch	6.894757	kilopascals
square feet	0.09290304	square metres
square inches	6.4516	square centimetres

* To obtain Celsius (C) temperature readings from Fahrenheit (F) readings, use the following formula: $C = (5/9)(F - 32)$. To obtain Kelvin (K) readings, use $K = (5/9)(F - 32) + 273.15$.

STRENGTH DESIGN OF REINFORCED CONCRETE HYDRAULIC STRUCTURES

LOAD-MOMENT CHARACTERISTICS OF REINFORCED CONCRETE CIRCULAR CONDUITS

PART I: INTRODUCTION

1. The investigation summarized herein was undertaken to determine the effect of curvature on the resistance of axially flexurally loaded reinforced concrete members and to recommend any appropriate modifications to normal strength design practice for circular conduits used by the US Army Corps of Engineers. In the analysis of reinforced concrete (RC) members loaded by combined moment and thrust, the effects of initial curvature on the response of RC conduits beyond the elastic range have in the past been neglected. The Corps of Engineers constructs many curvilinear conduits with curvatures considerably greater than those of structural members encountered in usual practice.

2. A survey of the Corps' existing and planned conduits was conducted to see the ranges of R/h ,* ρ_g , ρ'_g , d , and f_y which exist for these structures, where: R = radius of initial curvature to middepth of section, h = overall depth of section, ρ_g = gross tension steel ratio, ρ'_g = gross compression steel ratio, d = effective depth of tension steel, f_y = yield strength of reinforcing steel. This survey is shown in Table 1 and sketches of the different shapes are shown in Figure 1. For the range of R/h values listed, Timoshenko's curved beam theory (Timoshenko 1941) can be applied. In Figure 2, this theory indicates that maximum stresses computed without considering curvature would be incorrect (unconservative by at least 10 percent) if the Corps structures behaved elastically. To the best of the authors' knowledge, the effect of curvature on an inelastic RC beam has not been studied.

3. The investigation consisted of analytical and experimental studies. The analytical study involved a curved beam analysis to predict capacities of RC sections with curvature effects as well as an application of a nonlinear finite element (FE) model for concrete. The experimental study involved

---

* For convenience, symbols are listed and defined in the Notation (Appendix E).

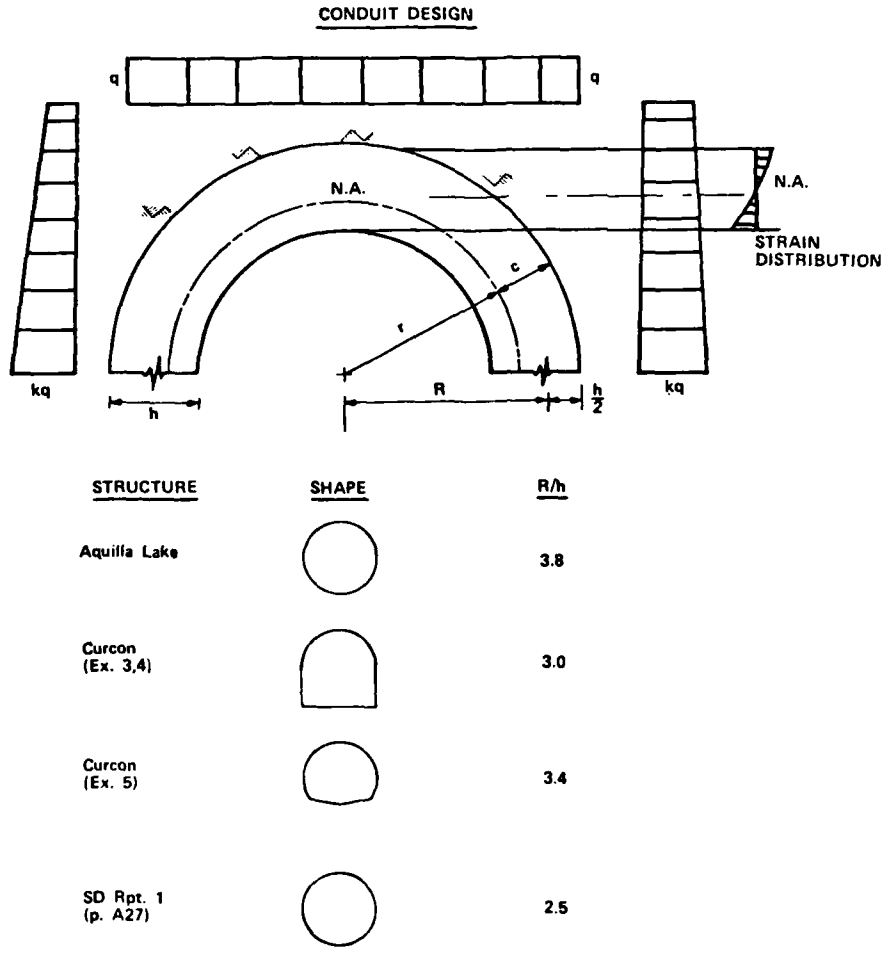

Figure 1. Sketches of curvilinear conduit shapes, Corps of Engineers (US Army Engineer District, Fort Worth 1978; Harter, Bircher, and Wilson 1980)

For Elastic Materials - Error Between Linear and Hyperbolic Maximum Stress Value

$\frac{R}{h}$	%
1	35
2	17
3	10.9
4	9.2
10	3.2

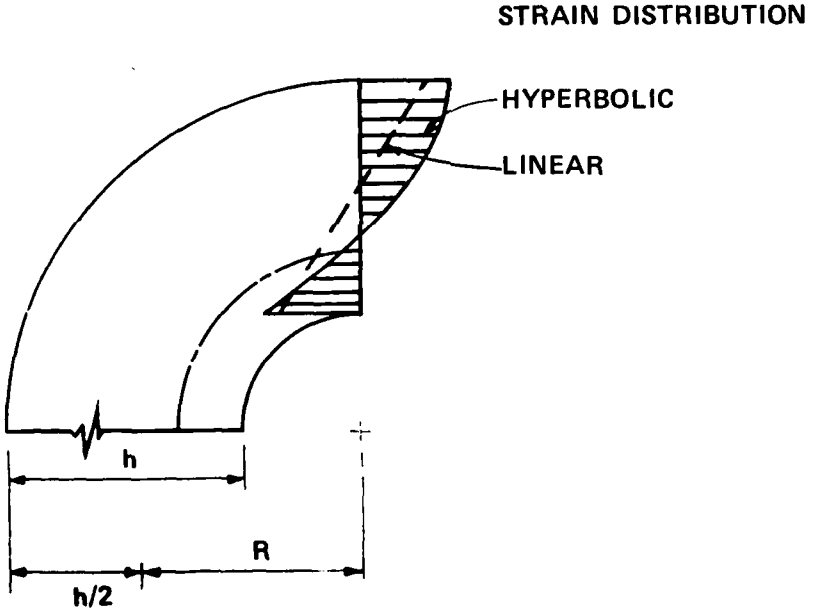

Figure 2. Comparison of stress calculations, with and without consideration for curvature

one-dimensional (1-D) structural and two-dimensional (2-D) linear elastic analyses of RC conduit models. Three RC conduit models were fabricated, instrumented, and tested. The results of the experiments are plotted as moment-thrust values and are compared to predicted capacities (interaction diagrams). Results are discussed, conclusions are drawn, and recommendations made.

4. This investigation provides an in-depth look at the flexural response of circular conduits, but applies only to a known set of loading conditions. Although the response of conduits is a soil-structure interaction problem, this first step toward its solution considers only the design loadings prescribed in EM 1110-2-2902 (Headquarters, Department of the Army 1969). Since the conduit shapes used by the Corps include circular and noncircular geometries, an understanding of the circular structure's behavior is a logical prerequisite before analyzing the structural response of more complex conduit shapes. The behavior of these thick elements in shear must be considered at some future time.

PART II: STRESS AND STRAIN VARIATIONS FOR THE STRENGTH DESIGN OF CURVED CONCRETE BEAMS

5. A curved beam analysis was formulated to evaluate the response of RC conduits. The curved beam analysis was chosen since the top portion of each shape for a conduit represents a thickly curved beam. There is very good agreement between curved beam theory and the elasticity solution (Airy stress function) (Timoshenko 1941) for stresses in a thick hollow cylinder under a given load condition as shown in Figure 3. The Hognestad constitutive law for concrete is used to investigate the inelastic response of thick, RC curved beams. The curved beam analysis shows that the present American Concrete Institute (ACI) practice for determining flexural resistance of RC straight beam members (ACI 1983) is appropriate for the Corps' RC curved members.

Curved Beam Analysis

6. Consider the curved beam subjected to a positive bending moment and axial thrust in Figure 4. Notation for Figure 4 is as follows:

b = width of section

c = depth of section in compression

r = radius of initial curvature to neutral axis of section

$d\phi$ = small angle between two neighboring cross sections

$\Delta d\phi$ = small angle of rotation due to moment and thrust

The distance from the neutral axis, y, is positive in the compressive region and negative in the tensile region. If it is assumed that plane sections of the beam initially remain plane under the action of combined moment and thrust, it then follows that the strain distribution when the inner surface is in tension is given by (Timoshenko 1941):

$$\varepsilon(y) = \frac{y}{r + y} \frac{\Delta d\phi}{d\phi} \tag{1}$$

where ε = strain. In this hyperbolic strain distribution, compressive strains are positive values. Similarly, when the outer surface is in tension (subjected to a negative moment) the strain distribution is:

PURE BENDING OF CURVED BEAMS FOR
A LINEARLY ELASTIC MATERIAL.

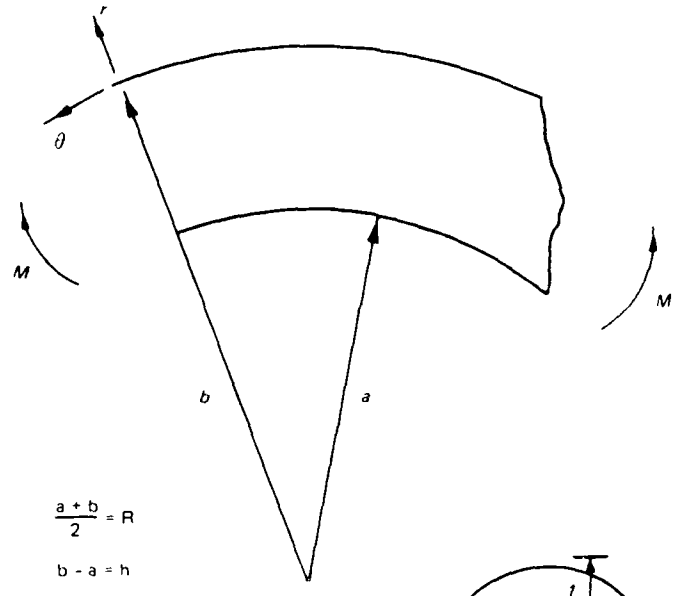

$$\frac{a+b}{2} = R$$

$$b - a = h$$

$$\frac{R}{h} = \frac{1}{2}\left(\frac{a+b}{b-a}\right)$$

$$= \frac{1}{2}\left(\frac{1+\frac{b}{a}}{\frac{b}{a}-1}\right)$$

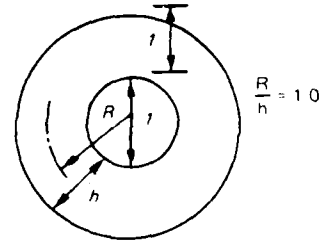

$\frac{a}{b}$	$\frac{b}{a}$	$\frac{R}{h}$	LINEAR STRESS DISTRIBUTION	HYPERBOLIC	EXACT
0.75	1.3	3.83	±66.67	+72.98, -61.27	+73.05, -61.35
0.33	3.0	1.0	±1.500	+2.285, -1.095	+2.292, -1.130

EQ. (h) — $\sigma_\theta = m\frac{M}{a^2}$

Figure 3. Pure bending of curved beams for a linearly elastic material (from Timoshenko and Goodier (1951))

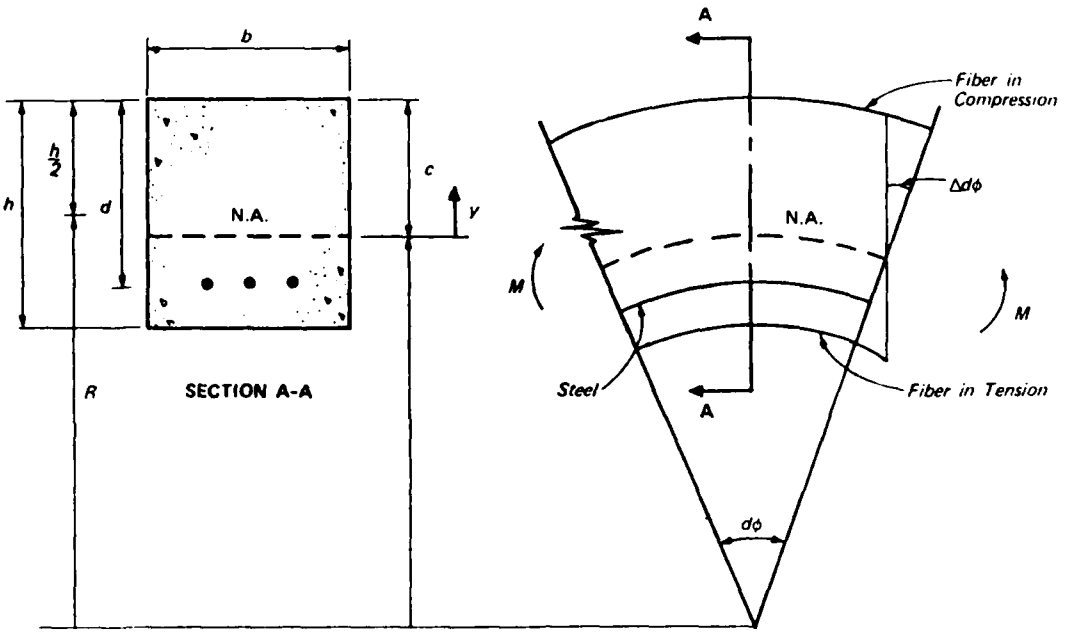

Figure 4. Reinforced concrete curved beam section subjected to positive moment

$$\varepsilon(y) = \frac{y}{r - y} \frac{\Delta d\phi}{d\phi} \tag{2}$$

where positive y is now measured from the neutral axis (N.A.) toward the center of curvature. The term $\Delta d\phi/d\phi$ in Equations 1 and 2 is a constant that is evaluated by setting $\varepsilon(y)$ equal to ε_u at y equal to c. Therefore, $\Delta d\phi/d\phi$ equals $\varepsilon_u \frac{(r \pm c)}{c}$, where the plus sign is used for a positive moment section and the minus sign is used for a negative moment section. It is further supposed that the stress-strain relationships for concrete in compression (Hognestad, Hanson, and McHenry 1955) and for steel reinforcement in tension and compression are as shown in Figure 5, where:

E_s = modulus of elasticity of steel (29,000,000 psi*)

f_c = concrete stress

f'_c = 28-day compressive strength of standard 6- by 12-in. concrete cylinder

f''_c = compressive strength of concrete in reinforced concrete members (0.85 f'_c)

f_s = steel stress; for this study GR60 (grade 60 steel) is used

---

* A table of factors for converting non-SI units of measurement to SI (metric) units is presented on page 3.

ϵ_o = strain at which the maximum concrete stress f''_c occurs (0.002)

ϵ_u = limiting useful concrete strain (0.003)

Finally, in accordance with accepted procedure, assume the tensile strength of concrete to be negligible.

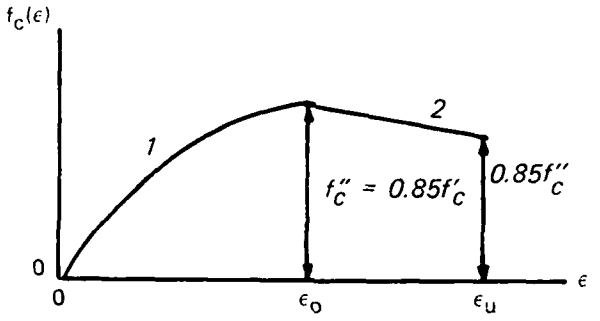

a. Concrete in compression

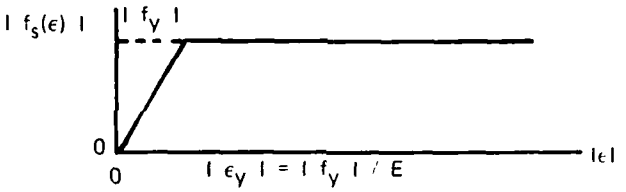

b. Steel in tension or compression

Figure 5. Stress-strain relationships

7. Under these assumptions the load-moment characteristics of a given initially curved reinforced concrete cross section can be obtained as shown in Figures 6 and 7 through the following steps adopted from an analysis for an initially straight member (Pfrang, Siess, and Sozen 1964). For Figures 6 and 7 C_s , C_c , and T_s are defined below:

C_s = Resultant force in the compressive steel

C_c = Resultant compressive concrete force

T_s = Resultant force in the tensile steel

M = Moment applied to section ("+" indicates positive moment, "-" negative moment

N.A. = Neutral Axis

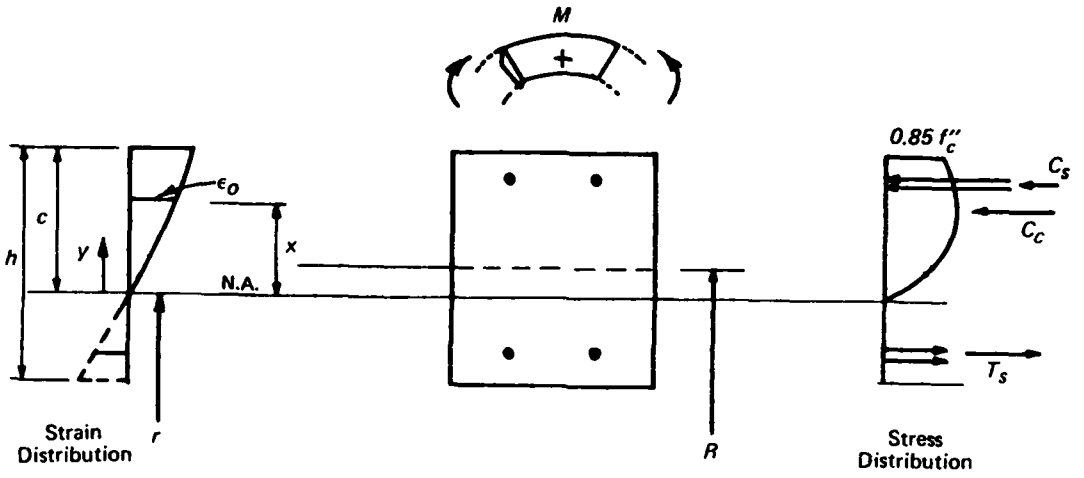

Figure 6. Reinforced concrete curved beam section: resultant strain and stress distributions due to a positive moment

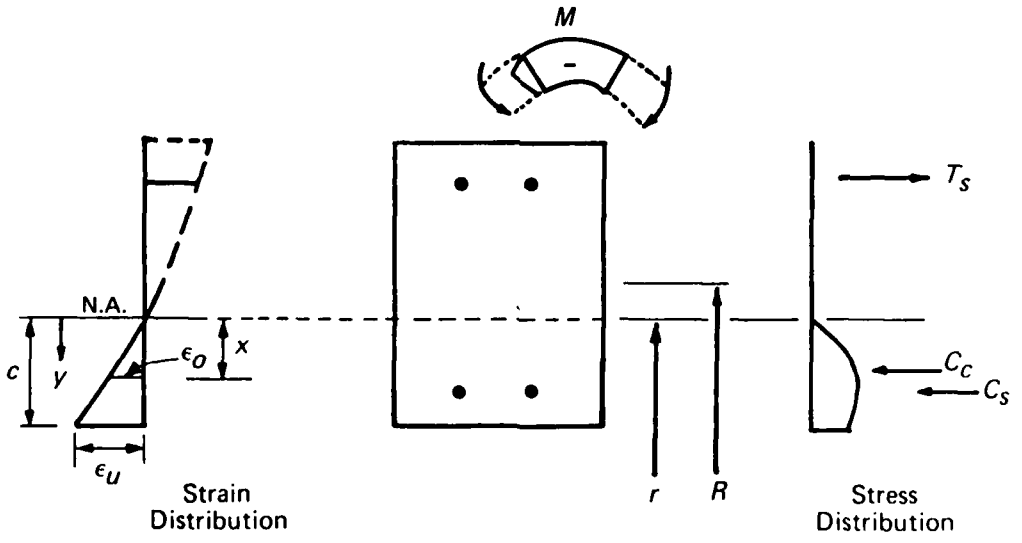

Figure 7. Reinforced concrete curved beam section: resultant strain and stress distributions due to a negative moment

a. Define the shape of a hyperbolic strain distribution over the depths of the section by assuming a neutral axis location r in Equation 1 for positive moment or Equation 2 for negative moment.

b. Determine the concrete stress distribution consistent with the assumed strain distribution through the constitutive relation of Figure 2a and calculate its resultant axial thrust.

$$b \int_0^c f_c(\varepsilon,y)\, dy = C_c \tag{3}$$

and moment about the neutral axis

$$b \int_0^c y f_c(\varepsilon,y)\, dy = M_c \tag{4}$$

where $f_c(\varepsilon,y)$ is given by the relationship illustrated in Figure 5a. The governing equations for Figure 5a are

$$f_c(\varepsilon,y) = f''_c \left[\frac{2\varepsilon(y)}{\varepsilon_o} - \left(\frac{\varepsilon(y)}{\varepsilon_o}\right)^2\right]$$

for $o \le \varepsilon \le \varepsilon_o$

and

$$f_c(\varepsilon,y) = f''_c \left[1 - 0.15 \left(\frac{\varepsilon - \varepsilon_o}{\varepsilon_u - \varepsilon_o}\right)\right]$$

for $\varepsilon_o \le \varepsilon \le \varepsilon_u$ and $\varepsilon(y)$ defined by Equations 1 and 2.

c. Determine the reinforcement forces, C_s and T_s, corresponding to the assumed strain distribution by the constitutive relation of Figure 5.

d. Calculate the centric thrust, P, and the bending moment, M, acting on the cross section which are statically equivalent to this distribution.

8. If a series of such strain distributions is established whose magnitude corresponds to a failure of the cross section, then the resulting (M, P) points are the ultimate interaction diagram. For purposes of practical design, a failure occurs in tension if the tensile reinforcement strain ε_s equals its tensile yield strain $-f_y/\varepsilon_s$; or in compression, if the maximum concrete strain ε_c equals the ultimate concrete strain ε_u and the middepth concrete strain is less than ε_o; or in compression, if the middepth concrete strain equals ε_o and ε_c is less than ε_u.

Results

9. The resultants C_c and M_c of the concrete stress distribution in an initially curved cross section can be determined by closed-form integrations under the postulates and procedures of the preceding section.

10. Consider first a member loaded by a positive moment which causes compression on the cross section's outer surface as shown in Figure 6. For a failure governed by the yield of the tensile steel

$$C_c = f''_c b \left\{ \frac{2k}{\varepsilon_o} \left[x - r \ln \left(\frac{r + x}{r} \right) \right] - \left(\frac{k}{\varepsilon_o} \right)^2 \left[x - 2r \ln \left(\frac{r + x}{r} \right) - \frac{r^2}{(r + x)} + r \right] + (c - x) - \left(\frac{0.15}{\varepsilon_u - \varepsilon_o} \right) \left[(k - \varepsilon_o)(c - x) - kr \ln \left(\frac{r + c}{r + x} \right) \right] \right\} \quad (5)$$

and

$$M_c = f''_c b \left(\frac{2k}{\varepsilon_o} \left[\frac{x^2}{2} - rx + r^2 \ln \left(\frac{r + x}{r} \right) \right] - \left(\frac{k}{\varepsilon_o} \right)^2 \left[\frac{x^2}{2} - 2rx + 3r^2 \ln \left(\frac{r + x}{r} \right) - \frac{r^2 x}{r + x} \right] + \frac{c^2 - x^2}{2} - \left(\frac{0.15}{\varepsilon_u - \varepsilon_o} \right) \left\{ (k - \varepsilon_o) \left(\frac{c^2 - x^2}{2} \right) - kr \left[c - x - r \ln \left(\frac{r + c}{r + x} \right) \right] \right\} \right) \quad (6)$$

where

$$k = \frac{(R + h/2)\varepsilon_u}{c}$$

For a failure in which $\varepsilon_c = \varepsilon_u$

$$C_c = f''_c b \left\{ \frac{2k}{\varepsilon_o} \left[(x - x') - r \ln \left(\frac{r + x}{r + x'} \right) - \left(\frac{k}{\varepsilon_o} \right)^2 \left[(x - x') \right. \right. \right.$$

$$\left. - 2r \ln \left(\frac{r + x}{r + x'} \right) + \frac{r^2 (x - x')}{(r + x)(r + x')} \right] + (c - x)$$

$$\left. \left. - \left(\frac{0.15}{\varepsilon_u - \varepsilon_o} \right) \left[(k - \varepsilon_o)(c - x) - kr \ln \left(\frac{r + c}{r + x} \right) \right] \right\} \right\} \qquad (7)$$

and

$$M_c = f''_c b \left(\frac{2k}{\varepsilon_o} \left[\frac{x^2 - x'^2}{2} - r(x - x') + r' \ln \left(\frac{r + x}{r + x'} \right) \right] \right.$$

$$- \left(\frac{k}{\varepsilon_o} \right)^2 \left[\frac{x^2 - x'^2}{2} - 2r (x - x') + 3r^2 \ln \left(\frac{r + x}{r + x'} \right) \right.$$

$$\left. \left. - r^2 \left(\frac{x}{r + x} - \frac{x'}{r + x'} \right) \right] + \frac{c^2 - x^2}{2} - \frac{0.15}{\varepsilon_u - \varepsilon_o} \right.$$

$$\left. \times \left\{ (k - \varepsilon_o) \left(\frac{c^2 - x^2}{2} \right) - kr \left[c - x - r \ln \left(\frac{r + c}{r + x} \right) \right] \right\} \right) \qquad (8)$$

where $x' = c - h$. For a failure governed by the middepth strain equal to ε_o the resultants are given by Equations 7 and 8 with:

$$k' = \frac{R}{c - \frac{h}{2}} \varepsilon_o \qquad (9)$$

and substituting k' for k .

11. A member subjected to a negative moment behaves as in Figure 7. C_c and M_c are given by

$$C_c = f''_c b \left\{\frac{2k_1}{\varepsilon_o}\left[-r \ln\left(\frac{r-x}{r}\right) - x\right] - \left(\frac{k_1}{\varepsilon_o}\right)^2 \left[x + 2r \ln\left(\frac{r-x}{r}\right) + \frac{r^2}{r-x} - r\right] + c - x + \left(\frac{0.15}{\varepsilon_u - \varepsilon_o}\right)\left[(k_1 + \varepsilon_o)(c-x) + k_1 r \ln\left(\frac{r-c}{r-x}\right)\right]\right\} \quad (10)$$

and

$$M_c = f''_c b \left\{\frac{2k_1}{\varepsilon_o}\left[\frac{-x^2}{2} - rx - r^2 \ln\left(\frac{r-x}{r}\right)\right] - \left(\frac{k_1}{\varepsilon_o}\right)^2 \left[\frac{x^2}{2} + 2rx + 3r^2 \ln\left(\frac{r-x}{r}\right) + \frac{r^2 x}{r-x}\right] + \frac{c^2 - x^2}{2} + \left(\frac{0.15}{\varepsilon_u - \varepsilon_o}\right) \times \left[k_1 r^2 \ln\left(\frac{r-c}{r-x}\right) + k_1 r (c-x) + (k_1 + \varepsilon_o)\left(\frac{c^2 - x^2}{2}\right)\right]\right\} \quad (11)$$

in the case of a tensile failure of the steel, where $k_1 = \left[R - (h/2)\right]/c\varepsilon_u$
For a failure controlled by $\varepsilon_c = \varepsilon_u$

$$C_c = f''_c b \left\{\frac{2k_1}{\varepsilon_o}\left[-(x - x') - r \ln\left(\frac{r-x}{r-x'}\right)\right] - \left(\frac{k_1}{\varepsilon_o}\right)^2 \left[(x - x') + 2r \ln\left(\frac{r-x}{r-x'}\right) + \frac{r^2}{r-x} - \frac{r^2}{r-x'}\right] + c - x + \left(\frac{0.15}{\varepsilon_u - \varepsilon_o}\right)\left[(k_1 + \varepsilon_o)(c-x) + k_1 r \ln\left(\frac{r-c}{r-x}\right)\right]\right\} \quad (12)$$

and

$$M_c = f''_c b \left\{ \frac{2k_1}{\varepsilon_o} \left[- \left(\frac{x^2 - x'^2}{2} \right) - r\,(x - x') - r^2 \ln \left(\frac{r - x}{r - x'} \right) \right] \right.$$

$$- \left(\frac{k_1}{\varepsilon_o} \right)^2 \left[\frac{x^2 - x'^2}{2} + 2r\,(x - x') + 3r^2 \ln \left(\frac{r - x}{r - x'} \right) \right.$$

$$\left. + \frac{r^2 x}{r - x} - \frac{r^2 x'}{r - x'} \right] + \frac{c^2 - x^2}{2} + \left(\frac{0.15}{\varepsilon_u - \varepsilon_o} \right) \left[k_1 r^2 \ln \left(\frac{r - c}{r - x} \right) \right.$$

$$\left. \left. + k_1 r\,(c - x) + \left(k_1 + \varepsilon_o \right) \left(\frac{c^2 - x^2}{2} \right) \right] \right\} \qquad (13)$$

For a failure in which the middepth strain equals ε_o, C_c and M_c are found by substituting k' from Equation 9 for k_1 in Equations 12 and 13.

Discussion of Analysis

12. To assess the implication of the above results, one must know the range of curvatures and other variables encountered in Corps conduit construction. To this end, recent Corps publications revealing variable values for conduit structures were quickly surveyed as summarized in Table 1. If this survey is taken to be representative of Corps practices, it would seem that the values of dimensionless curvatures R/h range from 2.5 to 3.8.

13. The effect of the most severe curvature in this domain is superimposed on a previously published (Mattock, Kriz, and Hognestad 1961) analysis of concrete stress distribution in Figure 8. In this figure, a dimensionless measure of the concrete resultant thrust is given by:

$$k_1 k_3 = \frac{C_c}{f'_c b c} \qquad (14)$$

while a dimensionless measure of this resultant's location is:

$$k_2 = 1 - \frac{M_c}{c C_c} \qquad (15)$$

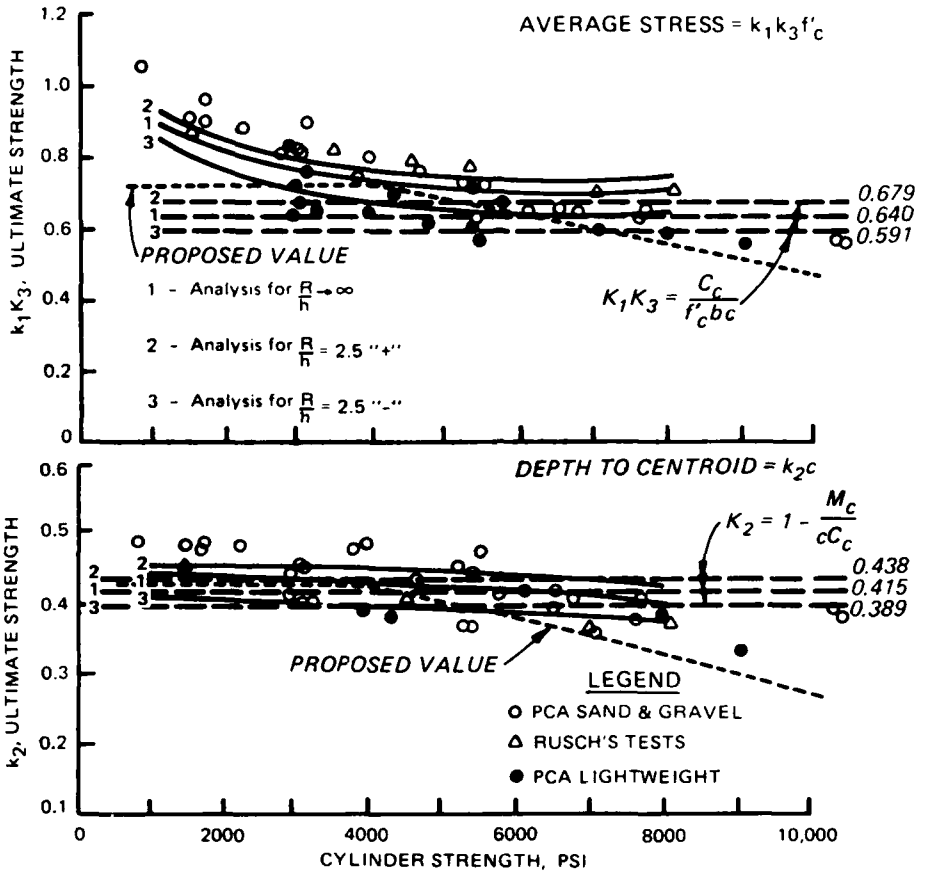

Figure 8. Properties of concrete stress distribution at ultimate strength determined from tests on plain concrete (Mattock, Kriz, and Hognestad 1961)

The equations describing the solid curves in Figure 8 are presented in Appendix D. The dashed curves using Equations 5 through 13 are not a function of the cylinder strength. There is good agreement between the analytical results of this study for $R/H \to \infty$ and independently acquired experimental results for members with no initial curvature. It is also noted that the effect on k due to the most severe initial curvature in Corps practice is within the scatter of carefully conducted laboratory experiments on uncurved members. The solid lines suggest that the present ACI β_1 factor, which was shown as the "Proposed Value" in Figure 8, is about as appropriate for Corps practice as for normal ACI practice. The dashed curves for the most extreme case of curvature at the springing line section do lie slightly below the scatter between 3,000 and 5,000 psi cylinder strengths. Results from the tests on

the model conduits will be used to evaluate further using the ACI β_1 factor for Corps practice for designing RC circular conduits.

14. Determining cross-section resistance of straight members under combined moment and thrust is compared to the capacity of Corps curved members. This can be seen from the interaction diagrams of Figures 9 and 10 for cross sections representative of Table 1. In these figures, the resistance of a member initially curved at $R/h = 2.5$ is shown by the symbols. It is seen that the hyperbolic strain distribution induced by the initial curvature causes a smaller resistance in negative moment than in positive moment. However, when these resistances are compared to the resistance of a straight beam ($R/H \rightarrow \infty$ corresponds to a straight beam), a decrease is only seen near the balance point, and this difference is within 10 percent.

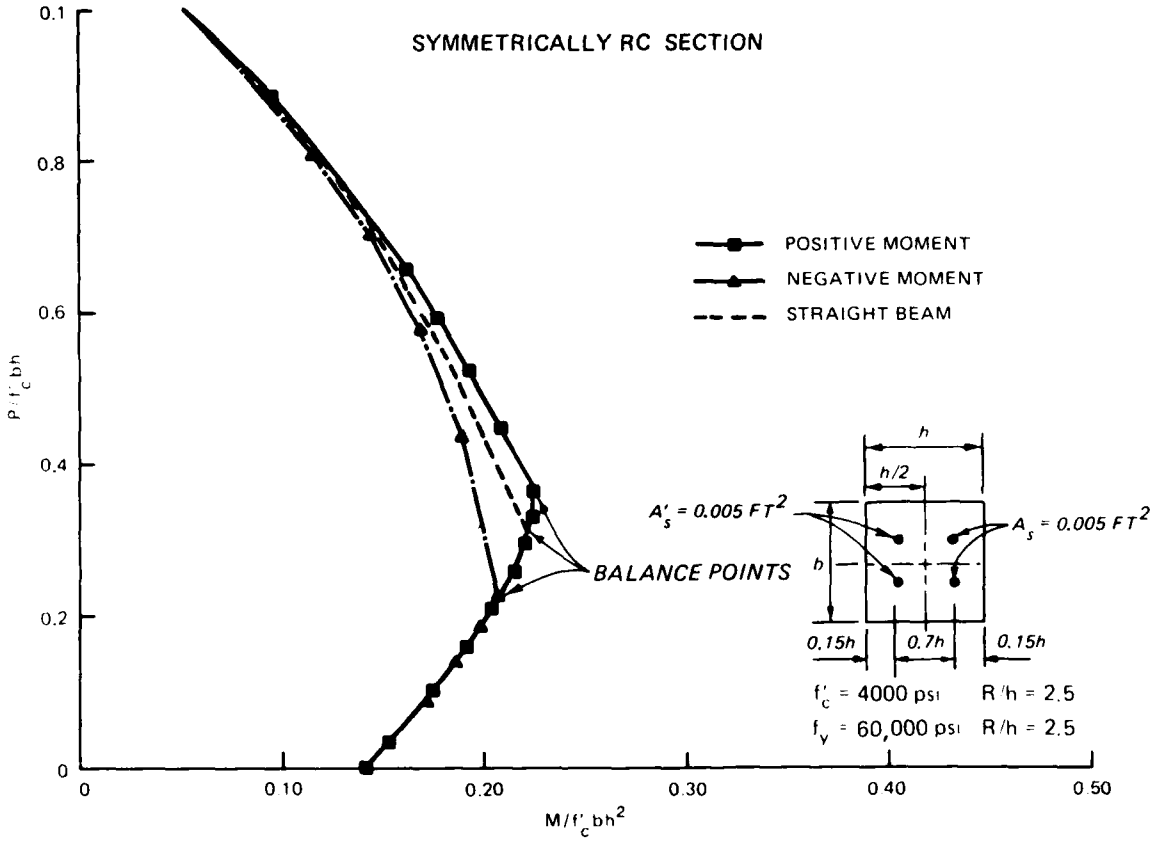

Figure 9. Interaction diagram, symmetrically reinforced cross section representative of Table 1

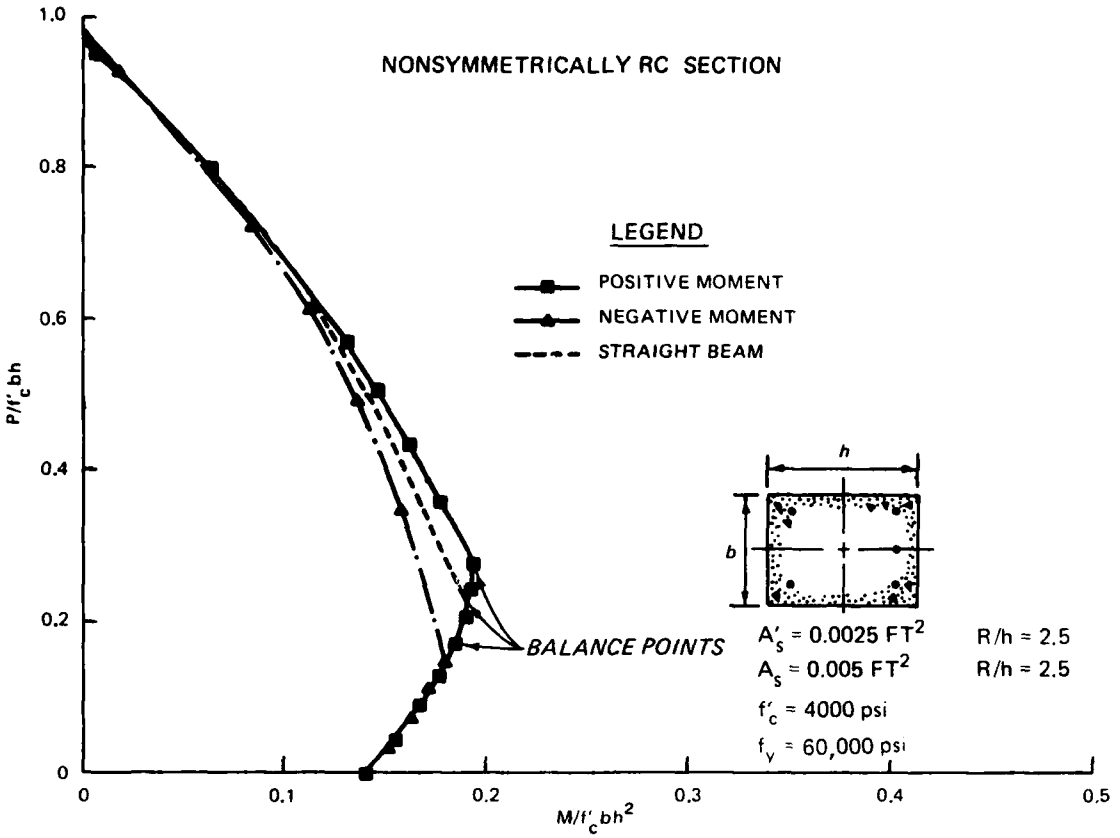

Figure 10. Interaction diagram, nonsymmetrically reinforced cross section representative of Table 1

Nonlinear Finite Element Model

15. The nonlinear FE program NONSAP was used to study the behavior of a plain concrete curved beam. An elastic-plastic hardening model which accounts for fracturing in the nonlinear material it represents and assumes small strains in rotation was used to represent the plain concrete (Chen and Chen 1975). It should be noted that this model only represents the portion of the concrete stress-strain curve up the maximum stress, f''_c . In Figure 11, the Chen and Chen model and the Hognestad stress-strain curve are compared. The symbols depict results computed from the application of the Chen and Chen model to a simply supported beam under combined moment and thrust loading. The stress-strain curves in Figure 11 are both for uniaxial stress conditions.

16. The differences noted between the two curves in Figure 11 are the maximum concrete stresses allowed and the strain value at which the maximum

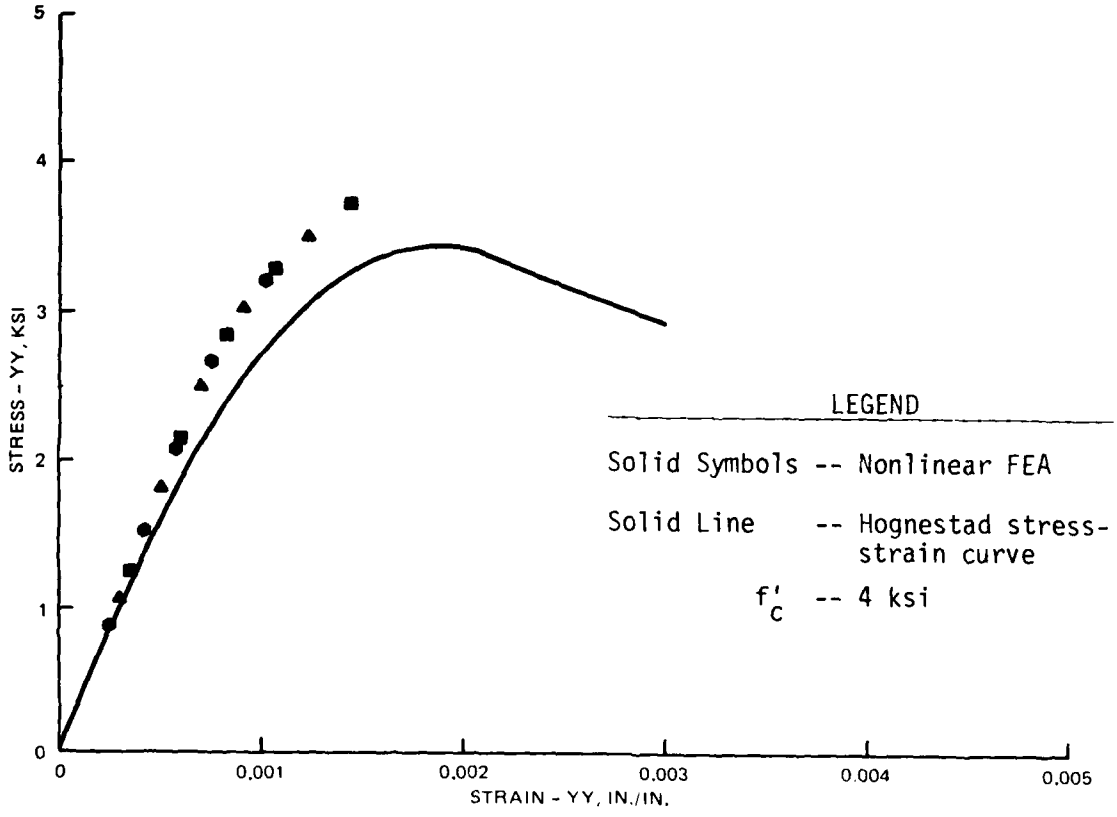

Figure 11. Comparison of the Hognestad stress-strain curve (solid) with uniaxial nonlinear FE data (Chen and Chen model, depicted by symbols)

stress occurs. In the Hognestad model, there is a factor that controls the value of the maximum stress.

17. A nonlinear FE analysis was performed on a plain concrete curved beam to verify the validity of a hyperbolic strain distribution for loading in the inelastic range. In Figure 12, the grid is shown for this analysis. The grid consisted of 192 total elements, of which 112 were 2-D linear elements in the outer thirds and 80 were 2-D nonlinear elements located in the middle third of the plain concrete member. The curved beam was simply supported at the geometric centroid of the section. Horizontal load couples placed at the ends of the beam applied a constant moment, and an external pressure applied on the extrados of the curved beam produced a constant thrust throughout the beam. The two load curves (force couple and pressure) were defined so that the neutral axis remained close to the edge such that the entire cross section was in compression. This simulated the procedure used by the Portland Cement Association (PCA) to conduct eccentric column tests to determine stress-strain

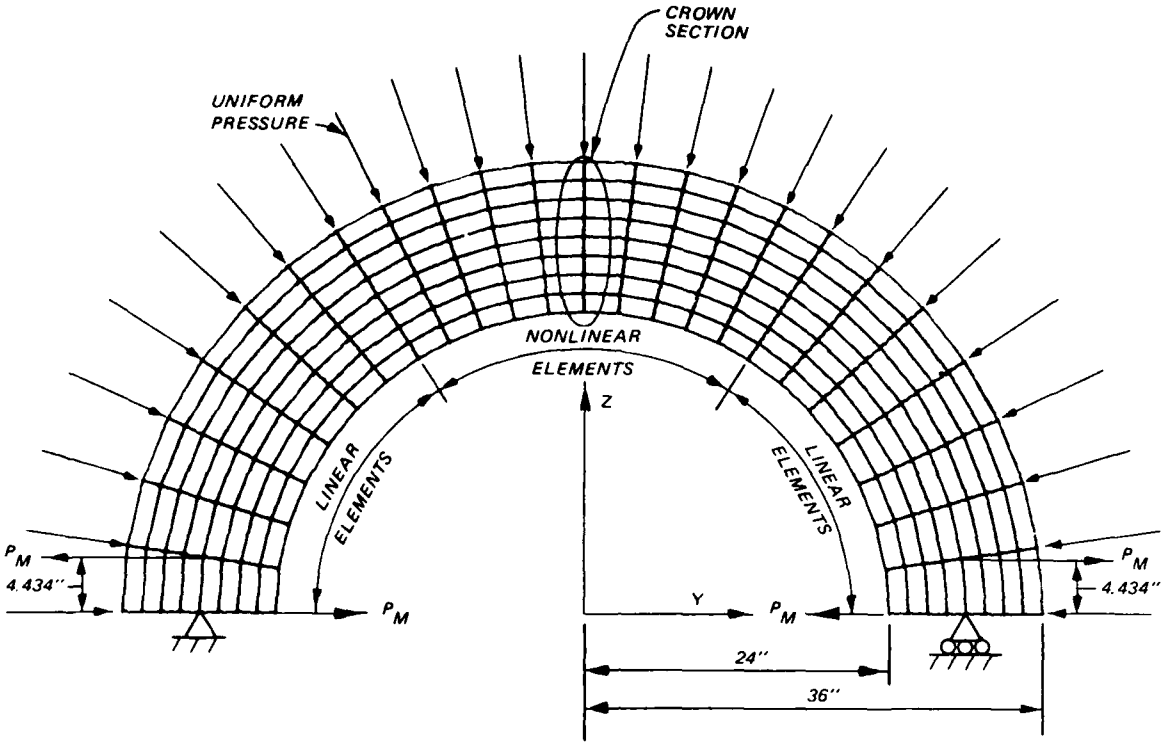

Figure 12. Grid used for the NONSAP analysis of RC curved beam (undeformed grid)

characteristics of reinforced and plain concrete rectangular sections (Kaar, Hanson, and Capell 1977; Kaar et al. 1978). In Figure 12 the loading and boundary conditions used in this analysis are illustrated.

18. Figure 13 shows the verification of the hyperbolic strain distribution by the nonlinear FE model, up to a strain of 0.0015 in./in. compression. The strain profiles are from the middle vertical cut of the beam. The curve marked by $t = 20$ (load step 20) depicts elastic behavior of the section whereas the curve marked by $t = 50$ depicts a portion of the section behaving plastically near the edge of the section. At $t = 20$, the pressure is 495 psi and the horizontal load couple is (4.424 in.) $(0.85 \times 10^5$ lb) = 376,890 in.-lb. At $t = 50$, the pressure is 750 psi and the horizontal load couple is (4.434 in.) $(0.114 \times 10^6$ lb) = 505,476 in.-lb.

19. Also listed in Figure 13 are the internal forces denoted with subscript I and the applied forces denoted with subscript A. The internal forces were calculated from the stress output and the applied forces were the horizontal load couple and the thrust due to uniform pressure. The comparison

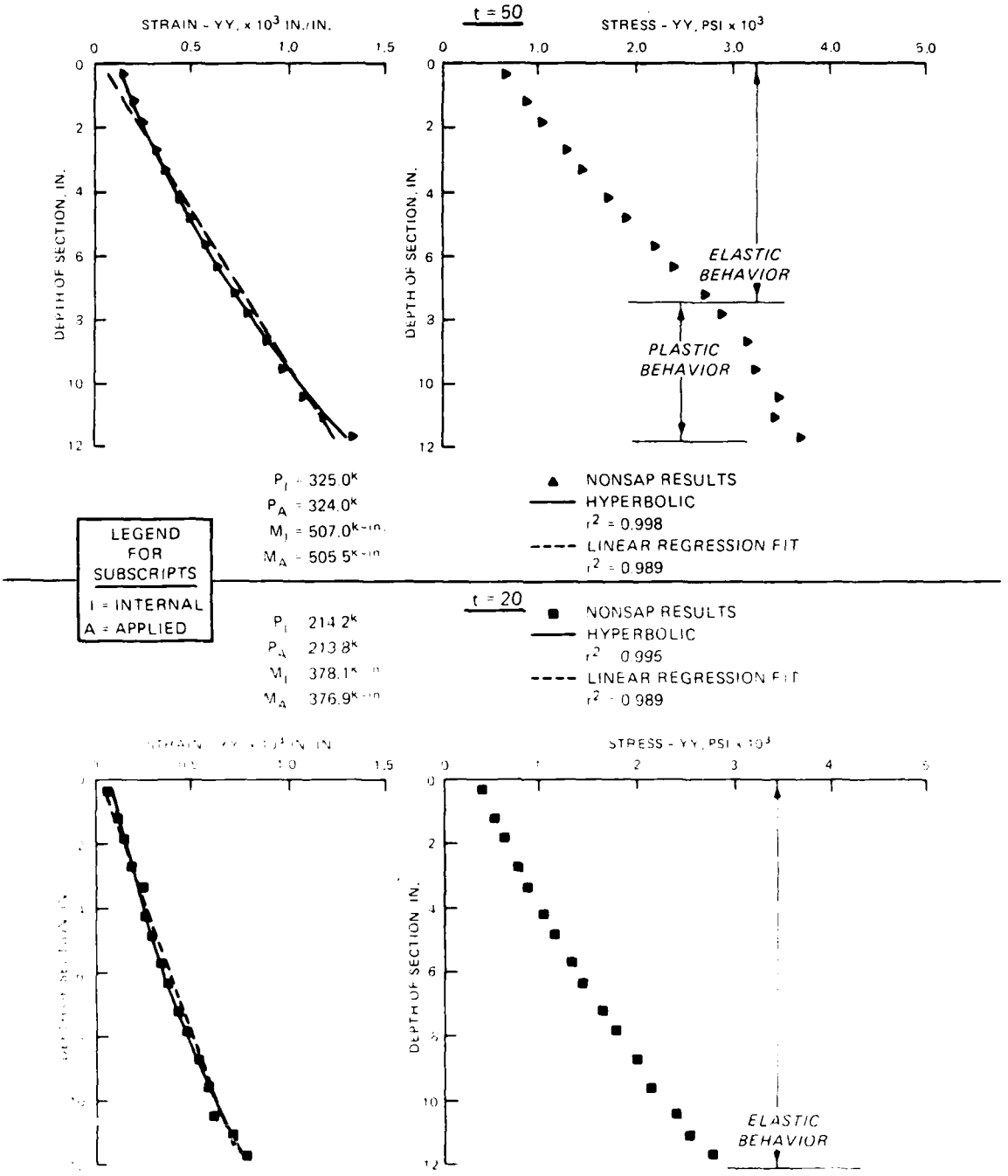

Figure 13. Verification of the hyperbolic strain distribution by a nonlinear FE model

between the internal and applied forces shows good agreement. Also shown is a comparison between the hyperbolic and linear fits to the numerical results. The correlation coefficient squared, r^2 , is listed for each load level. (Refer to Appendix C for the statistical analysis.)

PART III: STRUCTURAL ANALYSIS OF MODEL RC CIRCULAR CONDUITS

20. A 1-D structural analysis was performed to compute the internal forces of a one-quarter symmetrically loaded circular conduit. Three loading cases were analyzed: continuous normal pressure (Anderson, Haelsig, and Reifel 1966), the 3:1 Engineer Manual (EM) design load condition (Headquarters, Department of the Army 1969), and a five-point load simulating the normal load component of the 3:1 EM design load condition. The 3:1 EM loading is shown in Figure 14. The equations for the internal moments, thrusts, and shears are shown in Appendix A.

21. A closed-form solution, Airy stress, of the stresses with a given wall thickness was published in an Air Force Weapons Laboratory (AFWL) report (Anderson, Haelsig, and Reifel 1966). The equations for the resultant moments, thrusts, and shears from the stress distributions due to the continuous normal pressure distribution are also presented in Appendix A.

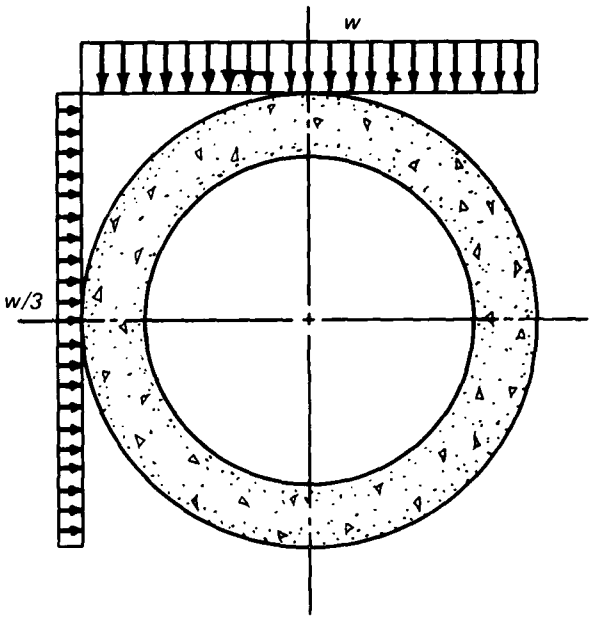

Figure 14. EM 3:1 loading

22. In Figure 15, the 2-D conduit is idealized by the 1-D linear elastic line structure. The one-quarter symmetric structure is 1 degree indeterminate; therefore, both the equilibrium equations and a geometric compatibility condition were required to solve for the internal forces. All of the material properties were assumed to be represented by the line structure at the geometric center of the section. (Actually, it is more accurate to assume that these properties are concentrated at the neutral axis, but the neutral axis is not known a priori.) Only the normal loading can be modelled experimentally in this study. If an actual soil is used, the 3:1 EM loading can be more accurately modelled such that shear transfer exists at the conduit-soil interface.

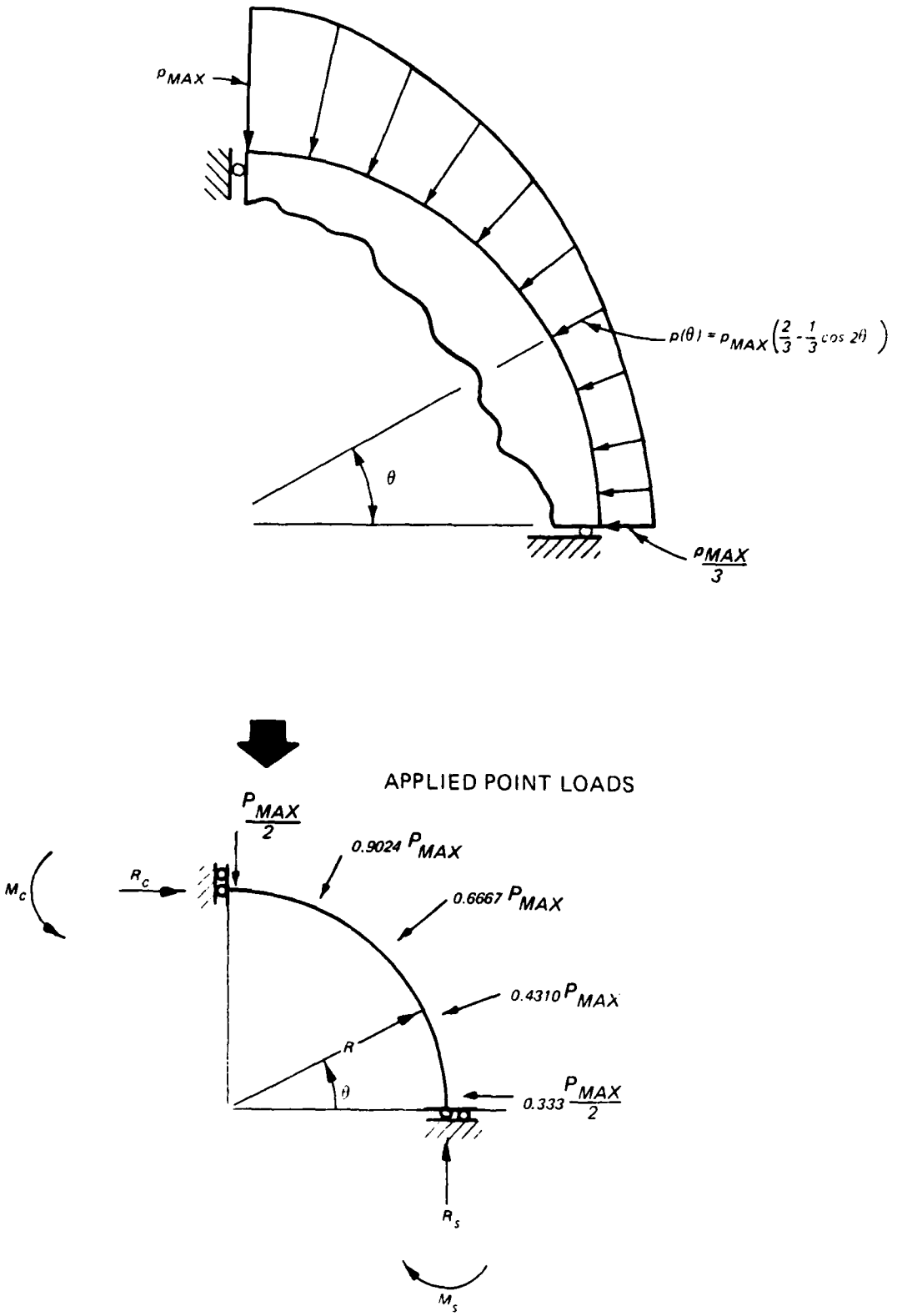

Figure 15. 1-D idealization of RC conduit

23. Comparisons between the EM and the two AFWL loadings (1-D and Airy) are presented in Figure 16. The analyses were normalized with respect to the applied maximum pressure and the radius of curvature to middepth. The 2-D results were obtained from a problem with $R = 15$ in. and $h = 6$ in. Comparing the EM loading with the AFWL 1-D loading, the EM loading gives 50 percent greater moment and shear, 29 percent more thrust at the springing line, and 40 percent less thrust at the crown. Comparing the Airy stress solution with the AFWL 1-D solution, the largest differences between the thrusts, shears, and moments are, respectively, 20, 20, and 100 percent (at $\theta = 45$ deg, where the 1-D analysis gives zero moment, and the Airy stress solution gives $-0.009\ wR^2$ for moment).

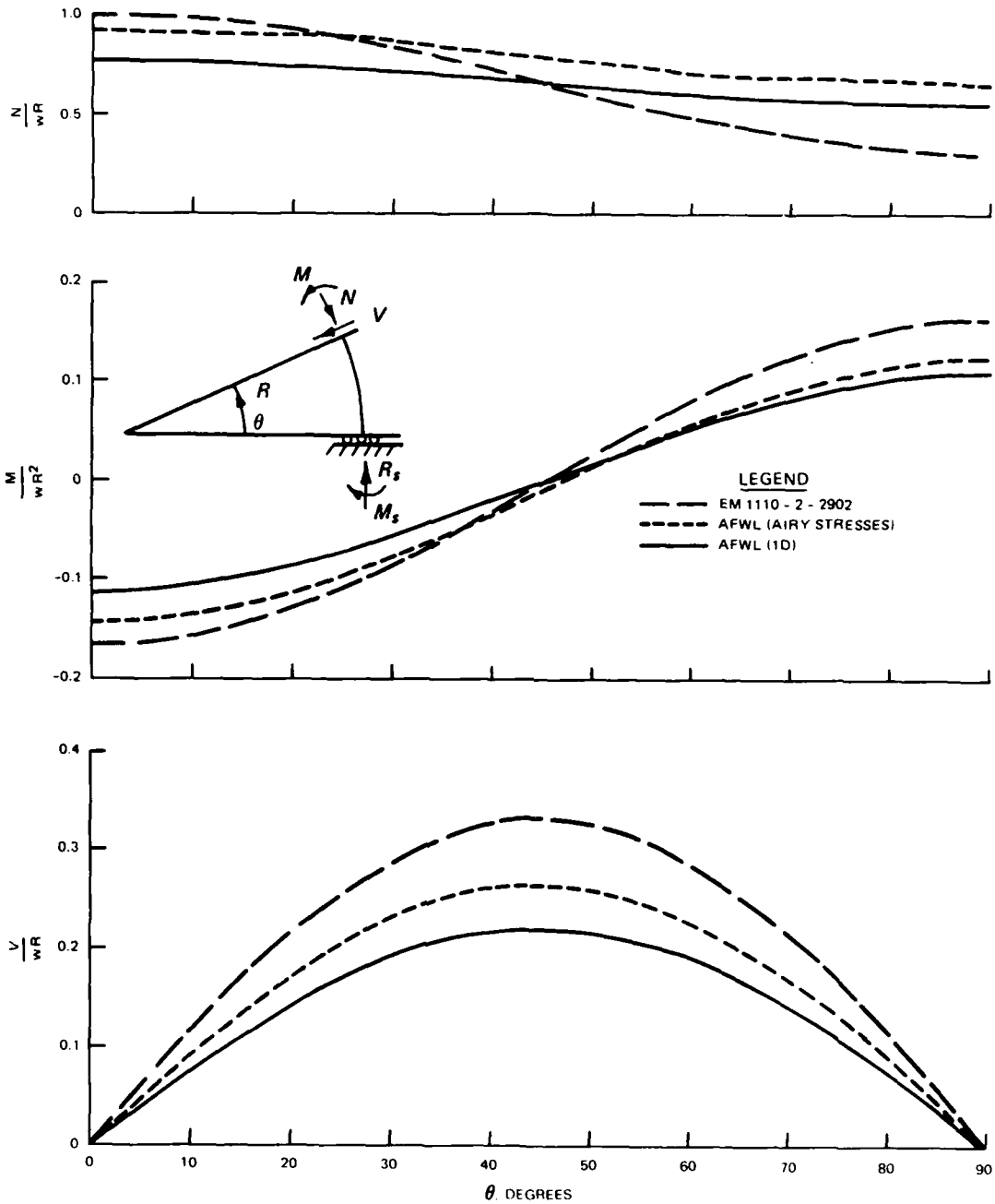

Figure 16. Comparison of internal forces computed using EM, AFWL 1-D, and Airy stress structural analysis

PART IV: EXPERIMENTAL STUDY OF THICK-WALLED CIRCULAR CONDUITS

24. An experimental study was performed to verify a conventional 1-D structural analysis of thick-walled RC circular conduits. The curved beam analysis described in Part II was used to predict the ultimate capacity curves of the curved beam RC sections. In this part of the report, only the experimental results will be presented; the test results are discussed in Part V. Failure loads were predicted for each of the experiments.

25. In addition to the experimental study a structural analysis of a circular conduit subjected to the EM design loading (Headquarters, Department of the Army 1969), a continuous pressure loading, and a multipoint loading was performed. The pressure and the test loading simulate normal components of the 3:1 EM design loading condition. The multipoint loading represents loads by hydraulic rams positioned radially about a circular conduit test specimen.

Test Descriptions

26. The purpose of the tests in the experimental study was to evaluate the behavior and failure modes of RC circular conduit with different initial curvatures. Three RC conduit models were fabricated. Two were identical (with the same section design and curvature (R/h = 2.5)) and the third differed only in curvature (R/h = 4.0). The test specimens represent a scaled slice of a circular RC conduit. Cross sections of C1, C2, and C3 are shown in Figures 17 and 18. The circular shape was chosen since it is the least complex and the tests will not be affected by any abrupt change in geometry that might complicate interpreting the observed behavior. Also the first series of tests establishes a standard testing procedure for future tests of other conduit shapes.

27. The section designs of the models are representative of the initial curvatures, steel percentages, and materials of the range of prototype structures surveyed, as listed in Table 2.

28. Normal-weight concrete was used with a maximum size aggregate of 1/2-in. sand and normal type cement. Steel reinforcement was modelled using No. 2 and No. 3 Grade-60 rebars. A symmetrically reinforced section was designed for the tests.

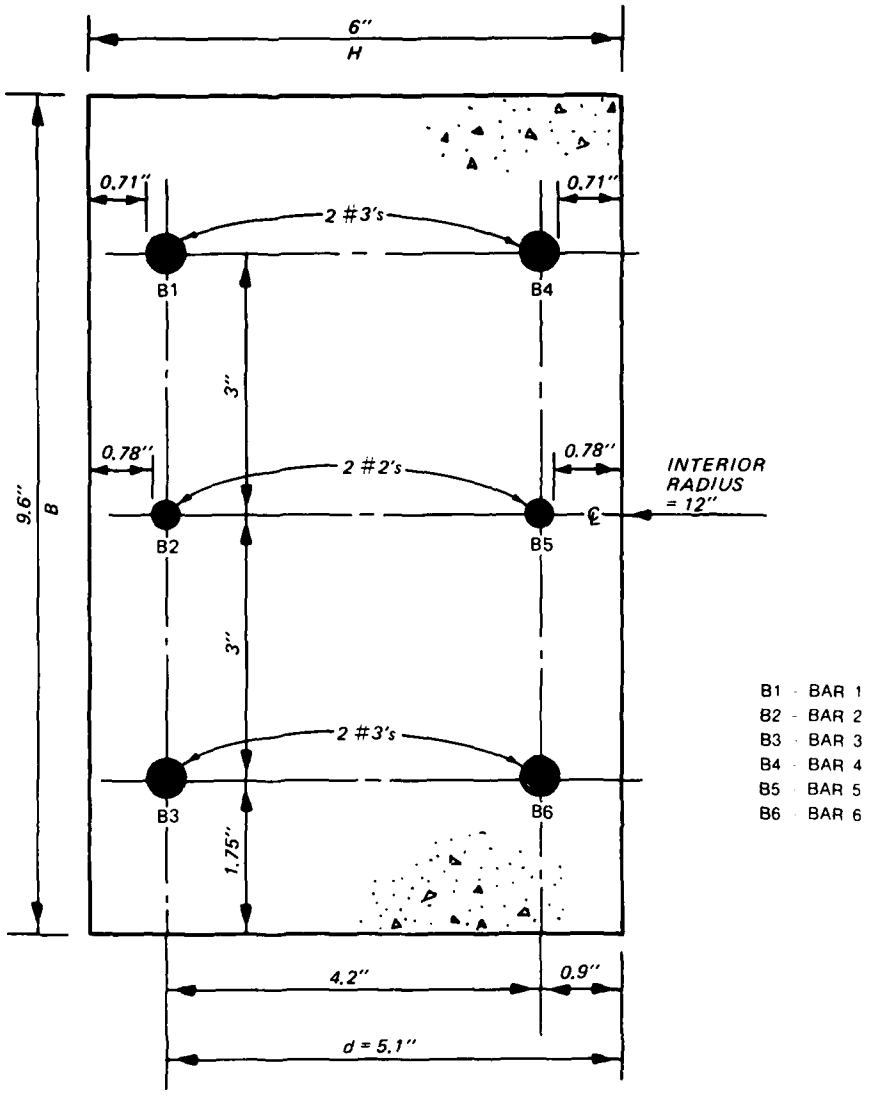

$A_{s_{TOTAL}} = 0.54\ IN.^2$

$$\rho_g = \frac{A_{s_{TOTAL}}}{BH} = \frac{0.54}{57.6} = \underline{0.938\%}$$

$\frac{d}{H} = 0.85$

$\frac{d'}{H} = 0.15$

$$\rho = \frac{As}{Bd} = \frac{0.27\ IN.^2}{(9.6\ IN.)\ (5.1\ IN.)} = \underline{0.00552}$$

Figure 17. Section design of specimens C1 and C2

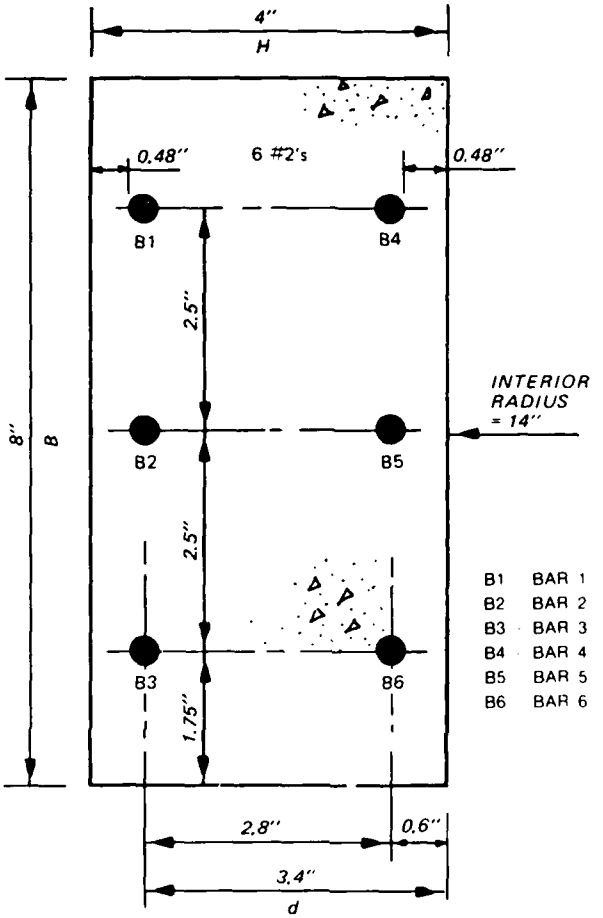

$A_{S_{TOTAL}} = 0.30\ IN.^2$

$$\rho g = \frac{A_{S_{TOTAL}}}{BH} = \frac{0.30\ IN.^2}{32} = 0.938\%$$

$\frac{d}{H} = 0.85$

$\frac{d'}{H} = 0.15$

$d = 3.4"$

$$\rho = \frac{As}{Bd} = \frac{0.15\ IN.^2}{(8")\ (3.4\ IN.)} = 0.00552$$

Figure 18. Section design of specimen C3

Instrumentation

29. The tests used 48 channels, as follows:

Load cells	16
Deflection gages	4
Gages on rebars	22 (Gage No. 1-4, 6, 7, 9-12, 14, 15, 17-20, 22, 23, 25-28)
Gages on interior surface of conduit mode	6

The deflection gages were positioned to measure the diametric changes at $\theta = 0$ and 180 deg; 45 and 225 deg; 90 and 270 deg; and 135 and 315 deg. The 16 load channels were connected to 50,000-lb Precision Universal Interface load cells, one mounted on each rod end of the hydraulic jacks. The load cells measured the actual load distribution applied. All data were recorded on two 32-track magnetic tapes. Gage locations are shown in Figure 19.

Loading Apparatus

30. The load distribution was simulated by 16 double-acting Hydroline cylinders, each rated for a maximum operating pressure of 3,000 psi. The hydraulic jacks were mounted to a steel frame designed 10 times stiffer than a test specimen and for adequate strength to resist maximum bending from two opposing point loads equal to 100 kips and maximum tensile thrust from 16 radial loads equal to 100 kips. Each cylinder can produce a static force of 59.8 kips at 3,000 psi. A hydraulic power supply rated for 3,000-psi maximum output supplied the hydraulic fluid pressure.

31. To produce the desired load distribution, a Challenger Model 10M multiple pressure hydraulic load maintainer manufactured by John S. Edison, Inc., of Burbank, Calif., was used. The Challenger 10M can deliver up to 10 different outlet pressures which can be increased simultaneously. Of the total, eight channels were used to deliver pressure to the push ports of the jacks and the two remaining channels used as return lines from the circuit connecting all the pull ports. In Figure 20, a schematic of the hydraulic circuit is shown. A plan view of the testing aparatus is shown in Figure 21. The experimental equipment is listed in Table 3.

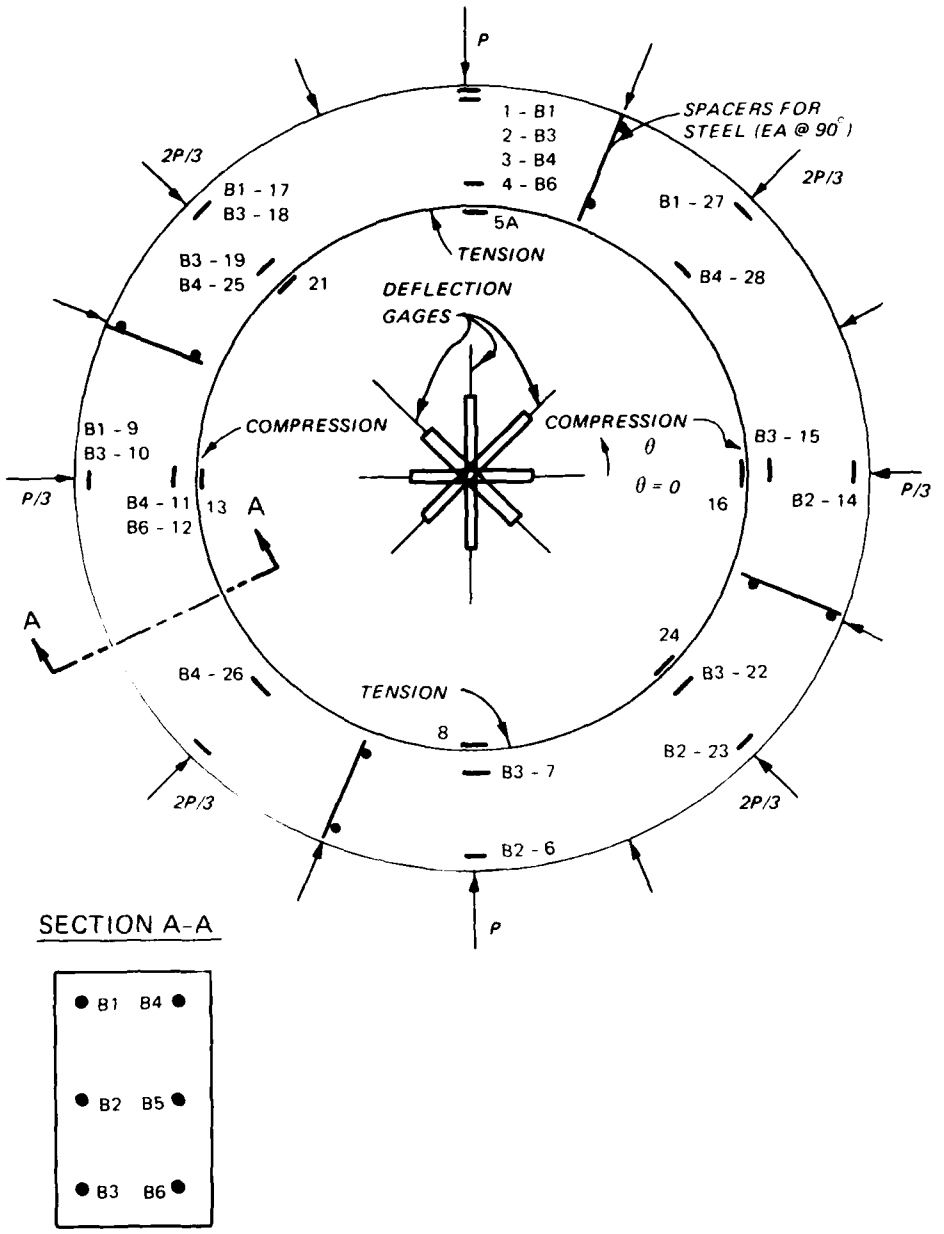

Figure 19. Strain and deflection gage locations

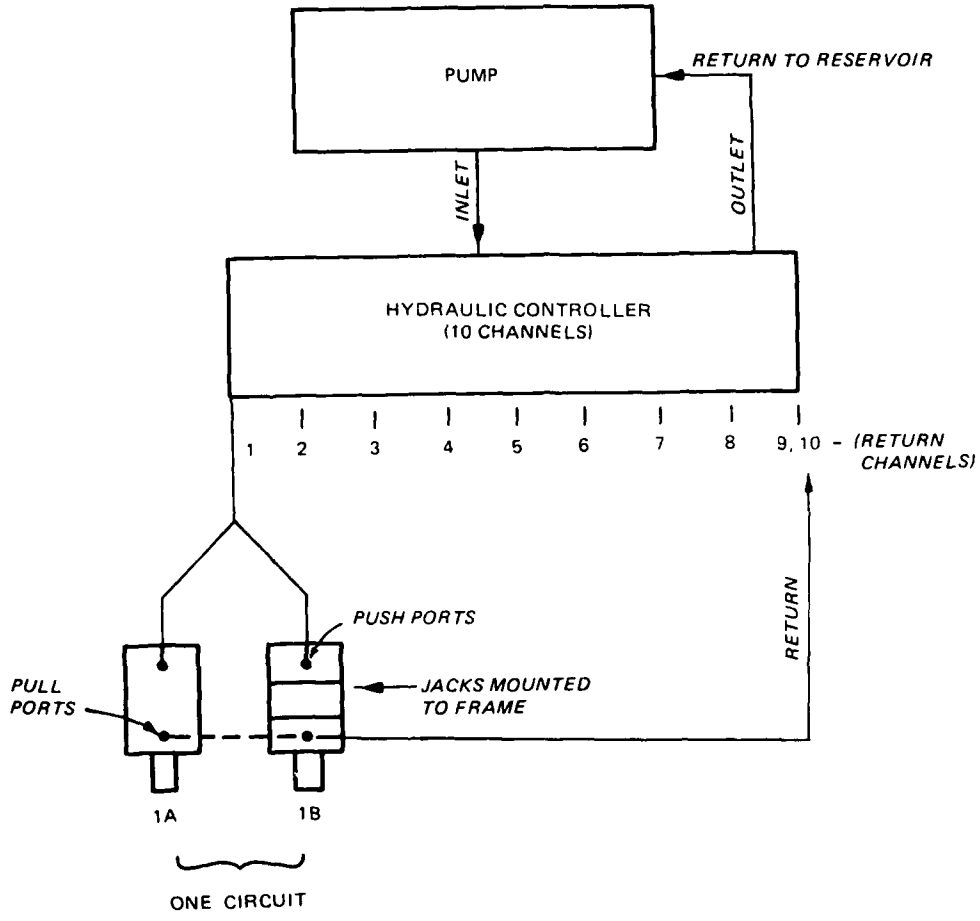

Figure 20. Schematic of hydraulic system

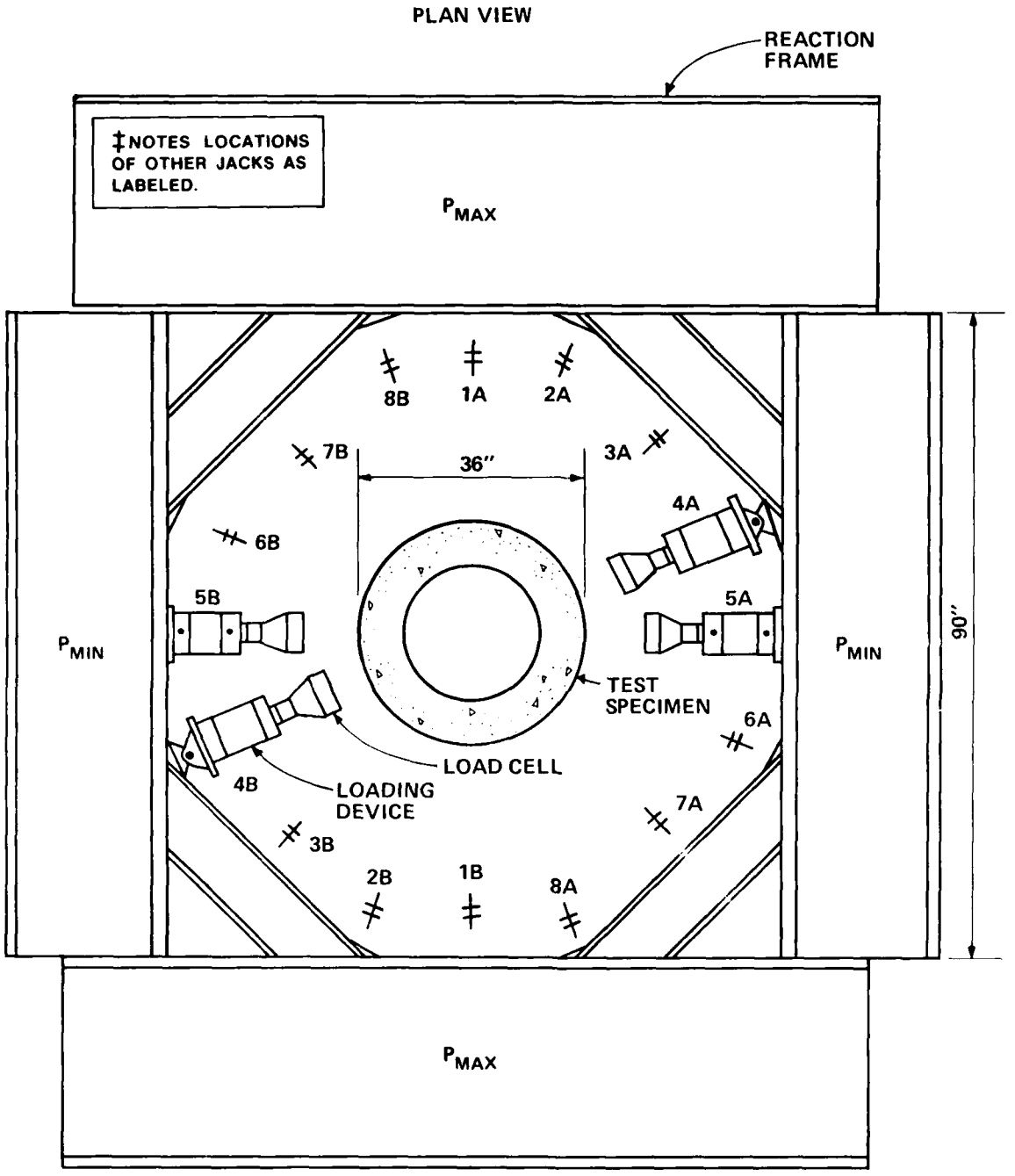

Figure 21. Plan view of testing apparatus

PART V: TEST RESULTS

Material Properties

32. For analyzing the test results, the following material properties were required: 28-day uniaxial compressive concrete strength; uniaxial compressive concrete strength at day of test; and yield, ultimate, and rupture value of the steel reinforcement. In Table 4 the results from the uniaxial compressive tests and the tensile tests of the steel reinforcement are listed. The design material properties representative of values from Table 1 for the concrete 28-day strength, f'_c , and the steel reinforcement yield strength are 4 and 60 ksi, respectively (remembering that new common practice is to use Grade-60 steel instead of Grade 40). Three standard 6- by 12-in. concrete cylinders were tested at 28 days. Very good control was achieved for a three-cylinder average 28-day strength of 3,980 psi. The other three dates in Table 4 were the days that models C1, C2, and C3 were each first tested.

33. The values of f'_c on the test day are used as parameters for the concrete material property according to Hognestad's constitutive law (Hognestad, Hanson, and McHenry 1955). In models C1 and C2, a weighted average was performed to compute an appropriate value for the yield strength, f_y , of the steel reinforcement.

34. Test cylinders and models were cured in separate buildings because of the convenience of the location of appropriate test equipment. However, it is noted that the average temperature difference probably ranged from 5° to 10° F (i.e., the temperatures would be 80° to 85° F compared with 85° to 95° F). It is not known exactly how much of a difference this makes in the actual f'_c for the model. However, there are effects other than temperature that account for actual differences between f'_c for test cylinders and the models (ACI 1970). It is assumed in this study that this difference is negligible compared to other experimental errors encountered.

Test Procedure

35. Before the first specimen was tested, a load test was conducted to check the prescribed load distribution. A very stiff circular specimen with the same outside dimensions as the model conduits was tested with the same

setup proposed for the conduit tests. The results from the load verification are presented in Table 5 and agree closely with the predicted loads. The measured loads provided a check on the load distribution.

36. After the load distribution was set, a model conduit was placed in the reaction frame such that the center line of the ram aligned with the center line of the model. The model was supported at four points by steel plate shims and two 4 by 4 by 1/2-in. pieces of Teflon. The Teflon pads were cleaned with a solvent beforehand and provided a very good low-friction surface to allow free translation of the model during loading. With the model in place, the model instrumentation channels were connected.

37. Before loading, each rod was positioned to be just touching load-bearing plates positioned against the model. The pressures in the jacks were simultaneously increased and all the data channels were recorded on two 32-track magnetic tape machines. The loading rate for each of the tests was approximately 100 psi/min (2,000 lb/min in the jack with the largest load). Cracking was detected by ear, but was not easily seen. Immediate output was in the form of an x-y plot (one load channel used as a reference versus any two-strain channels) and strip charts for all channels. The strip charts gave an approximate look at numerical results and indicated which gage channels were ineffective (either because of noise or a bad gage). The data stored on the 32-track tapes were then digitized and placed in computer files accessible through time-sharing terminals.

Observations

38. The first two specimens, C1 and C2, remained virtually intact when tested with the full capacity of the loading system. Cracking was detected by ear during the tests but no cracks or distress in C1 or C2 could be seen without closely inspecting each after the tests were complete. Retests on both specimens showed similar results; however, more tensile cracks were visible. Hence, C1 and C2 were not tested to failure under the prescribed load distribution. The first yield was expected to occur at the crown and the second at the springing line for a dominant flexural failure mode. The crack patterns observed are shown in Figure 22.

39. Model C3 was tested to failure and the progression of the collapse mechanism being formed was observed. First yield and plastic hinge were

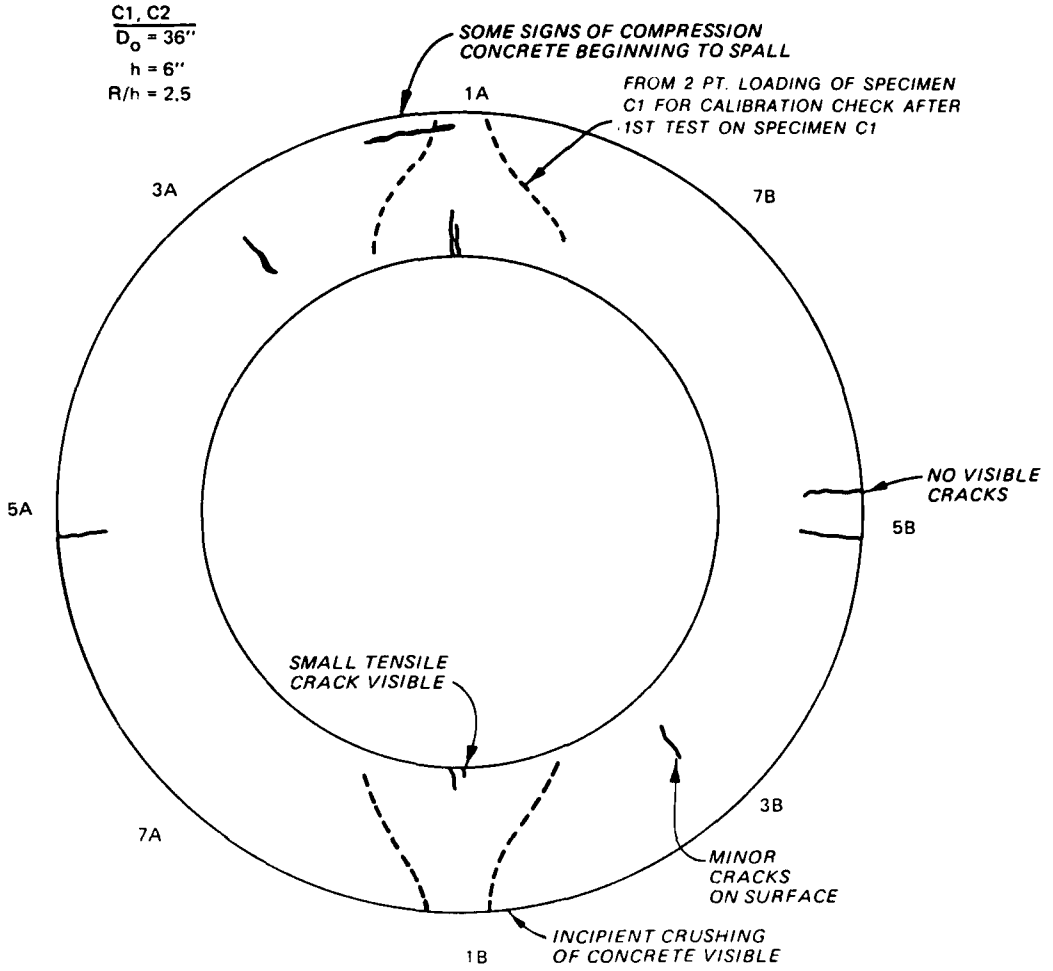

Figure 22. Crack patterns of models C1 and C2

expected to occur at one of the crown sections. The formation of the first hinge did occur at the crown such that the tension concrete was cracked and the compression concrete crushed. Then plastic hinges were formed at the two springing line sections formin , a three-pinned arch structure. The last hinge was formed following a secondary-type compression failure at the other crown section forming the four-hinge collapse mechanism. The final crack patterns are shown in Figure 23 with the observed order of cracking and crushing of concrete labelled.

Acoustic Emissions

40. After the test on C1 was completed, it was suggested that it may

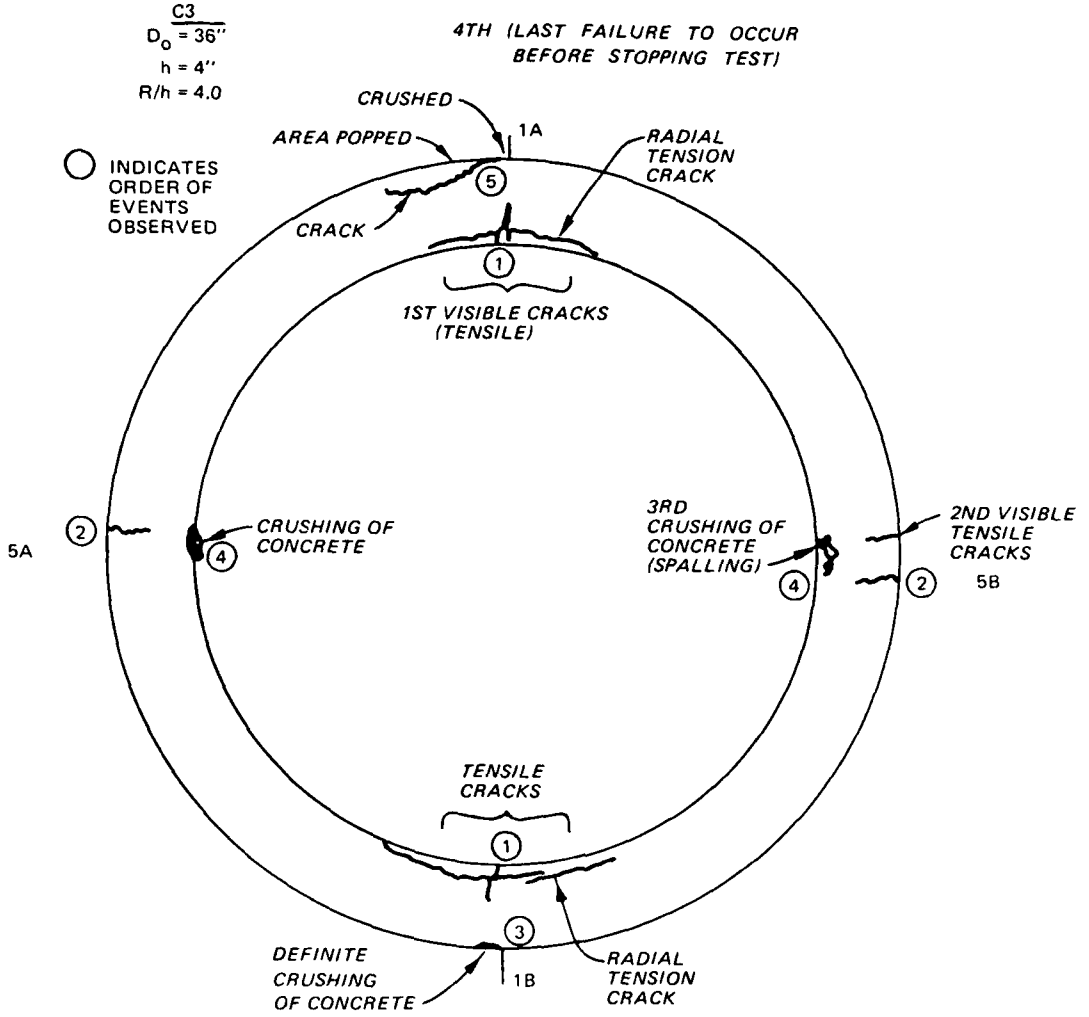

Figure 23. Crack patterns of model C3

be possible to detect qualitatively where cracking occurs first--the crown or the springing line. Disturbances in the model under load are sources of energy that cause waves to propagate within the model at very high frequencies. The events of disturbances can be counted electronically with acoustic emission transducers (Mlakar, Walker, and Sullivan 1981). An array of two transducers was placed each on C2 and C3. During these two tests, the transducers AE1 and AE2 were positioned at 67.5 and 22.5 deg from a springing line section on the middepth height of the intrados as shown in Figure 24. In this setup, one transducer (positioned at 67.5 deg) would detect disturbances from the crown before the other transducer.

41. Results are in the form of number of counts (events of disturbances

measured as accelerations occurring above a threshold acceleration value) versus load. In Figure 24, the location of the transducer is superimposed on the crack pattern for models C2 and C3. In Figure 25, the number of counts are plotted for the first and second (retest) test of C2. Note that the vertical scale for the number of counts is a factor of 10 smaller for the retest than the first test. In Figure 26, the count-load plot is shown for the test of C3 to failure. Distinct differences in the count-load plots are observed between a failed specimen (C3) and an intact specimen (C2).

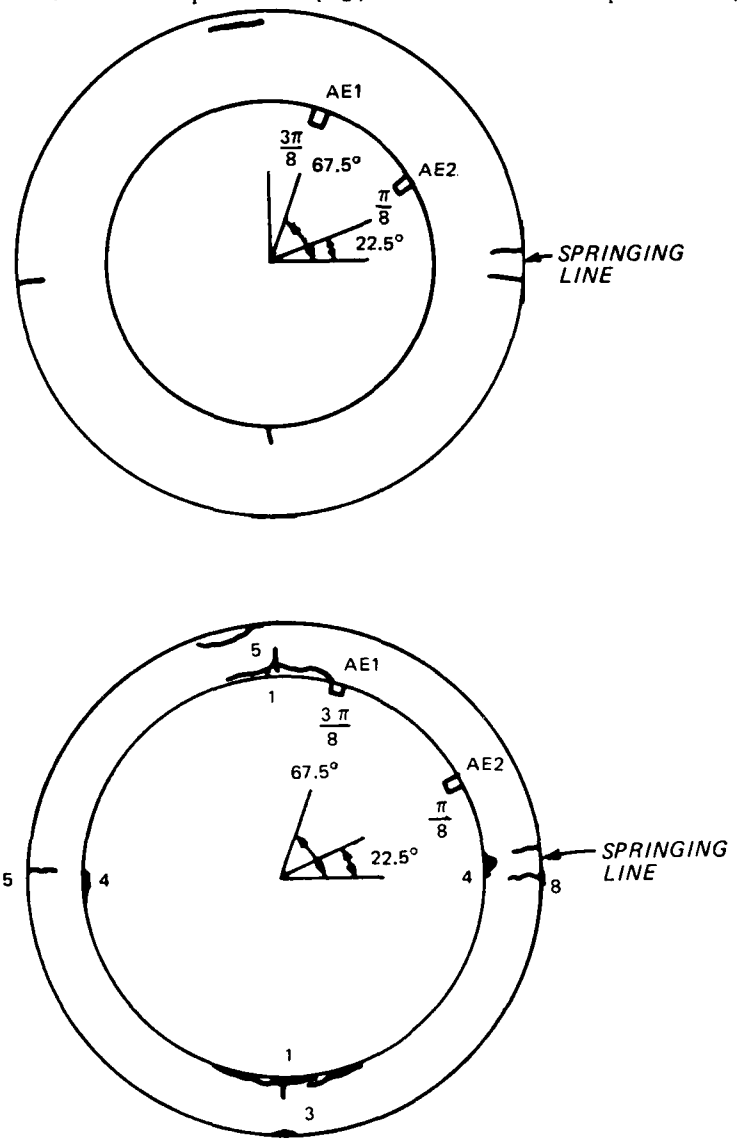

Figure 24. Location of acoustic emission transducer superimposed on crack patterns for models C2 and C3

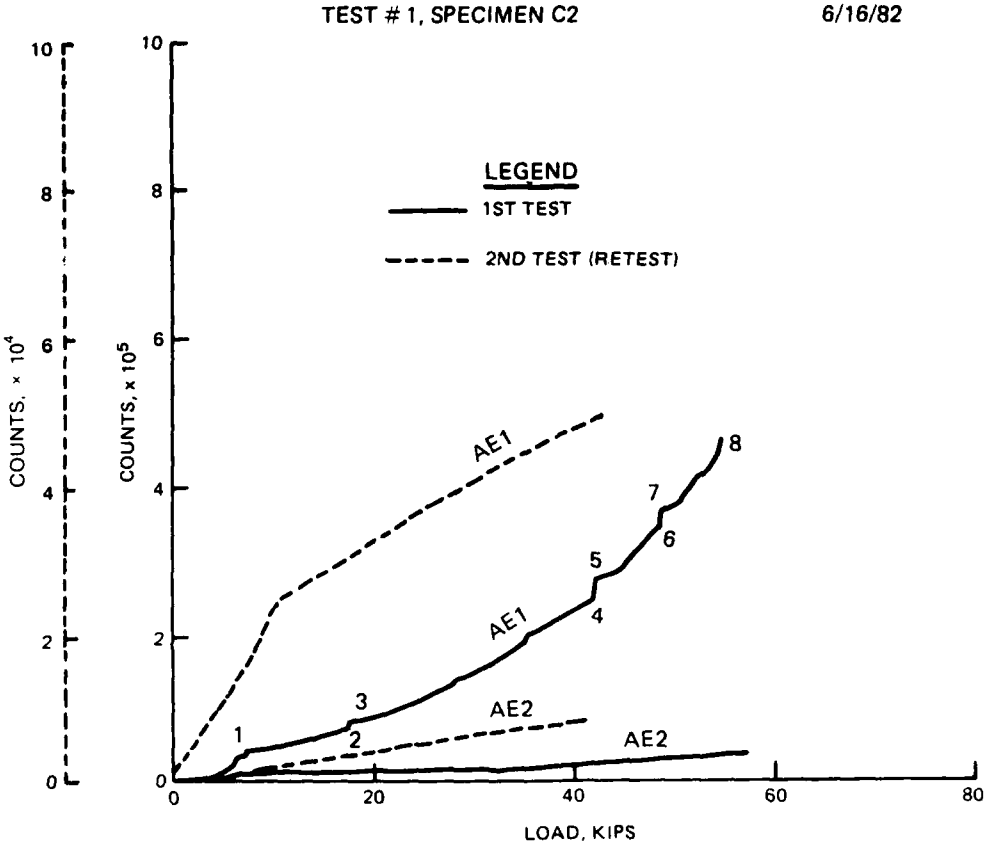

Figure 25. Plot of number of counts for first and second (retest) test of C2

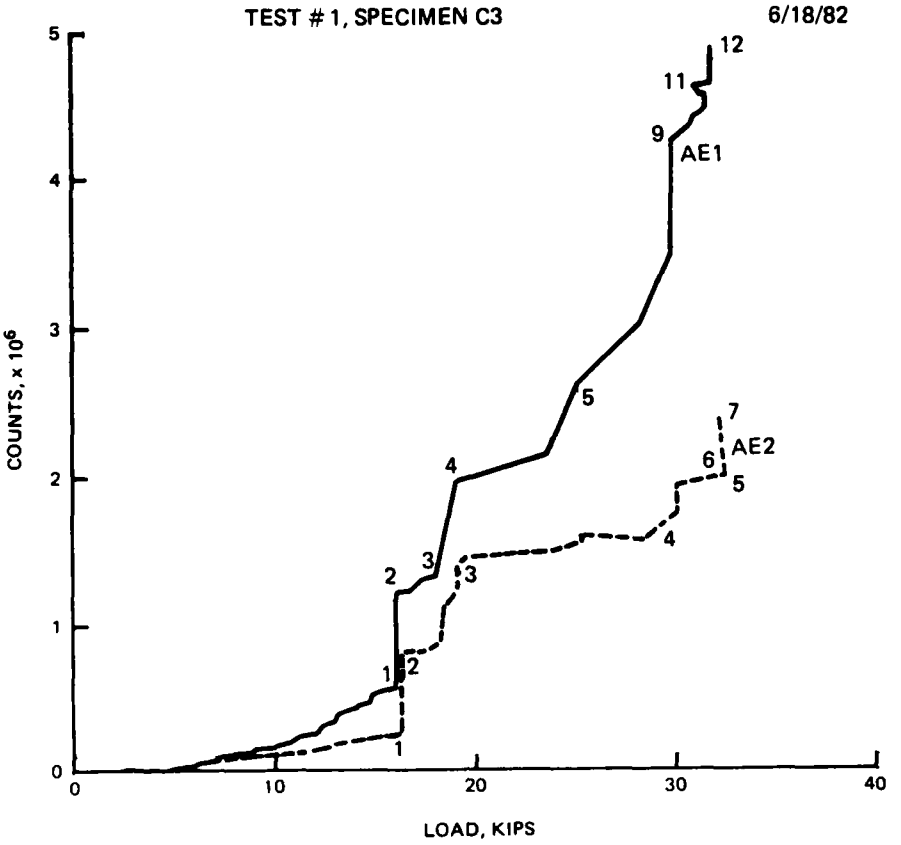

Figure 26. Count-load plot for test of model C-3 to failure

Load Distributions

42. Data from the load cells are presented in radial load distribution plots. Load distributions at a given time are plotted on the same axis to give the picture of the growing load distribution with increasing pressure. Star symbols represent the predicted load distribution for the last load step. Figures 27, 28, and 29 contain examples of the load distributions recorded. All the loads check to within 0.5 to 4 percent of static equilibrium. Equilibrium checks were performed on the measured load distributions to evaluate errors in computing static equilibrium. Looking at Figure 27 (load distributions) the equilibrium checks were performed by summing all negative vertical and horizontal force components and comparing the sums to all positive vertical and horizontal force components. The differences range from 0.09 to 4.56 percent, as shown in Table 6.

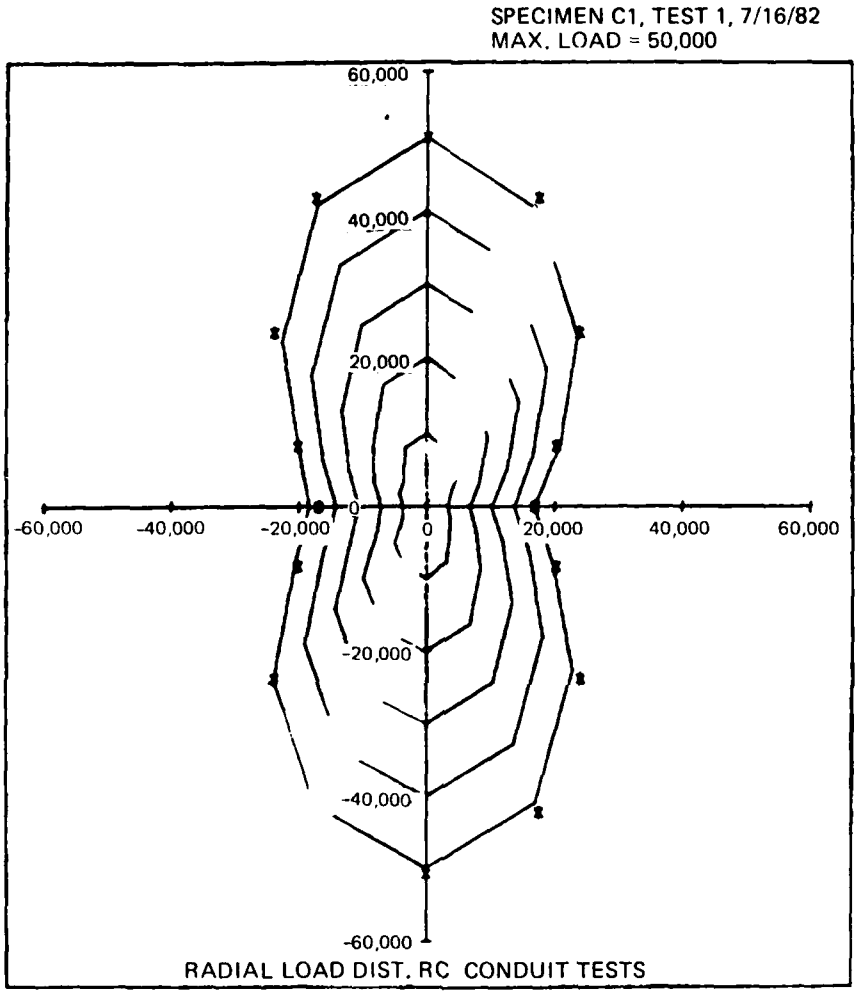

Figure 27. Load distributions recorded, specimen C1

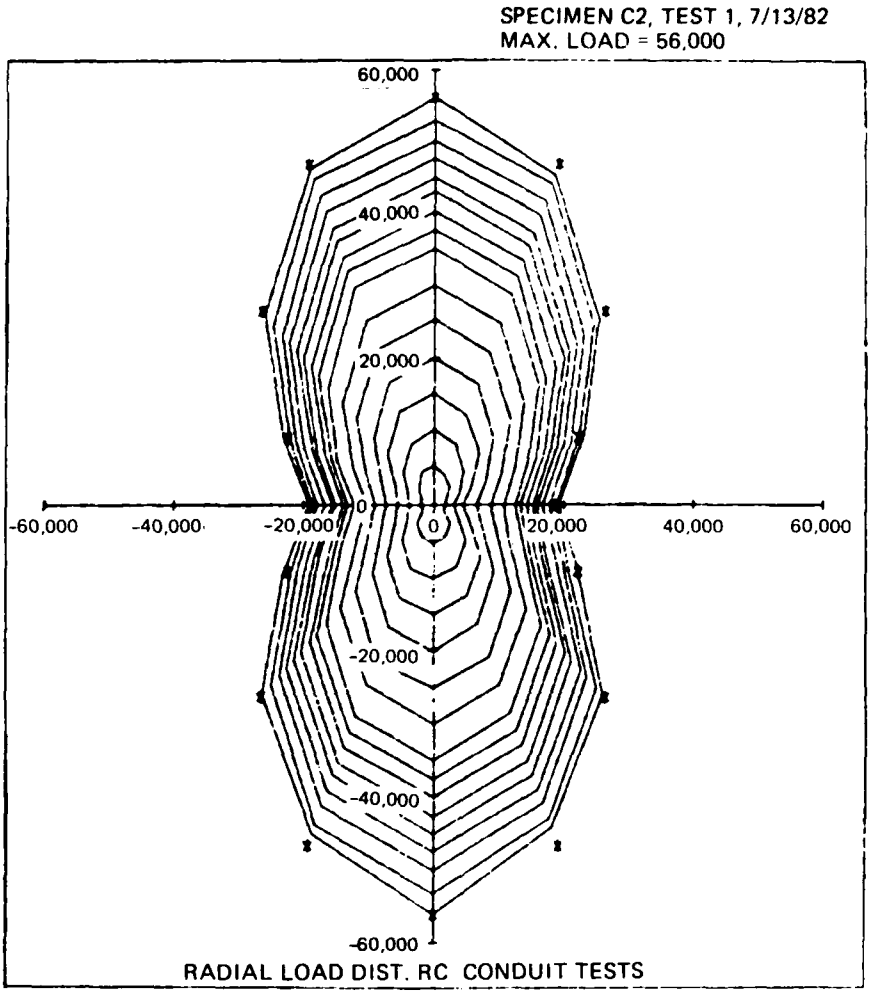

Figure 28. Load distributions recorded, specimen C2

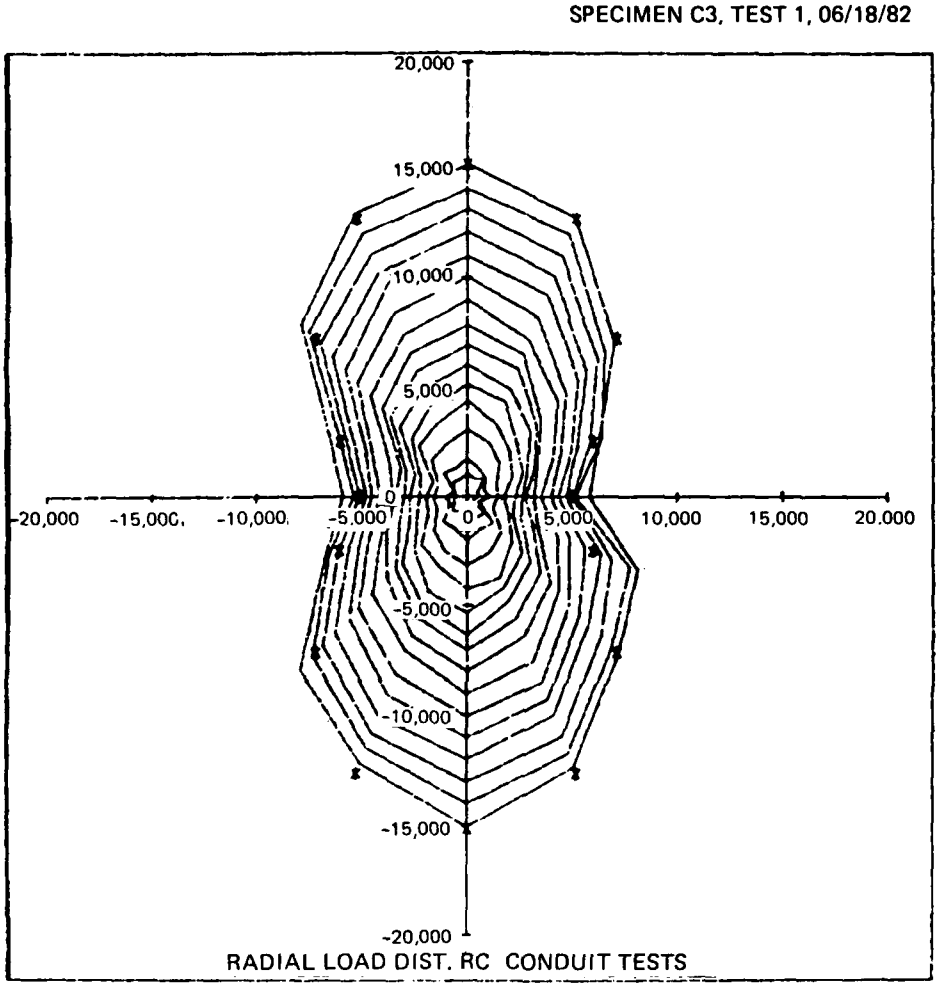

Figure 29. Load distributions recorded, specimen C3

Load-Strain Plots

43. The data from the strain gages on the steel reinforcement and concrete are plotted as load versus strain. Averaged load-strain plots for tests of C2 and C3 are shown in Figures 30 through 33. The load-strain plots for each good gage channel for tests of C1, C2, and C3 are shown in Appendix B. As mentioned earlier, the positive- and negative-moment sections refer to the crown and springing line sections, respectively.

Strain Distributions

44. Strains were plotted with all gages in the two positive-moment sections lumped into one section (assuming symmetry of loading and model deformation). Likewise, for the negative-moment and the zero-moment sections (the 45-deg sections), the strains were plotted in one section. This gives a graphical view of the scatter in the data.

45. The strain distributions of the positive- and negative-moment sections were fitted with both a hyperbolic and a linear curve. The formulations for the curve fits are included in Appendix C. A least-squares criterion was used for the curve fit. Figures 34 and 35 are examples of the curve fits representing the strain distributions in the positive- and negative-moment sections, respectively, in C2 for the same time load step (or time increment). Figure 36 is a typical plot of the strain distribution at the 45-deg section (theoretically the zero-moment section).

46. In Table 7 the results from the curve fits are listed. The results in the column labelled r^2 are the values of the correlation coefficient squared. This value is a measure of the scatter in data from the assumed strain distribution (linear or hyperbolic). The two values solved by the curve fits are the location of the neutral axis, c , or the depth of the compressive zone and the maximum compressive strain, ε_u .

Resolving Moments and Thrusts from Data Fit

47. Moments and thrusts were computed for each strain distribution using the section designs in Figures 17 and 18 and the material properties in Table 4. These values were used as input to a computer program of the curved

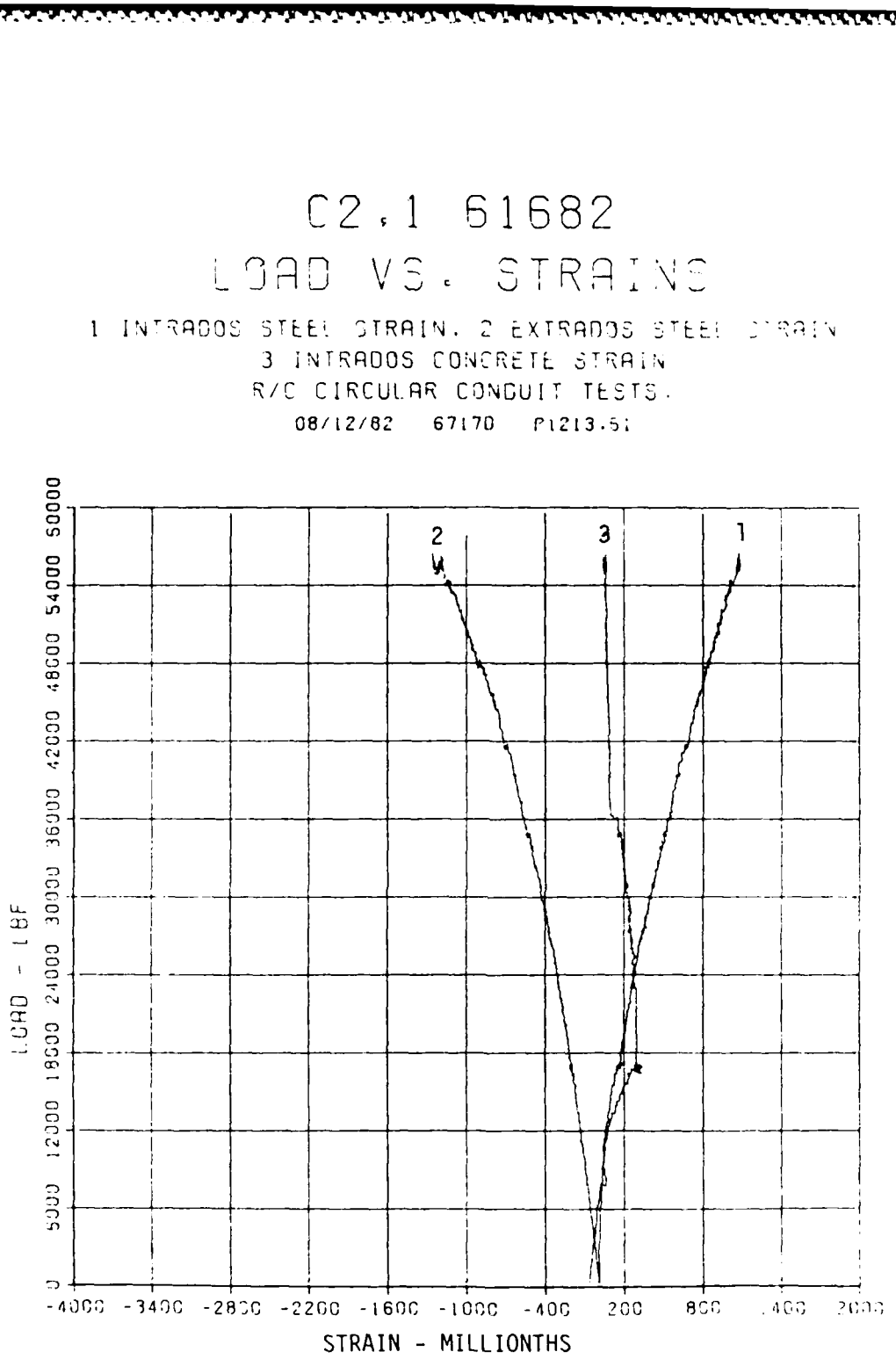

Figure 30. Average of load-strain plots: (1) gages 2 and 6; (2) gages 4 and 7; (3) gages 5 and 8

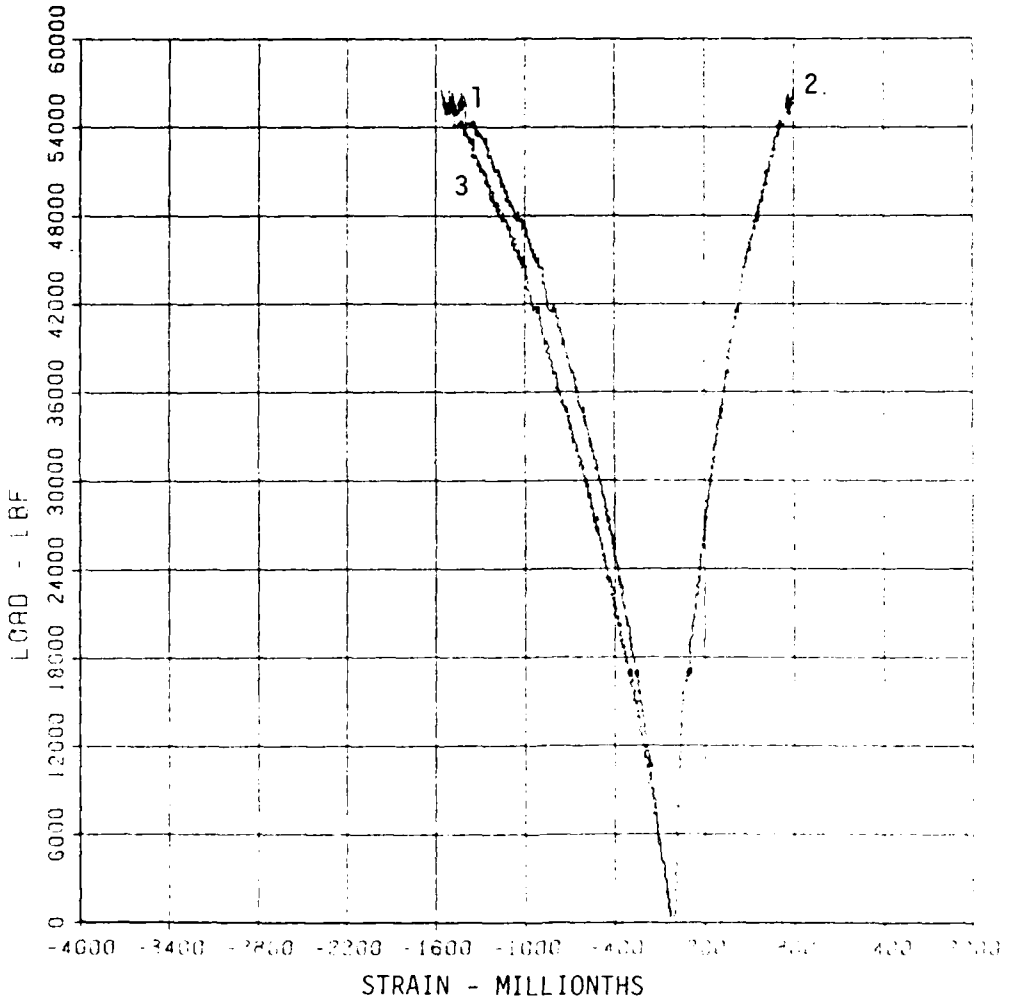

Figure 31. Average of load-strain plots: (1) gages 11, 12 and 15; (2) gages 9, 10, and 14; (3) gages 13 and 16

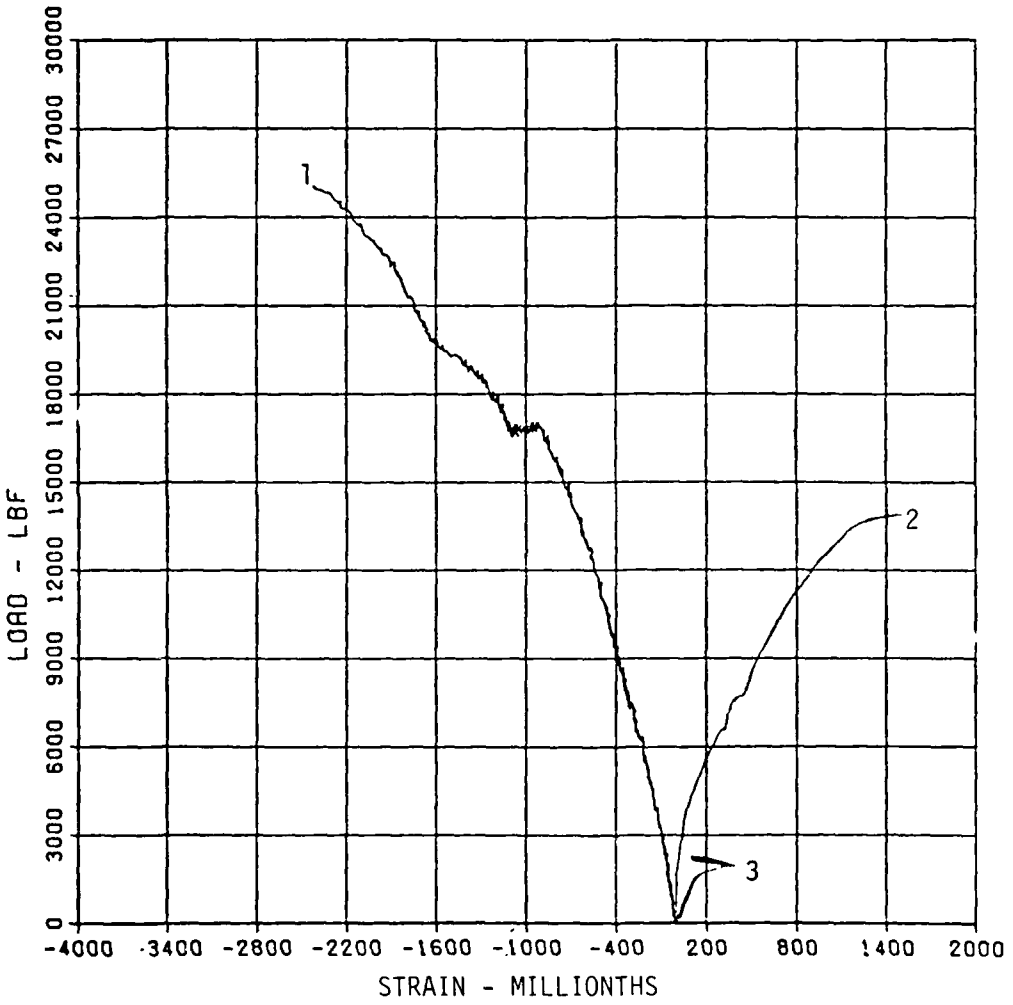

Figure 32. Average of load-strain plots: (1) gages 1, 2, and 6; (2) gages 3, 4, and 7; (3) gages 5 and 8

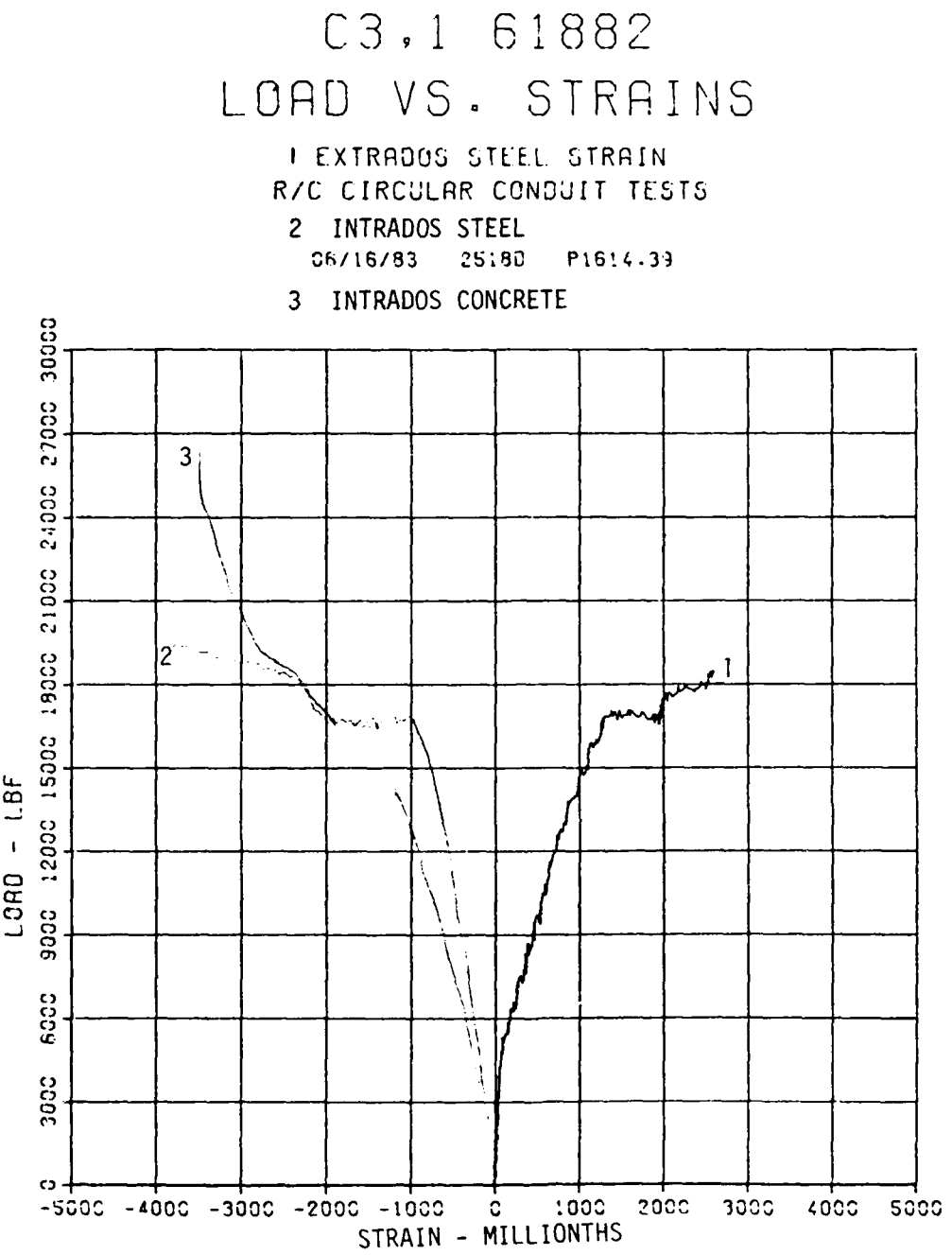

Figure 33. Average of load-strain plots:
(1) gages 9 and 10; (2) gages 11 and 12;
(3) gages 13 and 16

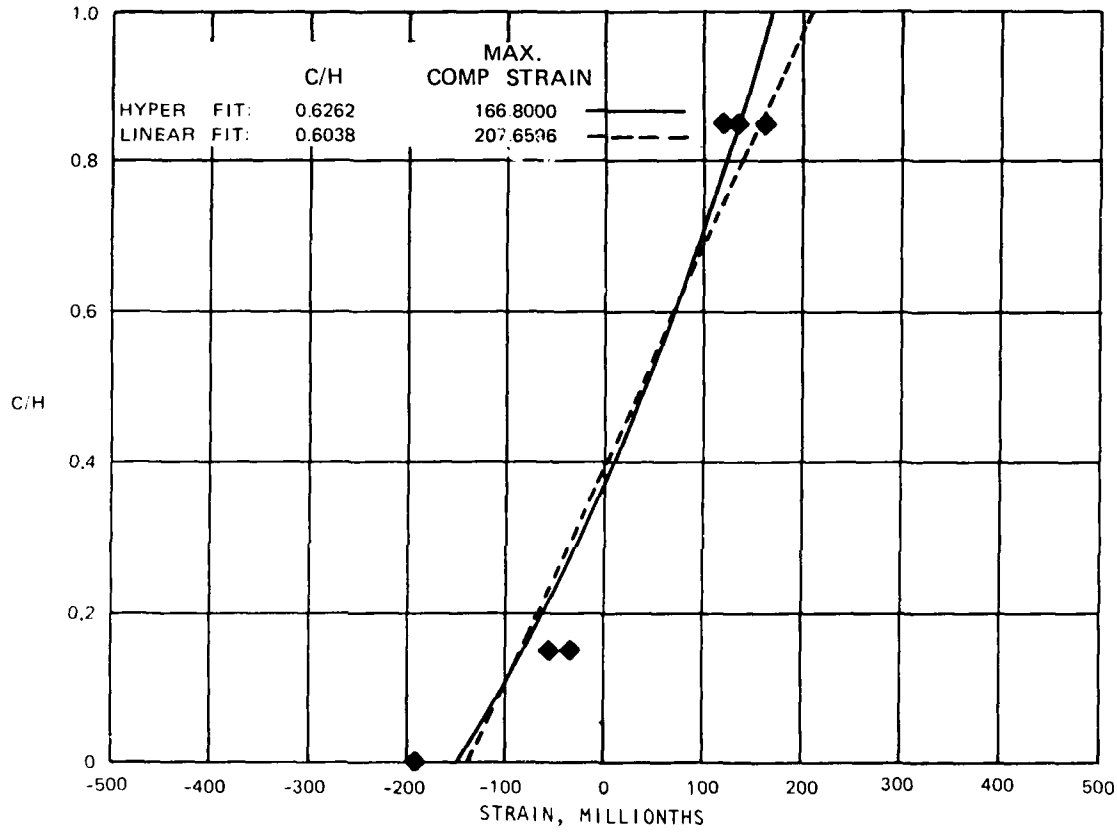

Figure 34. Strain distribution in positive-moment section, C2

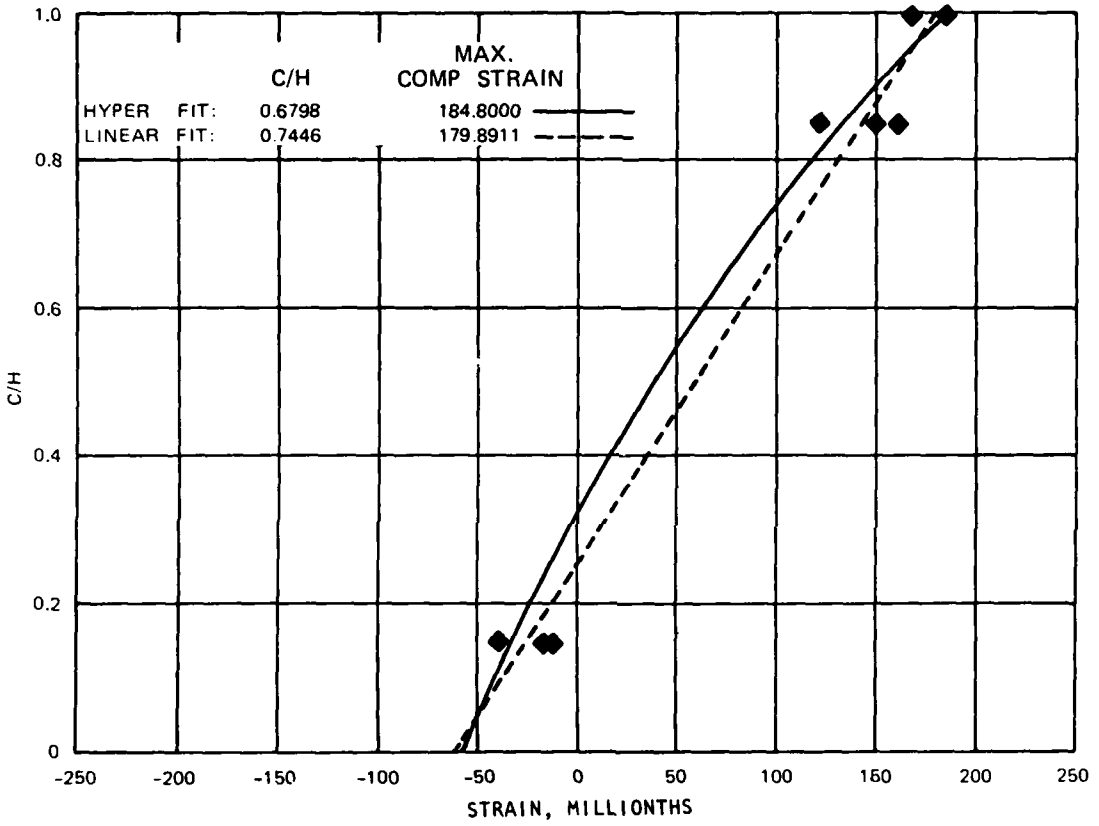

Figure 35. Strain distribution in negative-moment section, C2

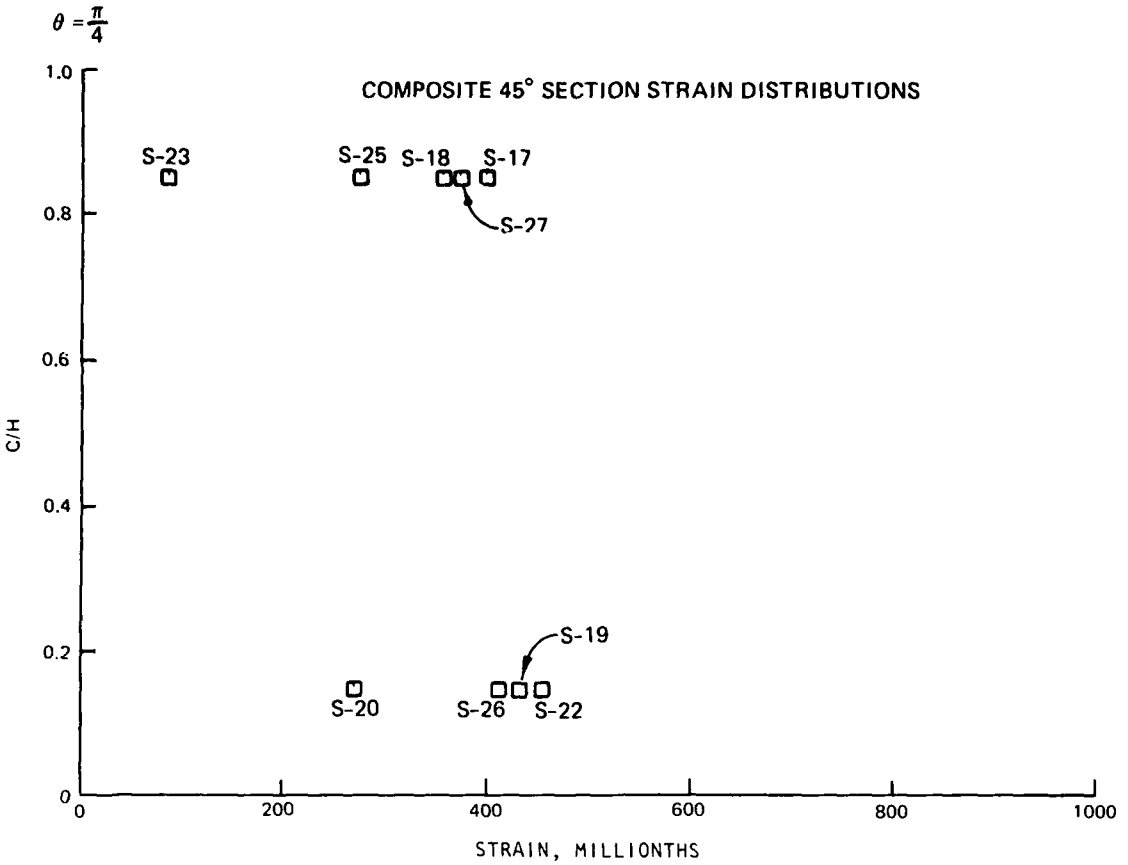

Figure 36. Typical strain distribution at 45-deg sections (zero-moment sections)

beam analysis. Moments and thrusts were computed from both the hyperbolic and linear strain distributions once the neutral axis location and the maximum compressive strain were known with the input of the material properties. For the curved beam analysis outlined in Part II, either strain distribution may be assumed to compute the moments and thrusts. In Table 8, all the moments and thrusts are listed for different load levels. For each load level, three comparisons for moments and thrusts are made among: (a) curved beam theory (application to RC curved beam), (b) straight beam theory, and (c) a 1-D linear elastic structural analysis.

48. Values from Table 8 are plotted on the interaction diagrams (plot of thrust and moment capacity of a section) shown in Figures 37 to 41. The five-point loading load path is the predicted 1-D elastic response due to five-point loads per quarter of the model. The load path marked by $p(\theta)$ is the predicted 1-D elastic response due to a continuous normal pressure. The

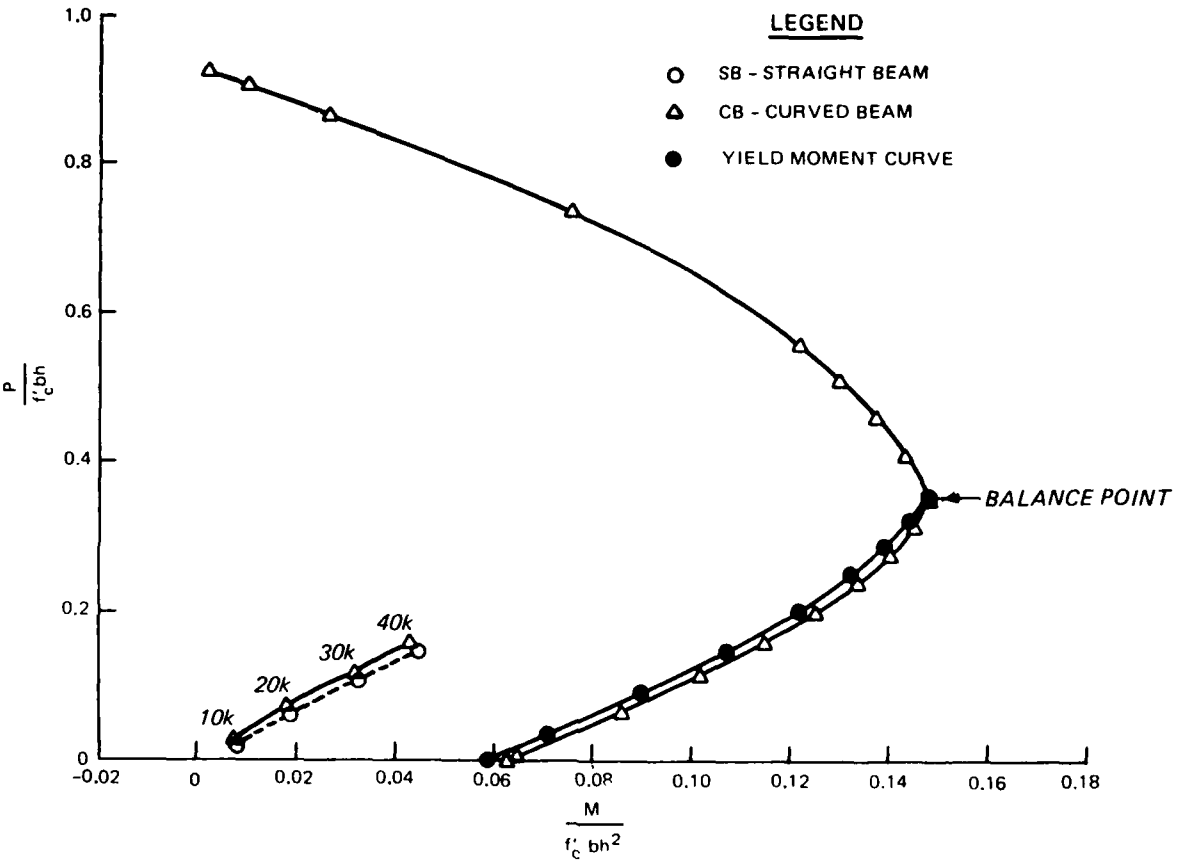

Figure 37. Resolved moments, thrusts, and load paths, specimen C1, positive-moment section

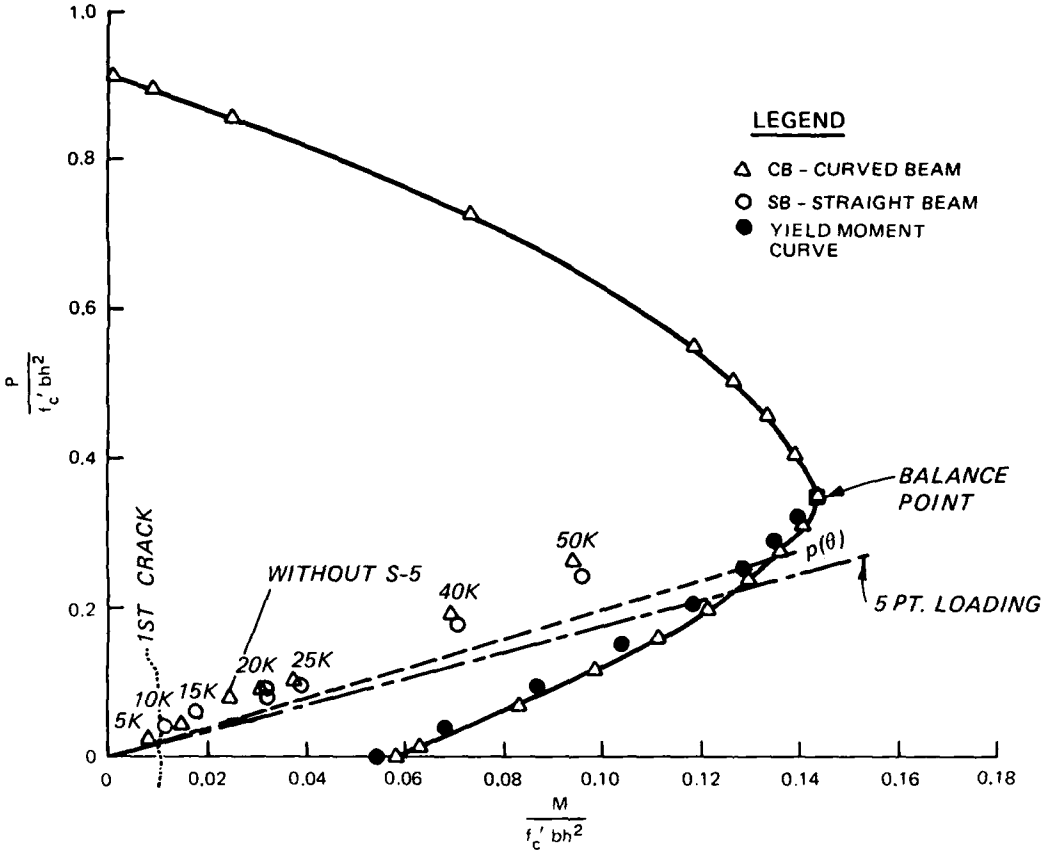

Figure 38. Resolved moments, thrusts, and load paths, specimen C2, positive-moment section

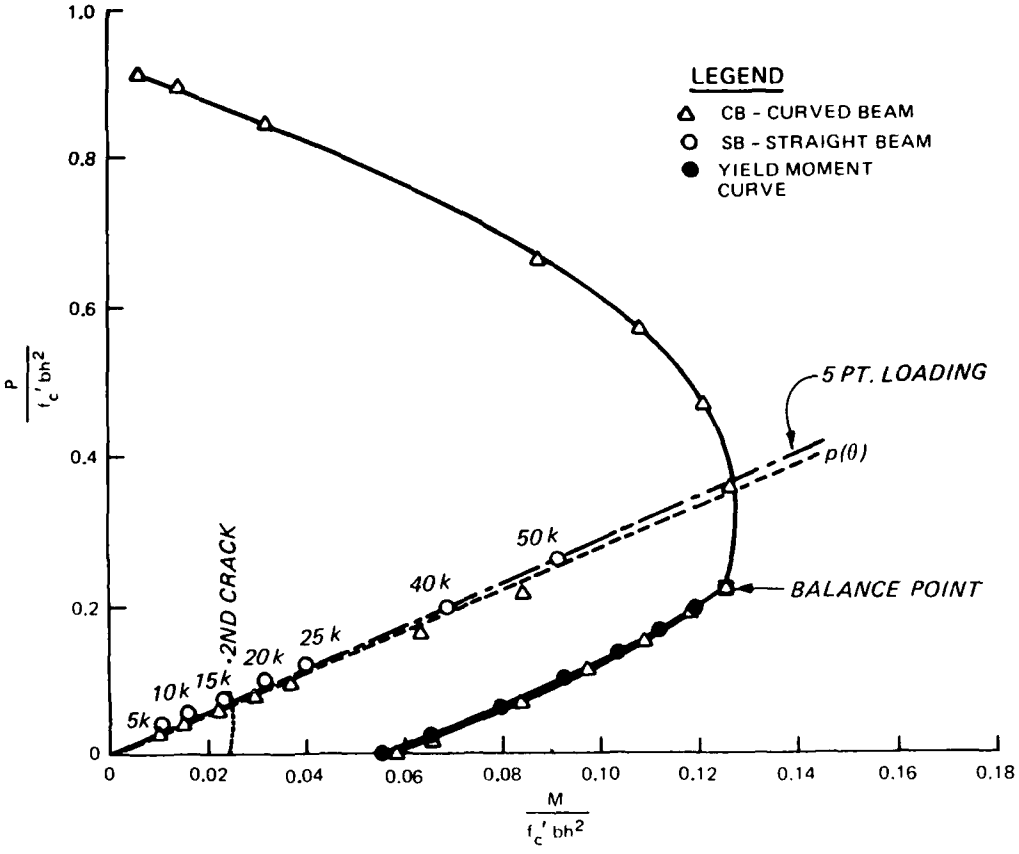

Figure 39. Resolved moments, thrusts, and load paths, specimen C2, negative-moment section

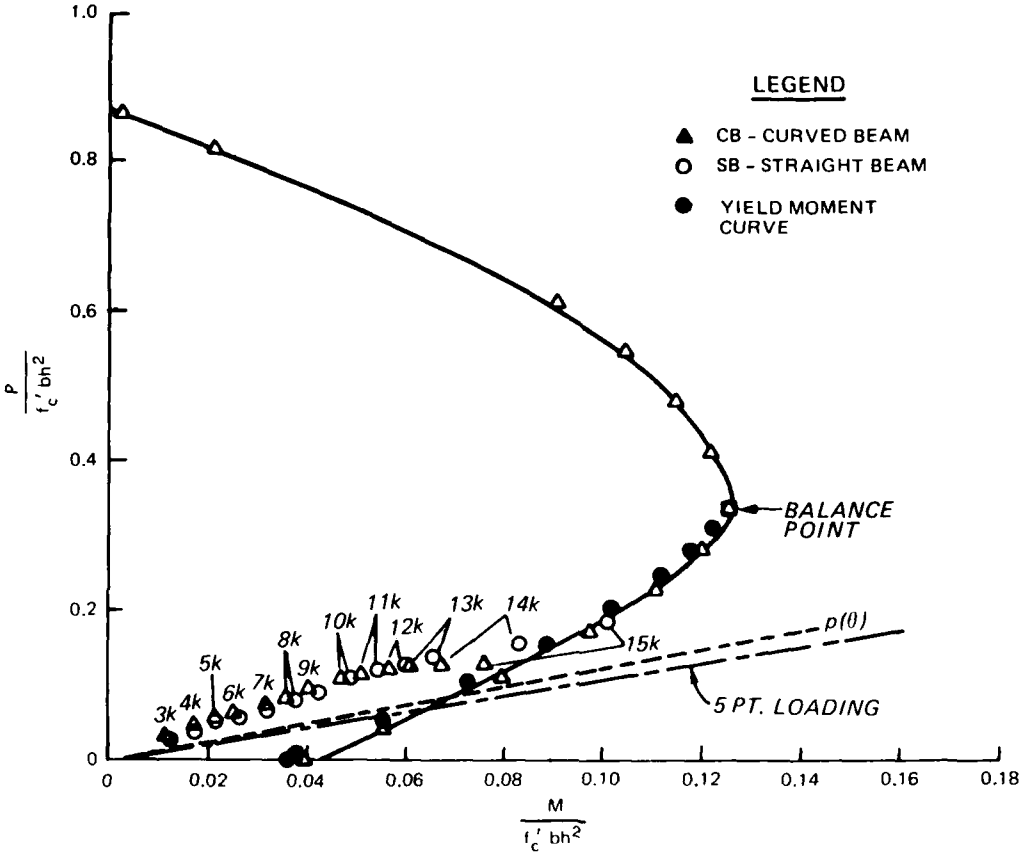

Figure 40. Resolved moments, thrusts, and load paths, specimen C3, positive-moment section

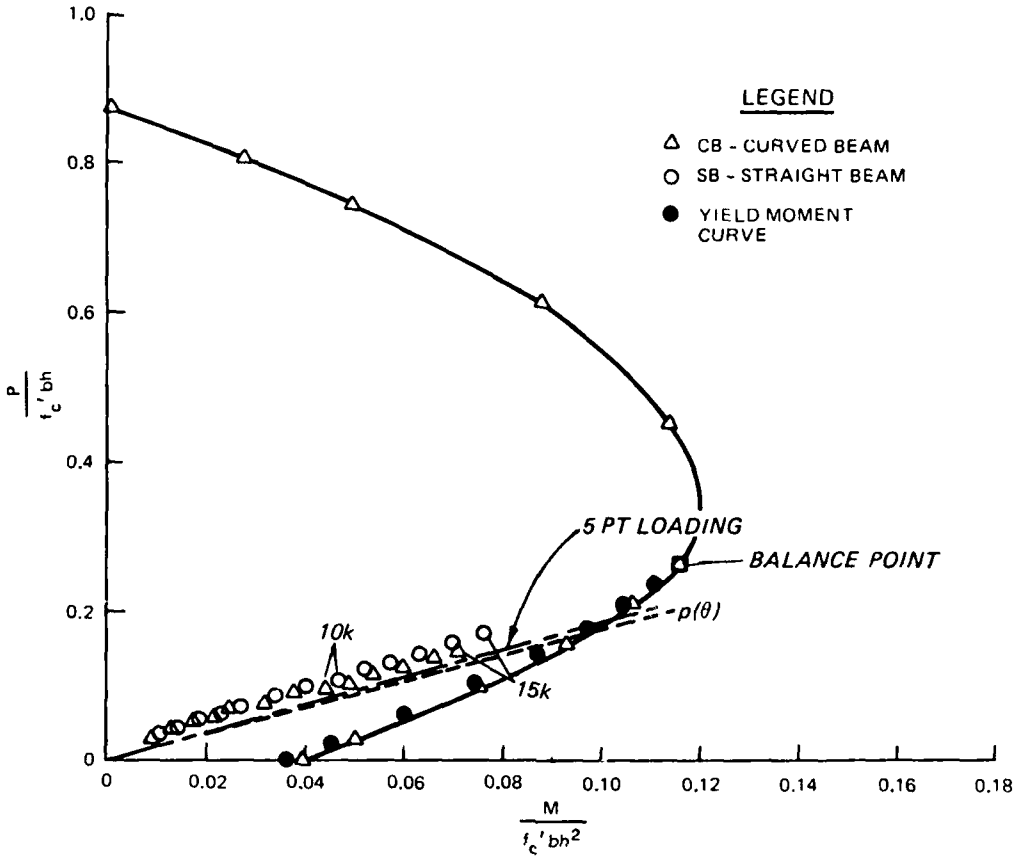

Figure 41. Resolved moments, thrusts, and load paths, specimen C3, negative-moment section

open circular and triangular symbols marked with numbers near the predicted load paths represent resolved moments and thrusts for a particular reference load level as computed by assuming a straight or curved beam response. The interaction diagrams have been computed assuming a curved beam response. In the interaction diagrams, the triangle symbols connected with solid lines represent the ultimate curve and the solid symbols represent the yield moment curve.

49. Data for the negative-moment section of C1 were recorded on another analog 32-track tape and were not complete because of a malfunction.

PART VI: DISCUSSION OF EXPERIMENTAL RESULTS

50. The first two specimens, C1 and C2, did not fail when tested to the full capacity of the loading apparatus. Specimen C3 failed in flexure initially and ultimately.

51. The first test on C1 indicated no visible signs of distress on the model. After the test, it was discovered that one of the hydraulic circuits had inadvertently been shut off; thus, all of the load that was believed to be on the specimen was not. The hydraulic circuit for jacks 8A and 8B was closed (see Figure 21). With the absence of the loads in 8A and 8B, there is a slight skewness to the load distribution. The pressure in this circuit is 90.24 percent of the maximum pressure in circuit 1 (jacks 1A and 1B). At the crown, the effect of the load in jacks 8A and 8B accounts for 8.5 percent of the total thrust and 37.1 percent of the total moment. To account for the absence of load in jacks 8A and 8B, the entire conduit response is analyzed and the results shown in Appendix A (Figure A2).

52. Specimen C2 was by design a replica of C1. The purpose of conducting two identical tests was to establish consistency. Retests on C1 (and C2) established consistency within a specimen. Because of the slight discrepancy between the initial load distributions of C1 and C2, the tests were not exactly the same. For the first test on C2, all pressure channels were checked to assure that all loads were acting on the model. Specimen C2 was not failed either when tested to full capacity of the loading system. After each retest (three on C1, one on C2) more cracks were visible.

53. Retests conducted on C1 and C2 evaluated the strength of each model through a cycle of loading. Even after a reloading of the models, no significant damage was observed.

54. Specimen C3 was the only model loaded to ultimate failure. The progression to failure was described in the test observations in Part IV. A flexure collapse mechanism formed such that "plastic hinges" developed at the crown, invert, and the two springing lines. No signs of shear failure were observed. Specimen C3 was the thinner model with $R/h = 4.0$.

55. In Table 7, all the results of the fits to the strain distributions are listed. The values of r^2 (the correlation coefficient squared) ranged from 0.749 to 0.989 for the hyperbolic fit and 0.666 to 0.985 for the linear fit. The value of r^2 implies what percentage of the scatter in the data can

be represented by the specific curve fit. The results in Table 7 show no significant difference between the hyperbolic and the linear fit. However, these results are based on data from three specimens, which is a limited statistical sample. Most of the strain gages were placed in two locations and some in three. More meaningful strain gradients should be obtained to better quantify the statistical comparison between the hyperbolic and linear fit. This could be accomplished by placing more circumferential strain gages across the section on future tests. Accordingly, more tests results will be needed to conclude whether the current straight beam analysis is appropriate for conduits with R/h as low as 2.5.

56. Table 8 and Figures 37 to 41 contain the results of the resolved moments and thrust for specimens C1, C2, and C3. In Figure 37, the moments and thrusts form a straight load path and are contained within the interaction diagram. In Table 8, the experimental values are compared to theoretical values (computed from the 1-D structural analysis). For specimen C1, differences in thrust range from 36 to 64 percent between the linear fit and the predicted value (theoretical). The differences in the moments ranged from 46 to 61 percent. The largest differences occurred at the lowest load levels. These results are for the internal forces resolved at the crown.

57. For specimen C2 at the crown, differences in the thrust values ranged from 0.51 to 26 percent, with the moment values differing from 30 to 40 percent. At the springing line, thrusts differed from 7.9 to 35 percent and moments differed from 24 to 61 percent. In Figure 38, the experimental values plot a consistently different load path than predicted. The moment and thrust at the last load level plots are within the interaction diagram and this is consistent with the observed experimental behavior. Specimen C2 did not fail as predicted by the five-point loading path (the predicted loading path is theoretically between the $p(\theta)$ and five-point loading paths). Even after the observed first crack the load path appears to be undisturbed. In Figure 39, the plotted experimental values of moment and thrust appear to agree closely, with the predicted values. Even though the experimental and theoretical load paths agree closely, there is a difference between the values at specific load levels. No signs of failure existed on specimen C2 at the springing line, which is consistent with plotted results.

58. For specimen C3, the only specimen tested to failure, the thrusts and moments at the crown differed from 12 to 35 percent and 23 to 57 percent,

respectively. At the springing line, the thrusts differed from 14 to 24 percent and the moments differed from 33 to 54 percent. In Figure 40, the experimental and theoretical load paths at the crown are plotted. Again the difference between the two load paths is observed. The structure yielded at about 14.5 kips (maximum load in jack 1A) as seen in the load-strain plots in Appendix B (strain gages 3 and 4) and as shown by the intersection of the experimental load path with the yield line of the interaction diagram. The predicted ultimate and yield moments are very close, as shown in Figures 40 and 41. However, a closer look at the load-strain plots on pages B55 and B56 (of Appendix B) reveal that the ultimate load resistance occurred at approximately the 32,500-lb reference load level. This is about twice the first yield load level. Reference to the load-strain plots of the tension steel at the crown (pages B45, B46, B49, and B57) indicates that the first yield occurs at about the 15,000-lb reference load level. Second yield occurs at the springing line (pages B51, B52, and B59). The plots on pages B55 and B56 are the load-strain results of the concrete compressive strains at the intrados of the springing line. The second and third plastic hinges formed to complete a three-pinned arch structure before final collapse due to the fourth hinge.

59. In Figure 41 it is shown that the capacity of the springing line section was not exceeded at 15 kips. This was observed. The analytical and experimental load paths at the springing line section agree very closely, but the values at specific load levels differ as discussed previously.

60. Three consistent observations among the tests are: (a) the discrepancy between analytical and experimental load paths at the crown, (b) agreement between analytical and experimental load paths at the springing lines, and (c) comparison of observed cracking failures with predicted location of cracking.

61. Three effects will be discussed that can account for the observed differences between predicted and experimentally computed internal forces at the crown and the springing line sections. First, the tensile capacity of the concrete has been ignored. Looking at Figures 42 and 43 (reprints of Figures 34 and 35, the strain distributions at 10 kips) the maximum thrust and moment due to tension carried by concrete are computed using the linear fit for convenience. The moments are seen to be affected more than the thrusts. However, in this test, 10 kips is a low load level and the effect of the tensile capacity of the concrete would be expected to be less for the higher load

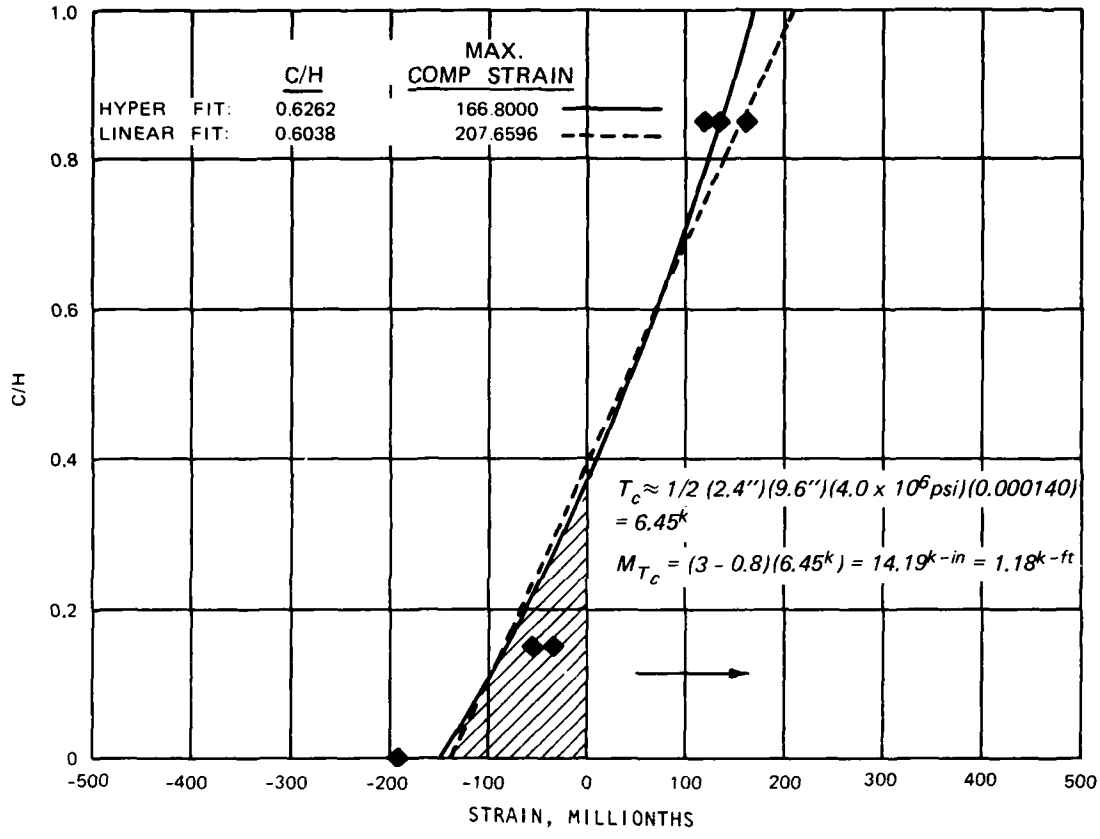

Figure 42. Strain distribution in positive-moment section, C2; computing resisting concrete tensile force

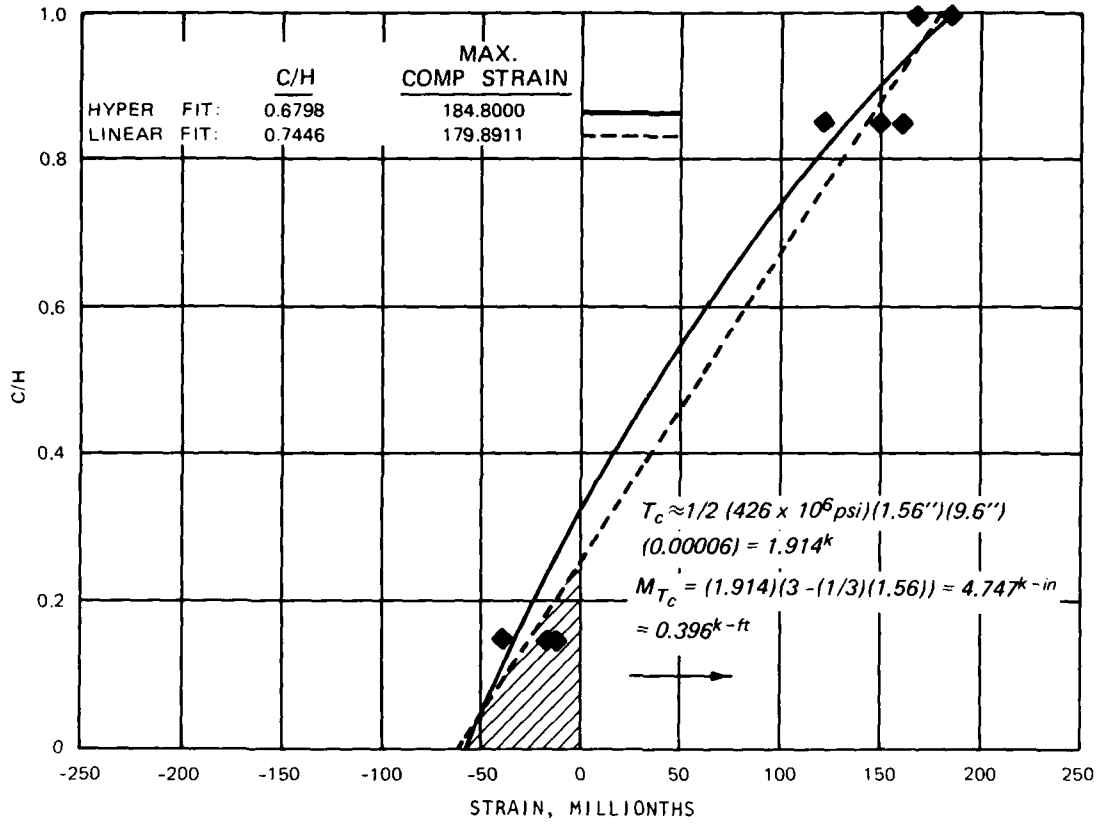

Figure 43. Strain distribution in negative-moment section, C2; computing resisting concrete tensile force

levels. (See Appendix C for the other strain distributions.) From the two tensile split tests (Table 4) the average strength was 410 psi. Using 4.26 $\times$ 10^6 psi as the average E_c, the average value for the cracking strain is approximately $410/(4.26 \times 10^6) = 0.000096$ in./in. or about 100 μin./in.

62. Another effect not accounted for in predicting capacity and resolving internal forces from the data is the biaxial response of concrete. This would increase the values of the interaction diagram for predicting capacity and the values of the resolved moments and thrusts from tests. The biaxial effect needs to be quantified. Uniaxial behavior is assumed, but there is actually a significant compressive confinement pressure present on the extrados of the entire conduit. An excerpt from Park and Paulay (1975) contained in Figure 44 explains this phenomenon.

63. Also, the plastic behavior of the conduit is not accounted for in the structural analysis. The nonlinear load path in Figure 40 suggests that there is nonlinear behavior above 10 kips. The plastic response is also seen

"A biaxial stress condition occurs if the principal stresses act only in two directions; that is, the stresses act in one plane and the third principal stress is zero...[Figure 42] presents the combination of direct stress in two directions which caused failure of concrete subjected to biaxial compression may be as much as 27 percent higher than the uniaxial strength. For equal biaxial compressive stresses, the strength increase is approximately 16 percent. The strength under biaxial tension is approximately equal to the uniaxial tensile strength. Note, however, that combined tension and compression loadings reduce both the tensile and the compressive stresses at failure" (from Park and Paulay (1975)).

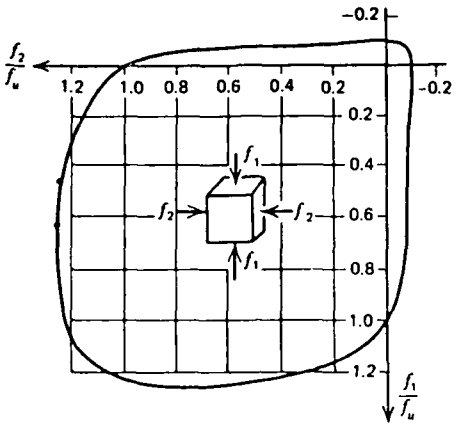

Figure 44. Biaxial strength of concrete, f_u = uniaxial strength (Park and Paulay 1975)

when the load-strain plots are compared betweeen the initial and the reloading test of C2 in Figures 45-48. In all the initial load-strain plots, a nonlinear response is observed. In all the load-strain plots of the corresponding reloaded channels, it appears that the structure is behaving linearly elastic. The structure was not reloaded past the maximum load of the initial test. According to the theory of plasticity, after an initial loading of a structure (or material) past yield, the structure will behave in an elastic manner until loaded past yield again (Anderson, Haelsig, and Reifel 1966).

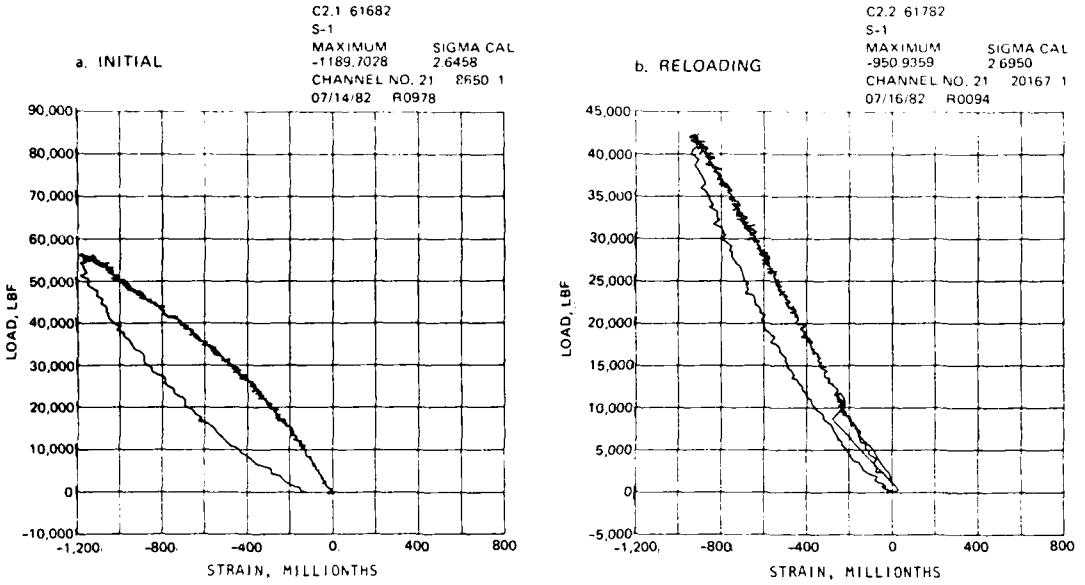

Figure 45. Comparison of load-strain plots, initial test and reloading

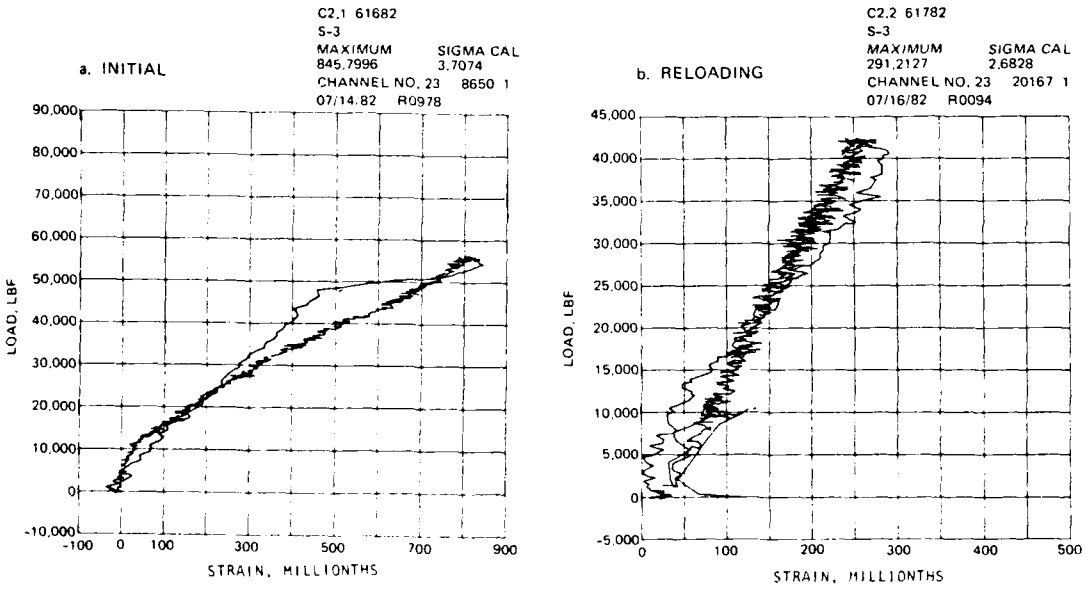

Figure 46. Comparison of load-strain plots, initial test and reloading

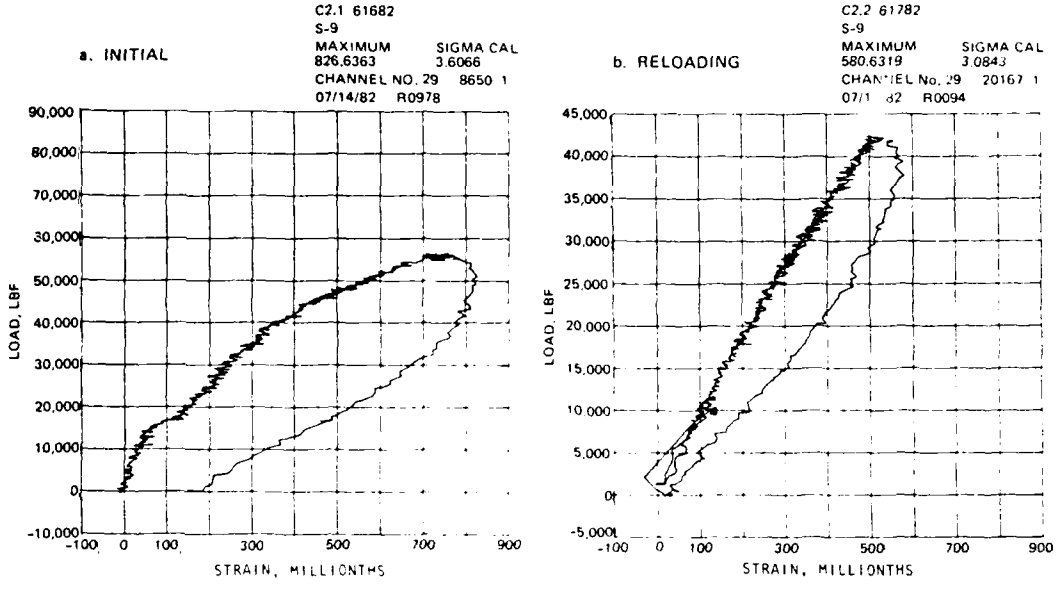

Figure 47. Comparison of load-strain plots, initial test and reloading

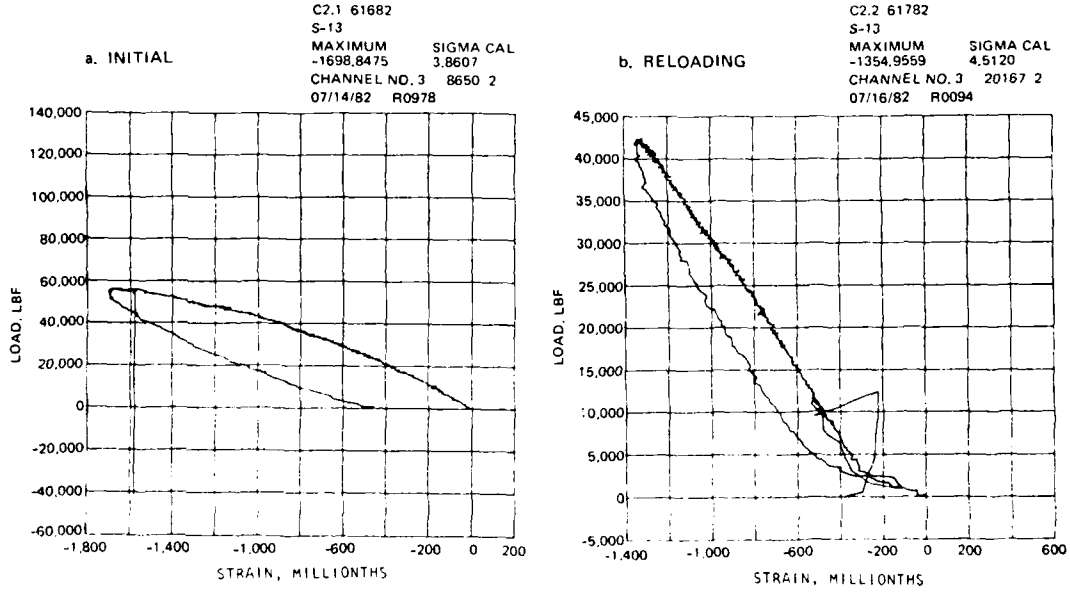

Figure 48. Comparison of load-strain plots, initial test and reloading

PART VII: FUTURE WORK

64. In FY 83, model RC circular conduits were planned for testing to ultimate failure. The results of these tests will provide qualitative information about failure modes and will be the subject of a future report.

65. Finite element studies will also continue, using both linear and nonlinear models. The effect of the biaxial response of concrete will also be studied.

66. The problem of shear capacity of the RC conduits will be addressed. New criteria will be evaluated and revised if necessary.

PART VIII: CONCLUSIONS

67. Initial curvatures of Corps curvilinear conduits do affect their flexural-axial resistance, but when compared to straight beam behavior, the effect of the initial curvature is apparently not significant. It has also been shown from curve fits to experimental strain data that there is statistically no difference between hyperbolic and linear strain distributions in circular conduits. More tests will be needed to obtain a better statistical sample and investigate even more extreme curvatures than studied in this report. From future tests it will be determined whether the normal design practice for computing the moment-thrust resistance of uncurved members provides an appropriate safety margin for Corps cross sections. The shear resistance of these Corps structures was not considered herein; therefore, it is the subject of a further investigation.

68. A nonlinear finite element model for concrete was shown applicable. Also a 1-D structural analysis and 2-D Airy stress solutions compared favorably for evaluating the response of the elastic behavior of RC conduits under static pressure loading. Three RC conduit specimens were loaded and these tests established a standard testing procedure. Of the three specimens only one failed ultimately. Cracking occurred during tests on specimens C1 and C2. The third specimen formed a flexural collapse mechanism as was predicted. The resultant moments and thrusts from the data differ from the internal forces predicted from the linear elastic 1-D structural analysis. Three reasons cited for these differences are:

a. The tensile capacity of concrete was neglected (this affects results at the smaller load levels).

b. Biaxial response of concrete was not accounted for in the constitutive model.

c. Plastic behavior of the structure was not accounted for in the structure analysis.

Items b and c are the two most important effects to be studied for future analysis.

REFERENCES

American Concrete Institute. 1970. "Models for Concrete Structures," ACI Publication No. 24, Detroit, Mich.

_____. 1983. "Building Code Requirements for Reinforced Concrete," ACI 318-83, Detroit, Mich.

Anderson, R. H., Haelsig, R. T., and Reifel, M. D. 1966 (Mar). "Structural Behavior of Ring Sections Under Nonuniform External Pressure," AFWL-TR-65-145, Air Force Weapons Laboratory, Kirtland Air Force Base, N. Mex.

Chen, A. C. T., and Chen, W. F. 1975 (Aug). "Constitutive Relations for Concrete," Journal, Engineering Mechanics Division, American Society of Civil Engineers, Vol 101, No. EM4, p 465.

Harter, M. M., Bircher, B. E., and Wilson, H. B. 1980 (Feb). "User's Guide: Computer Program for Design/Review of Curvilinear Conduits/Culverts (CURCON)," Instruction Report K-80-1, US Army Engineer Waterways Experiment Station, Vicksburg, Miss.

Headquarters, Department of the Army. 1969. "Design of Miscellaneous Structures, Conduits, Culverts, and Pipes," Engineer Manual 1110-2-2902, Washington, DC.

Hognestad, E., Hanson, N. W., and McHenry, D. 1955 (Dec). "Concrete Stress Distributions in Ultimate Strength Design," Journal, American Concrete Institute, Title No. 52-28, Vol 27, No. 4, pp 455-479.

Karr, P H., Hanson, N. W., and Papell, H T. 1977. "Stress-Strain Characteristics of High-Strength Concrete," RD051.01D, preprinted with permission from Douglas McHenry International Symposium on Concrete and Concrete Structures, American Concrete Institute, Detroit, Mich., Portland Cement Association.

Karr, P. H., Fiorato, A. E., Carpenter, J. E., and Corley, W. G. 1978. "Limiting Strains of Concrete Confined by Rectangular Hoops," RD053.01D, Portland Cement Association.

Liu, T. C. 1980. "Strength Design of Reinforced Concrete Hydraulic Structures; Report 1, Preliminary Strength Design Criteria," Technical Report SL-80-4, US Army Engineer Waterways Experiment Station, Vicksburg, Miss.

Mattock, A. H., Kriz, L. B., and Hognestad, E. 1961 (Feb). "Rectangular Concrete Stress Distribution in Ultimate Strength Design," Journal, American Concrete Institute, pp 875-928.

Miller, I., and Freund, J. E. 1977. Probability and Statistics for Engineers, 2d ed., Printice-Hall, Englewood Cliffs, N. J.

Mlakar, P. F., Walker, R. E., and Sullivan, B. R. 1981 (Sep). "Acoustic Emission from Concrete Specimens," Miscellaneous Paper SL-81-26, US Army Engineer Waterways Experiment Station, Vicksburg, Miss.

Park, R., and Paulay, T. 1975. Reinforced Concrete Structures, John Wiley, New York.

Pfrang, E. O., Siess, C. P., and Sozen, M. A. 1964 (Jul). "Load-Moment-Curvature Characteristics of Reinforced Concrete Cross Sections," Journal, American Concrete Institute, Title No. 61-44, Vol 61, No. 7, pp 763-777.

Timoshenko, S. 1941 (Aug). Strength of Materials; Part II, Advanced Theory and Problems, 2d ed., Chapter II, D. Van Nostrand, New York.

Timoshenko, S., and Goodier, J. N. 1951. Theory of Elasticity, McGraw-Hill, New York.

US Army Engineer District, Fort Worth. 1978 (Mar). "Plans for Initial Embankment, Partial Spillway Excavation and Outlet Works, Aquilla Lake, Aquilla Creek, Texas," Invitation No. DACW63-78-B-0042, Sequence No. 51, Fort Worth, Tex.

BIBLIOGRAPHY

Bathe, K. J., Wilson, E. L., and Peterson, F. E. 1973 (Jun). "SAP IV: A Structural Analysis Program for Static and Dynamic Response of Linear Systems," Report No. EERC 73-11 (Revised Apr 1974), University of California, Richmond, Calif.

Chen, W. F. 1982. Plasticity in Reinforced Concrete, McGraw-Hill, New York.

Edison, J. S., Inc. "Operation and Service Manual with Illustrated Parts Lists, Challenger Models 10fc and 10M, Multiple Pressure Hydraulic Load Maintainers and Cycling Units," Burbank, Calif.

Gupshup, V. N., and Shah, I. K. 1963 (Mar). "Static and Dynamic Behavior of Reinforced Concrete Circular Arches (Part 1)," Massachusetts Institute of Technology, Cambridge, Mass.

Ruzicka, G. C., Gamble, W. L., and Mohraz, B. 1976 (May). "Strength and Behavior of Thick Walled Reinforced Concrete Conduits," prepared by the University of Illinois at Urbana-Champaign, for the US Army Corps of Engineers, Washington, DC.

Winter, G., and Nilson, A. H. 1972. Design of Concrete Structures, 8th ed., McGraw-Hill, New York.

Table 1

Characteristics of Corps Curvilinear Conduits

Structure	Shape	f'_c ksi	ρ_g %	ρ'_g %	f_y ksi	$\frac{R}{h}$	$\frac{d}{h}$	$\frac{d'}{h}$	$\frac{e}{h}$
Liu (1980) Examples 1,2	Circular	4	0.72	0.36	40	3.0	0.875	0.125	0.417
Liu (1980) Examples 3,4	Oblong	4	0.72	0.36	40	3.0	0.875	0.125	0.289
Liu (1980) Example 5	Horseshoe	4	0.24	0	40	3.4	0.786	--	0.239
Mattock, Kriz, and Hognestad (1961)	Circular	4	0.95	0.36	40	3.8	0.75	0.25	--
Mattock, Kriz, and Hognestad (1961)	Circular	4	0.82	0.27	40	3.0	0.81	0.19	--
Hognestad, Hanson, and McHenry (1955)	Circular	4	0.44	0.22	40	2.5	0.88	0.10	--

Note: f'_c = design 28-day uniaxial compressive concrete strength; f_y = design yield strength of steel; ρ_g = total A_s/bh , gross steel ratio; $\rho'_g = A'_s/bh$, gross compression steel ratio; h = depth of section; R = radius to middepth of section; e = eccentricity = M/P (moment/thrust); d = effective depth of tension steel; d' = depth to compression steel.

Table 2

Testing Scheme

		All Tests - 3:1 Loading				
Test No.	$\frac{R}{h}$	f'_c ksi	f_y ksi	ρ_g %	ρ'_g %	Shape
1	2.5	4	60	0.938	0.469	Circular
2	2.5	4	60	0.938	0.469	Circular
3	4.0	4	60	0.938	0.469	Circular

Table 3

Experimental Equipment

Hydraulic System	
Hydraulic cylinder jacks	Double Acting Hydroline Series Hydroline Cylinders Model: N2R, Serial Suffix: 01R, Bore--5 in., Stroke--6 in. Rated for 58.9 kips at 3,000 psi
Hydraulic power supply	Built by Activation, Inc., Model #1-1671-1 Serial No. 80-1751 rated for 3,000 psi
Hydraulic controller (pressure regulator)	Hydraulic Load Maintainer Challenger Model 10M Serial No. 5M1142 rated for 5,000 psi
Instrumentation	
Load cells	Interface Model: 1220 AR50K, Precision Universal Load Cells, 50 kips
Strain gages	Micro Measurements
Deflection gages	Linear Variable Differential Transformer (LVDT)
2 tape recorders	32-track Sabre IV

Table 4

Strengths of Uniaxial Compressive Concrete, Split Cylinder Concrete, and Steel

Date Tested	Days		f'_c psi	Initial Elastic Concrete Modulus, E_c, 10^6 psi	Poisson's Ratio
			Compressive Strengths		
5/7/82	28		4,050	4.21	0.180
			4,000	4.44	0.193
			3,900	4.07	0.180
		Avg	3,983		
C1, 5/28/82	49		4,140	4.40	0.150
			4,160	4.50	0.16
			4,190	4.50	0.17
		Avg	4,163		
C2, 6/16/82	68		4,700	4.10	0.14
			4,530	4.0	0.14
		Avg	4,615		
C3, 6/18/82	70		4,350	4.0	0.18
			4,600	4.4	0.15
		Avg	4,475	4.26	0.164

Split Cylinder Strengths

		f'_{sp}, psi
6/17/82	69	350
6/18/82	70	470

Steel Reinforcement Properties (ksi) (from tensile tests):

		Yield	Ultimate	Rupture
#3's		70.2	100.5	96.4
		72.3	101.1	100.0
		69.7	101.1	95.5
	Avg	70.7		
#2's		65.0	96.6	80.0
		67.4	94.8	88.8
		68.4	94.2	88.8
	Avg	66.9		

Table 5

Load Verification Results

Load Position	(A) Reference at 20,000 lb	(B) Reference at 30,000 lb	Ratios of Recorded Loads to Reference Actual Column A ÷ 20,000	Actual Column B ÷ 30,000	Predicted* 1-A
1-A	20,000	30,000	1.00	1.00	1.00
2-A	18,250	27,500	0.9125	0.9167	0.9024
2-B	18,000	27,250	0.9000	0.9083	
3-A	13,000	20,000	0.6500	0.6667	0.667
3-B	13,500	20,000	0.6750	0.6667	
4-A	8,400	12,800	0.4200	0.4267	0.431
4-B	8,600	13,600	0.4300	0.4533	
5-A	7,000	10,400	0.3500	0.3467	0.333
5-B	7,200	10,200	0.3600	0.3400	
6-A	8,800	13,000	0.4400	0.4333	0.431
6-B	8,800	12.800	0.4400	0.4267	
7-A	14,000	20,500	0.7000	0.6833	0.667
7-B	14,000	20,000	0.7000	0.6667	
8-A	17,500	26,250	0.8750	0.8750	0.9024
8-B	18,250	27,500	0.9125	0.9167	

* These ratios represent the predicted load distribution to model the normal load component of the EM 3:1 design load condition.

Table 6

Load Equilibrium Checks

Test	Max Load lb	Maximum Differences, %, Force Components X	Y
C2	5,000	1.94	1.19
	10,000	3.39	1.37
	15,000	4.56	0.09
	20,000	2.58	0.15
	25,000	0.82	0.26
	40,000	0.36	0.92
	50,000	0.68	0.78
	Average: $\bar{X}$ = 2.05% ± 1.56%, $\bar{Y}$ = 0.68% ± 0.518%		
C3	3,000	3.98	1.55
	4,000	2.04	0.51
	5,000	0.75	1.13
	6,000	1.37	0.64
	7,000	1.05	1.03
	8,000	4.07	1.50
	9,000	0.99	1.16
	10,000	2.16	1.39
	Average: $\bar{X}$ = 2.05% ± 1.31%, $\bar{Y}$ = 1.11% ± 0.381%		

Table 7

Strain Distributions Fitted to Hyperbolic and Linear Curves

Hyperbolic Fit				Load	r^2		Linear Fit	
c , in.	c , ft	c/h	ε_u	Level	Hyperbolic	Linear	C , ft	ε_u
				Model C1 Crown				
3.181	0.2651	0.5302	0.0000858	10,000	0.966	0.965	0.4755	0.00009641
4.026	0.3355	0.6710	0.0002053	20,000	0.989	0.988	0.6275	0.0002214
4.245	0.3537	0.7074	0.0003557	30,000	0.955	0.953	0.6570	0.0003883
4.227	0.3522	0.7044	0.0005014	40,000	0.950	0.947	0.6520	0.0005491
				Model C2 Crown				
3.890	0.3242	0.6484	0.0000888	5,000	0.888	0.850	0.3137	0.0001181
3.757	0.3131	0.6262	0.0001668	10,000	0.931	0.907	0.3019	0.0002076
2.938	0.2448	0.4896	0.0002246	15,000	0.813	0.761	0.2616	0.0003945
3.594	0.2995	0.5990	0.0003543	20,000	0.981	0.981	0.2755	0.0003905
3.394	0.2828	0.5656	0.0004294	25,000	0.958	0.956	0.2581	0.0004876
3.408	0.2840	0.5680	0.0008805	40,000	0.980	0.980	0.2595	0.0009775
3.417	0.2848	0.5696	0.0012994	50,000	0.972	0.971	0.2602	0.0014544
				Model C2 Springing Line				
4.652	0.3877	0.7754	0.0001191	5,000	0.978	0.976	0.3973	0.0001159
4.079	0.3399	0.6798	0.0001848	10,000	0.970	0.980	0.3723	0.0001799
3.812	0.3177	0.6354	0.0002780	15,000	0.983	0.983	0.3416	0.0002693
3.529	0.2941	0.5882	0.0003816	20,000	0.967	0.971	0.3232	0.0003729
3.305	0.2754	0.5508	0.0004975	25,000	0.963	0.972	0.3100	0.0004883
3.132	0.2610	0.5220	0.0009402	40,000	0.964	0.974	0.2965	0.0009233
3.071	0.2559	0.5118	0.0013664	50,000	0.976	0.983	0.2912	0.0013310

(Continued)

Table 7 (Concluded)

Hyperbolic Fit				Load	r^2		Linear Fit	
c , in.	c , ft	c/h	ε_u	Level	Hyperbolic	Linear	C , ft	ε_u
				Model C3 Crown				
2.479	0.2066	0.6199	0.0001233	3,000	0.972	0.967	0.1976	0.0001373
2.371	0.1976	0.5929	0.0001910	4,000	0.970	0.970	0.1853	0.0002077
2.127	0.1773	0.5320	0.0002534	5,000	0.959	0.957	0.1670	0.0002800
2.008	0.1673	0.5020	0.0003079	6,000	0.959	0.957	0.1575	0.0003425
1.933	0.1611	0.4833	0.0003936	7,000	0.962	0.961	0.1516	0.0004381
1.859	0.1549	0.4647	0.0004693	8,000	0.961	0.959	0.1458	0.0005255
1.839	0.1533	0.4599	0.0005417	9,000	0.959	0.957	0.1442	0.0006089
1.835	0.1529	0.4587	0.0006325	10,000	0.954	0.952	0.1440	0.0007156
1.818	0.1515	0.4545	0.0007112	11,000	0.941	0.937	0.1431	0.0008187
1.785	0.1487	0.4461	0.0007987	12,000	0.941	0.938	0.1406	0.0009211
1.728	0.1440	0.4320	0.0008904	13,000	0.929	0.924	0.1366	0.0010480
1.578	0.1315	0.3945	0.0010542	14,000	0.841	0.810	0.1295	0.0014373
1.504	0.1253	0.3759	0.0012026	15,000	0.749	0.666	0.1292	0.0019338
				Model C3 Springing Line				
2.608	0.2173	0.6520	0.0001194	3,000	0.882	0.870	0.2182	0.0001246
2.549	0.2124	0.6373	0.0001717	4,000	0.926	0.916	0.2070	0.0001746
2.391	0.1993	0.5980	0.0002235	5,000	0.912	0.902	0.2014	0.0002300
1.992	0.1660	0.4980	0.0003080	6,000	0.946	0.941	0.1741	0.0003108
1.835	0.1529	0.4587	0.0003724	7,000	0.970	0.968	0.1642	0.0003703
1.757	0.1464	0.4392	0.0004825	8,000	0.969	0.965	0.1568	0.0004787
1.749	0.1458	0.4374	0.0005715	9,000	0.968	0.966	0.1567	0.0005679
1.703	0.1419	0.4257	0.0006729	10,000	0.976	0.974	0.1536	0.0006656
1.685	0.1404	0.4212	0.0007680	11,000	0.978	0.977	0.1526	0.0007592
1.667	0.1389	0.4167	0.0008586	12,000	0.981	0.980	0.1515	0.0008477
1.652	0.1377	0.4131	0.0009669	13,000	0.981	0.981	0.1507	0.0009559
1.619	0.1349	0.4047	0.0011053	14,000	0.983	0.983	0.1486	0.0010935
1.616	0.1347	0.4041	0.0012234	15,000	0.984	0.985	0.1483	0.0012088

Table 8

Moments and Thrusts

Load Level lb	Positive Moment Section: Moment (kip-foot) Specimen Hyperbolic Fit	Linear Fit	Predicted		Thrust (kips) Hyperbolic Fit	Linear Fit	Predicted	Negative Moment Section: Moment (kip-foot) Hyperbolic Fit	Linear Fit	Predicted	Thrust (kips) Hyperbolic Fit	Linear Fit	Predicted
				C1									
10,000	0.948	0.967	2.484	R = 15 in.	4.744	4.458	12.63						
20,000	2.253	2.281	4.968		15.24	14.19	25.25						
30,000	3.773	3.891	7.452		27.47	25.51	37.88						
40,000	5.170	5.339	9.936		37.54	34.79	50.50						
				C2									
5,000	1.374	1.336	1.975	R = 15 in.	7.006	8.366	6.90	1.261	1.298	1.706	9.531	10.63	9.850
10,000	1.987	2.302	3.950		12.42	13.87	13.80	1.936	2.013	3.412	12.908	15.24	19.70
15,000	2.955	4.136	5.925		19.24	21.46	20.70	2.847	2.977	5.118	17.90	20.48	29.55
20,000	4.071	4.136	7.900		24.11	22.68	27.60	3.794	4.039	6.824	22.32	26.20	39.40
25,000	4.845	5.018	9.875		26.69	25.64	34.50	4.788	5.162	8.531	26.62	32.07	49.25
40,000	9.141	9.228	15.80		50.47	47.21	55.20	8.274	8.949	13.65	43.89	53.22	78.80
50,000	12.40	12.51	19.75		68.49	63.89	69.00	11.05	11.87	17.06	57.51	69.29	98.50
				C3									
3,000	0.505	0.544	1.264	R = 16 in.	4.965	5.001	4.140	0.456	0.502	1.092	4.613	5.071	5.910
4,000	0.767	0.800	1.685		7.214	6.955	5.520	0.648	0.692	1.456	6.428	6.654	7.880
5,000	0.983	1.028	2.107		8.302	8.143	6.900	0.826	0.899	1.820	7.773	8.426	9.850
6,000	1.165	1.230	2.528		9.285	9.233	8.280	1.069	1.157	2.184	8.677	9.511	11.82
7,000	1.452	1.529	2.949		11.13	11.06	9.660	1.244	1.341	2.548	9.444	10.46	13.79
8,000	1.689	1.784	3.371		12.41	12.41	11.04	1.558	1.677	2.912	11.40	12.52	15.76
9,000	1.919	2.030	3.792		13.93	13.95	12.42	1.815	1.958	3.276	13.22	14.60	17.73
10,000	2.333	2.341	4.213		15.79	16.02	13.80	2.105	2.241	3.640	14.66	16.38	19.70
11,000	2.469	2.624	4.635		17.25	17.81	15.18	2.354	2.508	4.004	16.22	18.19	21.67
12,000	2.716	2.883	5.056		18.54	19.15	16.56	2.581	2.750	4.368	17.57	19.78	23.64
13,000	2.952	3.178	5.477		19.35	20.37	17.94	2.842	3.034	4.732	19.15	21.67	25.61
14,000	3.315	3.992	5.899		19.18	23.61	19.32	3.146	3.368	5.096	20.17	23.65	27.58
15,000	3.640	4.856	6.320		19.44	27.85	20.70	3.405	3.639	5.460	22.32	25.43	29.55

APPENDIX A
STRUCTURAL ANALYSIS

1. To obtain the resulting equilibrium equations at a given section above or below a load P, the following equations are derived (see Figure A1).

$$\Sigma M_{A'} = 0 \Rightarrow M(\phi) = M_s - P \sin\theta\,(r - r\cos\theta) \tag{A1}$$

for $\phi \leq \theta$,

$$\Sigma M_A = 0 \Rightarrow M(\phi) = M_s - Pr \sin\theta\,(1 - \cos\phi) + Pr \sin(\phi - \theta) \tag{A2}$$

for $\phi \geq \theta$.

2. Conserving continuity of curvature yields

$$\int_0^{\theta} (\text{Equation A1})\, d\phi + \int_{\theta}^{\pi/2} (\text{Equation A2})\, d\phi = 0 \,, \quad \theta \leq \frac{\pi}{2} \tag{A3}$$

Solving Equation A3 gives

for

$$\phi \leq \theta \,, \quad M(\phi) = Pr \left\{ -\frac{2}{\pi} \left[\sin\theta \left(1 - \frac{\pi}{2}\right) - \sin\theta + 1 \right] - \sin\theta\,(1 - \cos\phi) \right\} \tag{A4}$$

and for

$$\phi \geq \theta \,, \quad M(\phi) = Pr \left\{ -\frac{2}{\pi} \left[\sin\theta \left(1 - \frac{\pi}{2}\right) - \sin\theta + 1 \right] - \sin\theta\,(1 - \cos\phi) + \sin(\phi - \theta) \right\} \tag{A5}$$

Solving for M_s and M_c gives

$$M_s = Pr \left(\sin\theta - \frac{2}{\pi} \right) \tag{A6}$$

$$M_c = Pr \left(\cos\theta - \frac{2}{\pi} \right) \tag{A7}$$

and for R_s and R_c gives

$$R_s = P \sin\theta$$

$$R_c = P \cos\theta$$

3. The results from the structural analysis of a quarter-symmetric circular conduit loaded by five equally spaced radial loads are given by Equations A8-A13 which summarize the values of internal forces for $\phi \geq$ and $\leq \theta$. Refer to Figure A1 for the idealized quarter-symmetric one-dimensional (1-D) structure.

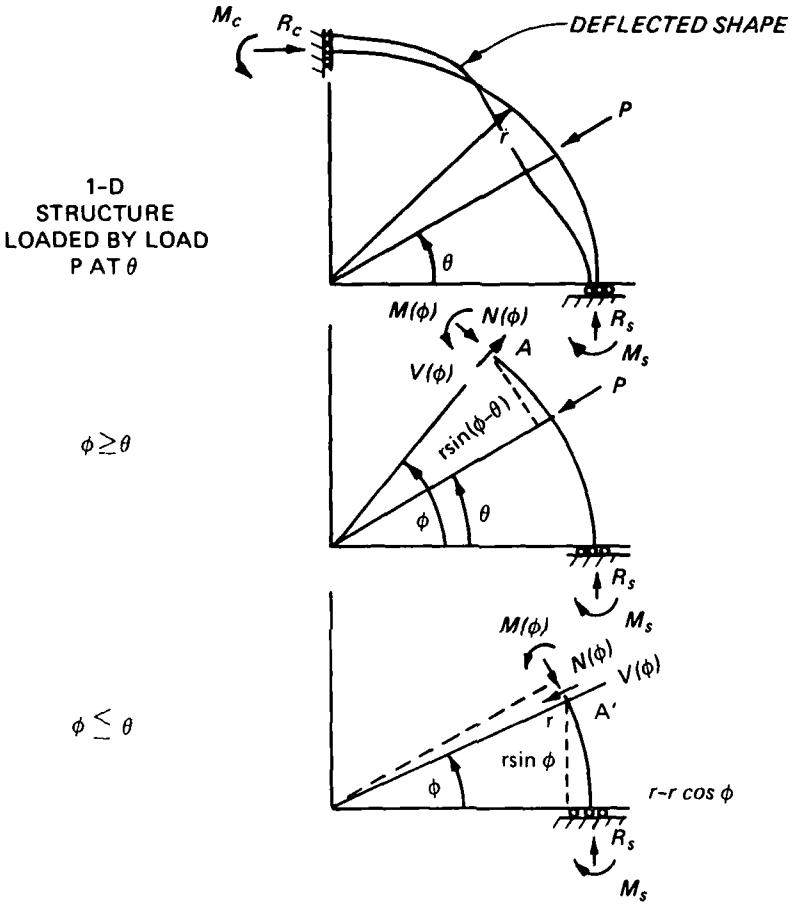

Figure A1. Idealized structure analyzed for an arbitrary load, P_r

$$M(\phi) = \begin{cases} Pr \left(\sin\theta \cos\phi - \frac{2}{\pi}\right) , & \phi \leq \theta \quad (A8) \\ Pr \left[\sin\theta \cos\phi - \frac{2}{\pi} + \sin(\phi - \theta)\right] , & \phi \geq \theta \quad (A9) \end{cases}$$

$$N(\phi) = \begin{cases} p \cos\phi \sin\theta , & \phi \leq \theta \quad (A10) \\ P \left[\cos\phi \sin\theta + \sin(\phi - \theta)\right] , & \phi \geq \theta \quad (A11) \end{cases}$$

$$V(\phi) = \begin{cases} P \sin\theta \sin\phi \ , & \phi \leq \theta \quad (A12) \\ P \left[\sin\theta \sin\phi - \cos(\phi - \theta)\right] \ , & \phi \geq \theta \quad (A13) \end{cases}$$

where

$N(\phi)$ = internal thrust

$N(\phi)$ = internal moment

$V(\phi)$ = internal shear

M_c = crown moment

M_s = springing line moment

R_c = crown thrust

R_s = springing line thrust

ϕ = angle from springing line to crown

θ = angle at which P is applied

P = normal load applied at θ

r = radius of 1-D structure

4. The resultant internal forces as given by a previous solution (Anderson, Haelsig, and Reifel 1966)* to the structure in Figure 15 (in the main text) under the continuous pressure distribution are given by

$$M(\theta) = \frac{wR_oR}{6} \left(K_V - K_L\right) \cos 2\theta$$

$$N(\theta) = \frac{w}{3} R_o \left[\left(2K_L + K_V\right) + \left(K_V - K_L\right) \cos^2\theta\right]$$

and

$$V(\theta) = \frac{w}{3} R_o \left(K_L - K_V\right) \sin 2\theta$$

where

θ = angle measured from the springing line

w = maximum pressure (p_{max})

R_o = outside radius

R = middepth section radius

K_L = lateral pressure coefficient

K_V = vertical pressure coefficient

---

* References cited in this appendix are included in the References at the end of the main text.

for 3:1 loading $\Rightarrow$ $K_L/K_V = 1/3 \Rightarrow K_L = 0.5$, $K_V = 1.5$

5. The EM 1110-2-2902 (Headquarters, Department of the Army 1969) design loadings give

$$M(\theta) = \frac{wR_oR}{4}\left(K_V - K_L\right)\cos 2\theta$$

$$N(\theta) = wR_o\left(K_L \sin^2\theta + K_V \cos^2\theta\right)$$

and

$$V(\theta) = \frac{wR_o}{2}\left(K_L - K_V\right)\sin 2\theta$$

6. The resulting internal forces from the Airy stress solution to the structure in Figure 15 (in the main text) under the continuous pressure distribution are

$$M(\theta) = \left\{\left[2A(b-a) + 4B(b^3 - a^3) - 2C\left(\frac{1}{b^3} - \frac{1}{a^3}\right)\right]\cos 2\theta + 2F(b-a) + H\left(\frac{1}{b} - \frac{1}{a}\right)\right\}\cdot e$$

where

$$e = r_m - \frac{\left\{\left[A(b^2 - a^2) + 3B\left(b^4 - a^4\right) - 3C\left(\frac{1}{b^2} - \frac{1}{a^2}\right)\right]\cos 2\theta + F\left(b^2 - d^2\right) - H\left[\ln(b) - \ln(a)\right]\right\}}{\left\{\left[2A(b-a) + 4B\left(b^3 - a^3\right) - 2C\left(\frac{1}{b^3} - \frac{1}{a^3}\right)\right]\cos 2\theta + 2F(b-a) + H\left(\frac{1}{b} - \frac{1}{a}\right)\right\}}$$

$$H(\theta) = \left\{\left[2A(b-a) + 4B(b^3 - a^3) - 2C\left(\frac{1}{b^3} - \frac{1}{a^3}\right)\right]\cos 2\theta + 2F(b-a) + H\left(\frac{1}{b} - \frac{1}{a}\right)\right\}$$

and

$$V(\theta) = \left\{\left[2A(b-a) + 2B(b^3 - a^3) + 2C\left(\frac{1}{b^3} - \frac{1}{a^3}\right) + 2D\left(\frac{1}{b} - \frac{1}{a}\right)\right]\sin 2\theta\right\}$$

where

$A = 3\alpha\frac{\rho}{q}\left(b^4 + a^2b^2 + 2a^4\right)$

b = outer radius

a = inner radius

$$B = -\alpha \frac{p}{q} (b^2 + 3a^2)$$

$$C = \alpha \frac{p}{q} (3a^4b^4 + a^6b^2)$$

$$F = -3\alpha \left(b^2 - a^2\right)^2$$

$$H = 6\alpha a^2 \left(b^2 - a^2\right)^2$$

$$D = -3\alpha \frac{p}{q} (2b^4a^2 + b^2a^4 + a^6)$$

$$r_m = R$$

$$\alpha = \frac{qb^2}{6\left(b^2 - a^2\right)^3}$$

p = varying pressure component magnitude, $\frac{(K_L - K_V)w}{2}$

q = uniform pressure component magnitude $\frac{(K_L + K_V)w}{2}$

7. Accounting for the absence of the load at locations 8A and 8B, the effect of this absence is solved by looking at the entire conduit (1-D) loaded by a two-point load and subtracting the effects contributed at the crown and the springing line. In Figure A2, the results of the classical two-point loading on a ring (Timoshenko 1941) are shown.

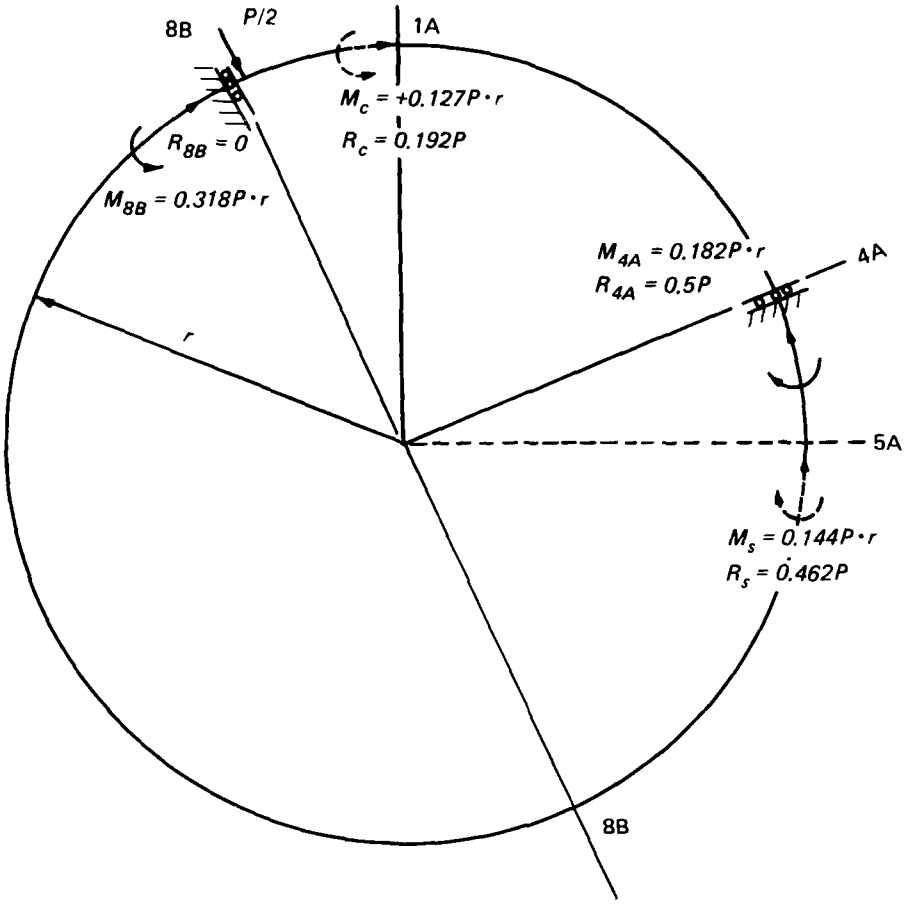

Figure A2. Accounting for absence of load at 8B and 8A

APPENDIX B

LOAD-DISPLACEMENT AND LOAD-STRAIN PLOTS

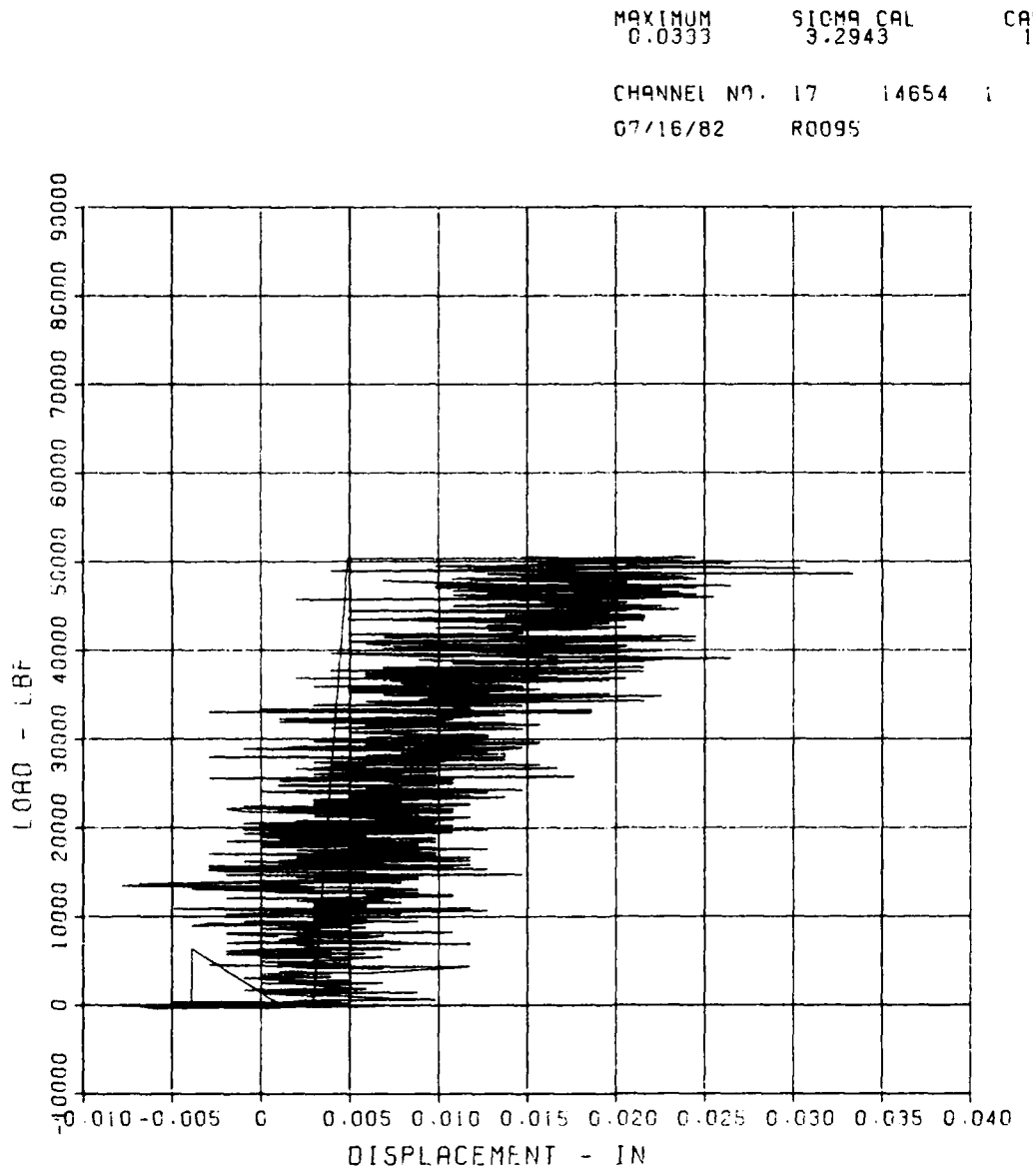

First test of C1

C1.1 52882
D-2

MAXIMUM	SIGMA CAL	CAL VAL
-0.0164	4.1052	1.6

CHANNEL NO. 18 14654 1
07/16/82 R0095

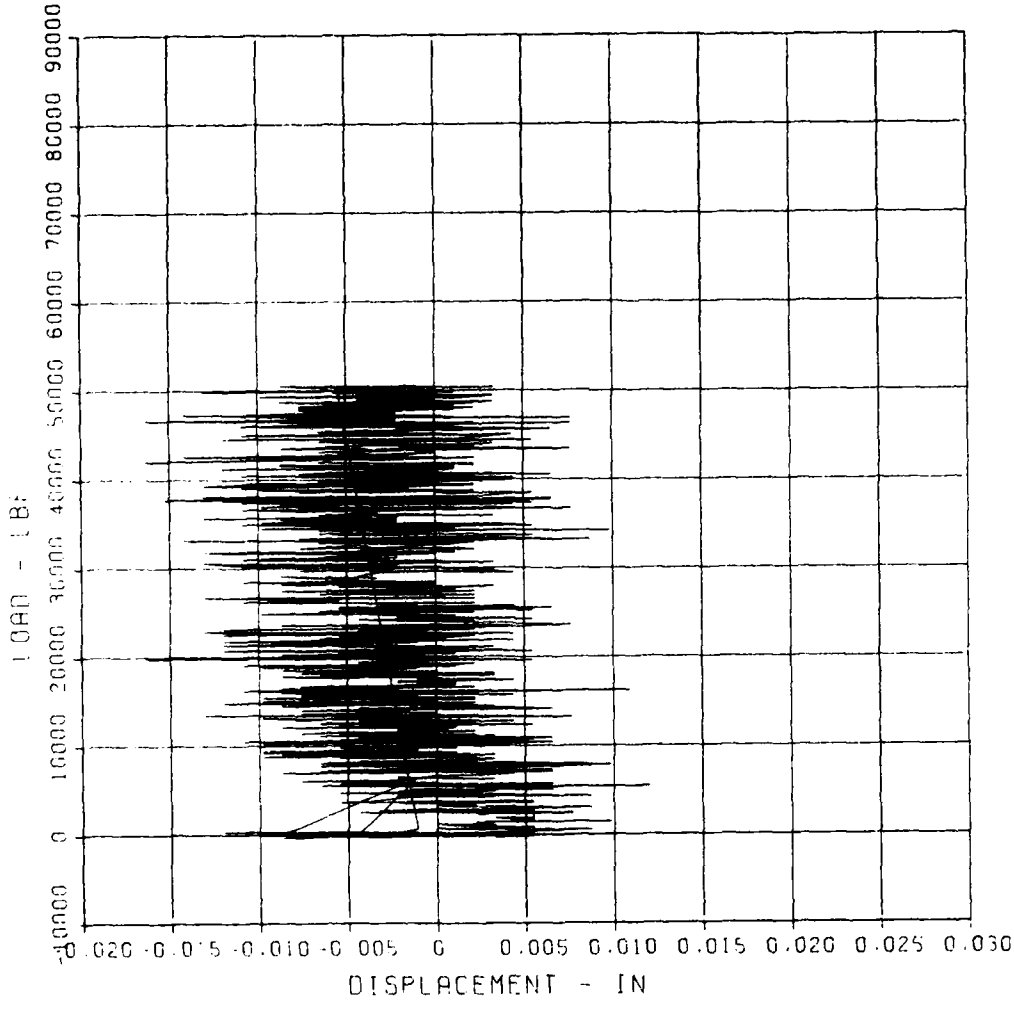

First test of C1

C1.1 52882
S-1

MAXIMUM	SIGMA CAL	CAL VAL
-667.7328	3.7609	2899.7

CHANNEL NO. 21 14654 1
07/16/82 R0095

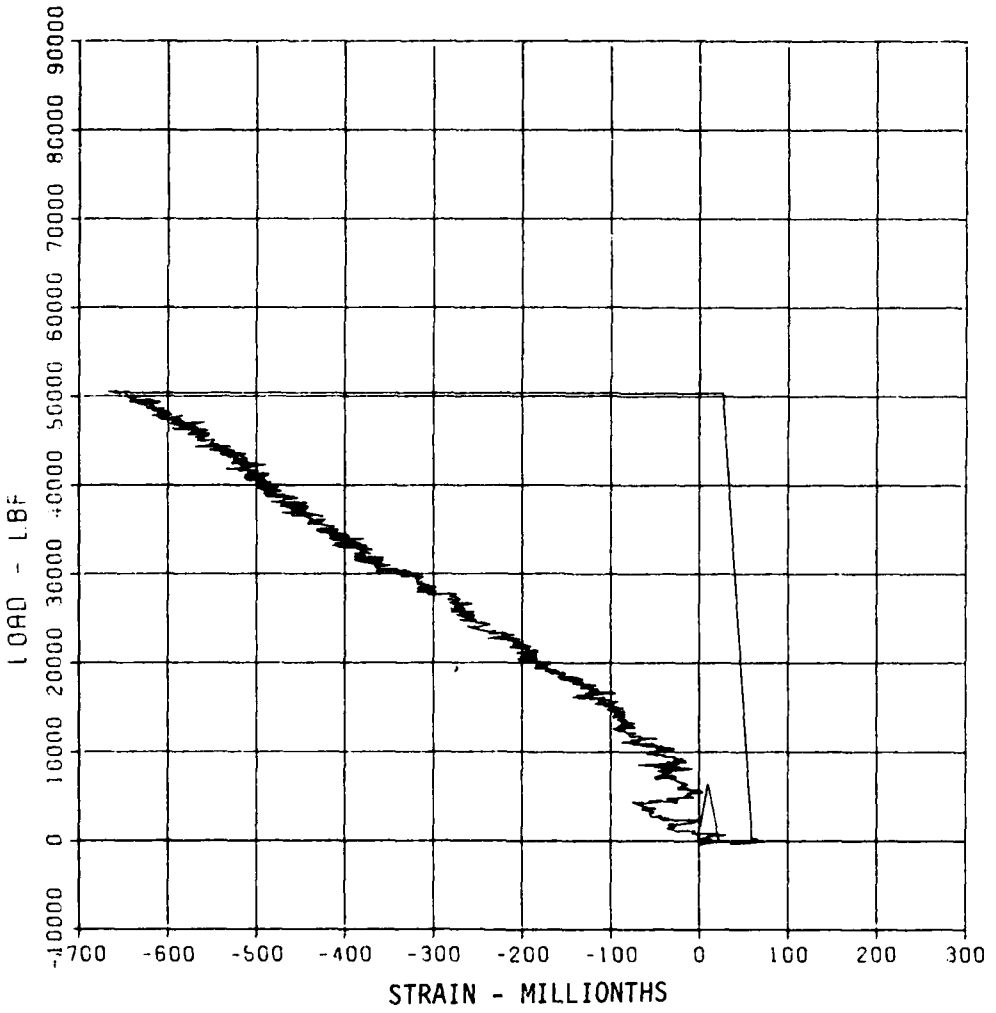

First test of C1

C1.1 52882
S-2

MAXIMUM	SIGMA CAL	CAL VAL
-599.3469	2.0667	2899.7

CHANNEL NO. 22 14654 1
07/16/82 R0095

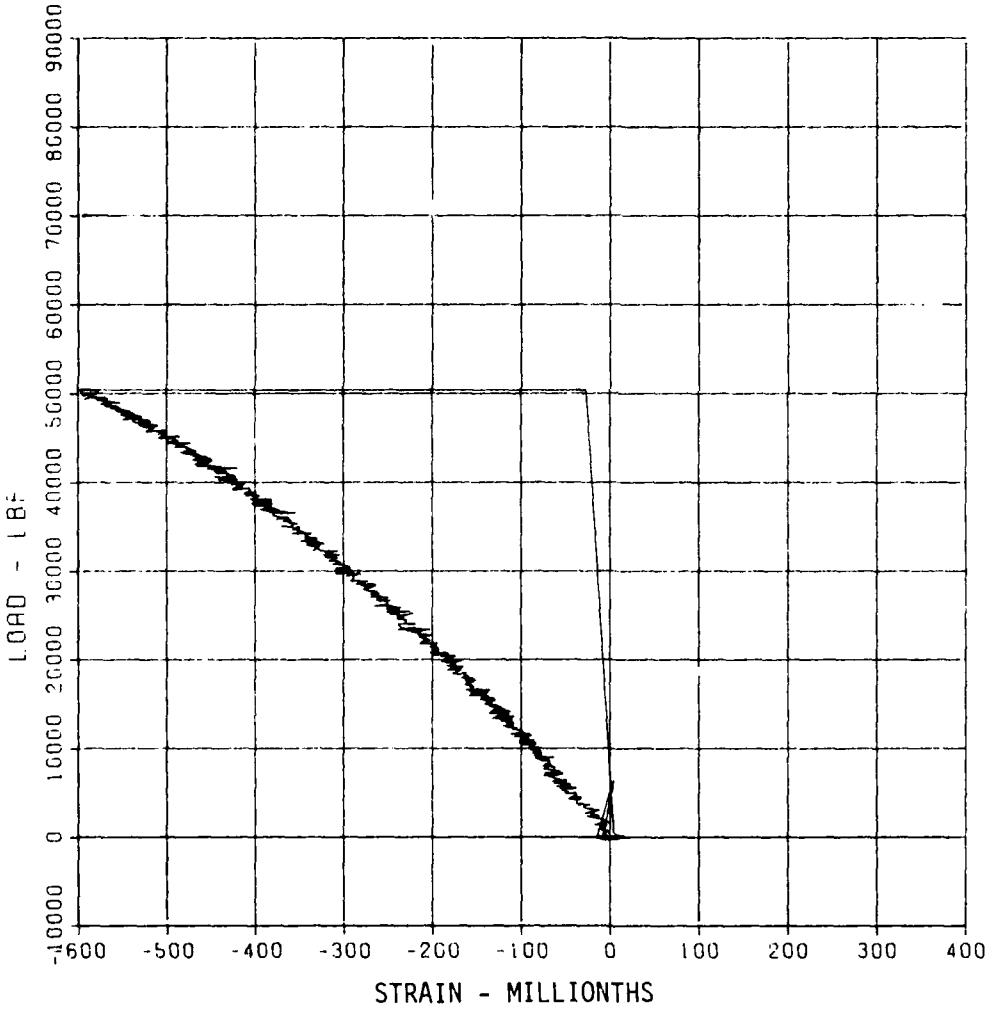

First test of C1

C1.1 52882
S-3

MAXIMUM	SIGMA CAL	CAL VAL
239.5895	2.5042	2899.7

CHANNEL NO. 23 14654
07/16/82 R0095

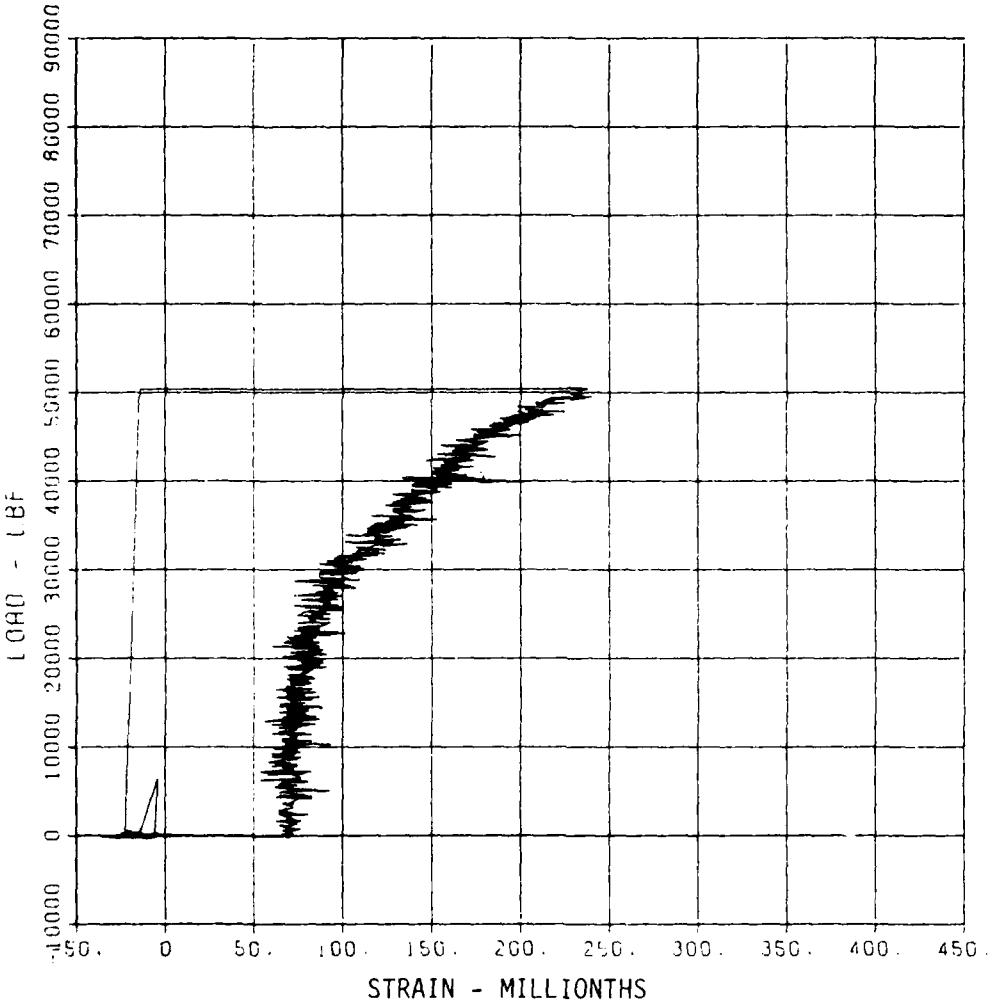

First test of C1

C1.1 52882
S-4

MAXIMUM	SIGMA CAL	CAL VAL
-550.6348	8.7598	2899.7

CHANNEL NO. 24 14654 1
07/16/82 R0095

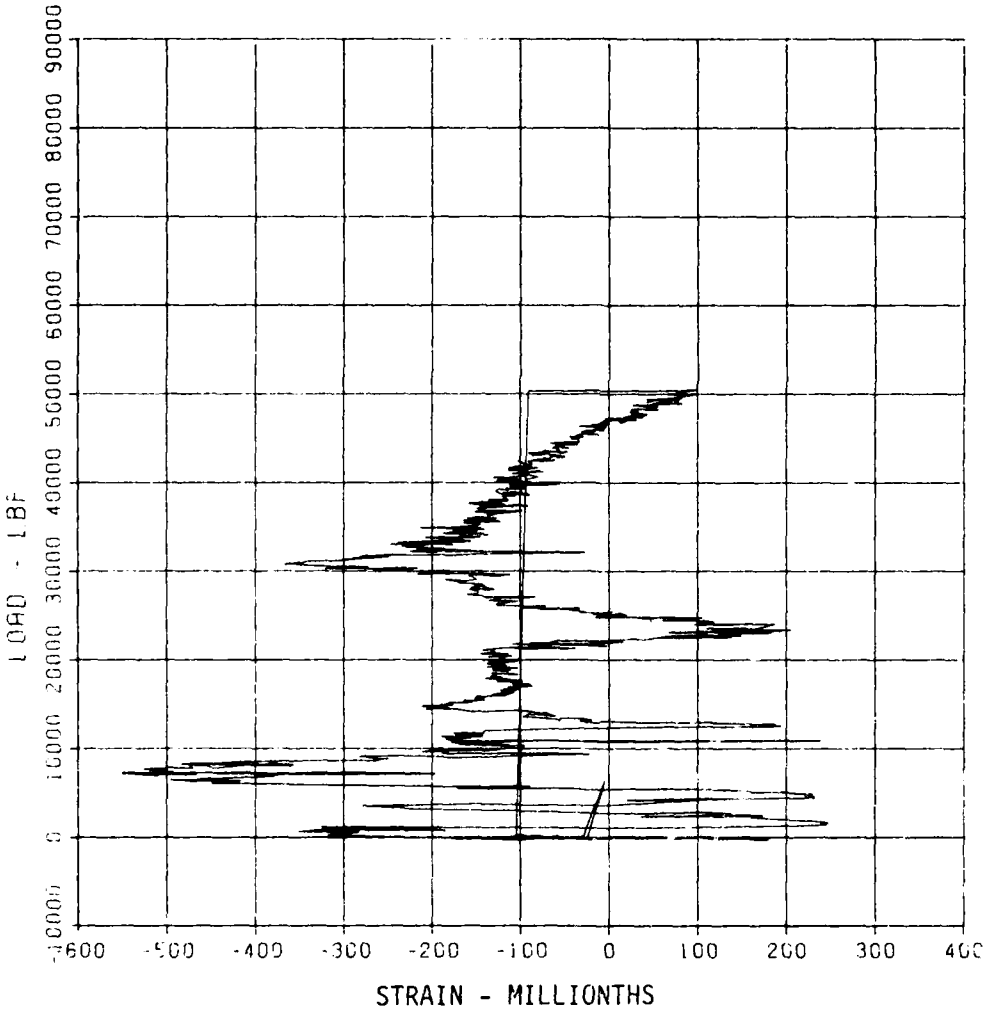

First test of C1

AD-A173 229 STRENGTH DESIGN OF REINFORCED CONCRETE HYDRAULIC STRUCTURES REPORT 4 LOAD..(U) ARMY ENGINEER WATERWAYS EXPERIMENT STATION VICKSBURG MS STRUC.. 2/2

UNCLASSIFIED V P CHIARITO ET AL. AUG 86 WES/TR/SL-80-4-4 F/G 13/13 NL

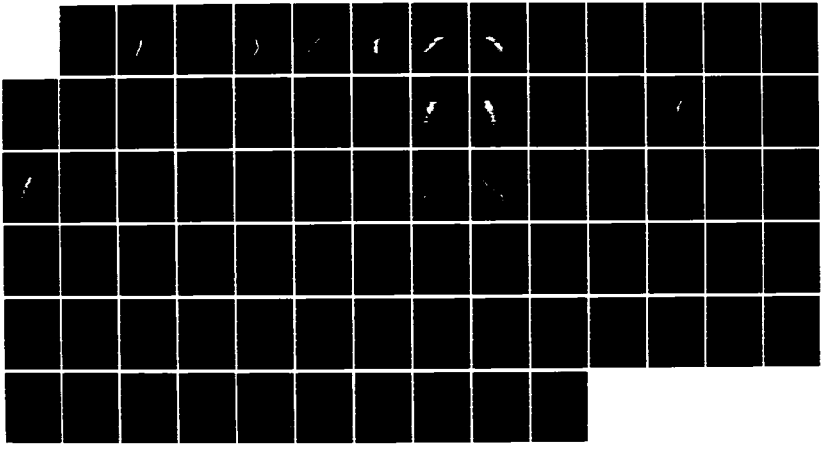

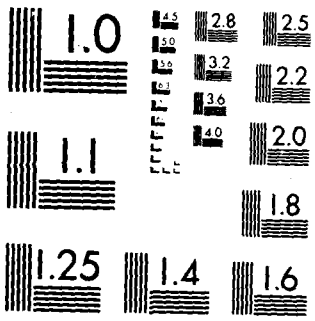

C1.1 52882
S-5

MAXIMUM	SIGMA CAL	CAL VAL
-126.4120	41.5792	2899.7

CHANNEL NO. 25 14654 1
07/16/82 R0095

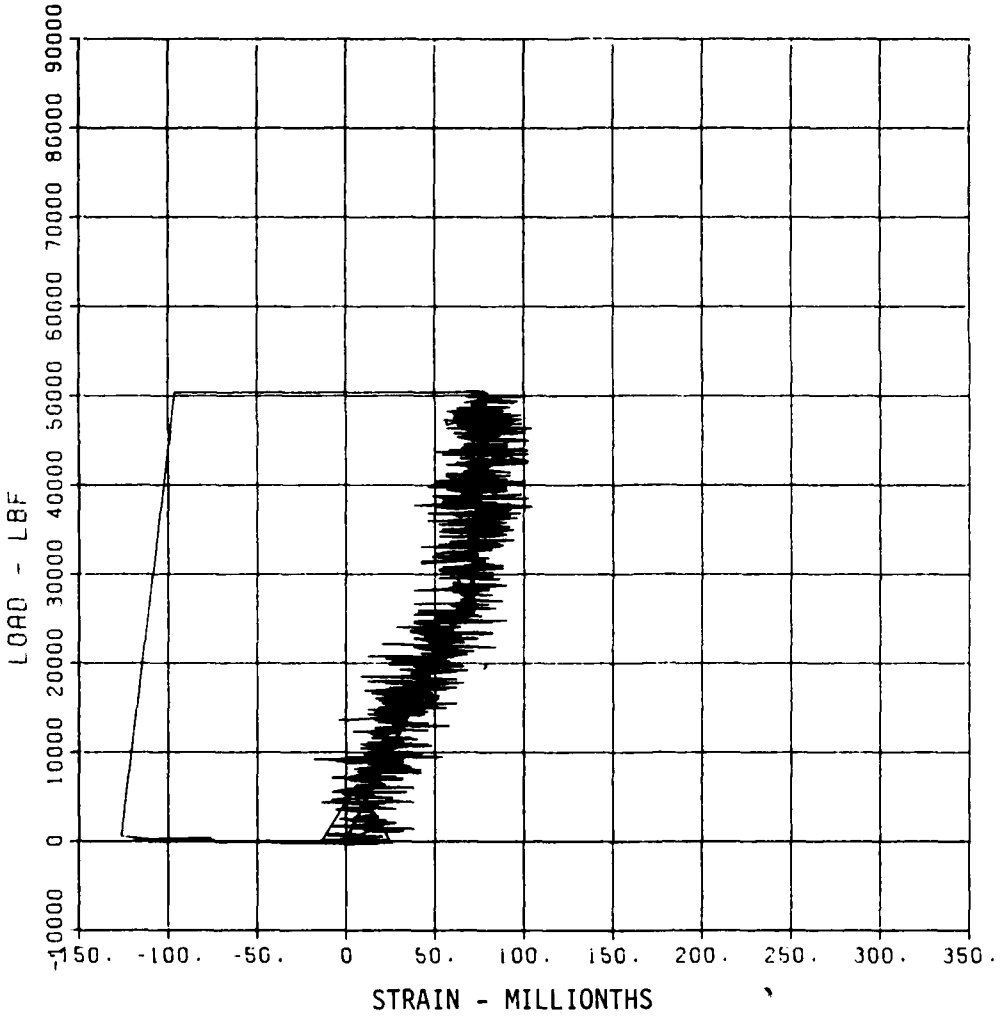

First test of C1

C1.1 52882
S-6

MAXIMUM	SIGMA CAL	CAL VAL
-480.4634	3.0843	2899.7

CHANNEL NO. 26 14654 1
07/16/82 R0095

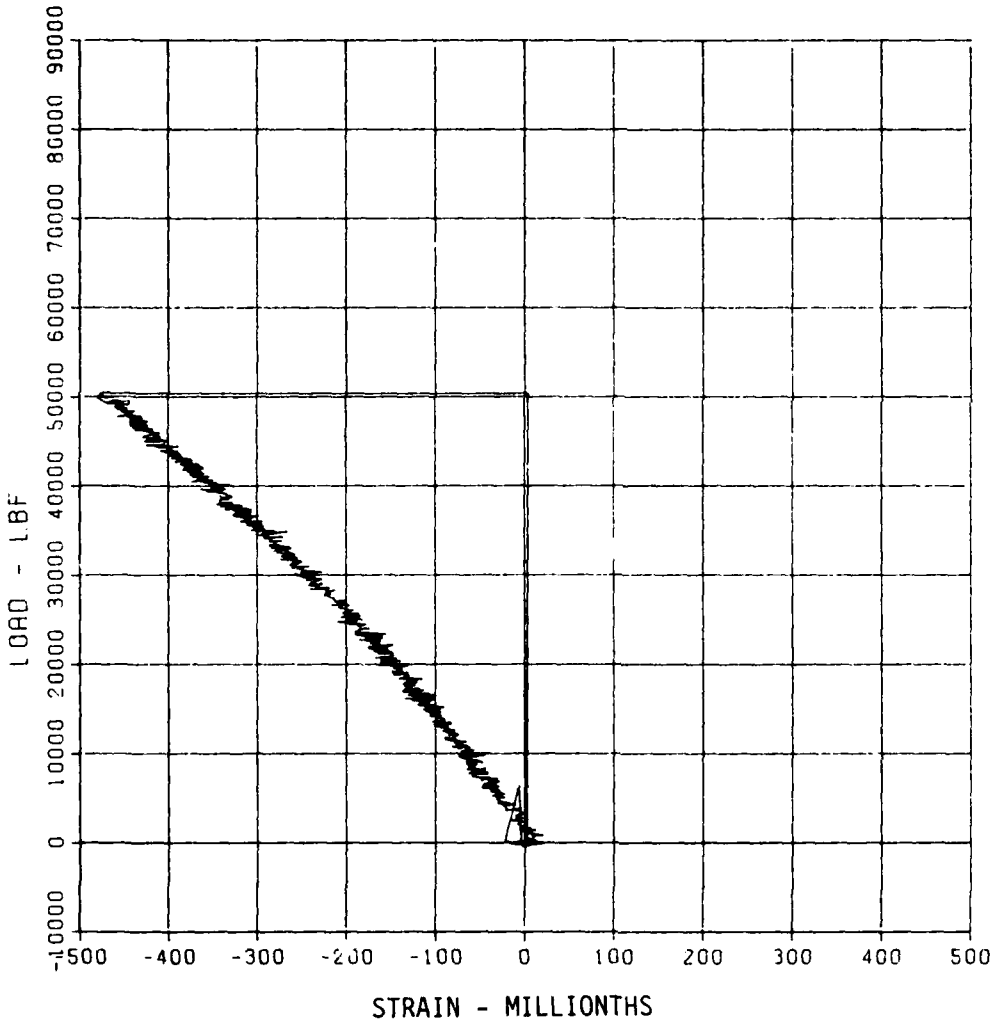

First test of C1

C1.1 52882
S-8

MAXIMUM	SIGMA CAL	CAL VAL
-110.9077	2.8636	2899.7

CHANNEL NO. 28 14654 1
07/16/82 R0095

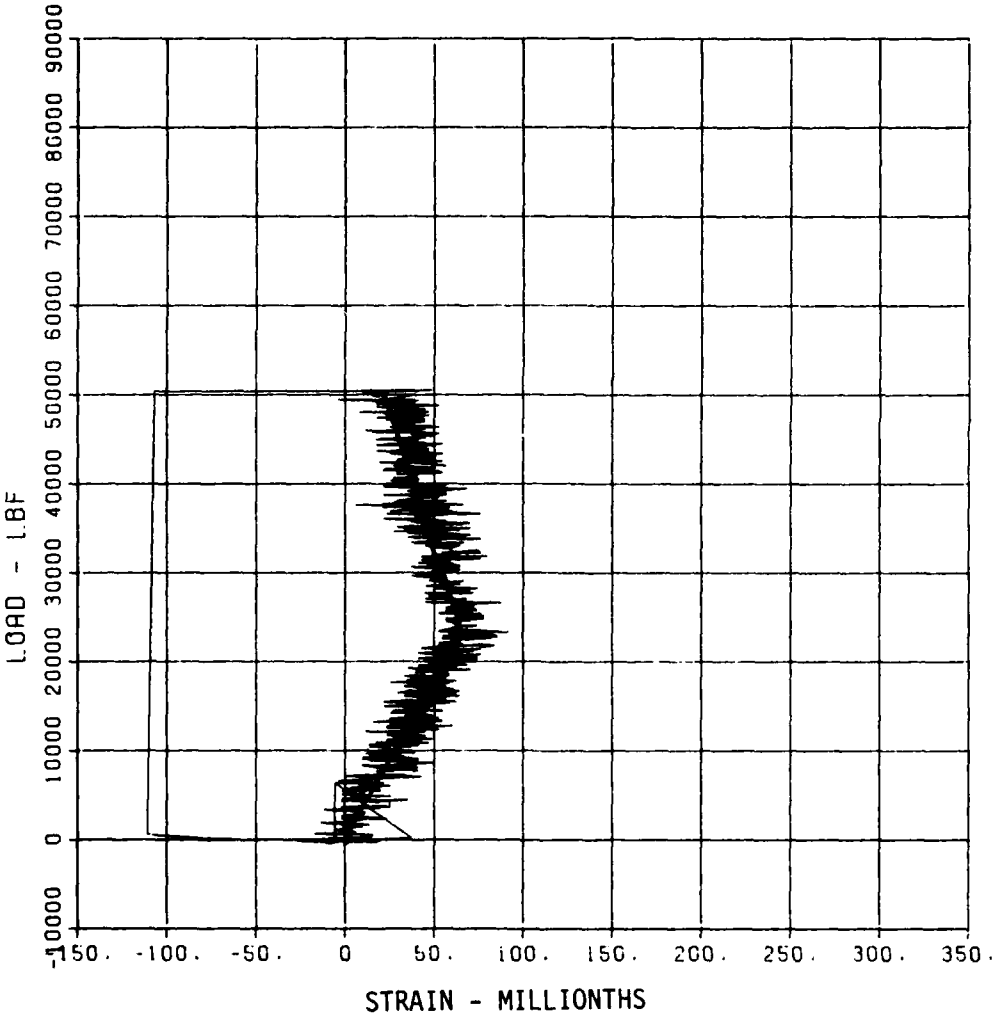

First test of C1

C1.1 52882
S-9

MAXIMUM	SIGMA CAL	CAL VAL
242.6819	3.1851	2899.7

CHANNEL NO. 29 14654 1
07/16/82 R0095

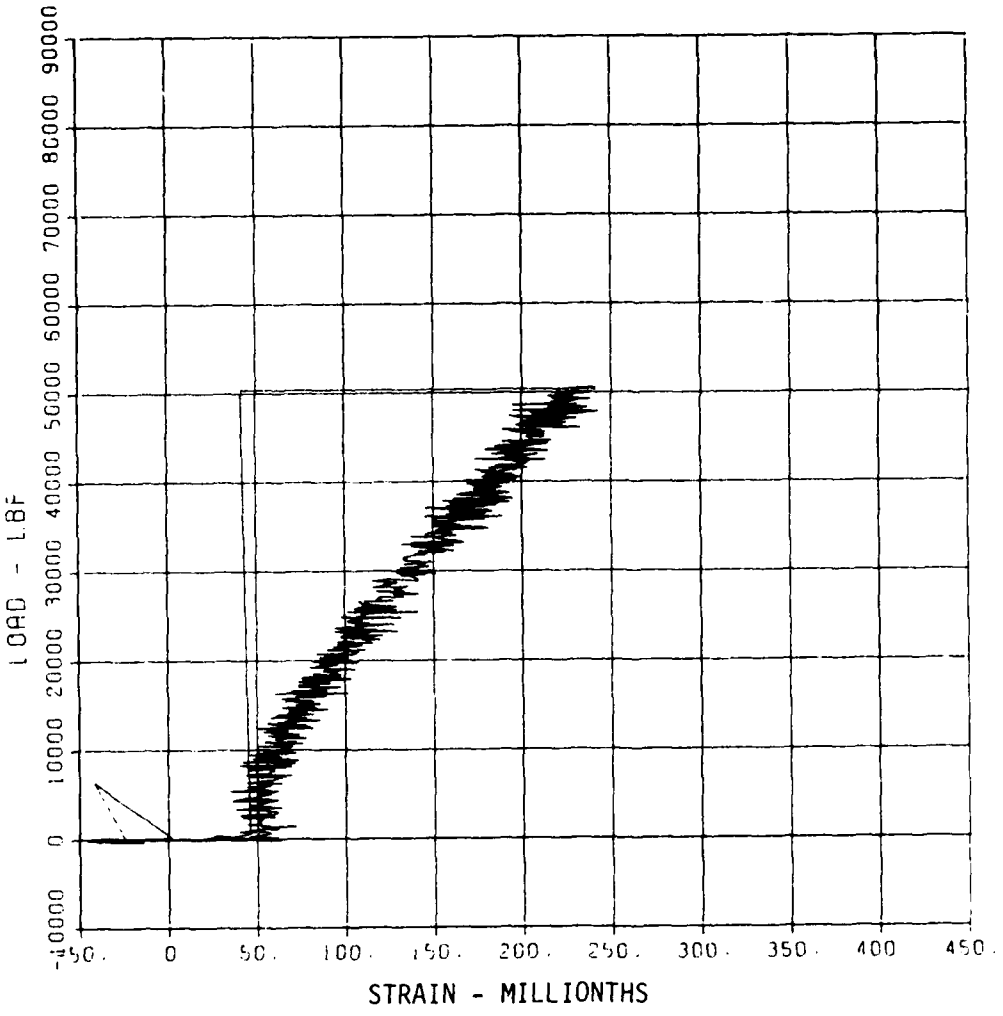

First test of C1

C1.1 52882
S-10

MAXIMUM	SIGMA CAL	CAL VAL
67.9530	3.7693	2899.7

CHANNEL NO. 30 14654 1
07/16/82 R0095

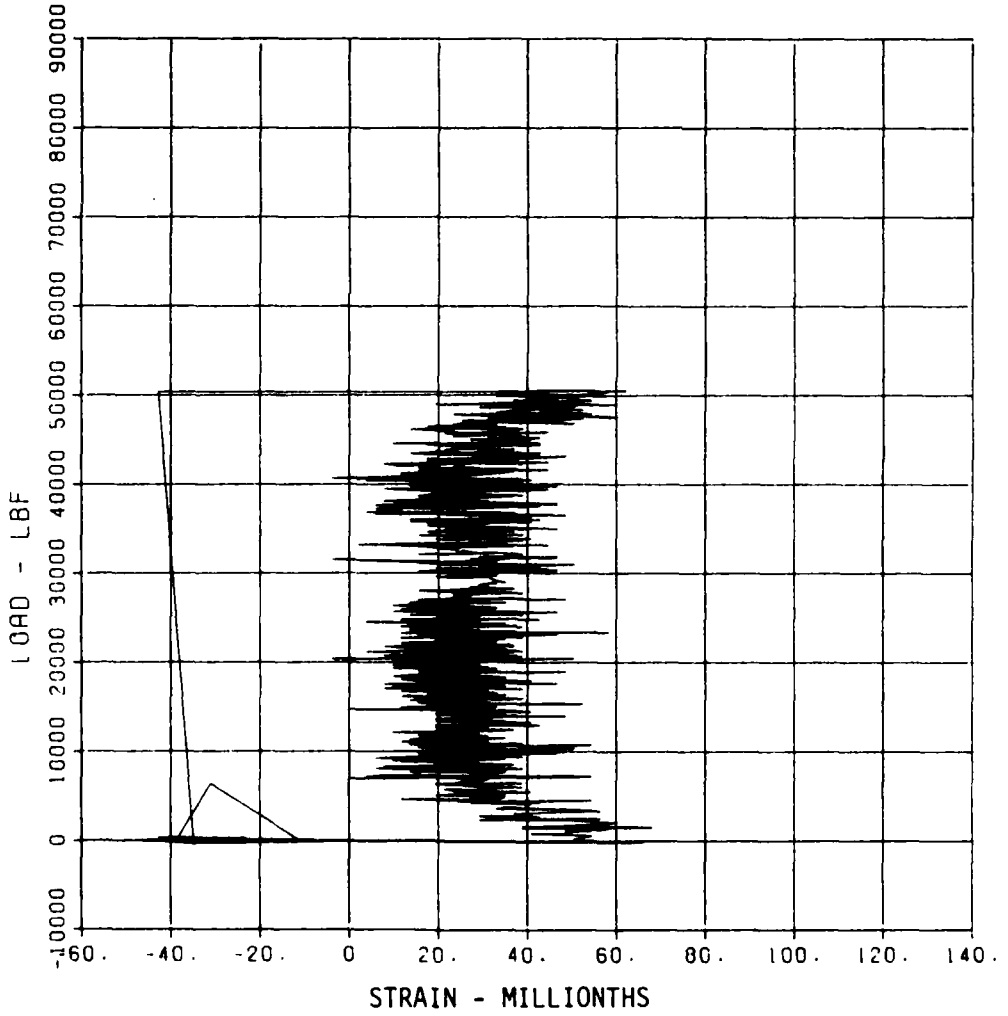

First test of C1

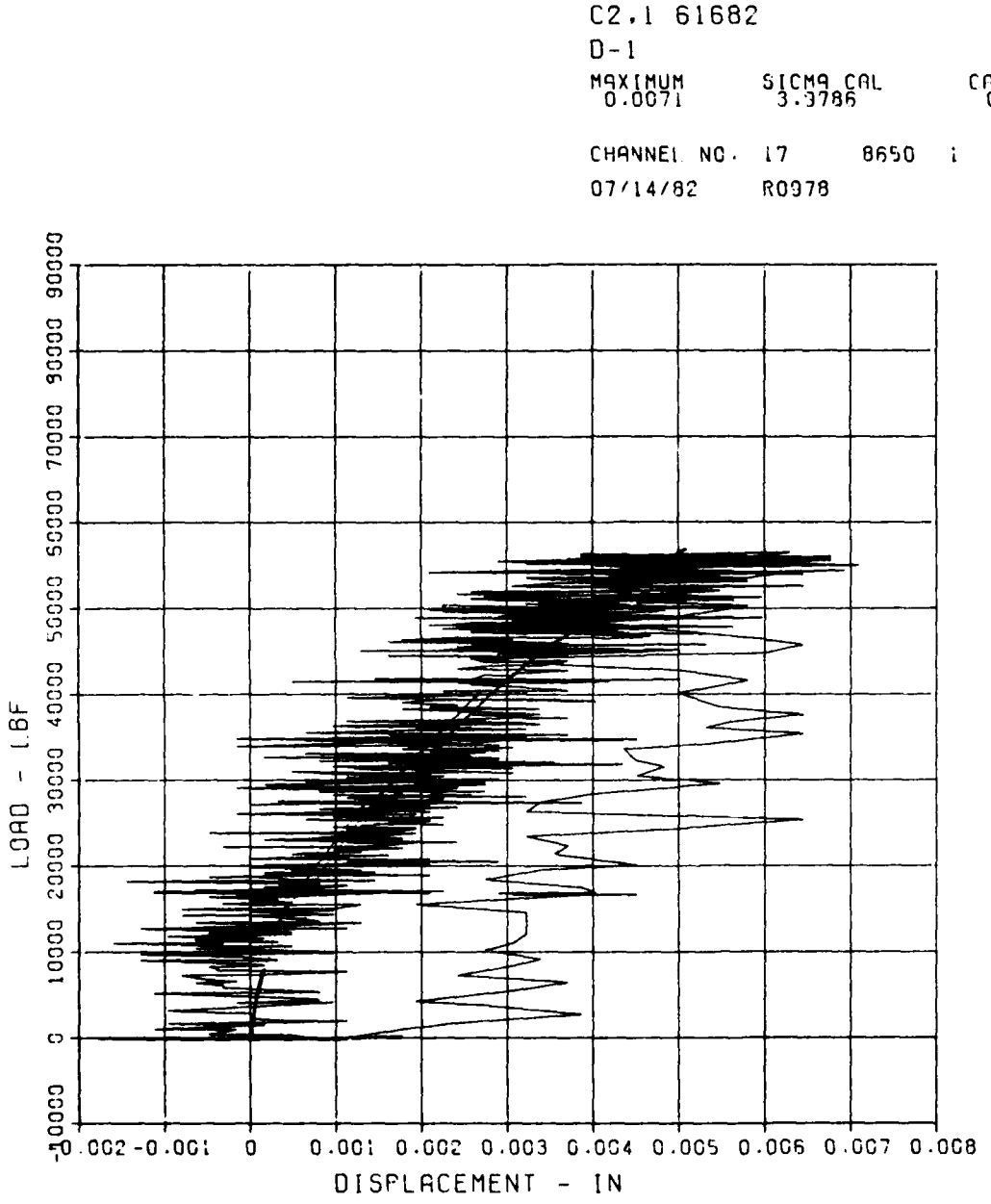

First test of C2

C2.1 61682
D-3

MAXIMUM	SIGMA CAL	CAL VAL
-0.0066	5.4105	0.3

CHANNEL NO. 18 8650 1
07/14/82 R0378

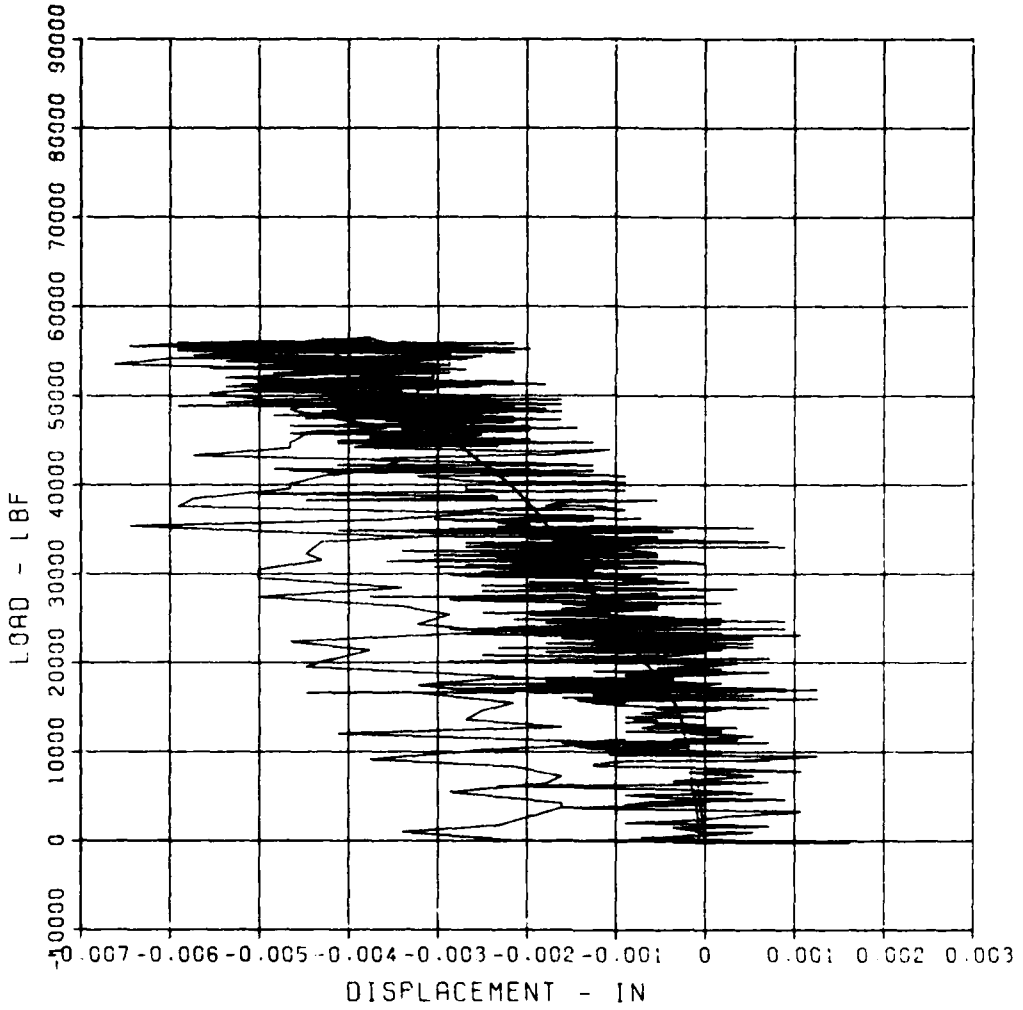

First test of C2

C2.1 61682
S-2

MAXIMUM	SIGMA CAL	CAL VAL
-1668.0519	2.2378	2899.7

CHANNEL NO. 22 8650 1
07/14/82 R0378

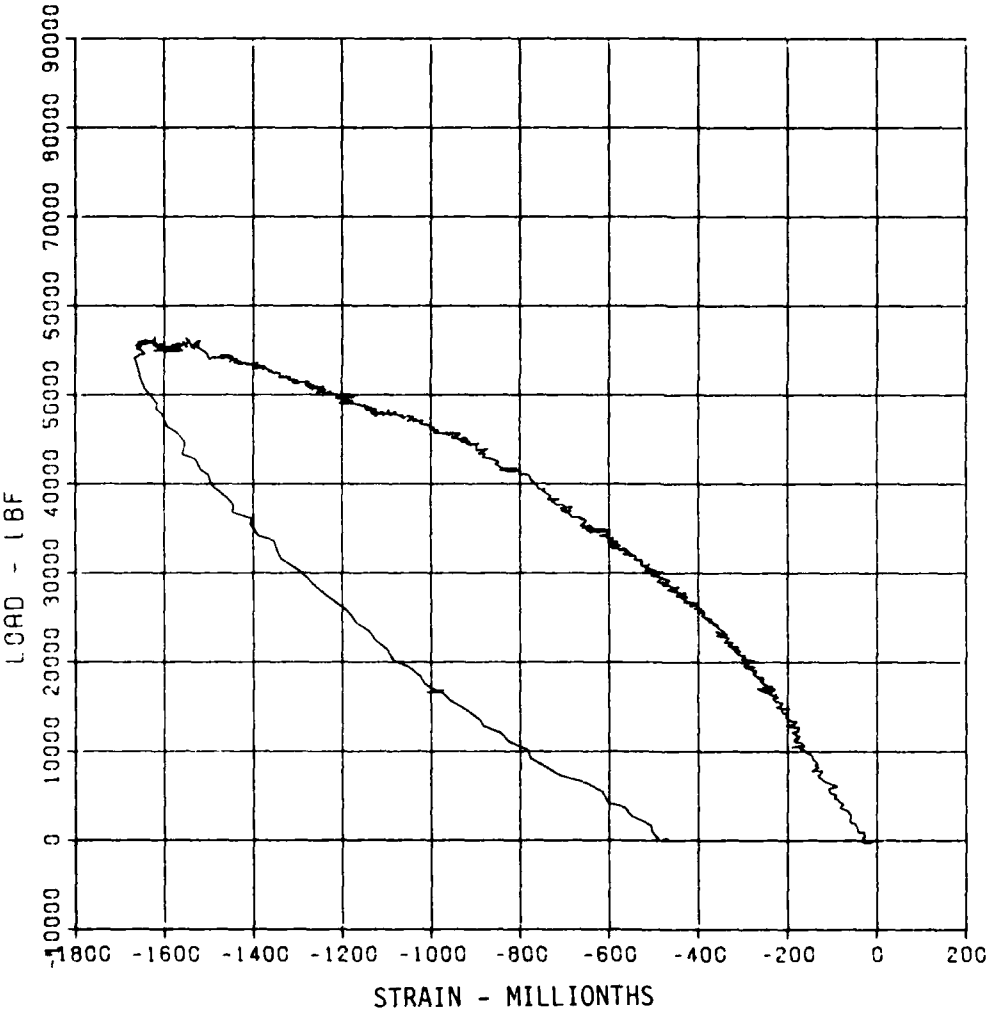

First test of C2

C2.1 61682
S-4

MAXIMUM	SIGMA CAL	CAL VAL
1317.0428	3.6332	2899.7

CHANNEL NO. 24 8650 1
07/14/82 R0978

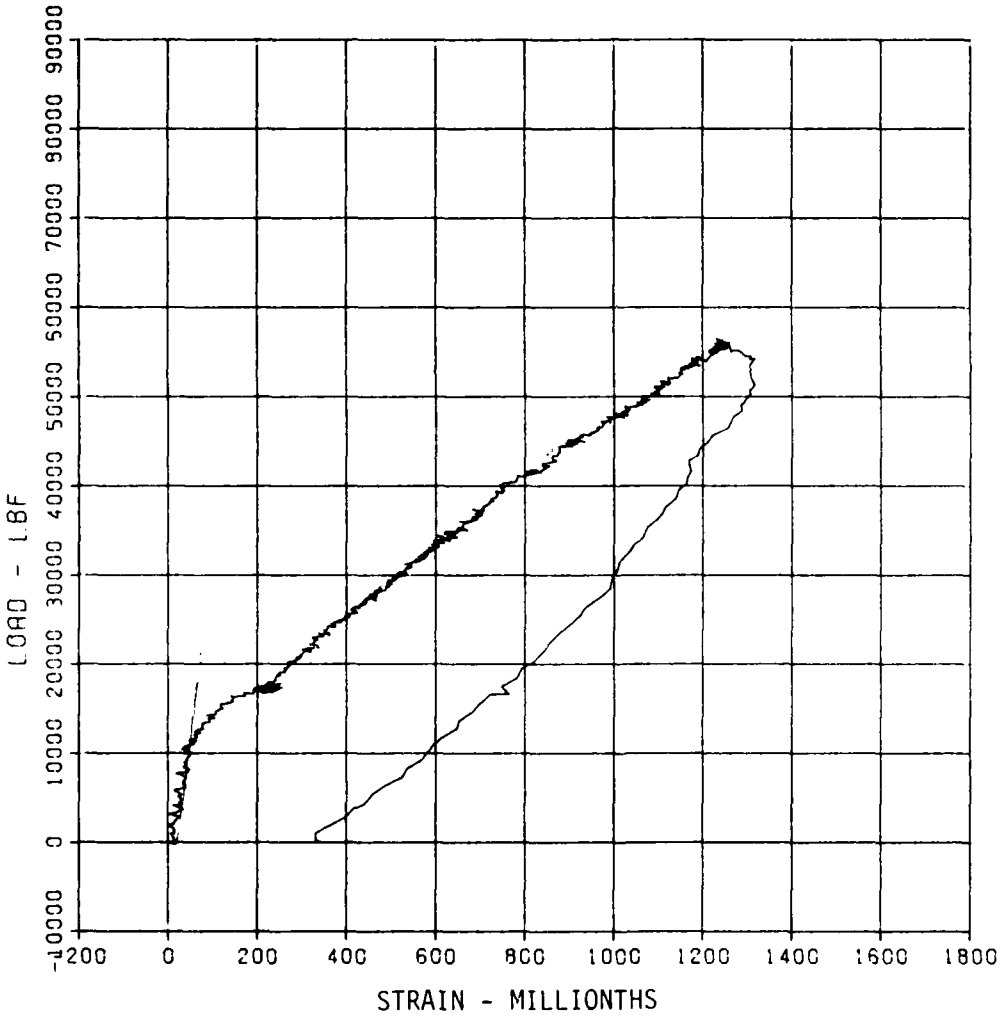

First test of C2

C2.1 61682
S-5

MAXIMUM	SIGMA CAL	CAL VAL
561.8067	41.1035	583.3

CHANNEL NO. 25 8650 1
07/14/82 R0378

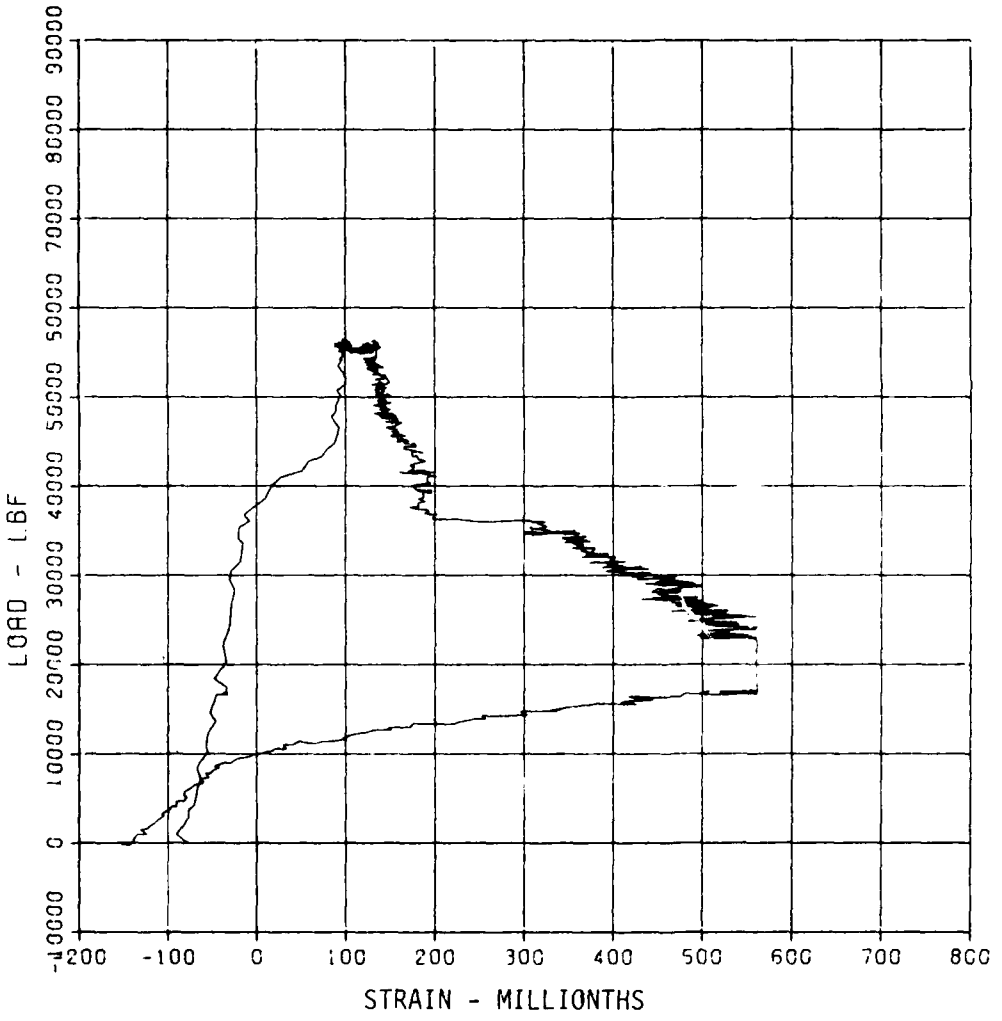

First test of C2

C2.1 61682
S-6

MAXIMUM	SIGMA CAL	CAL VAL
-1008.9850	2.7140	2899.7

CHANNEL NO. 26 8650 1
07/14/82 R0978

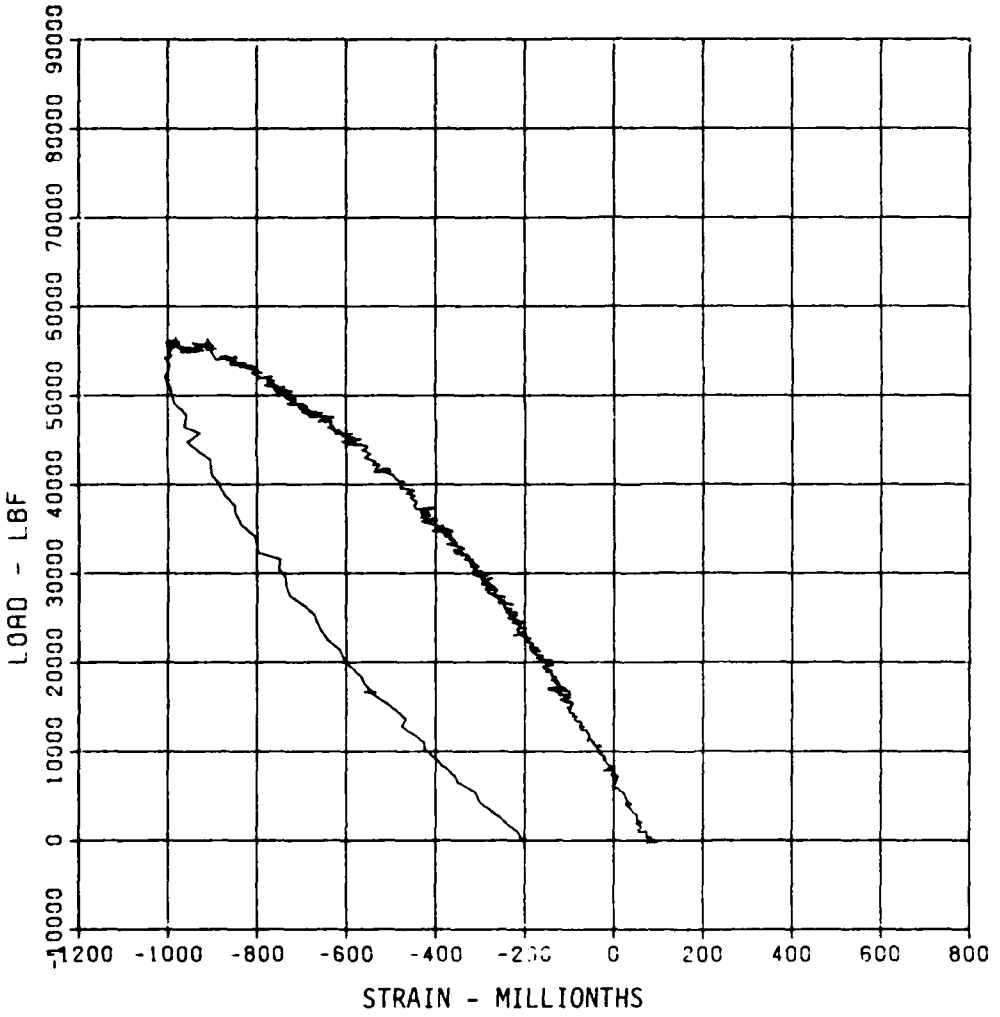

First test of C2

C2.1 61682
S-7

MAXIMUM	SIGMA CAL	CAL VAL
1508.7819	3.5448	2899.7

CHANNEL NO. 27 8650 1
07/14/82 R0978

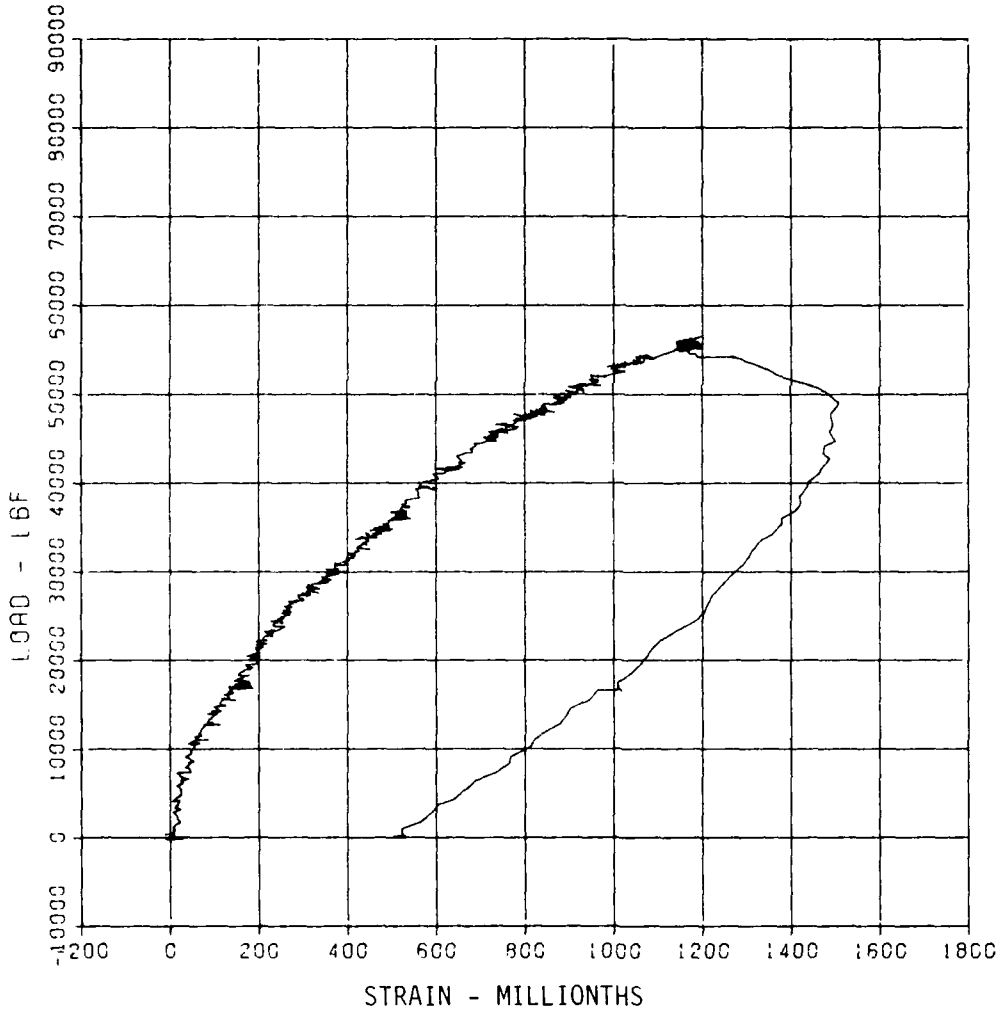

First test of C2

C2.1 61682
S-8

MAXIMUM	SIGMA CAL	CAL VAL
179.6705	7.5837	583.3

CHANNEL NO. 28 8650
07/14/82 R0978

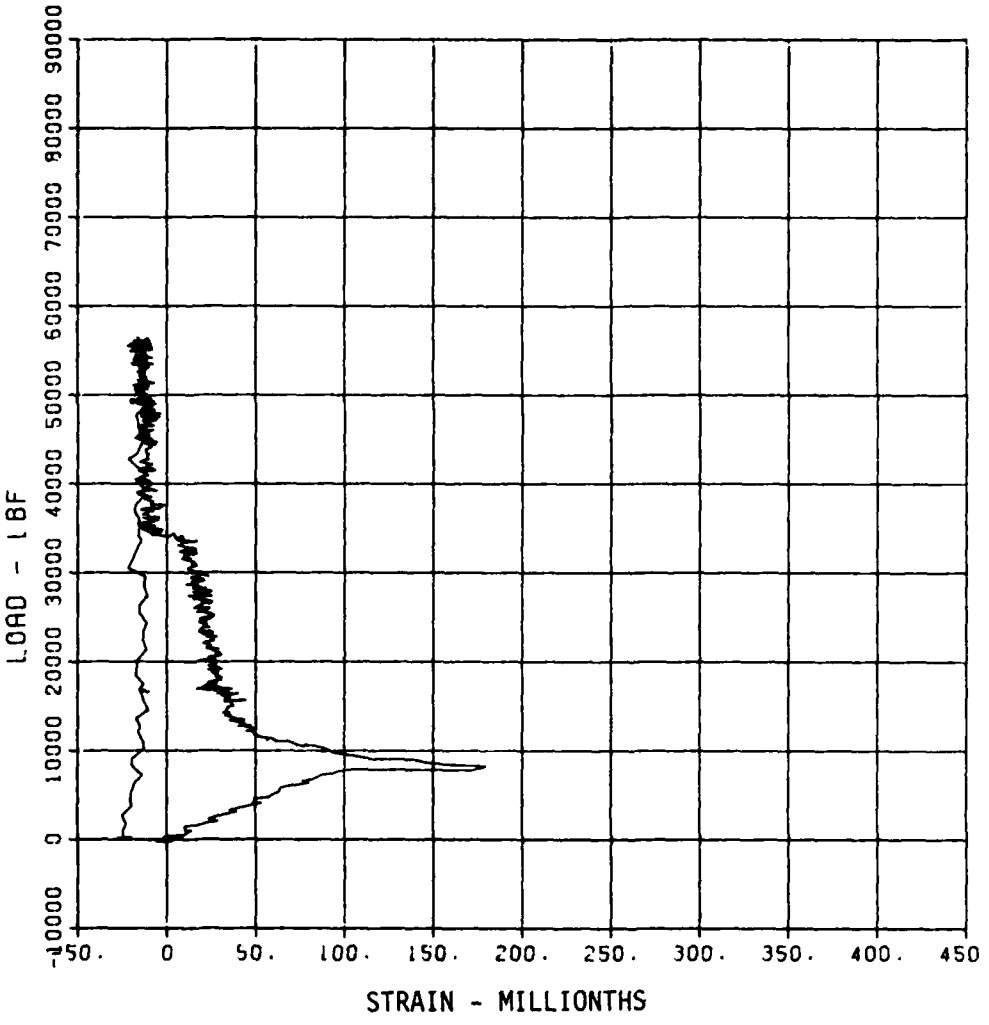

First test of C2

C2.1 61682
S-10

MAXIMUM	SIGMA CAL	CAL VAL
758.7385	5.7452	2833.7

CHANNEL NO. 30 8650 1
07/14/82 R0078

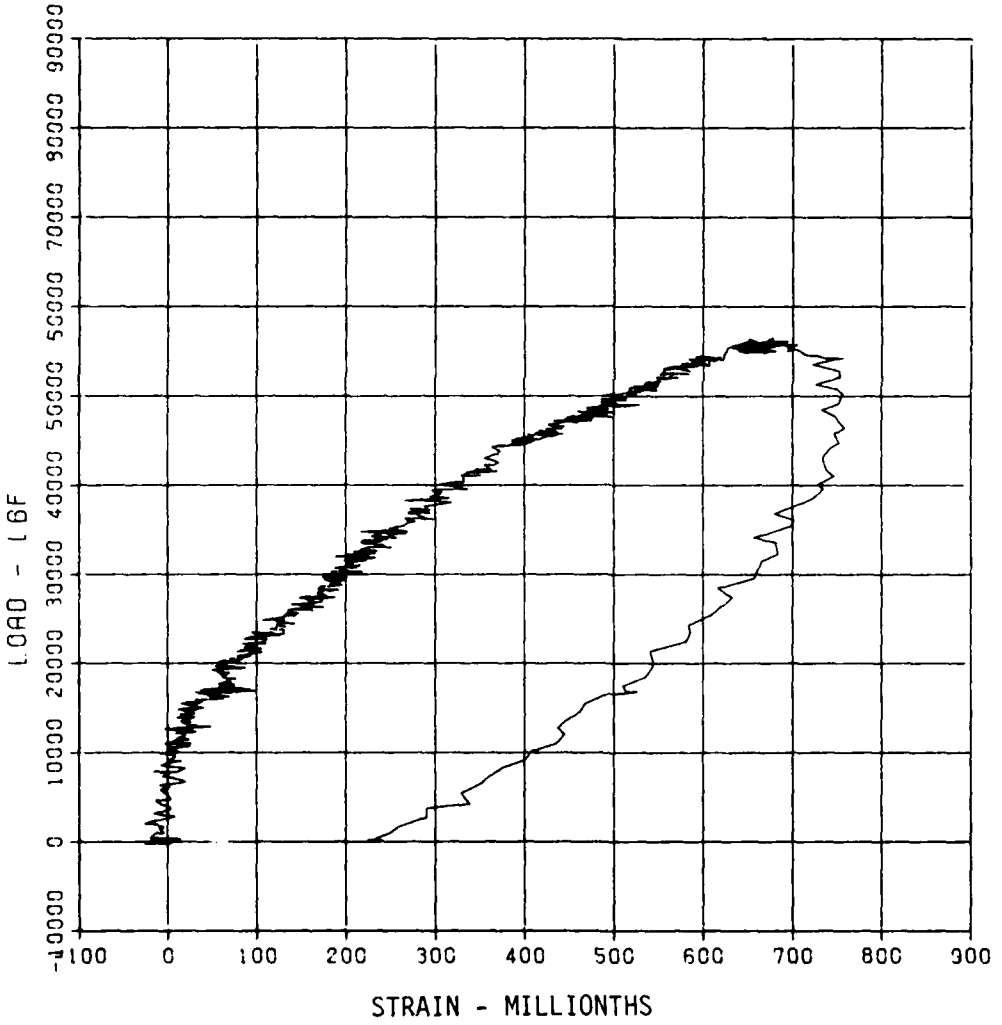

First test of C2

C2.1 61682
S-11

MAXIMUM	SIGMA CAL	CAL VAL
-10715.1962	2.7062	2899.7

CHANNEL NO. 1 8650 2
07/14/82 R0978

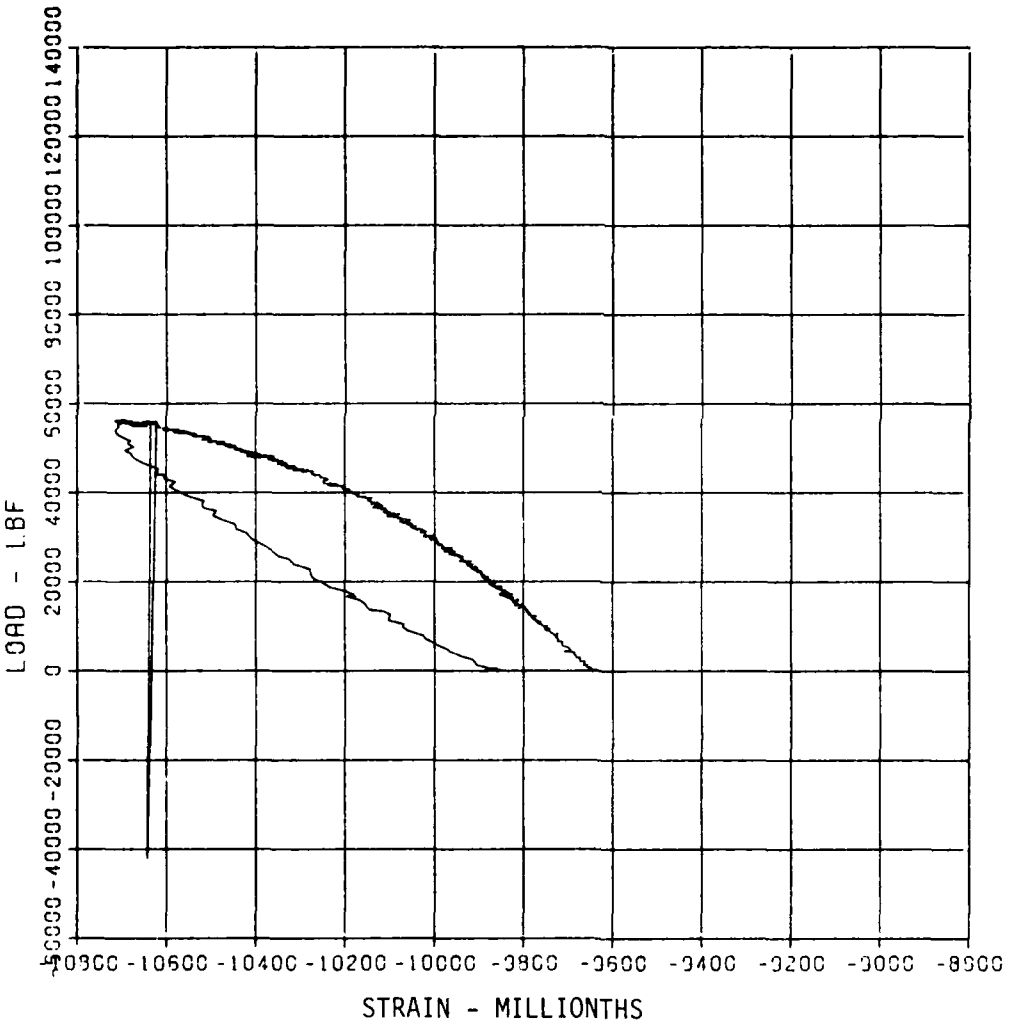

First test of C2

C2,1 61682
S-12

MAXIMUM	SIGMA CAL	CAL VAL
-1404.4241	3.5891	2899.7

CHANNEL NO. 2 8650 2
07/14/82 R0378

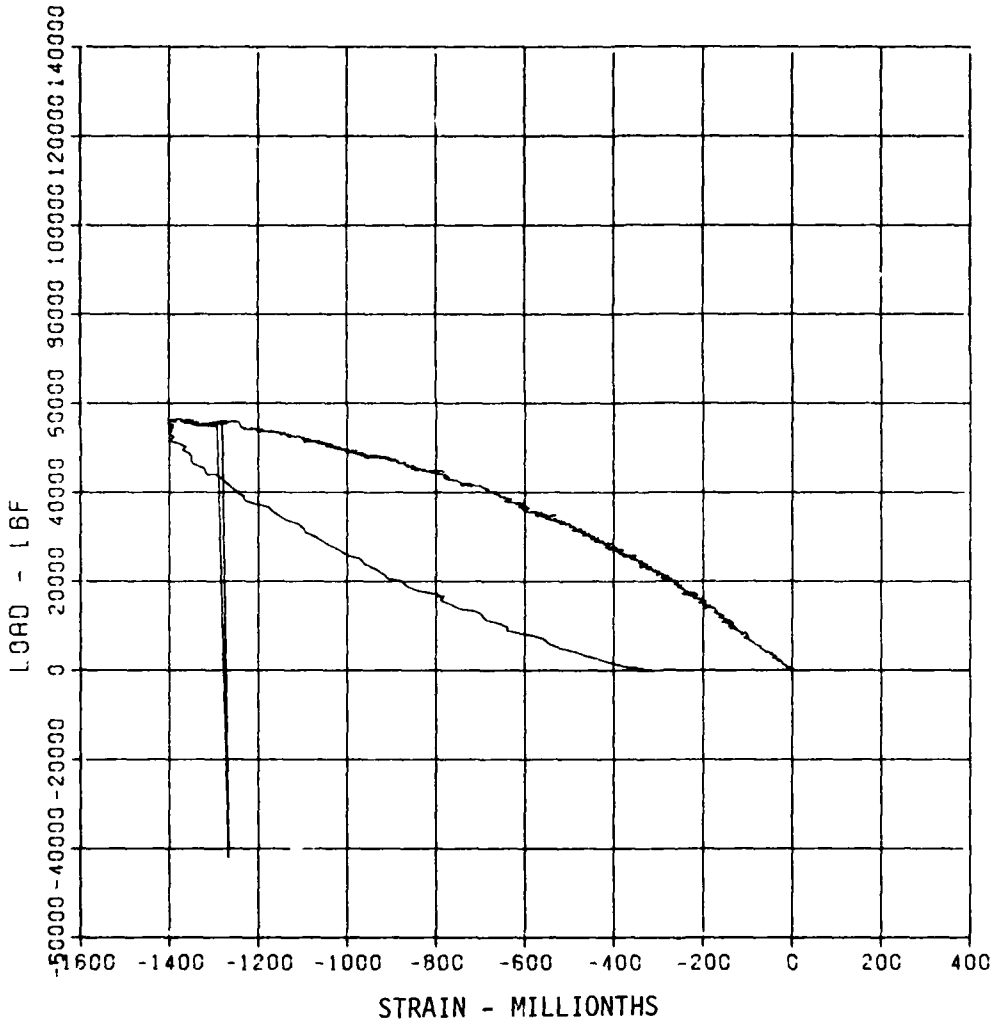

First test of C2

C2.1 61682
S-14

MAXIMUM	SIGMA CAL	CAL VAL
1055.1152	4.9244	2893.7

CHANNEL NO. 4 8650 2
07/14/82 R0378

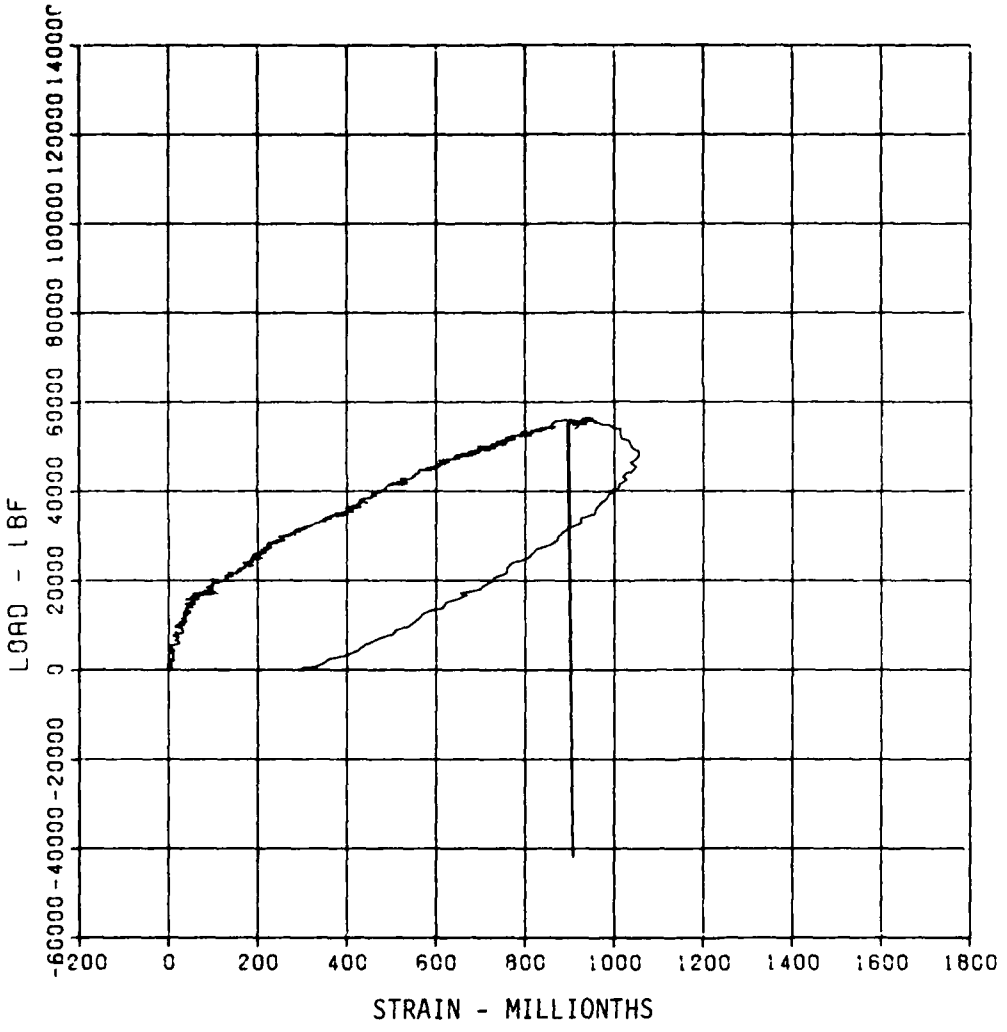

First test of C2

C2.1 61682
S-15

MAXIMUM	SIGMA CAL	CAL VAL
-1508.5489	3.7553	2803.7

CHANNEL NO. 6 8650 2
07/14/82 R0378

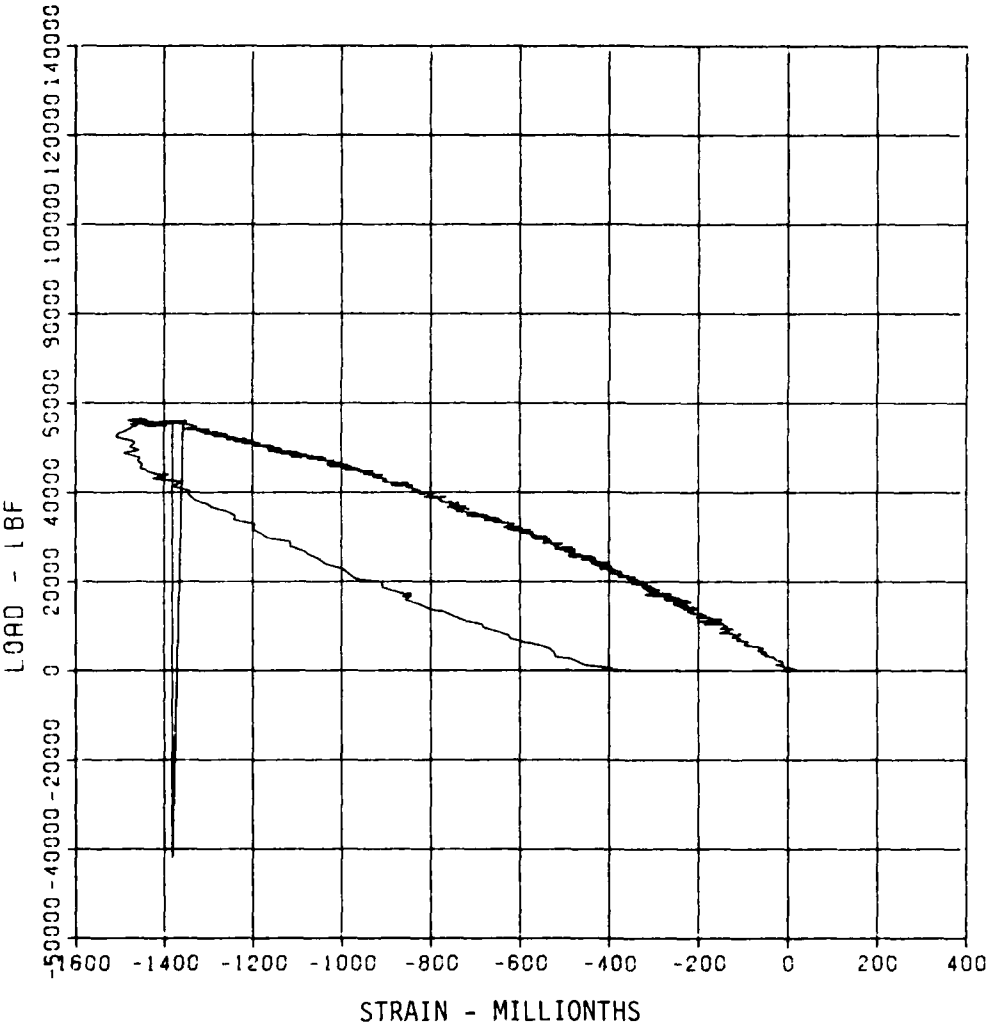

First test of C2

C2.1 61682
S-16

MAXIMUM	SIGMA CAL	CAL VAL
-1712.0630	2.8168	2899.7

CHANNEL NO. 5 8650 2
07/14/82 R0978

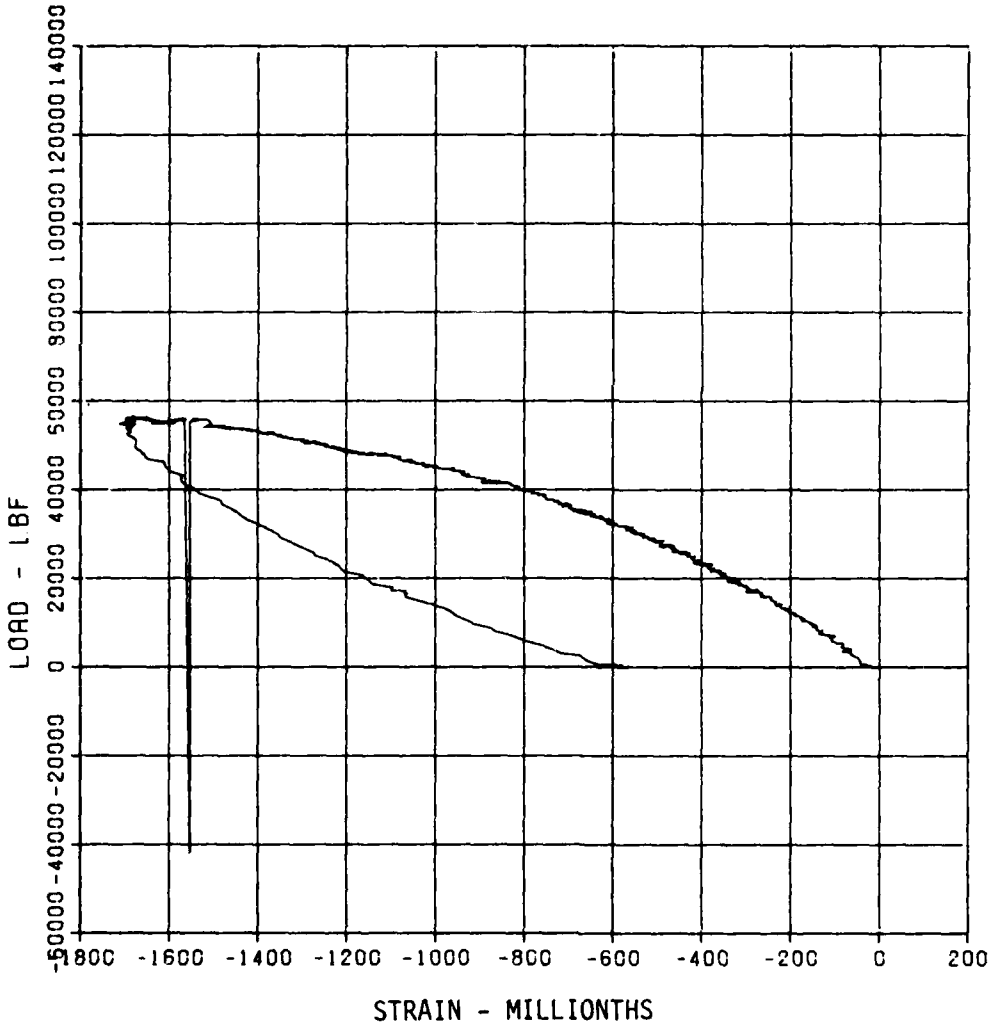

First test of C2

C2.2 61782
D-1

MAXIMUM	SIGMA CAL	CAL VAL
0.0052	4.9521	0.2

CHANNEL NO. 17 20167 1
07/16/82 R0094

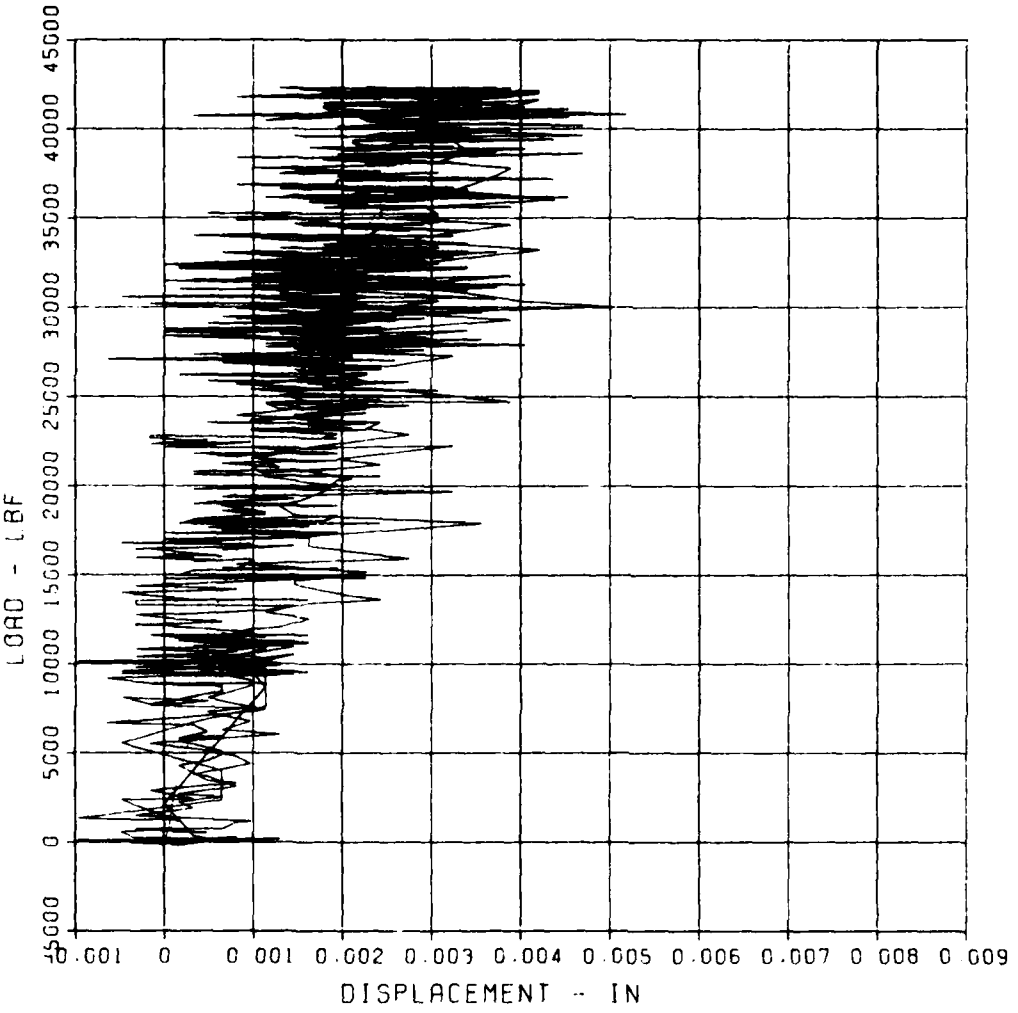

Second test of C2

C2.2 61782
D-3

MAXIMUM	SIGMA CAL	CAL VAL
-0.0049	4.6837	0.2

CHANNEL NO. 18 20167 1
07/16/82 R0094

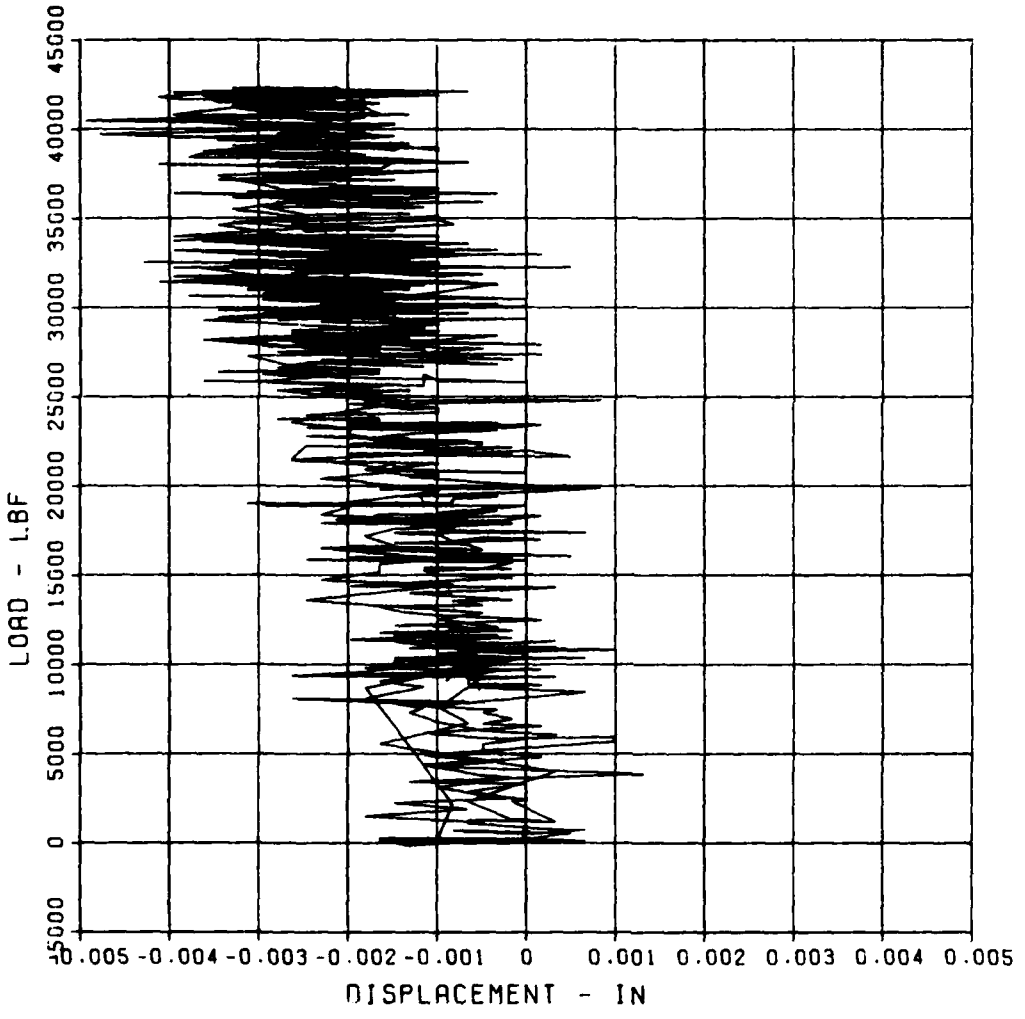

Second test of C2

C2.2 61782
S-2

MAXIMUM	SIGMA CAL	CAL VAL
-1050.2427	2.5361	2899.7

CHANNEL NO. 22 20167 1
07/16/82 R0094

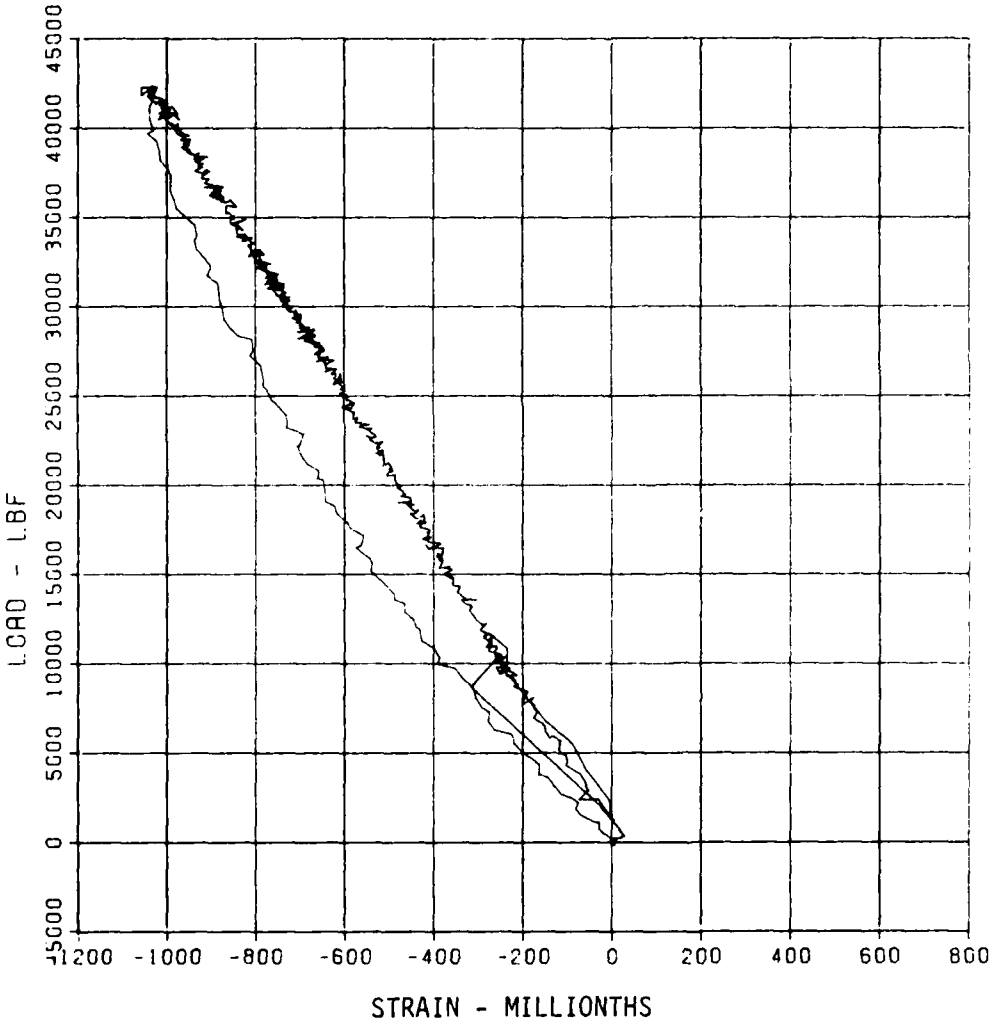

Second test of C2

C2.2 61782
S-4

MAXIMUM	SIGMA CAL	CAL VAL
729.2033	2.7453	2899.7

CHANNEL NO. 24 20167 1
07/19/82 R0149

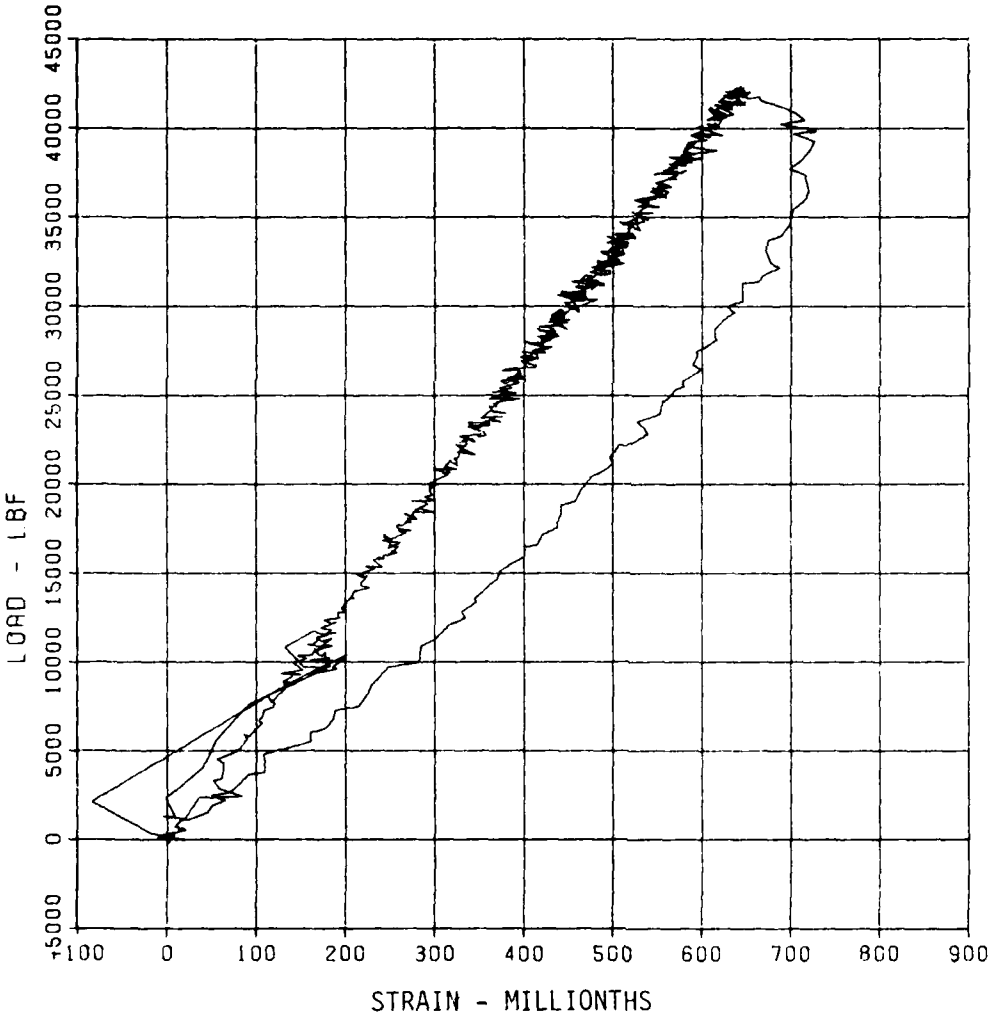

Second test of C2

C2.2 61782
S-5

MAXIMUM	SIGMA CAL	CAL VAL
76.0379	39.0282	583.3

CHANNEL NO. 25 20167 1
07/19/82 R0149

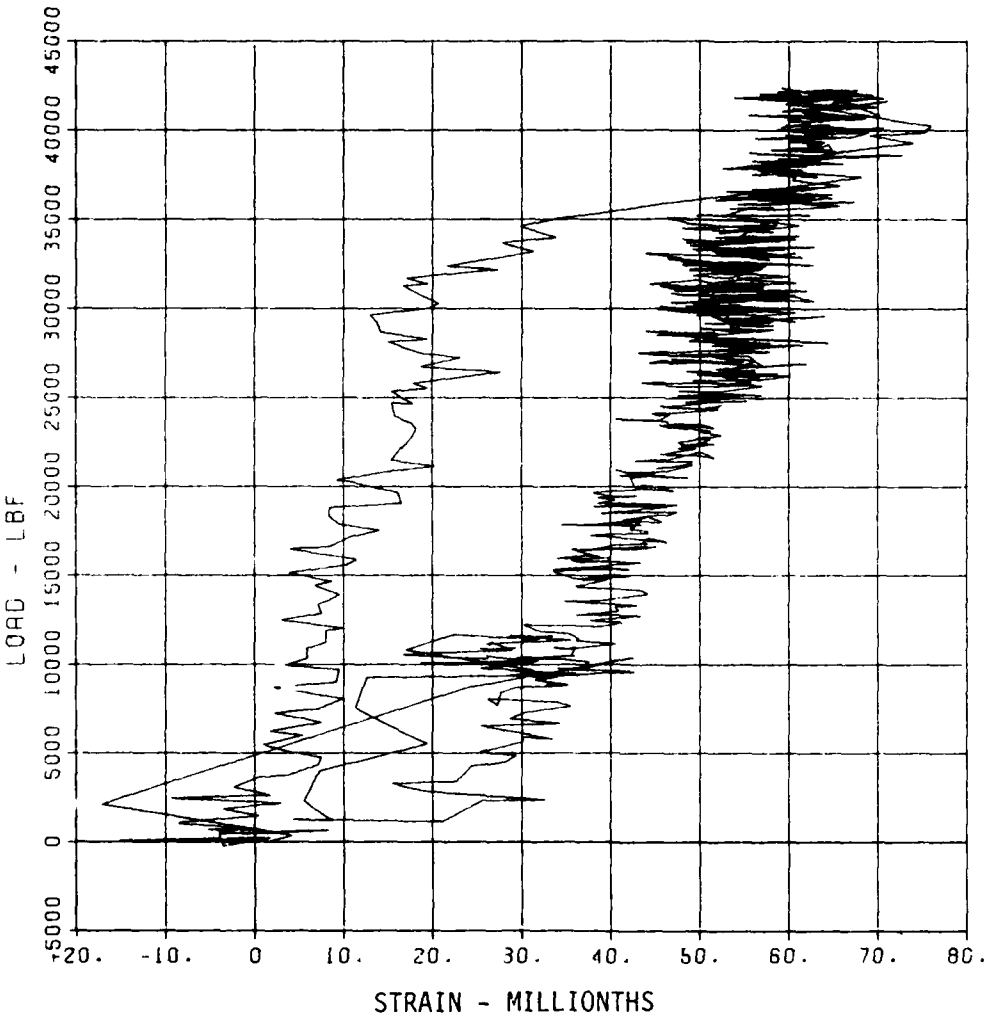

Second test of C2

C2,2 61782
S-6

MAXIMUM	SIGMA CAL	CAL VAL
-668.7272	3.3007	2899.7

CHANNEL NO. 26 20167 1
07/16/82 R0094

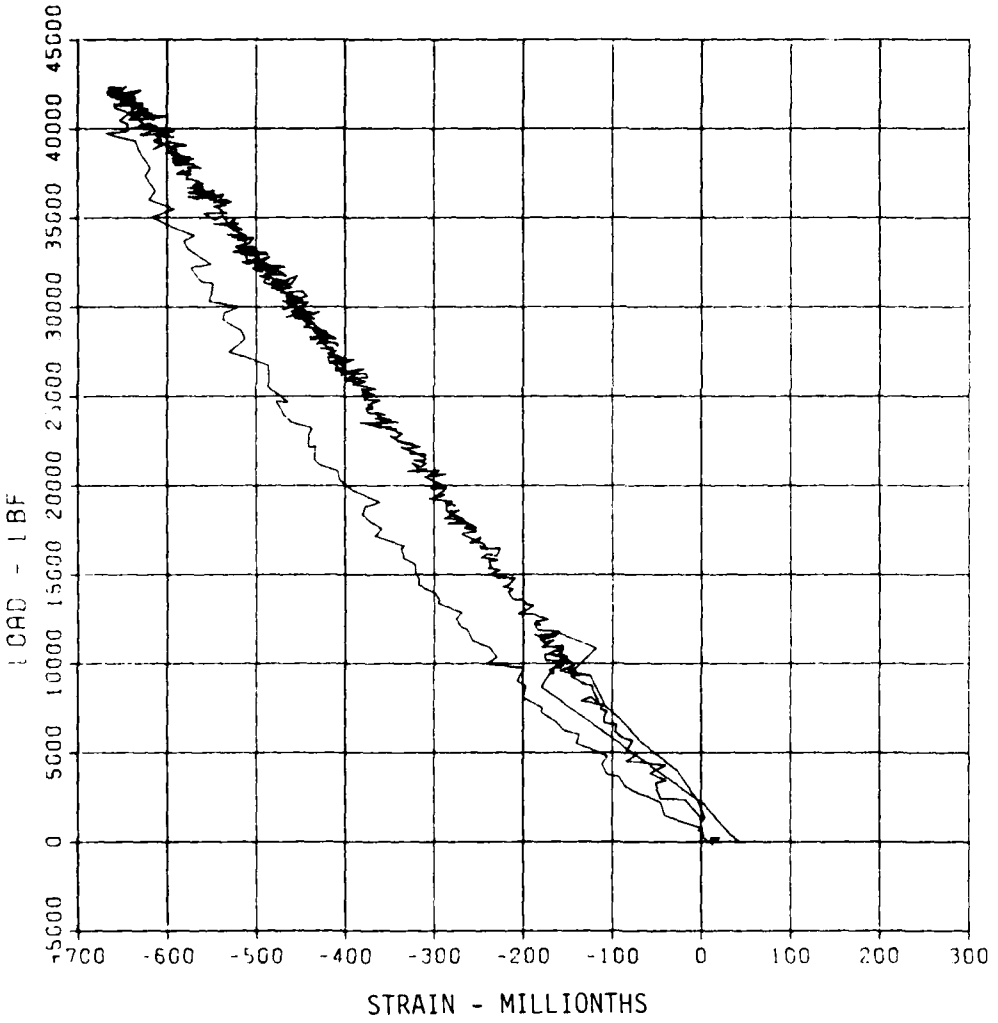

Second test of C2

C2.2 61782
S-7

MAXIMUM	SIGMA CAL	CAL VAL
876.2055	4.6109	2899.7

CHANNEL NO 27 20167
07/16/82 R0094

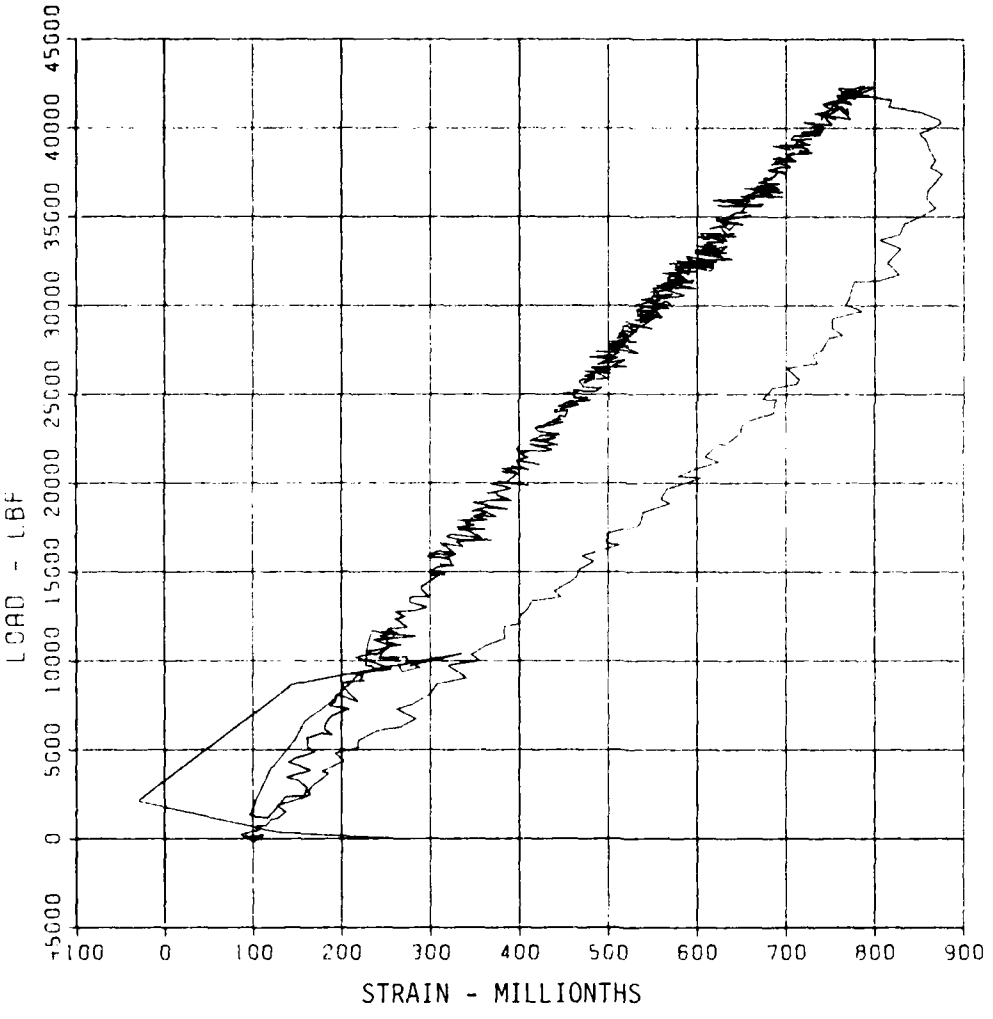

Second test of C2

C2.2 61782
S-8

MAXIMUM	SIGMA CAL	CAL VAL
28.0262	6.1000	583.3

CHANNEL NO. 28 20167 1
07/19/82 R0149

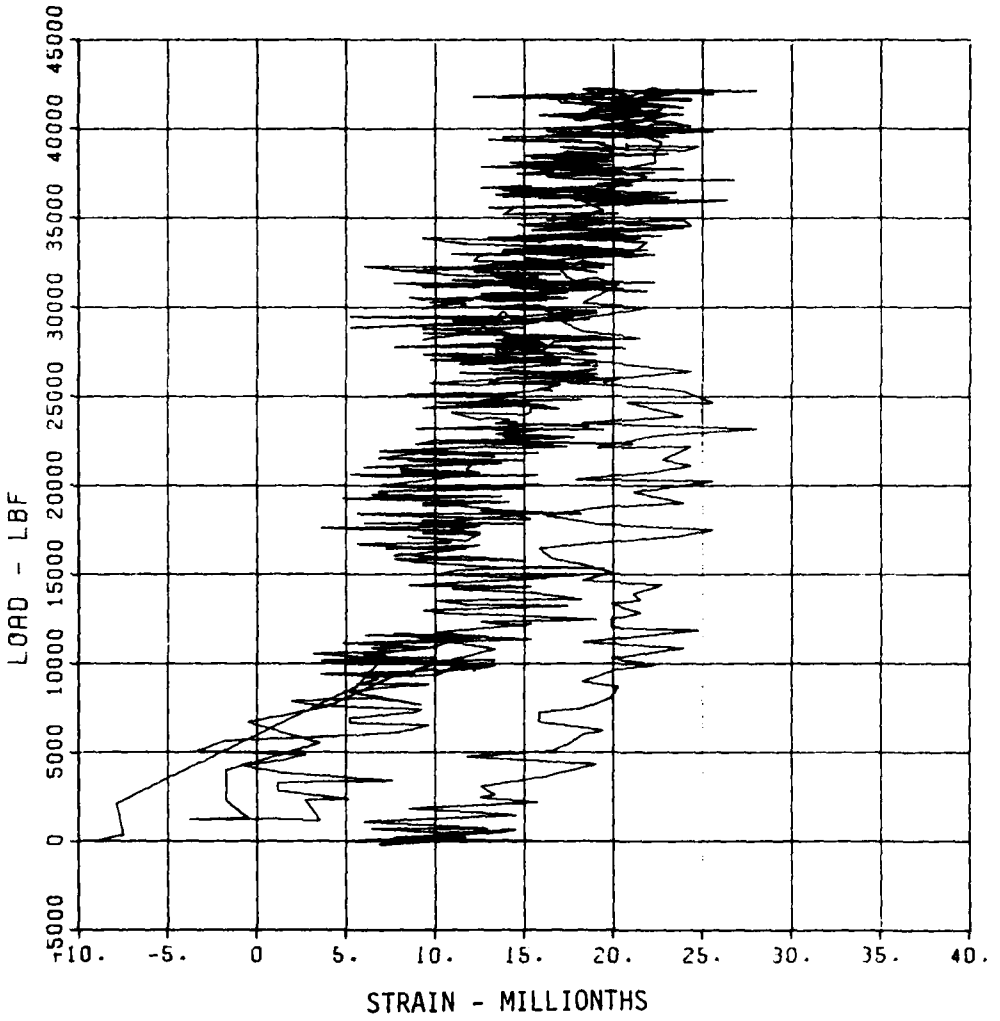

Second test of C2

C2.2 61782
S-10

MAXIMUM	SIGMA CAL	CAL VAL
495.0543	6.0903	2899.7

CHANNEL NO. 30 20167 1
07/16/82 R0094

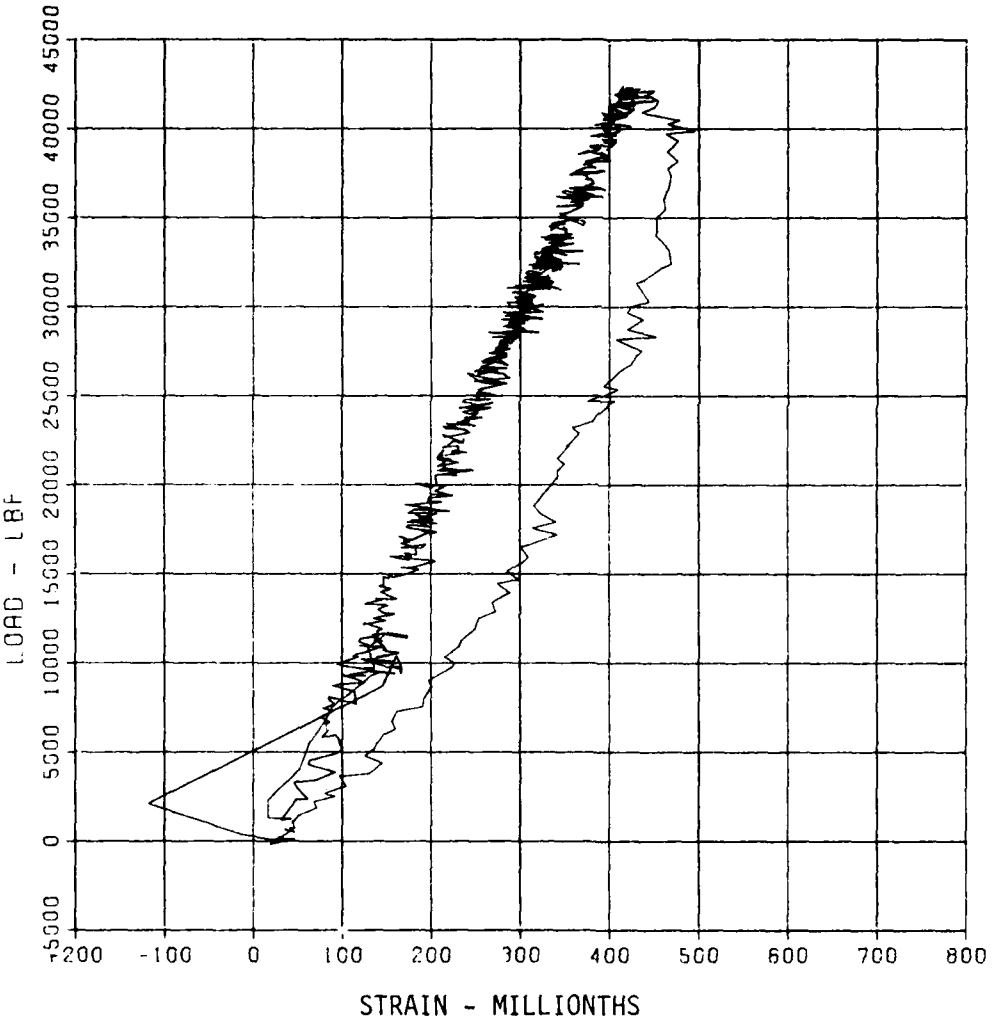

Second test of C2

C2.2 61782
S-11

MAXIMUM	SIGMA CAL	CAL VAL
-687.7310	2.6833	2899.7

CHANNEL NO. 1 20167 2
07/16/82 R0094

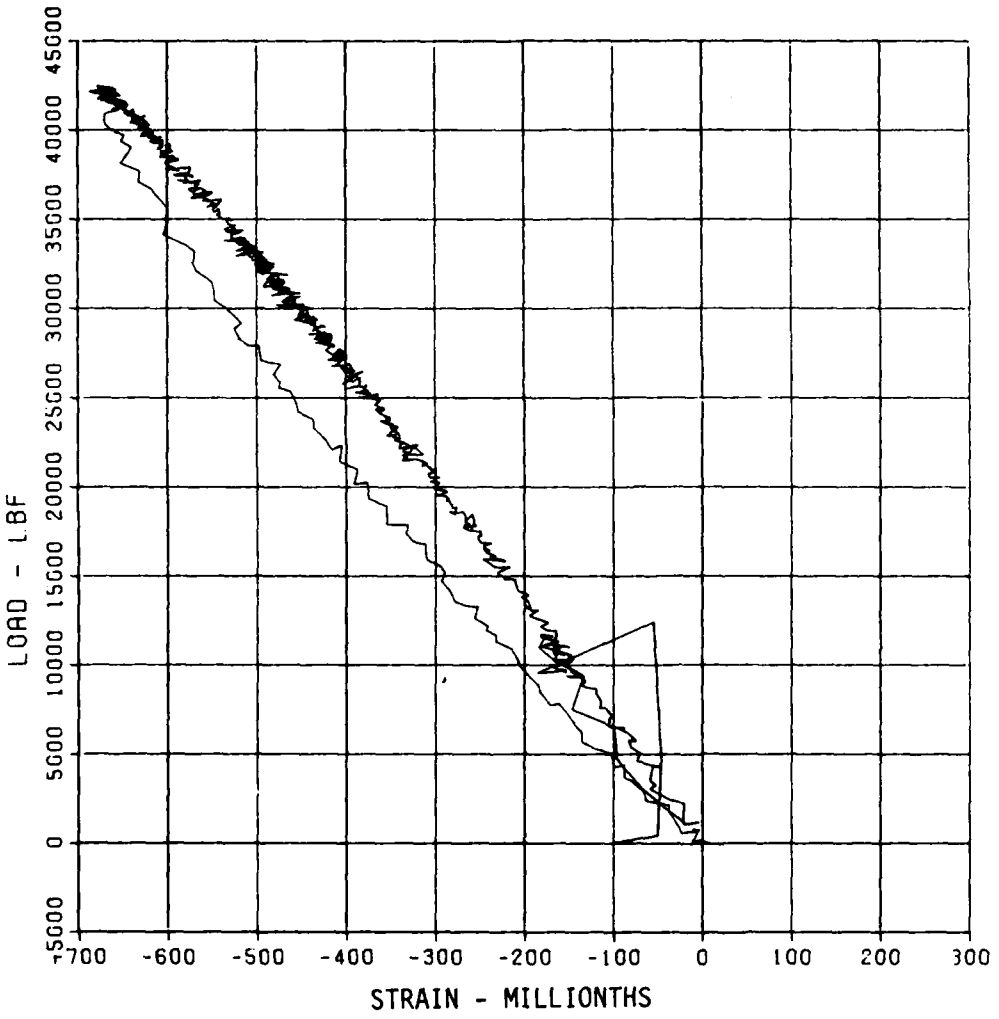

Second test of C2

C2.2 61782
S-12

MAXIMUM	SIGMA CAL	CAL VAL
-914.8262	3.6070	2899.7

CHANNEL NO. 2 20167 2
07/16/82 R0094

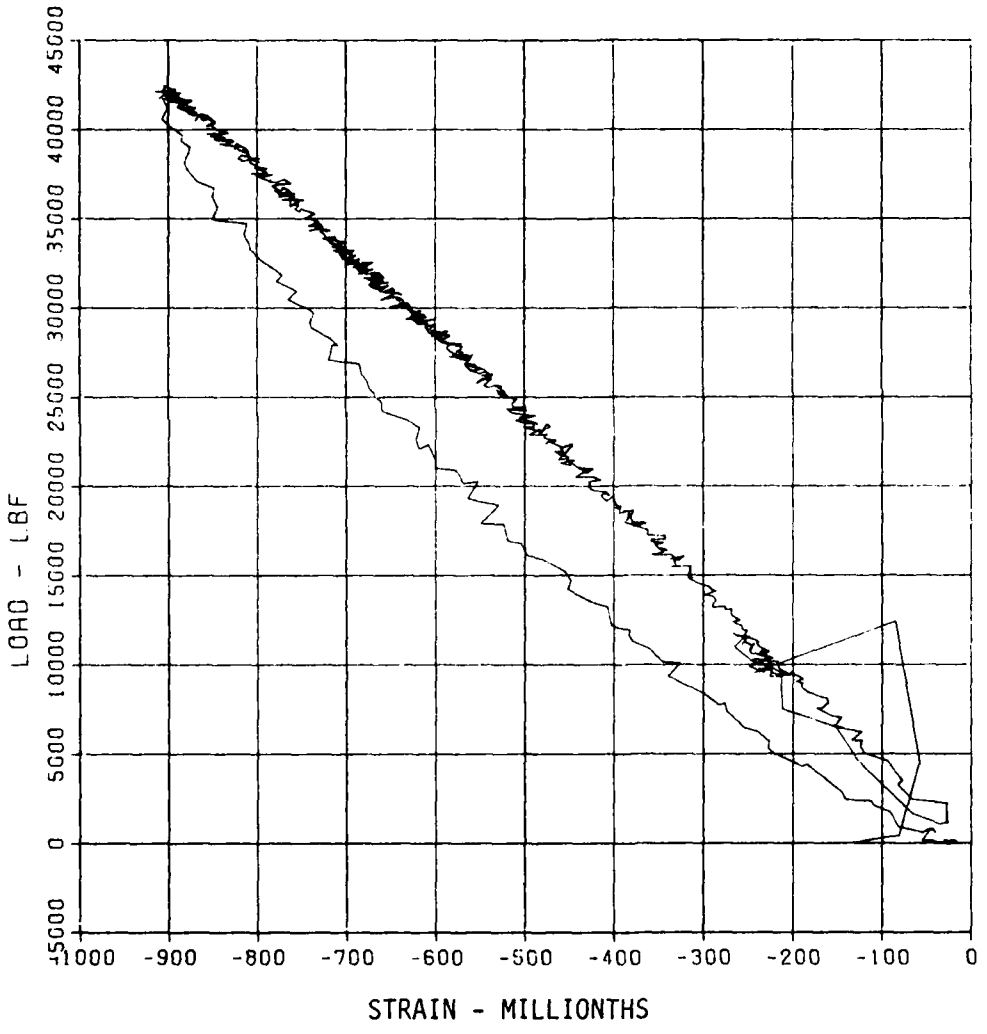

Second test of C2

C2.2 61782
S-14

MAXIMUM	SIGMA CAL	CAL VAL
660.2235	5.7930	2899.7

CHANNEL NO. 4 20167 2
07/16/82 R0094

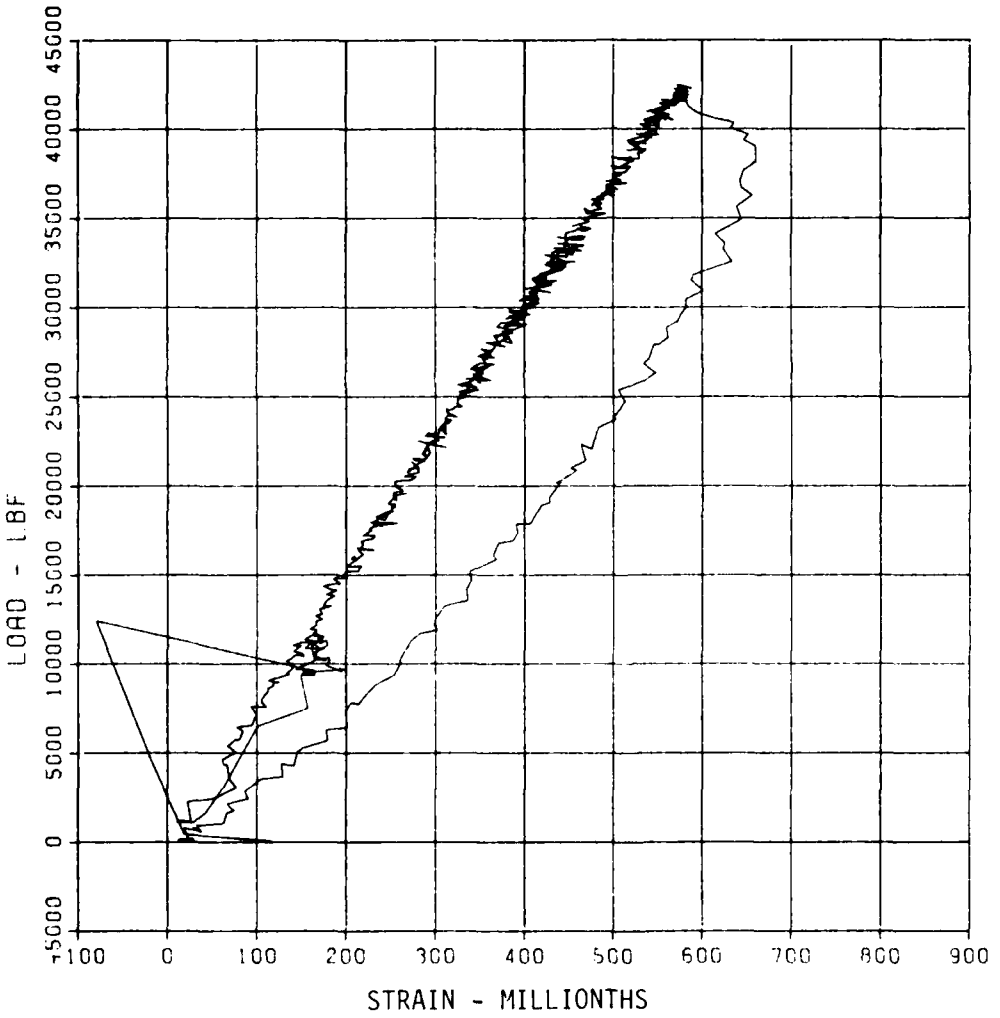

Second test of C2

C2,2 61782
S-15

MAXIMUM	SIGMA CAL	CAL VAL
-936.3574	3.3651	2899.7

CHANNEL NO. 5 20167 2
07/16/82 R0094

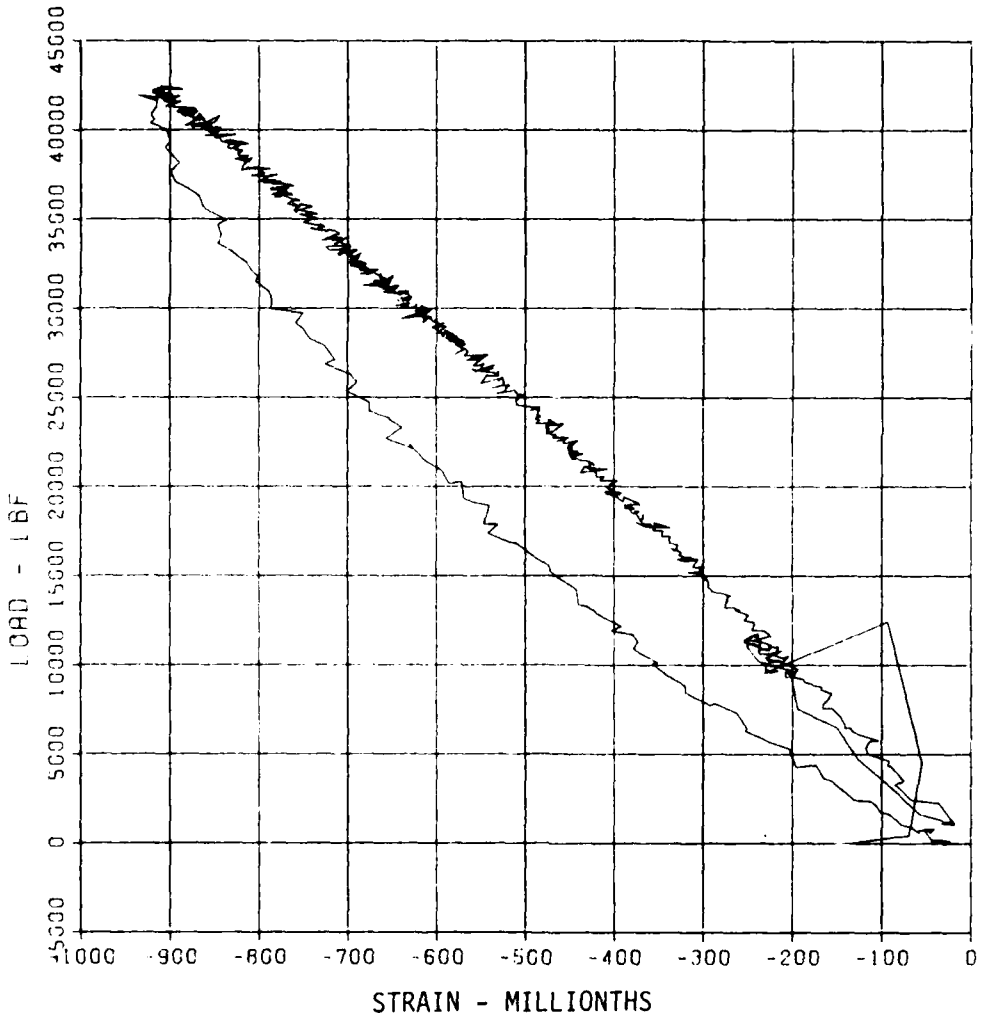

Second test of C2

C2.2 61782
S-16

MAXIMUM	SIGMA CAL	CAL VAL
-951.7065	5.4423	2899.7

CHANNEL NO. 6 20167 2
07/16/82 R0094

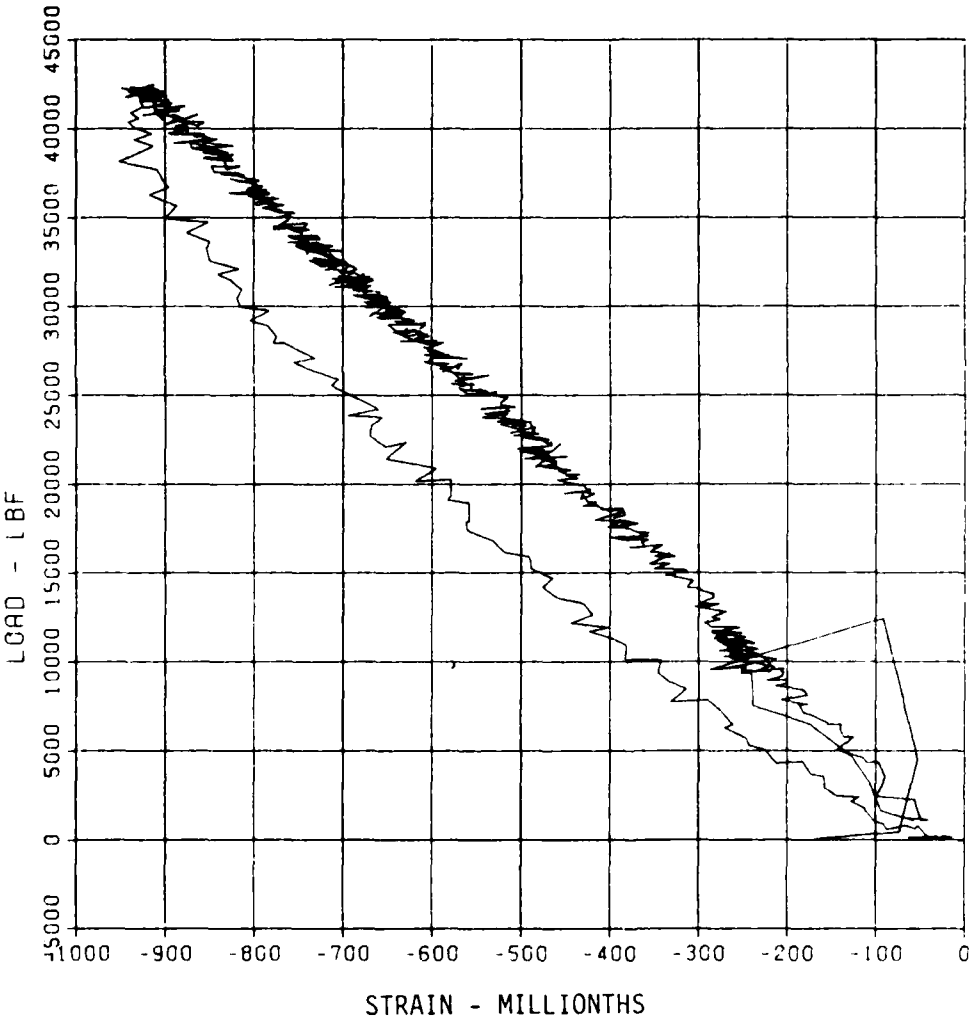

Second test of C2

C3.1 61862
D-1
MAXIMUM 0.0369 SIGMA CAL 4.0575 CAL VAL 0.2
CHANNEL NO 17 933 1
05/10/93 R0391

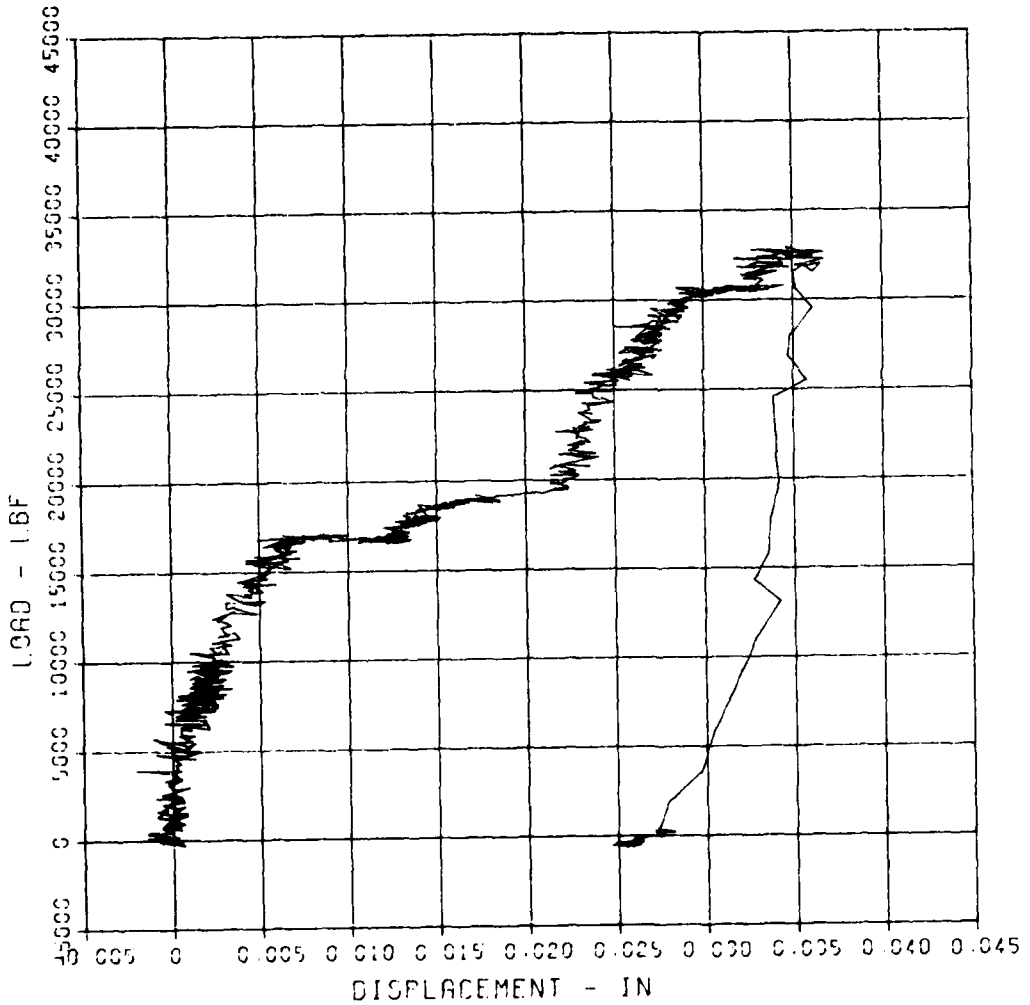

First test of C3

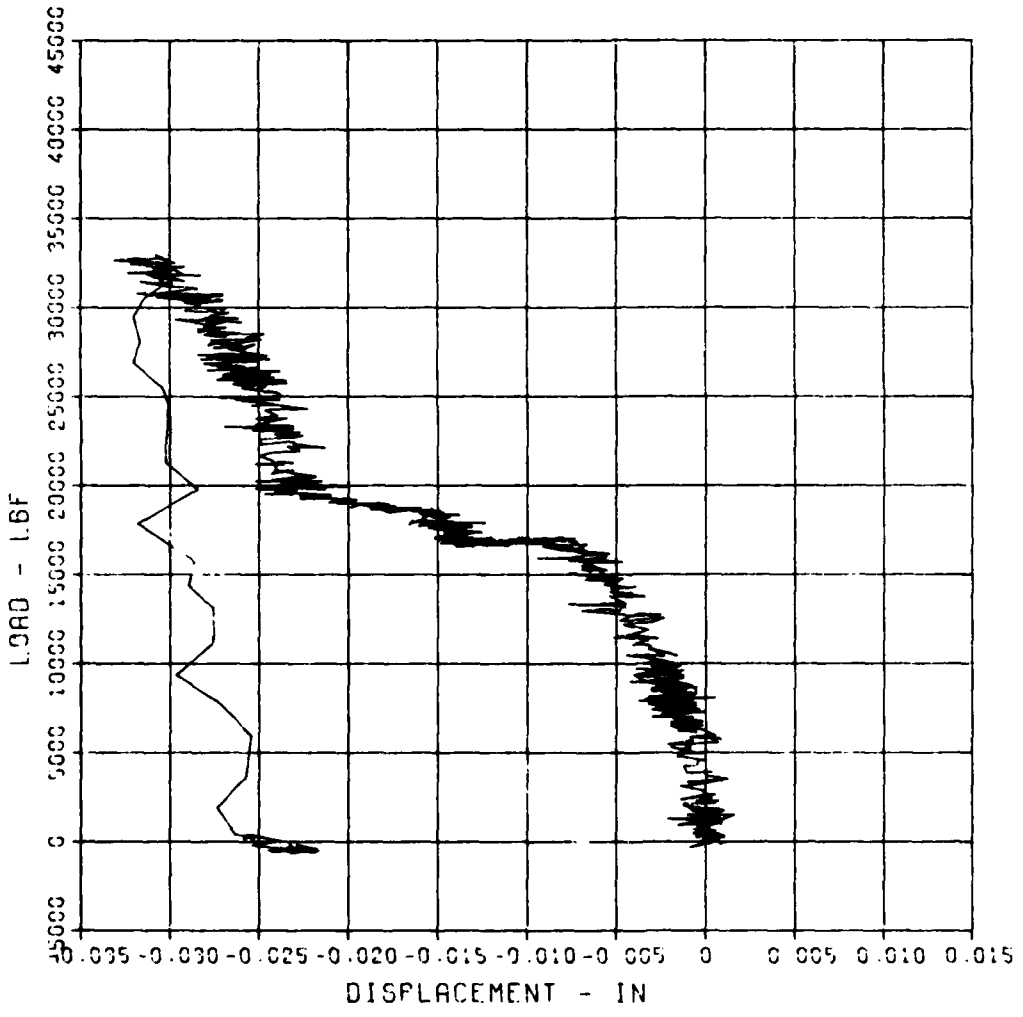

First test of C3

C3.1 51882
S-1
MAXIMUM SIGMA CAL CAL VAL
-4155.5037 3.1430 2893.7

CHANNEL NO. 21 803 1
05/10/93 R030:

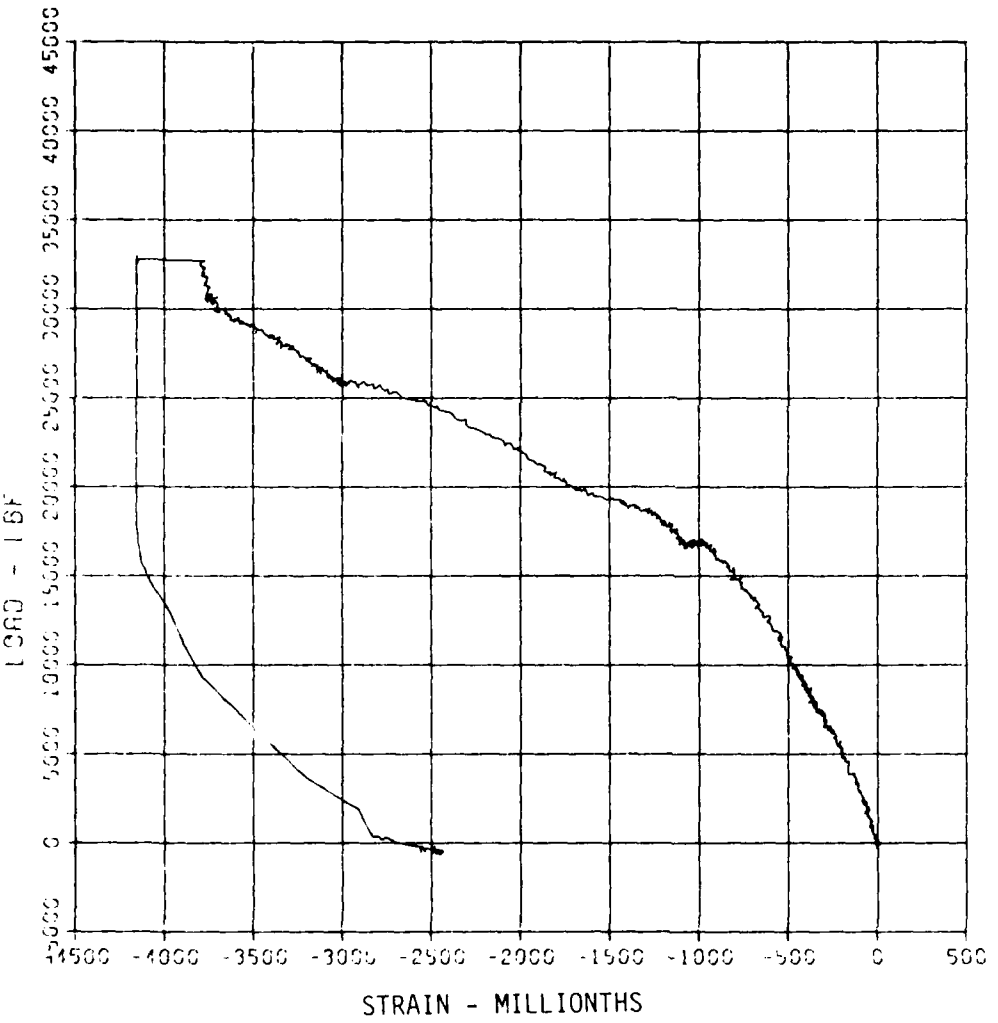

First test of C3

C3.1 61882
S-2
MAXIMUM -4145.8720 SIGMA CAL 2.6273 CAL VAL 2993.7

CHANNEL NO. 22 893 1
05/10/93 R0391

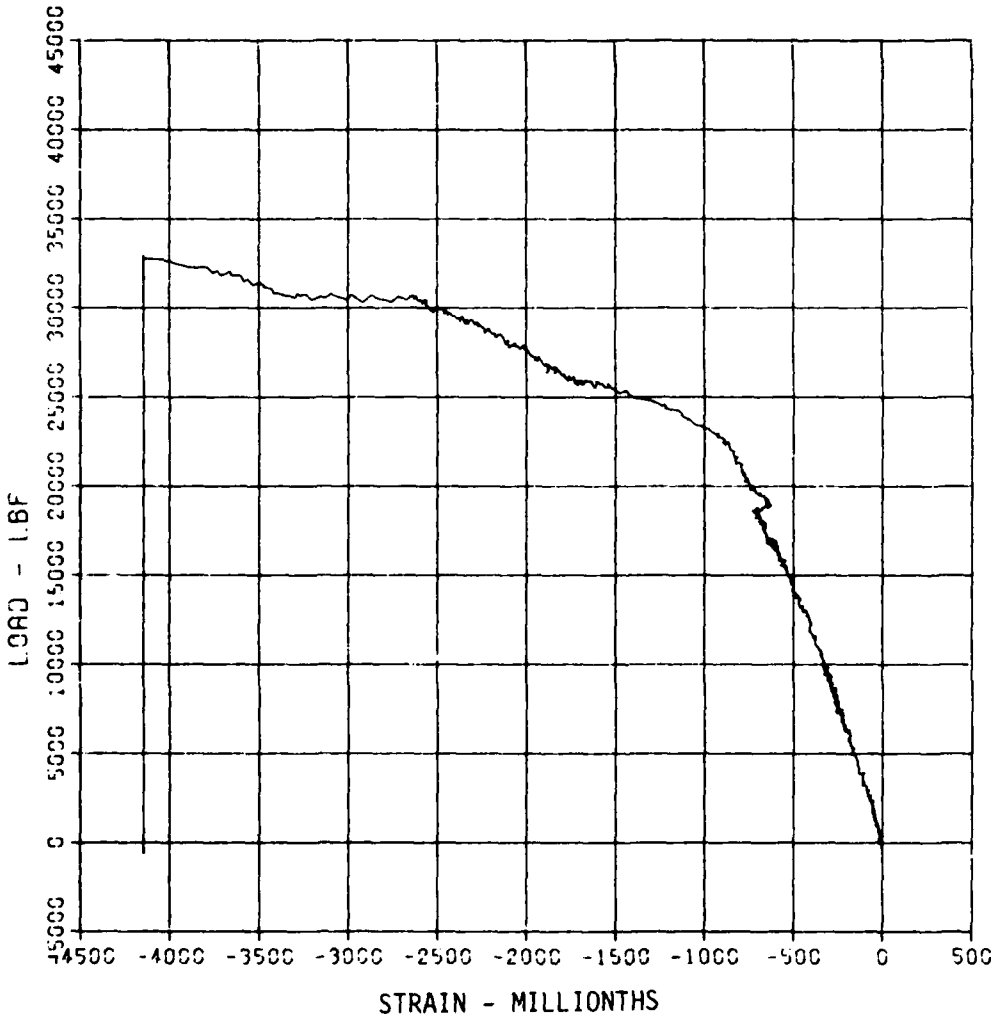

First test of C3

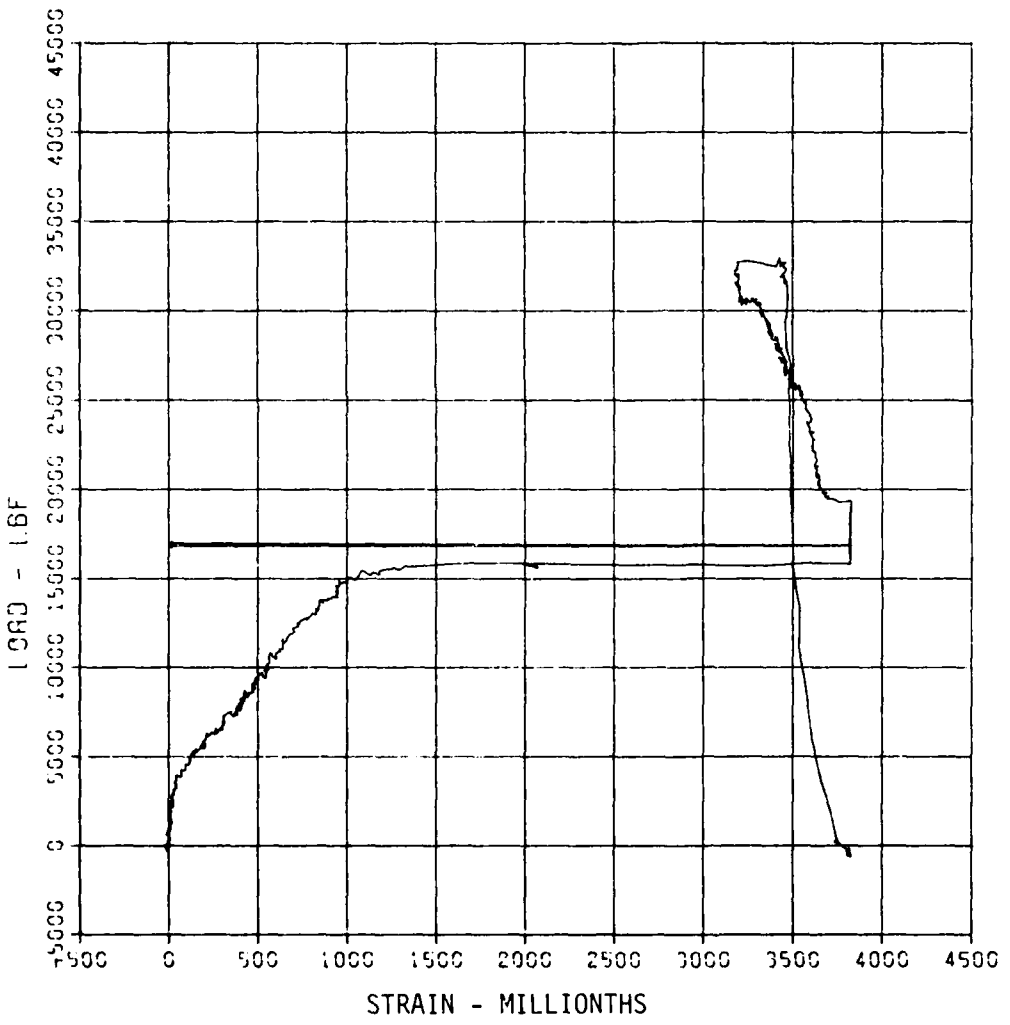

First test of C3

C3.1 61882
S-4
MAXIMUM 3367.8137 SIGMA CAL 2.5433 CAL VAL 2000.7
CHANNEL NO. 24 903 1
05/10/93 R0301

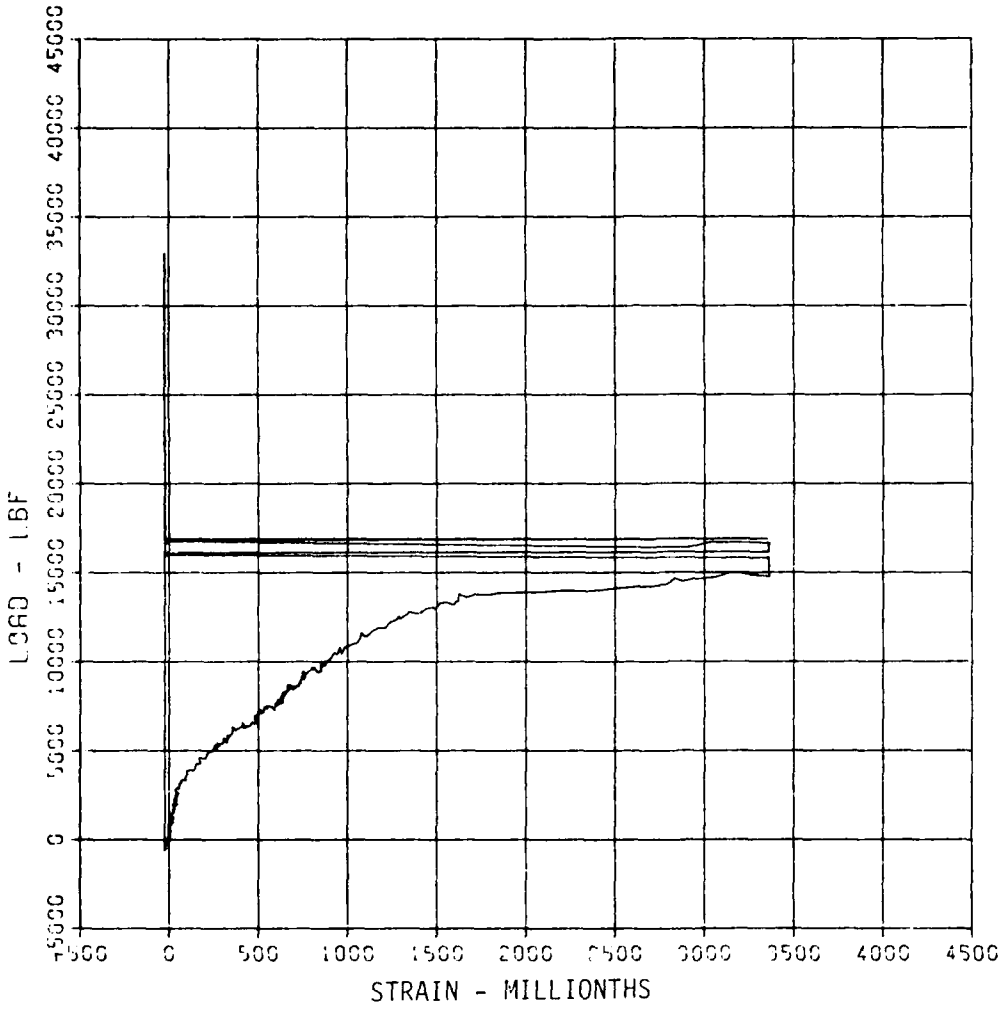

First test of C3

C3.1 61882
S-5

MAXIMUM	SIGMA CAL	CAL VAL
716.0520	39.4235	583.3

CHANNEL NO. 25 003 1
05/10/93 R0391

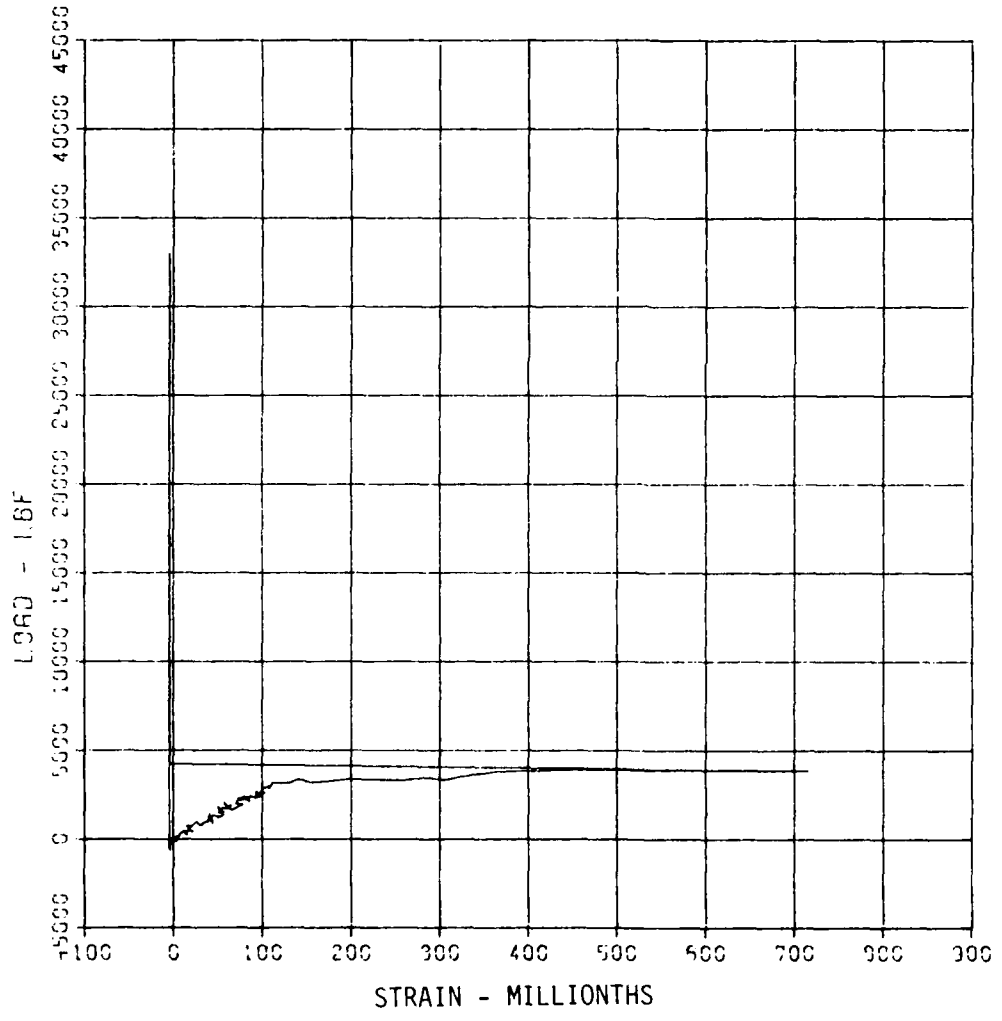

First test of C3

C3.1 61882
S-6
MAXIMUM SIGMA CAL CAL VAL
-3305.3063 2.0000 2800.7

CHANNEL NO 26 893 1
05/10/93 R0391

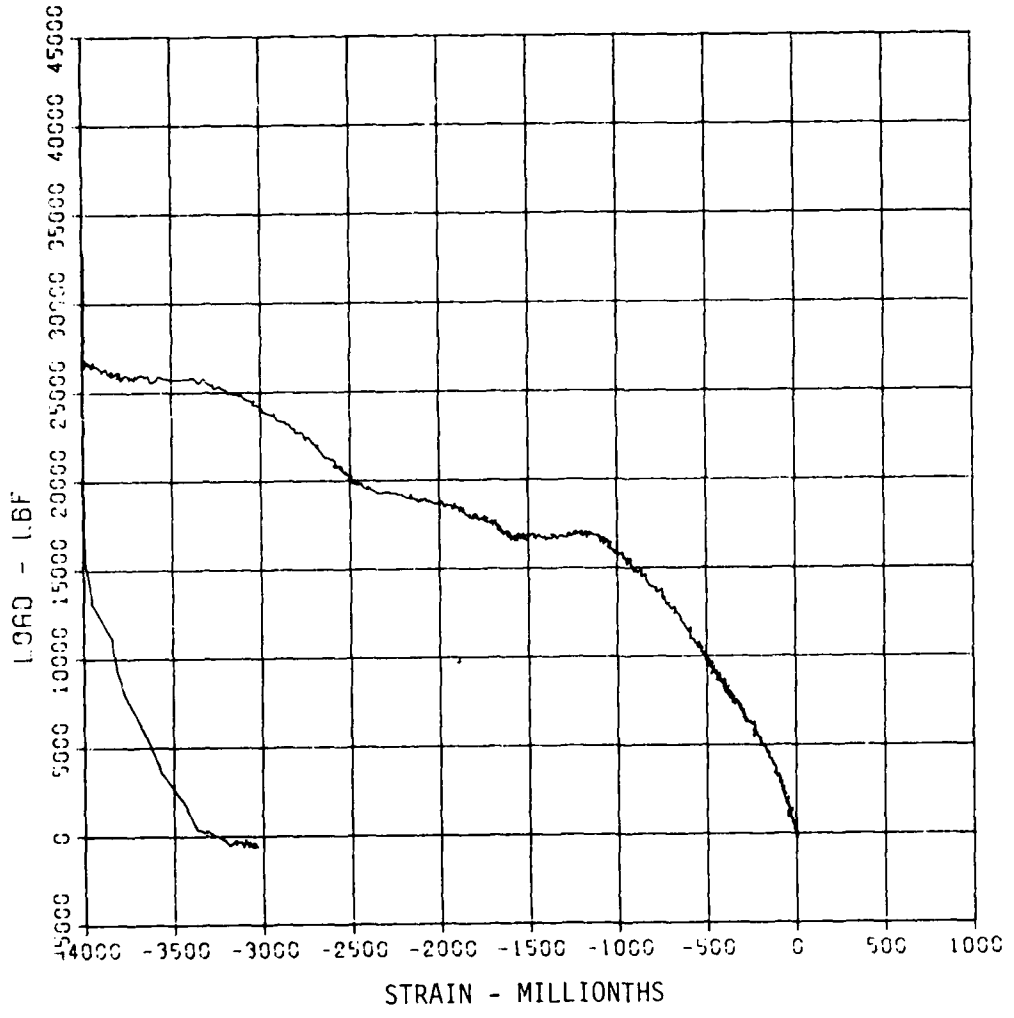

First test of C3

C3.1 61882
S-7
MAXIMUM SIGMA CAL CAL VAL
-1977.6801 3.4550 2000.7

CHANNEL NO 27 903 1
05/10/93 R0301

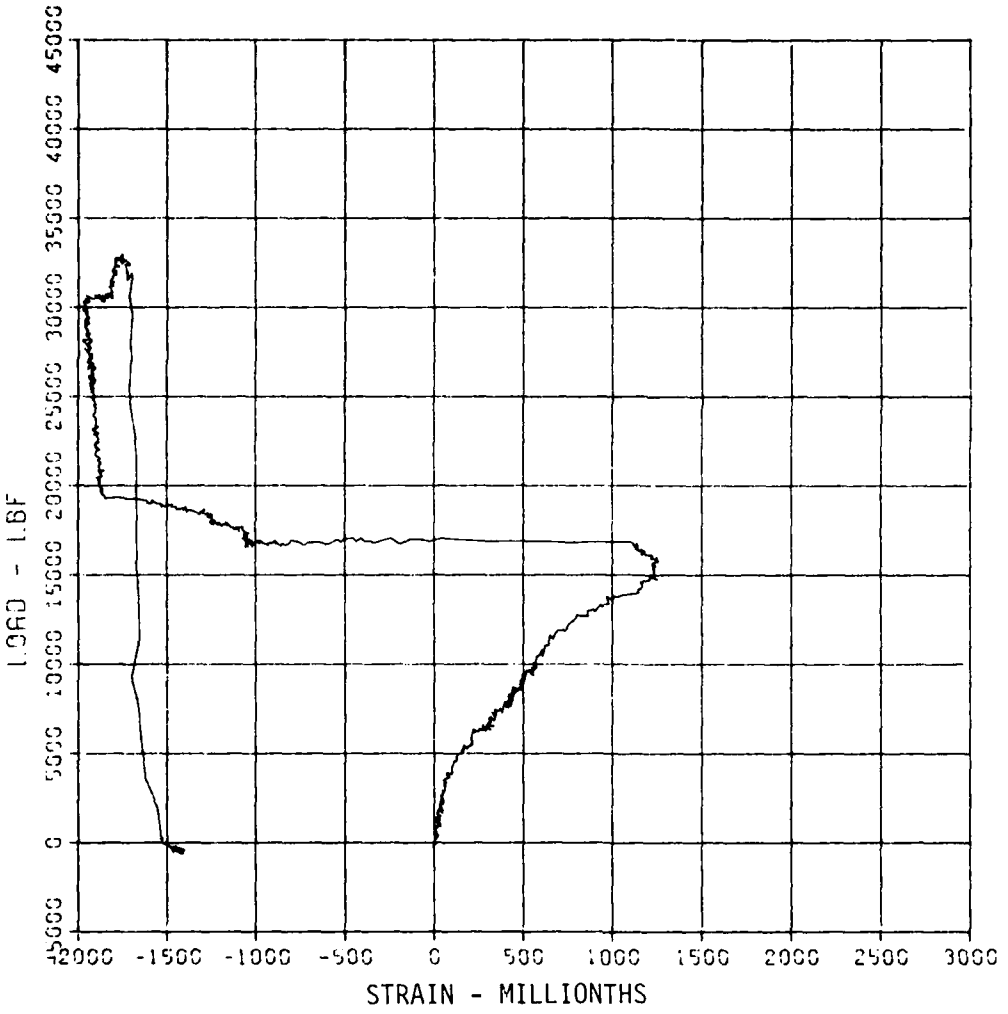

First test of C3

C3.1 61862
S-8

MAXIMUM	SIGMA CAL	CAL VAL
709.6976	5.9364	593.3

CHANNEL NO 28 893 1
05/10/93 R0301

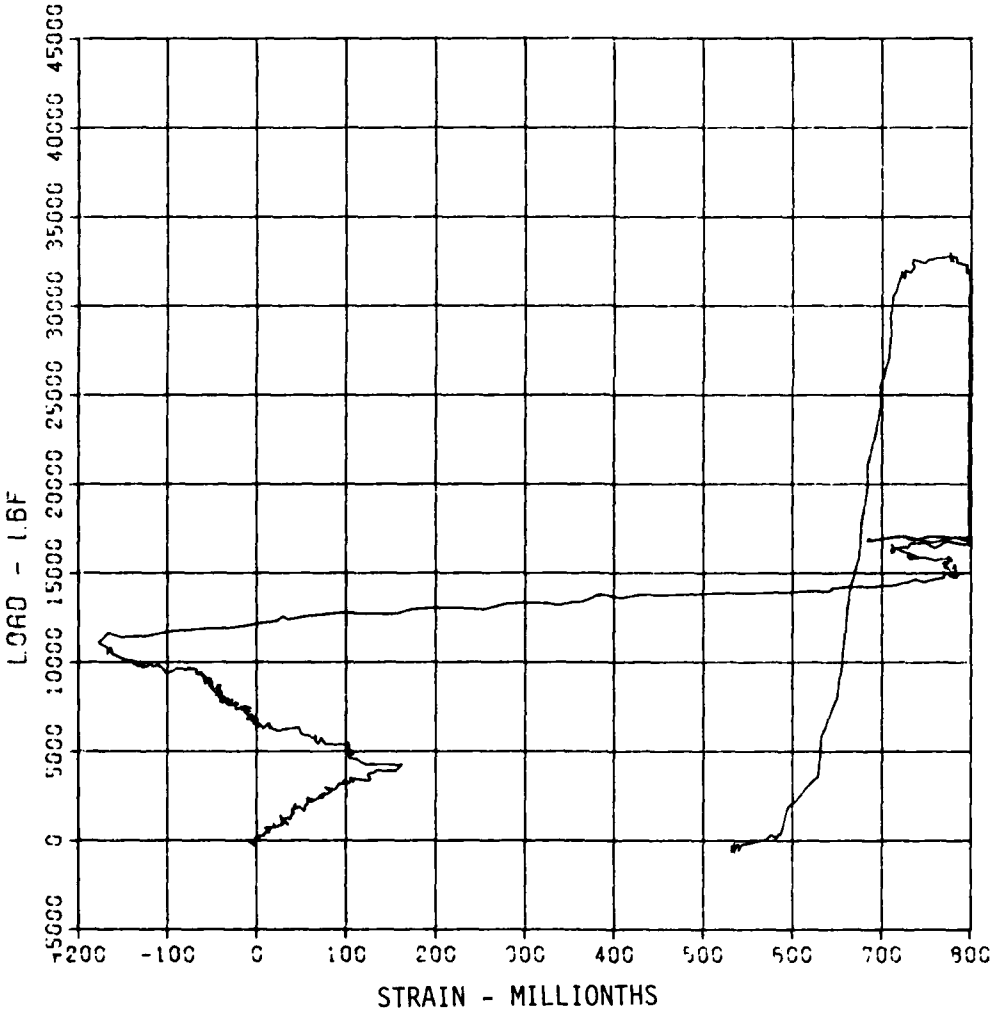

First test of C3

C3.1 61882
S-9
MAXIMUM 4050.4507 SIGMO CAL 2.5060 CAL VAL 2800.7

CHANNEL NO 20 803 1
05/10/83 R0301

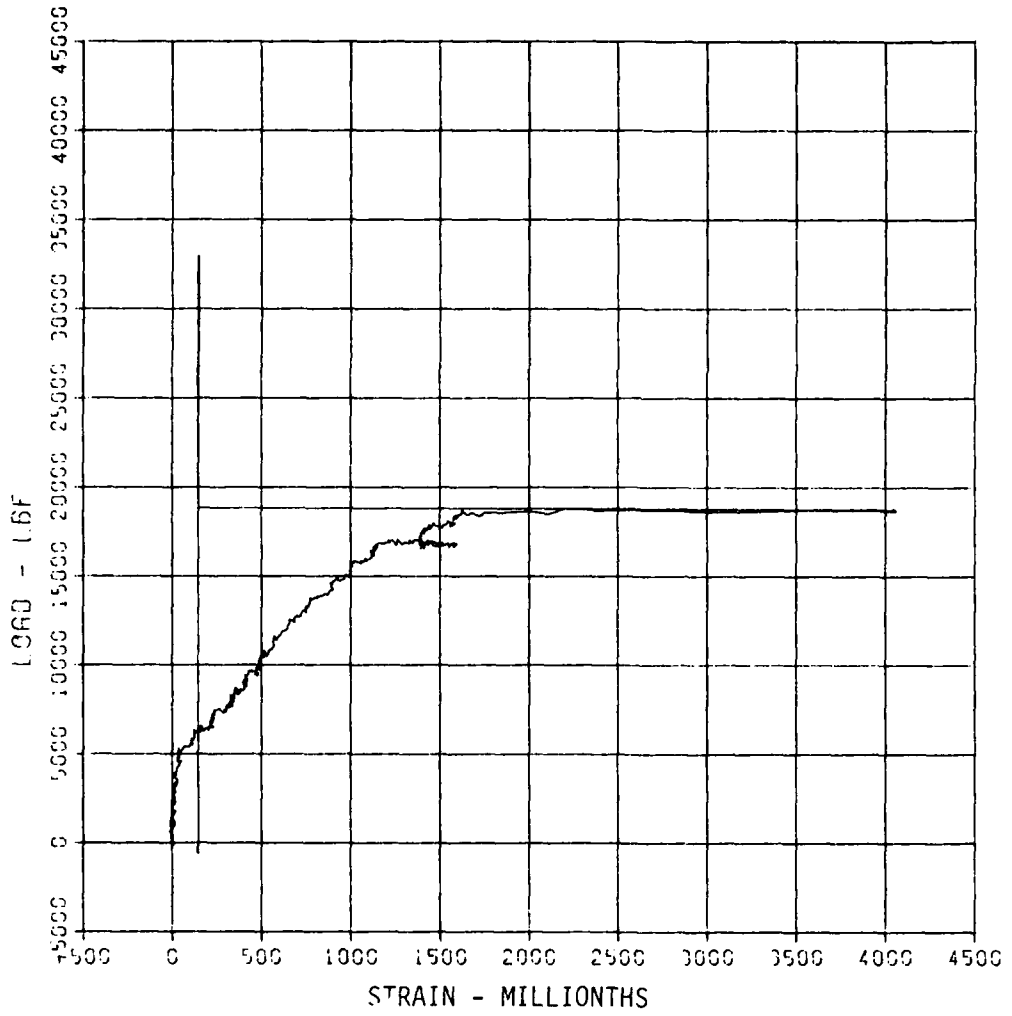

First test of C3

C3.1 61862
S-10
MAXIMUM 3924.5519 SIGMS CAL 2.9465 CAL VAL 2800.7

CHANNEL NO. 30 903 1
05/10/93 R0301

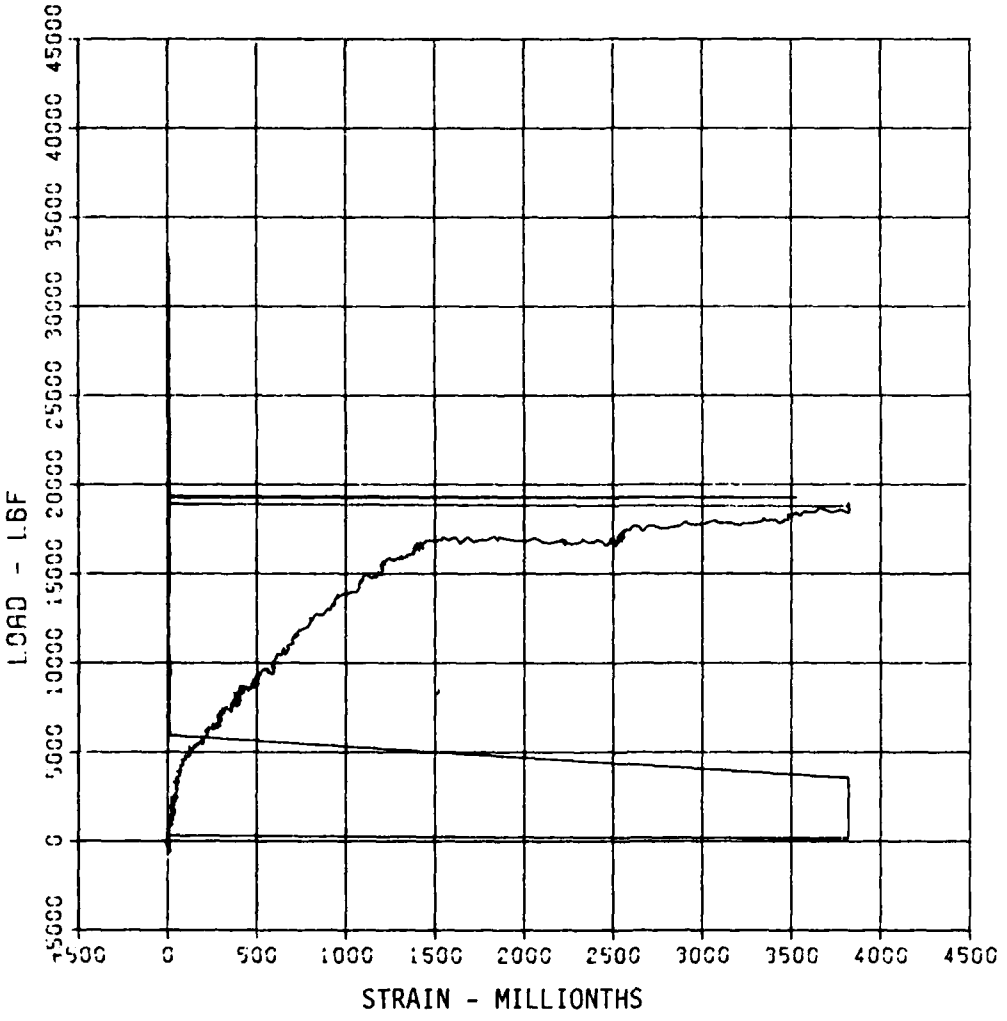

First test of C3

C3-1 61862
S-11
MAXIMUM SIGMS CAL CAL VAL
-3557.4834 5.2258 2303.7

CHANNEL NO . 3086 :
05/02/86 80306

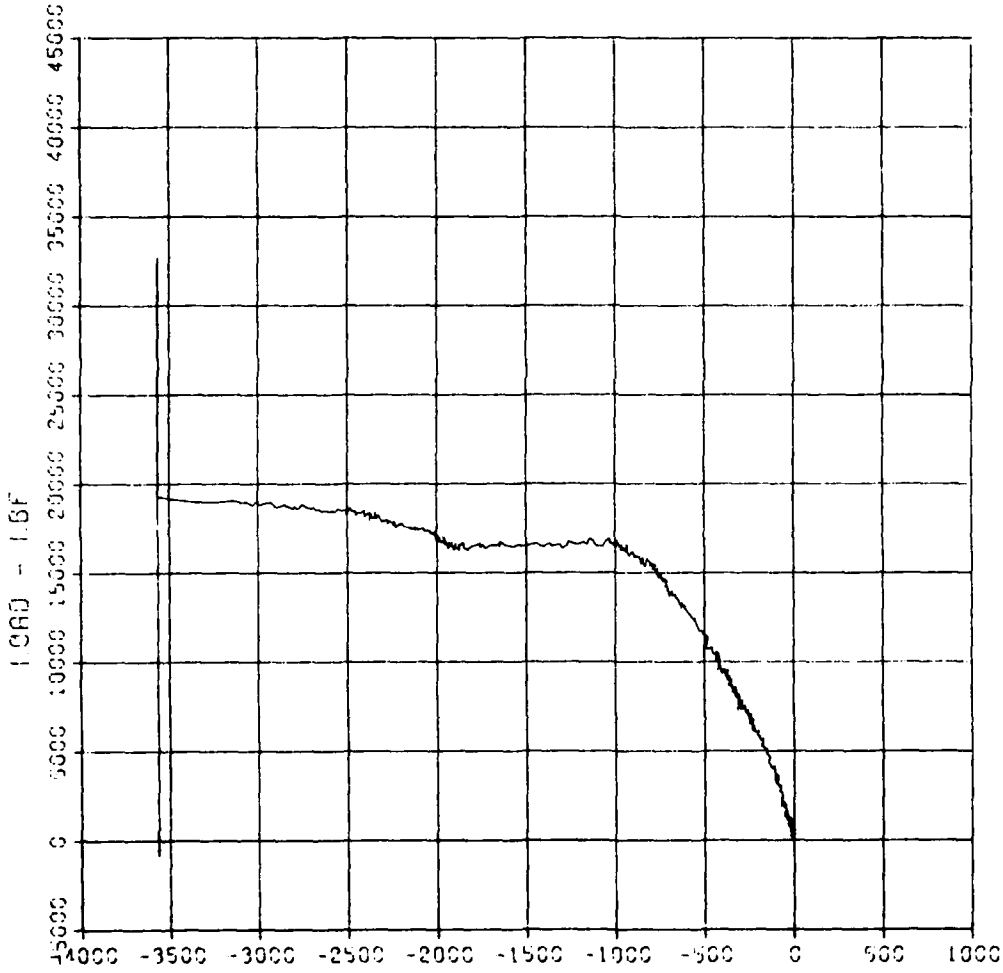

First test of C3

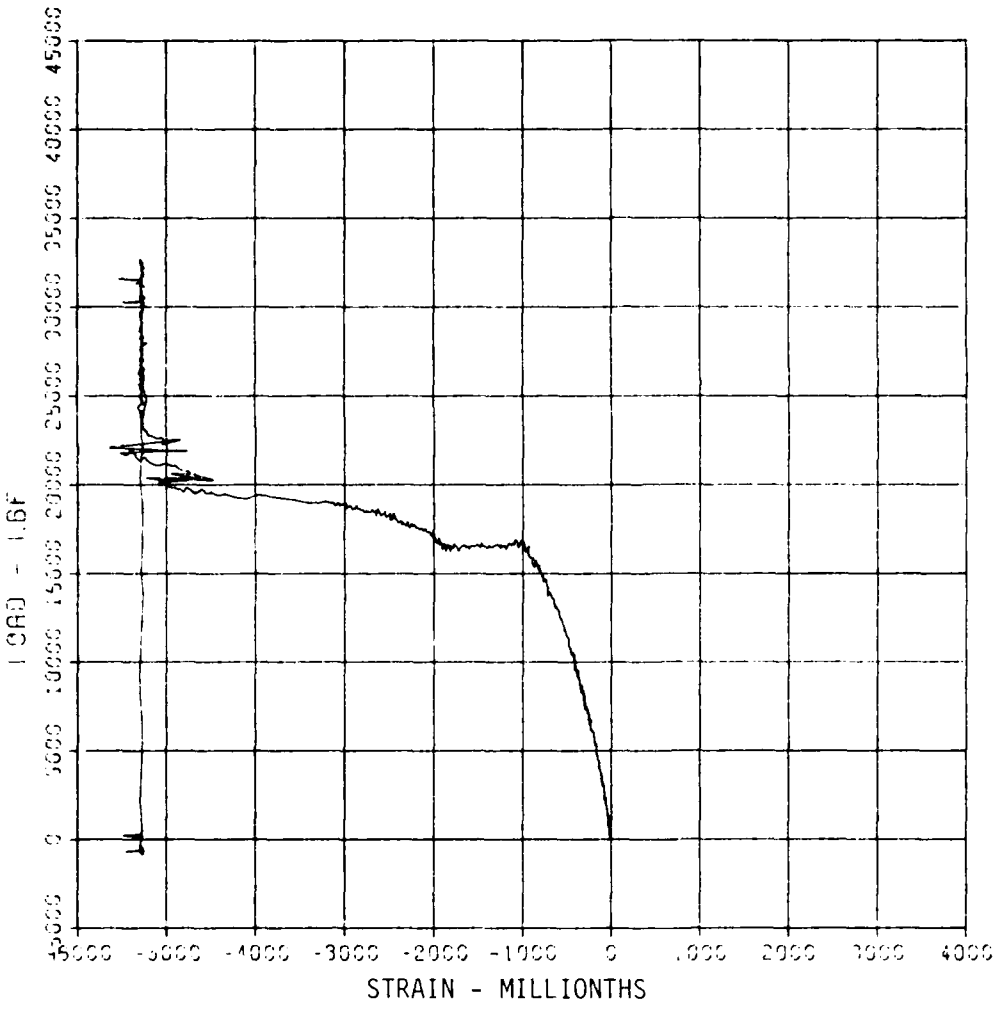

First test of C3

C3.1 61882
S-13
MAXIMUM SIGMS CAL CAL VAL
-2543.1487 3.4499 2893.7

CHANNEL NO 3 3085 1
05/02/85 R0306

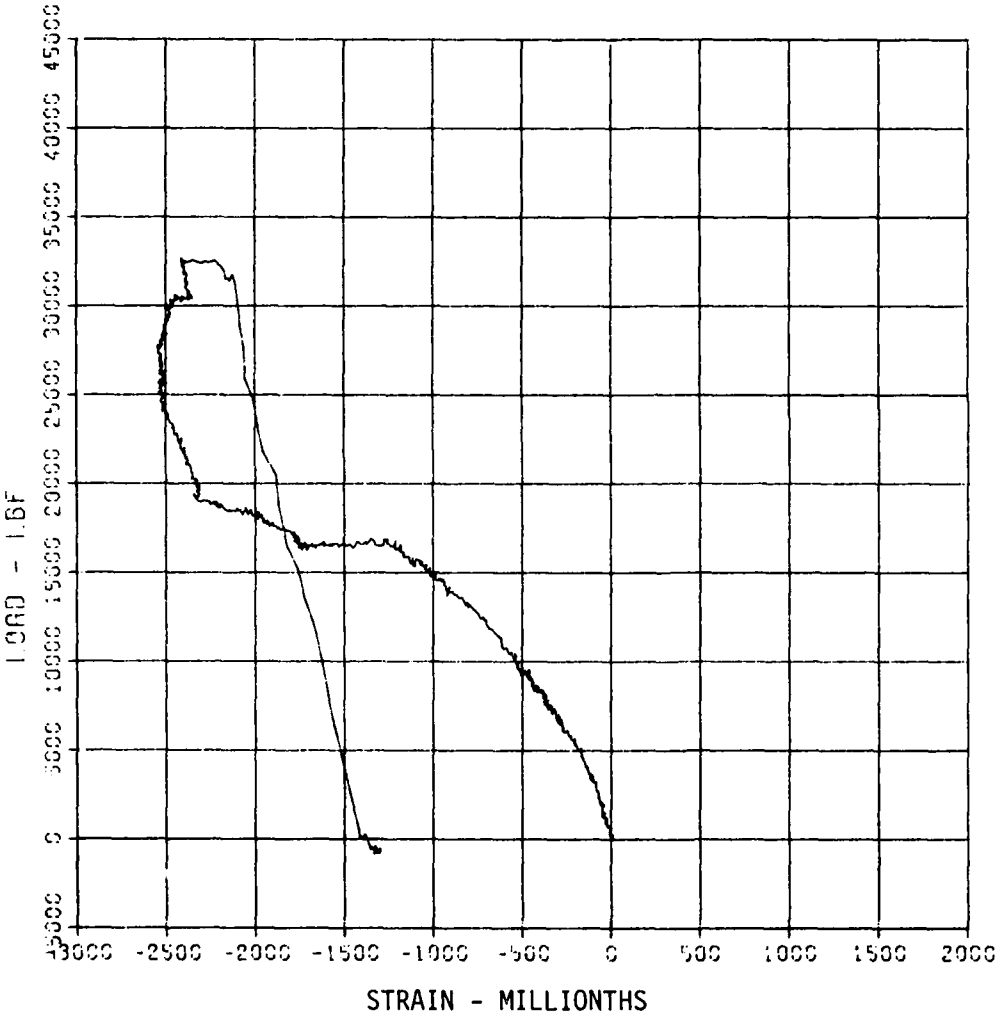

First test of C3

C3.1 61882
S-16
MAXIMUM SIGMS CAL CAL VAL
-4438.6120 1.0374 2803.7

CHANNEL NO. 6 3065 1
05/02/83 R0305

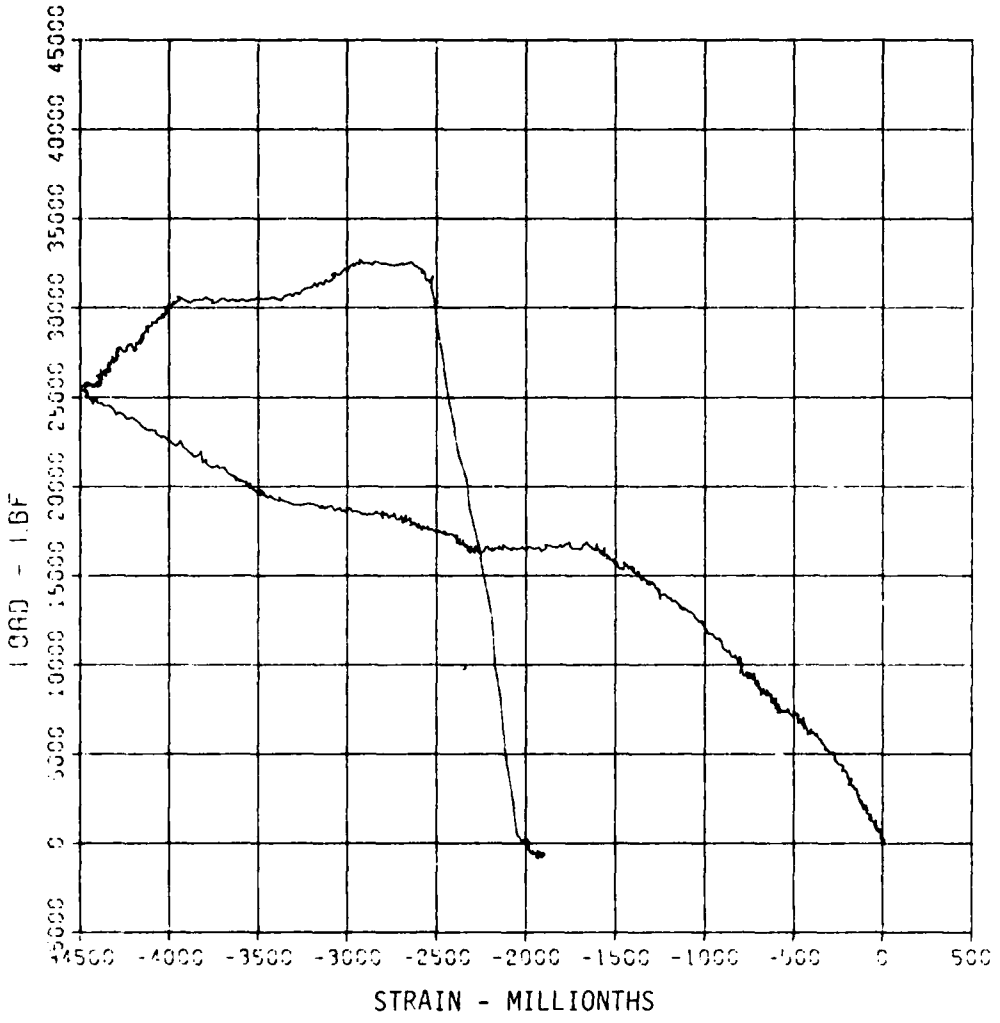

First test of C3

C3,1 61882
LOAD VS. STRAINS

INTRADOS STEEL STRAIN
R/C CIRCULAR CONDUIT TESTS.

08/13/82 0463E P1308.20

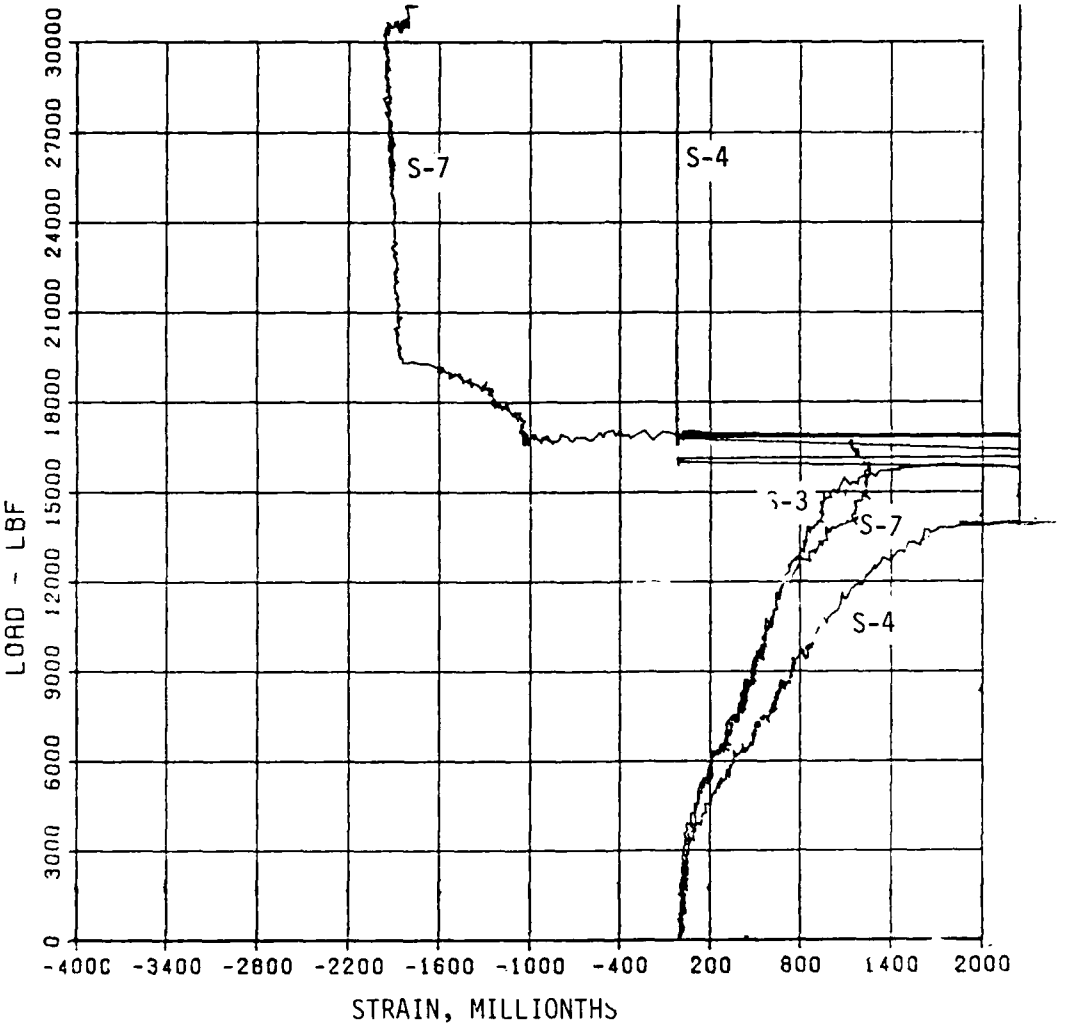

Summary of first test of C3

C3,1 61882
LOAD VS. STRAINS

INTRADOS CONCRETE STRAIN
R/C CIRCULAR CONDUIT TESTS.

08/13/82 0463E P1308.20

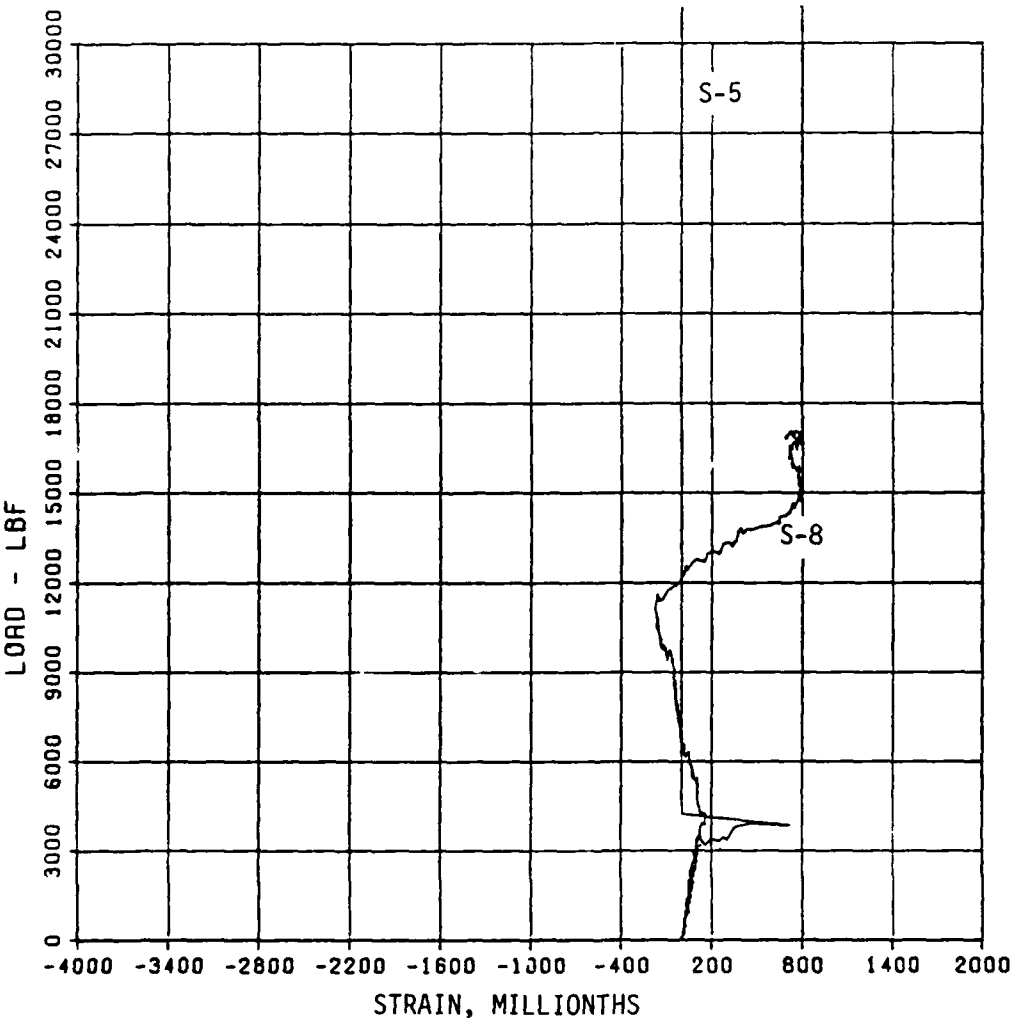

Summary of first test of C3

C3,1 61882
LOAD VS. STRAINS

EXTRADOS STEEL STRAIN
R/C CIRCULAR CONDUIT TESTS

06/16/83 25:80 P16:4.39

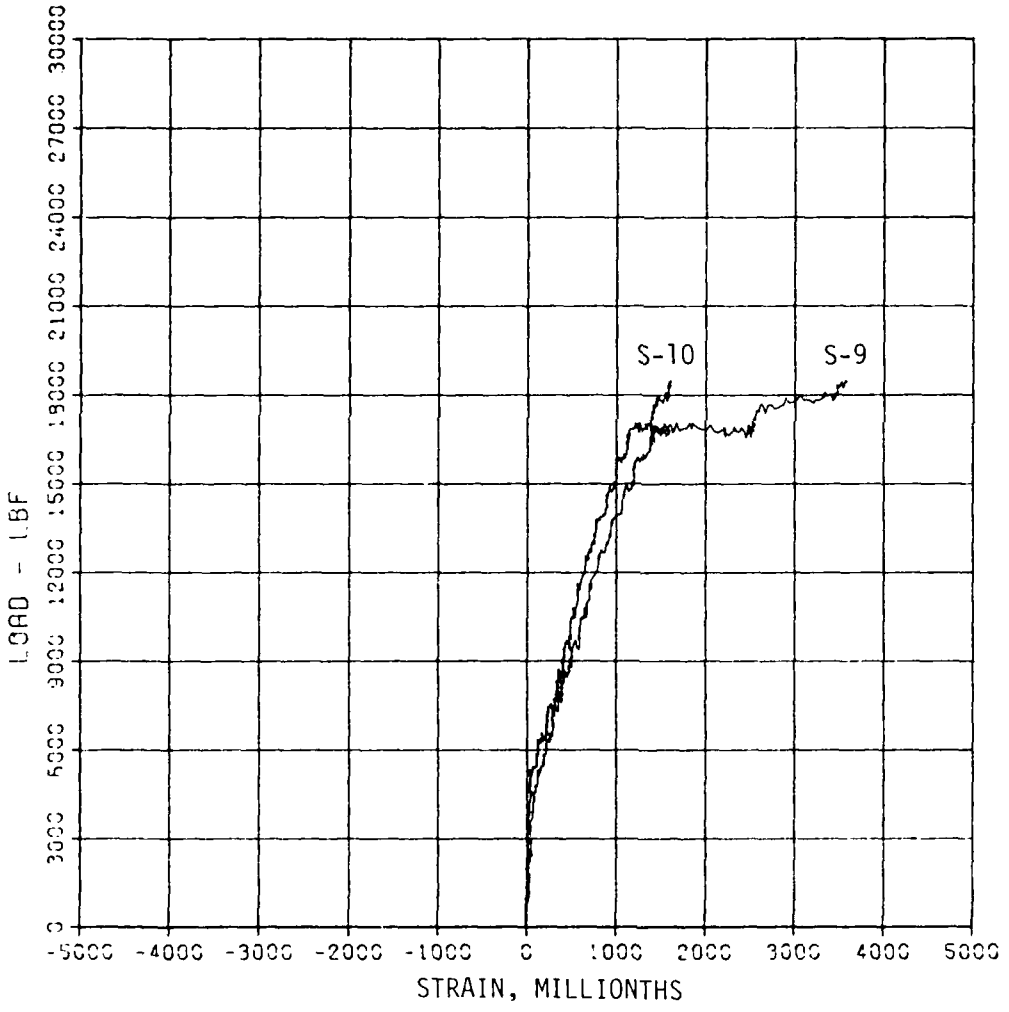

Summary of first test of C3

C3,1 61882
LOAD VS. STRAINS

INTRADOS STEEL STRAIN
R/C CIRCULAR CONDUIT TESTS.

06/16/83 25:80 P1614.39

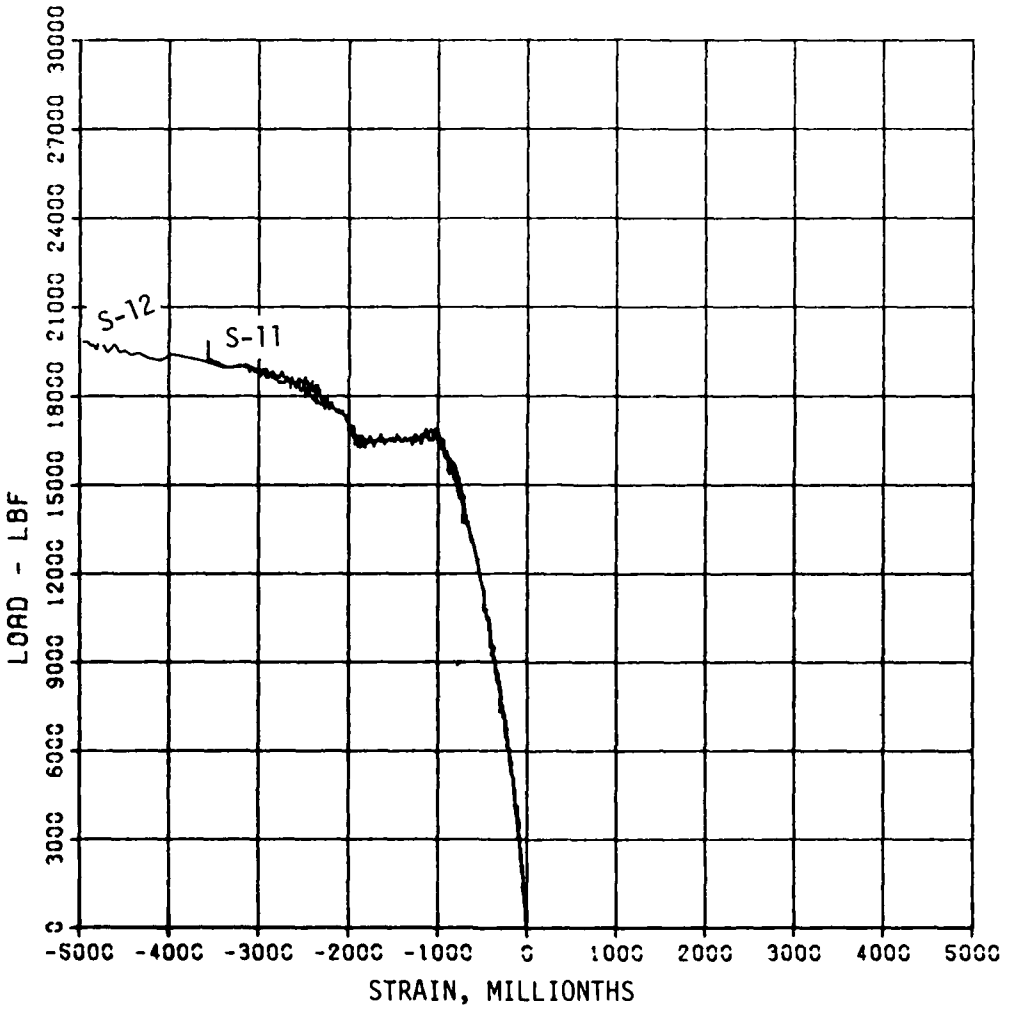

Summary of first test of C3

C3.1 61882

LOAD VS. STRAINS

INTRADOS CONCRETE STRAIN
R/C CIRCULAR CONDUIT TESTS.

06/16/83 2518D P1614.39

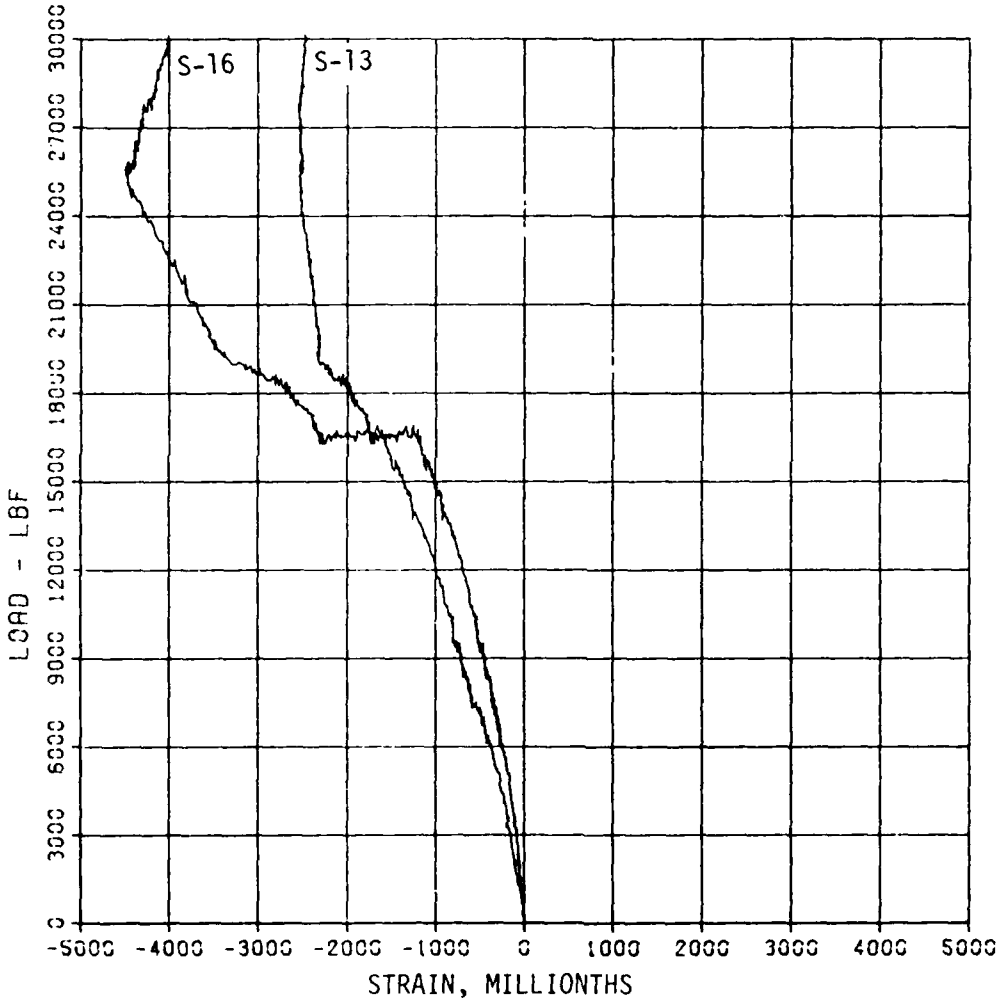

Summary of first test of C3

APPENDIX C

STRAIN DISTRIBUTIONS

Nonlinear Least-Squares Regression Analysis (Hyperbolic Strain Distribution)

1. The hyperbolic strain distribution according to Timoshenko's (1941) curved beam theory is (for the positive moment case):

$$\varepsilon(y) = \frac{y\left(R + \frac{h}{2}\right)\varepsilon_2}{\left(R + \frac{h}{2} - c + y\right)c}$$

Discretely, replace $\varepsilon(y)$ with $\varepsilon_i(y_i)$ or ε_i and y with y_i. Therefore the data will be curve fitted by the equation:

$$\varepsilon_i = \frac{R'y_i\varepsilon_u}{(R' - c + y_i)c} \tag{C1}$$

where

$R' = (R + \frac{h}{2})$

ε_u and c = undetermined coefficients to be solved for by the least-squares method

2. The error term e_i is:

$$e_i = \varepsilon_i = \frac{R'y_i\varepsilon_u}{(R' - c + y_i)c} \tag{C2}$$

The sum of the squares of the error term is:

$$\sum_{i=1}^{N} (e_i)^2 = \sum_{i=1}^{N} \left[\varepsilon_i - \frac{R'y_i\varepsilon_u}{(R' - c + y_i)c}\right]^2 \tag{C3}$$

where N is the number of data pairs $(\varepsilon_i,y_i)...(\varepsilon_N,y_N)$. Let $\varepsilon_u = \alpha$, maximum compressive strain and $c = \beta$, location of the neutral axis,

then the term in Equation C3 , $\sum_{i=1}^{N} (e_i)^2$, is to be minimized with respect to α and β .

3. To solve for α and β the following equations are formed:

$$\frac{\partial f(\alpha,\beta)}{\partial \alpha} = \sum_{i=1}^{N} \left[\epsilon_i - \frac{R' y_i \alpha}{(R' - \beta + y_i)\beta}\right] \left[\frac{y_i}{(R' - \beta + y_i)}\right] = 0 \qquad (C4)$$

and

$$\frac{\partial f(\alpha,\beta)}{\partial \beta} = \sum_{i=1}^{N} \left[\epsilon_i - \frac{R' y_i \alpha}{(R' - \beta + y_i)\beta}\right] (y_i) \left[\frac{R' + y_i - 2\beta}{(R' - \beta + y_i)^2}\right] = 0 \qquad (C5)$$

where

$$f(\alpha,\beta) = \sum_{i=1}^{N} \left[\epsilon_i - \frac{(R' y_i \alpha)}{(R' - \beta + y_i)\beta}\right]^2$$

4. Solving Equation C4 for α yields:

$$\alpha = \left\{\frac{\left[\sum_{i=1}^{N} \left(\frac{y_i \epsilon_i}{R' + y_i - \beta}\right)\right]}{\left[\sum_{i=1}^{N} \left(\frac{y_i}{R' + y_i - \beta}\right)^2\right]}\right\} \frac{\beta}{R'} \qquad (C6)$$

5. Solving Equation C5 implicitly for β then yields:

$$\beta = \frac{\left[\sum_{i=1}^{N} \frac{y_i^2 (R' + y_i - 2\beta)}{(R' + y_i - \beta)^3}\right]}{\left[\sum_{i=1}^{N} \frac{(R' + y_i - 2\beta) y_i \epsilon_i}{(R' + y_i - \beta)^2}\right]} (R'\alpha) \qquad (C7)$$

6. Therefore, using Equations C6 and C7, the following method was used to solve for α and β :

a. Choose a starting value for β (a realistic value is chosen using an "eyeball" fit to the data first).

b. Calculate α from Equation C6 where β is computed from a.

c. Rewrite Equation C7 as:

$$g(\beta) = \left\{ \sum_{i=1}^{N} \left[\frac{(R' + y_i - 2\beta)\varepsilon_i y_i}{(R' + y_i - \beta)^3} \right] \right\} \beta$$

$$- \left[\sum_{i=1}^{N} \frac{y_i^2 (R' + y_i - 2\beta}{(R' + y_i - \beta)^3} \right] R'\alpha \qquad \text{(C8)}$$

d. Using a root finder, determine a new value of β and repeat steps a through d until a convergence criterion is met such that

$$\left| g_1(\beta) - g_2(\beta) \right| \leq t$$

where g_1 and g_2 are two function values from successive iterations solving for α and β and t is a user-specified tolerance. There are practical limitations for the value of t ; the limit of t becomes clear when the above solution scheme is programmed and run on the computer. The solution for α and β for obtaining the hyperbolic curve fits to the strain data was obtained on a 4081 Tektronix computer.

7. Similarly, using the aforementioned procedure by substituting for Equations C6 and C8, respectively, by Equations C9 and C10:

$$\alpha = \left\{ \frac{\left[\sum_{i=1}^{N} \frac{\varepsilon_i y_i}{(R' - y_i + \beta)} \right]}{\left[\sum_{i=1}^{N} \frac{y_i^2}{(R' - y_i + \beta)^2 \beta} \right]} \right\} \frac{1}{R} \qquad \text{(C9)}$$

$$g(\beta) = \left\{ \sum_{i=1}^{N} \left[\frac{y_i \epsilon_i (R' - y_i + 2\beta)}{(R' - y_i + \beta)^2} \right] \right\} \beta$$

$$- \left\{ \sum_{i=1}^{N} \left[\frac{y_i^2 (R' - y_i + 2\beta)}{(R' - y_i + \beta)^3} \right] \right\} R'\alpha \qquad \text{(C10)}$$

8. Equations C9 and C10 were derived from Equations C11 and C12 below. The hyperbolic strain distribution for a negative moment section is:

$$\epsilon_i = \frac{y_i R' \epsilon_u}{(R' + c - y_i)c} \qquad \text{(C11)}$$

and where $R' = R - h/2$, the sum of the squares of the errors (or deviations) is:

$$\sum_{i=1}^{N} (e_i)^2 = \sum_{i=1}^{N} \left(\epsilon_i - \frac{R' y_i \epsilon_u}{(R' + c - y_i)c} \right)^2 \qquad \text{(C12)}$$

and letting $\alpha = \epsilon_u$ and $\beta = c$,

$$\frac{\partial f(\alpha,\beta)}{\partial \alpha} = \sum_{i=1}^{N} \left[\epsilon_i - \frac{R' y_i \alpha}{(R' - y_i + \beta)\beta} \right] \left(\frac{y_i}{R' - y_i + \beta} \right) = \phi \qquad \text{(C13)}$$

$$\frac{\partial f(\alpha,\beta)}{\partial \beta} = \sum_{i=1}^{N} \left[\epsilon_i - \frac{R' y_2 \alpha}{(R' + y_i + \beta)\beta} \right] \left[\frac{R' - y_i + 2\beta}{(R' - y_i + \beta)^2} \right] y_i = \phi \qquad \text{(C14)}$$

Correlation Coefficient
(Miller and Freund 1977)

9. The correlation coefficient squared gives statistical inference to quantify the correlation between the data and the fitted curve. The equation below measures the correlation by:

$$r^2 = 1 - \frac{\sum_{i=1}^{N} (\varepsilon_i - \varepsilon_i')^2}{\sum_{i=1}^{N} (\varepsilon_i - \bar{\varepsilon}_i)^2}$$

where

r^2 = the correlation coefficient squared

ε_i = measured value

ε_i' = predicted value

$\bar{\varepsilon}_i$ = average of measured values

10. The data that were fitted with the hyperbolic curve were also analyzed by the linear regression method. This gave a comparison of the statistical differences between a hyperbolic and a linear strain distribution for the same data. The linear regression formulas can be found in many statistics references. Some hand calculators also have linear regression equations preprogrammed by keystroke operations.

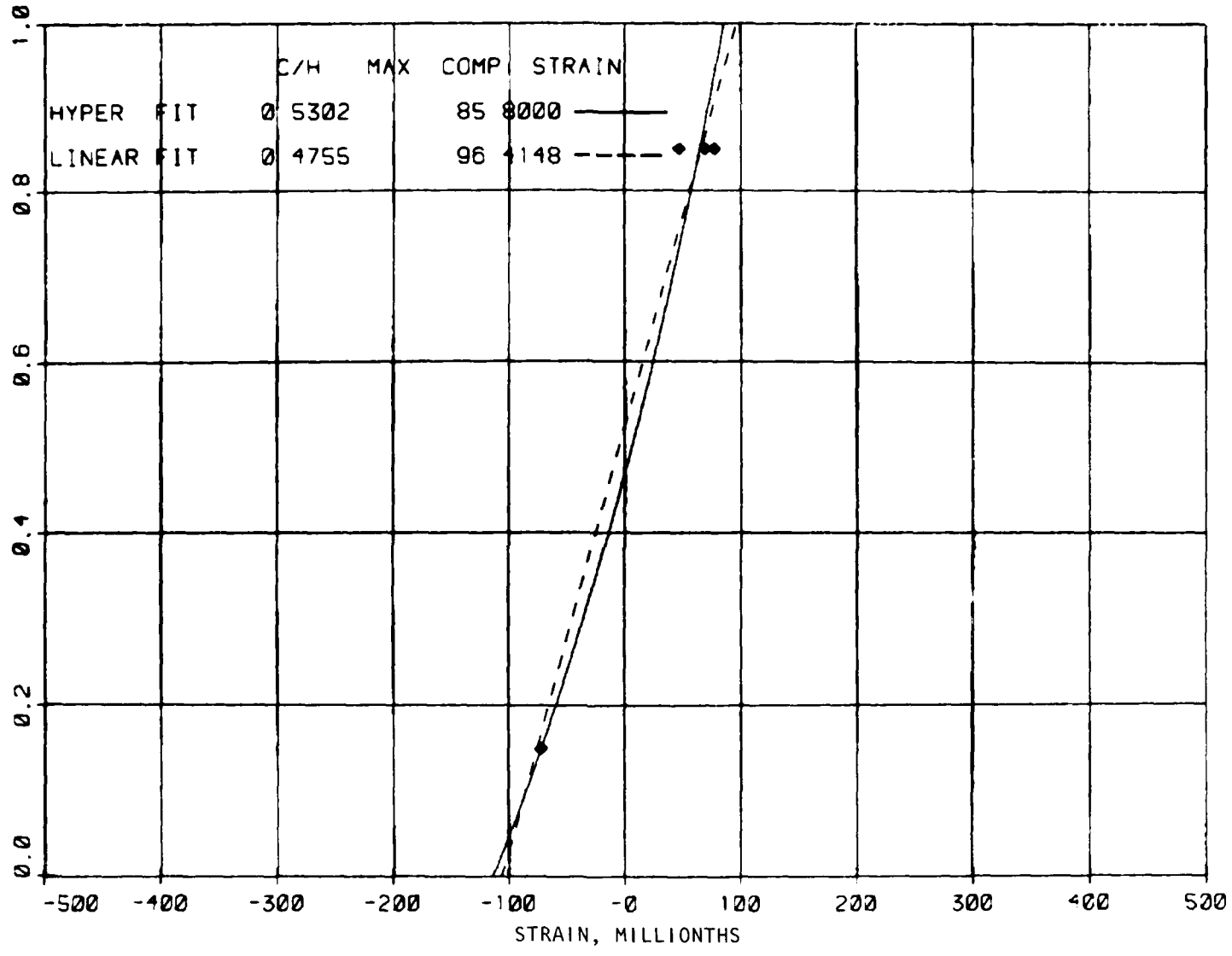

Specimen C1, positive moment, 10-kip load level

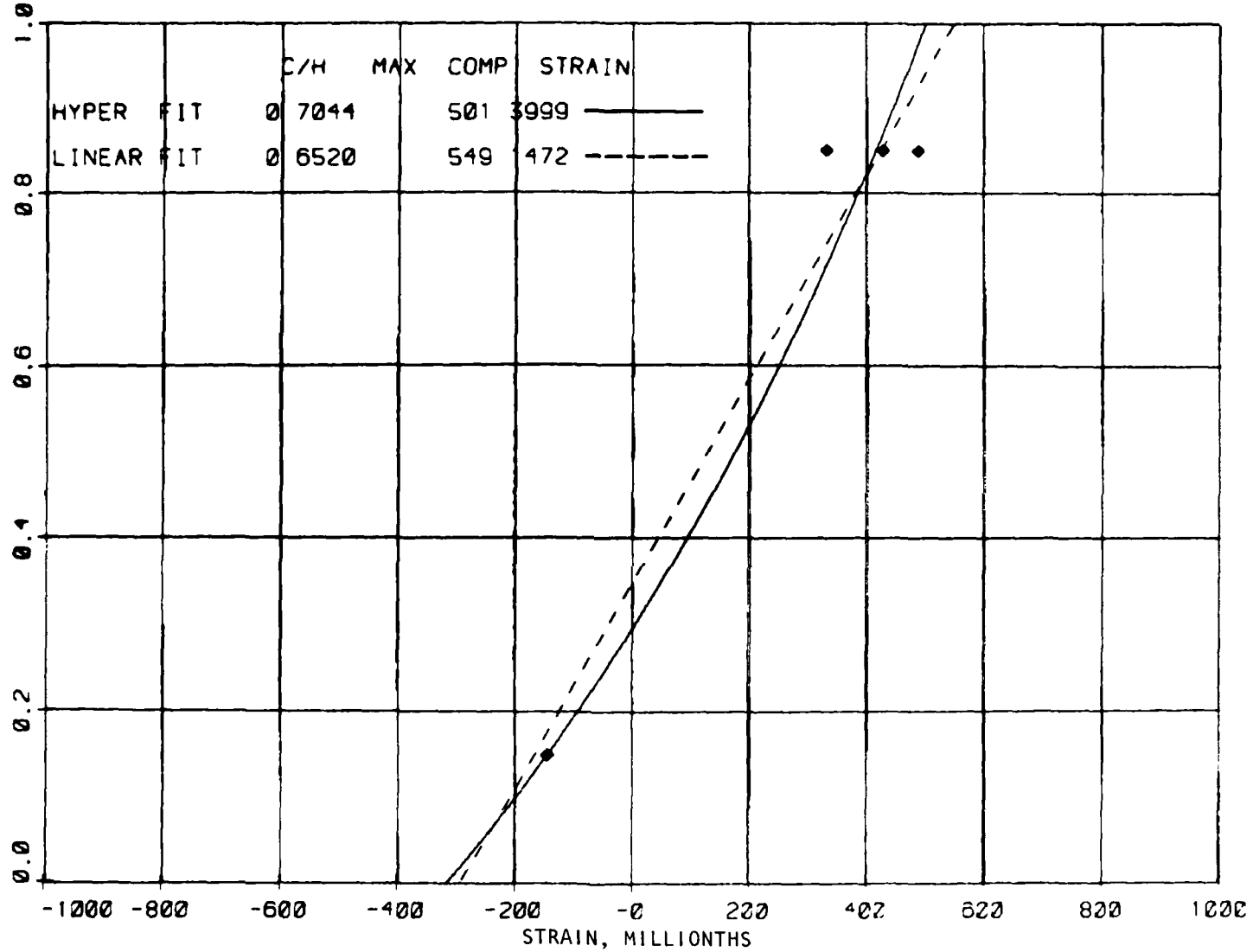

Specimen C1, positive moment, 40-kip load level

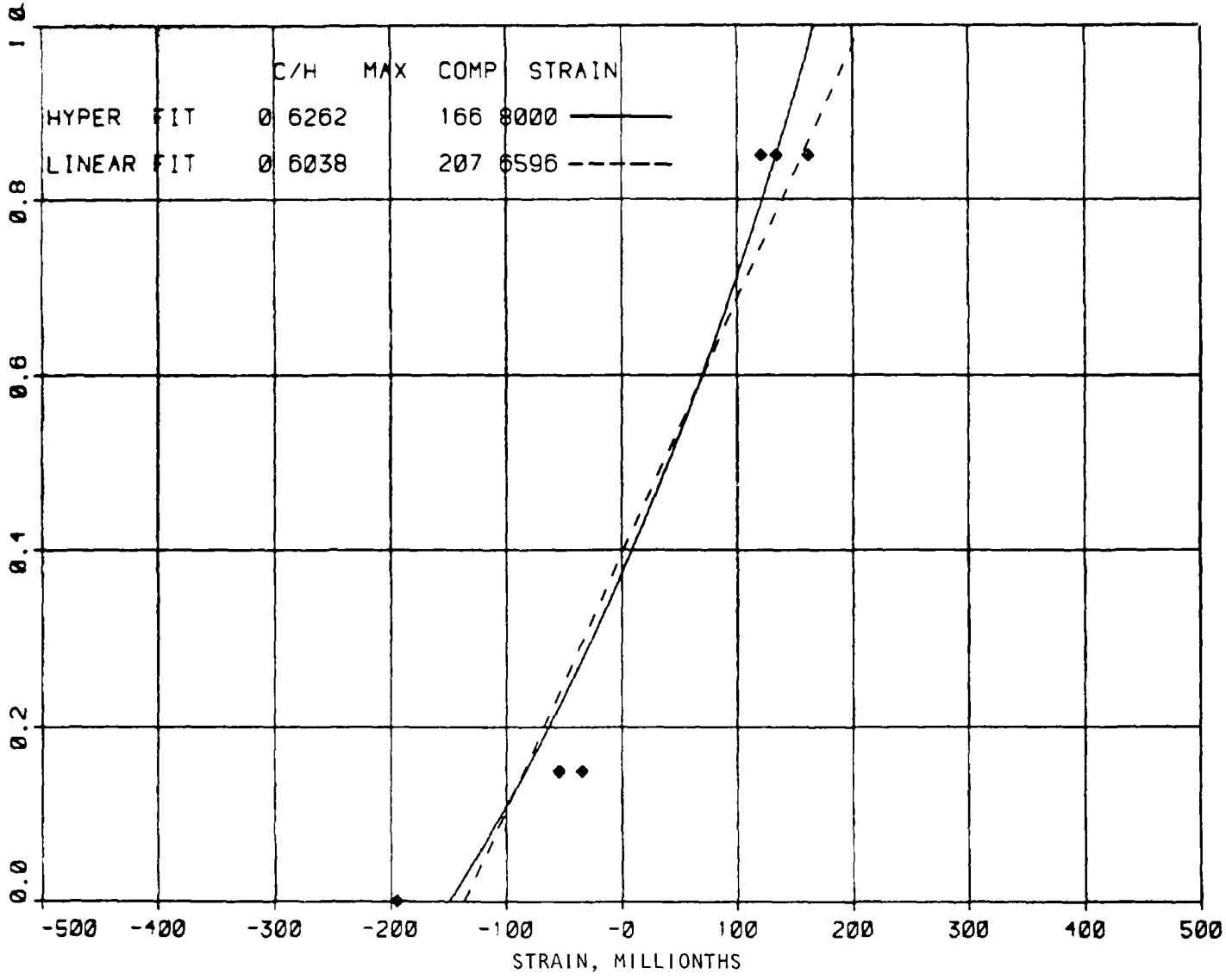

Specimen C2, positive moment, 10-kip load level

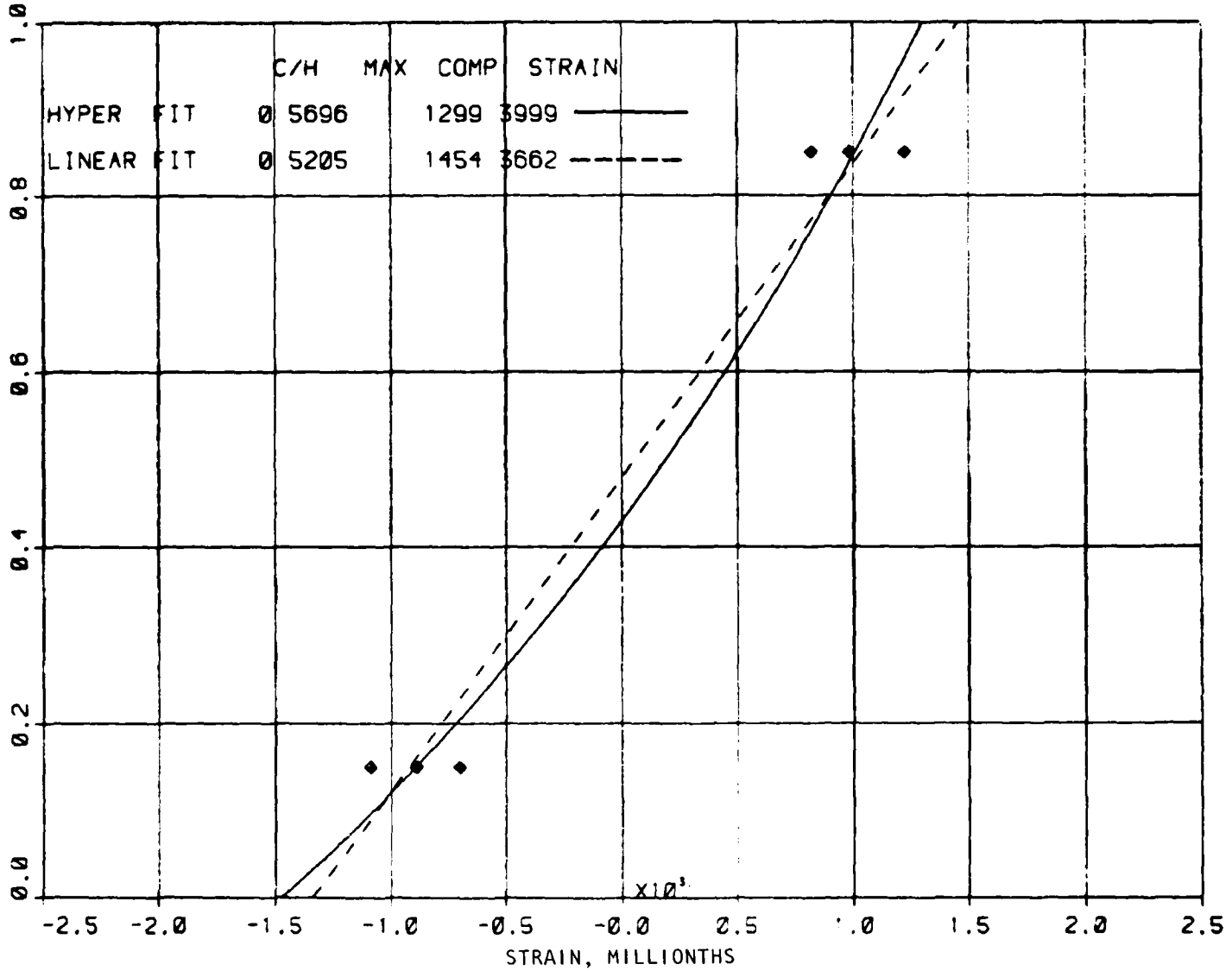

Specimen C2, positive moment, 50-kip load level

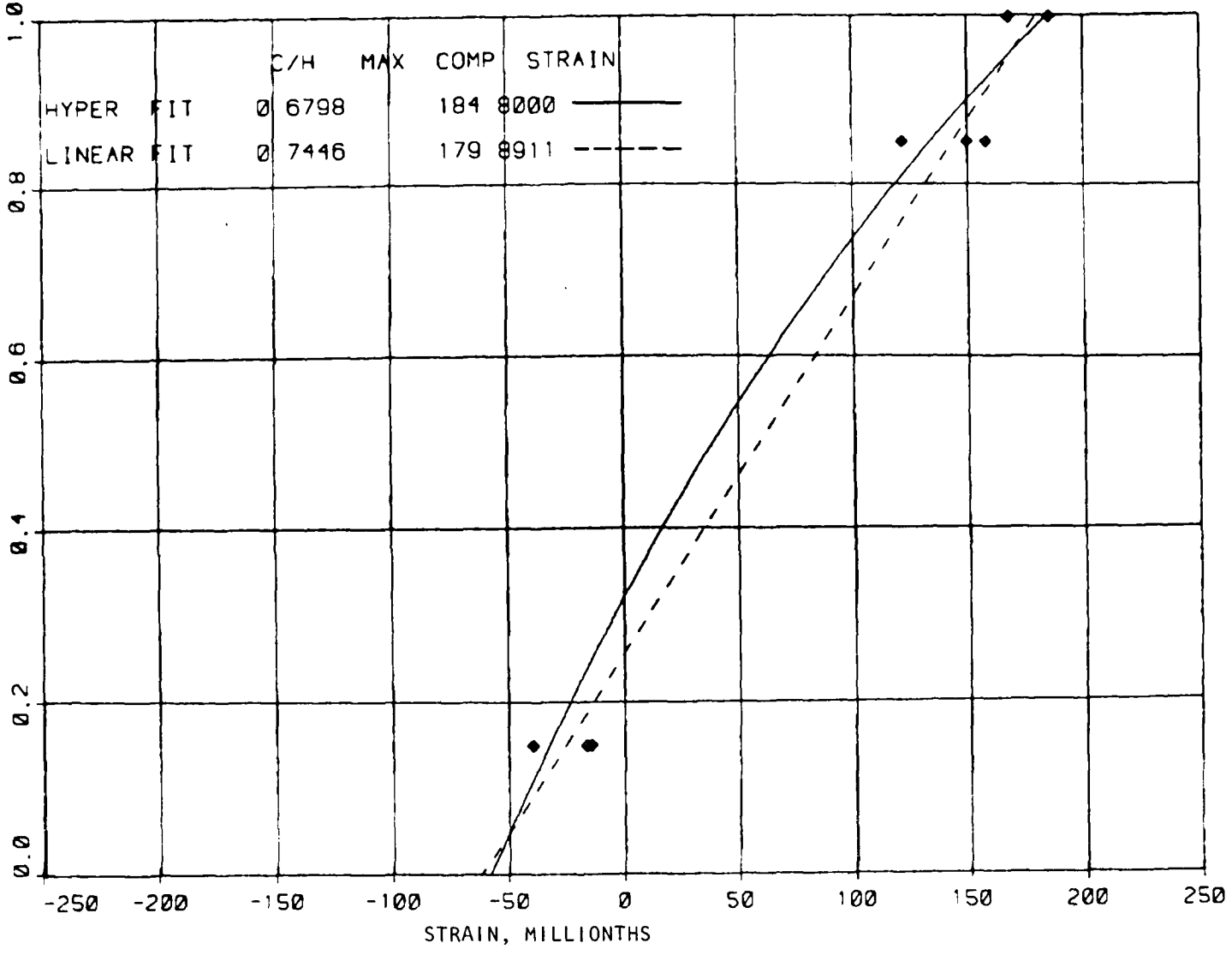

Specimen C2, positive moment, 10-kip load level

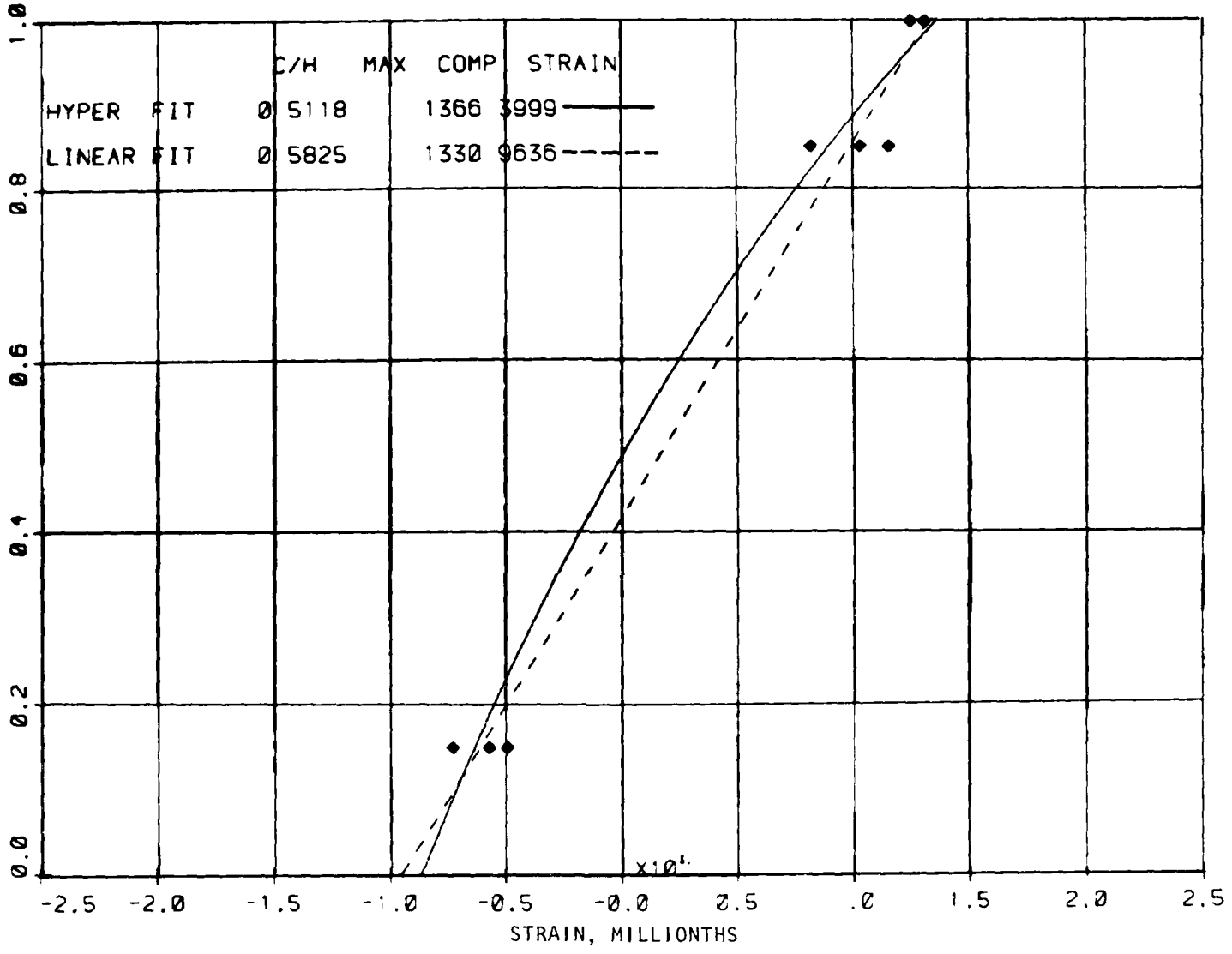

Specimen C2, positive moment, 50-kip load level

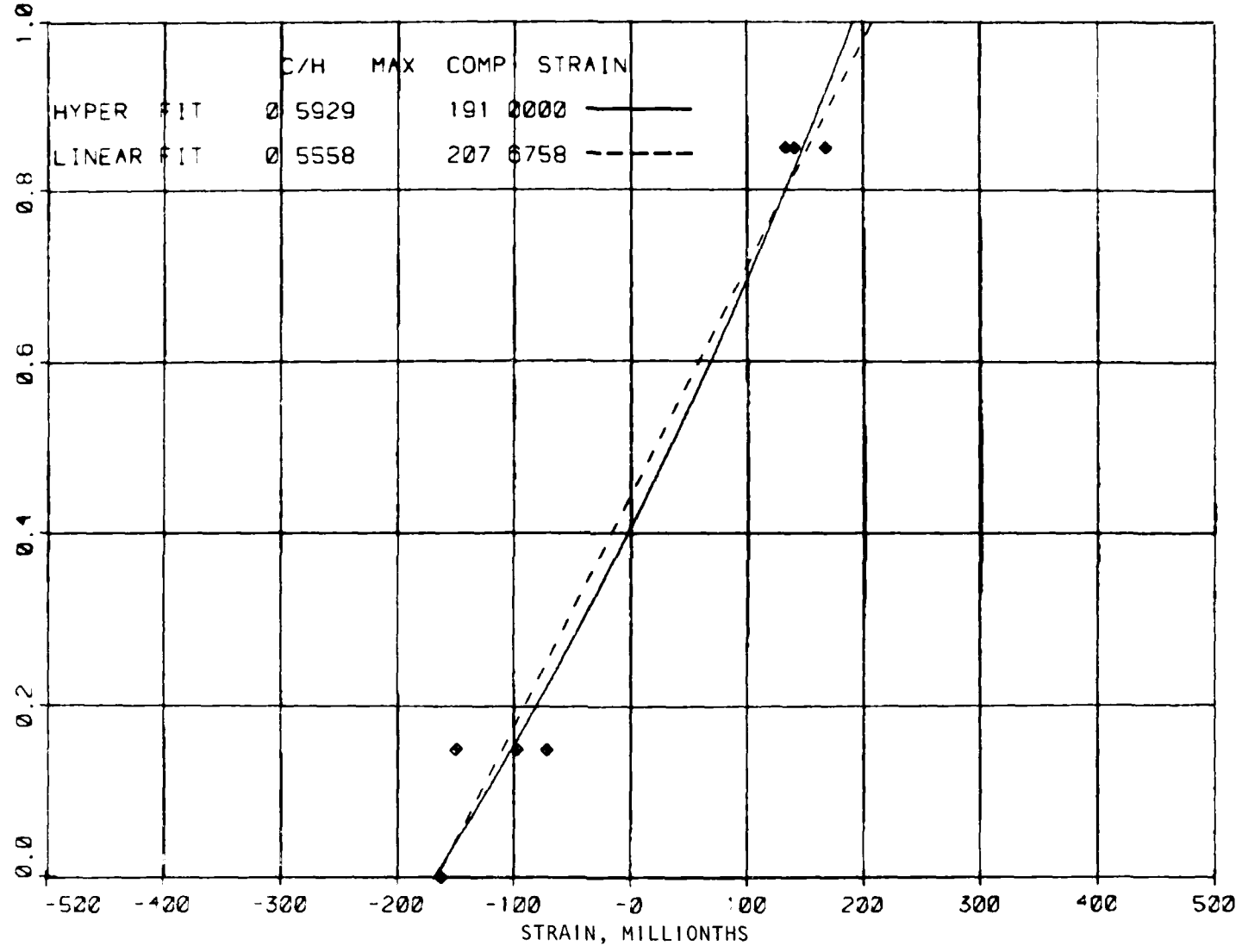

Specimen C3, positive moment, 4-kip load level

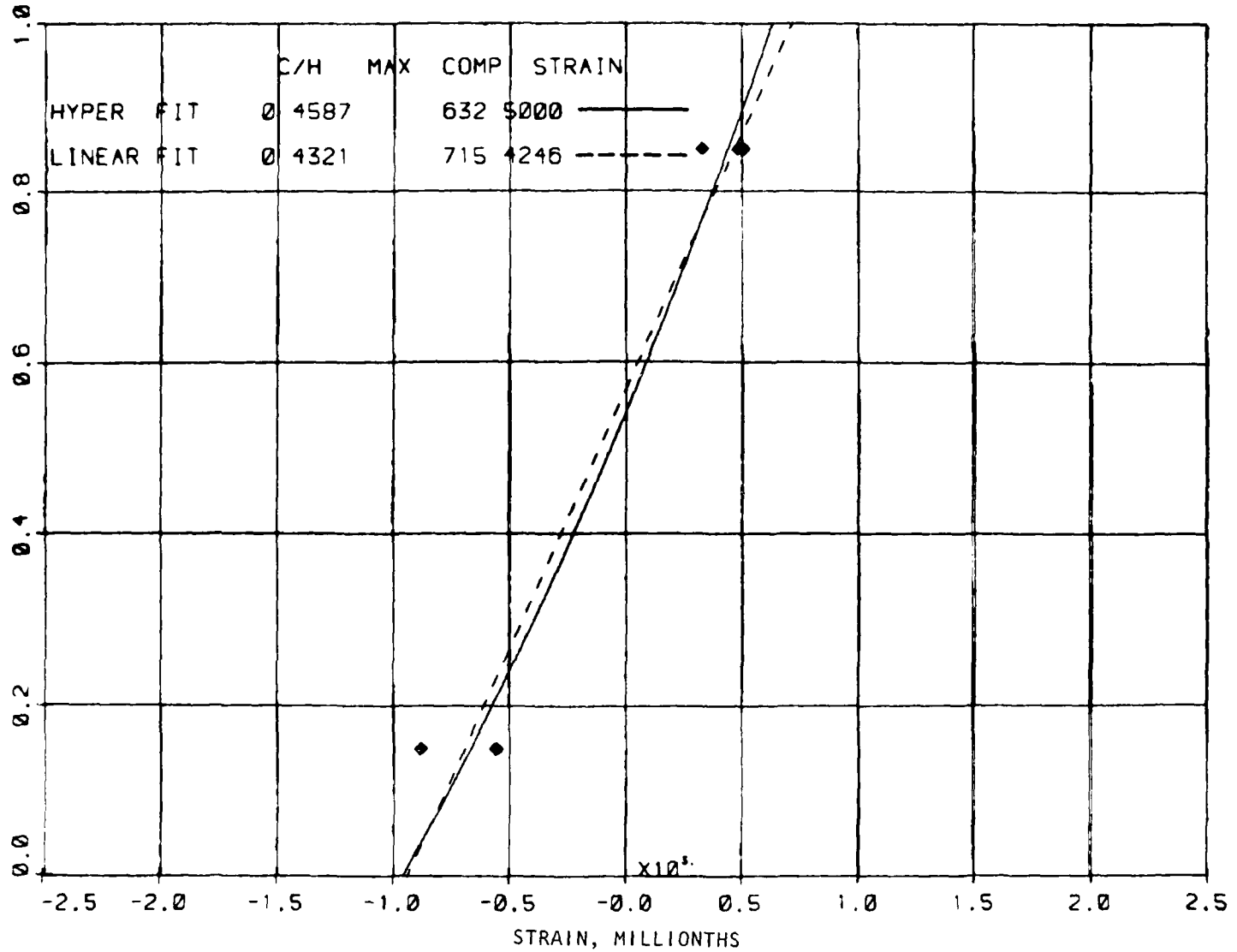

Specimen C3, positive moment, 10-kip load level

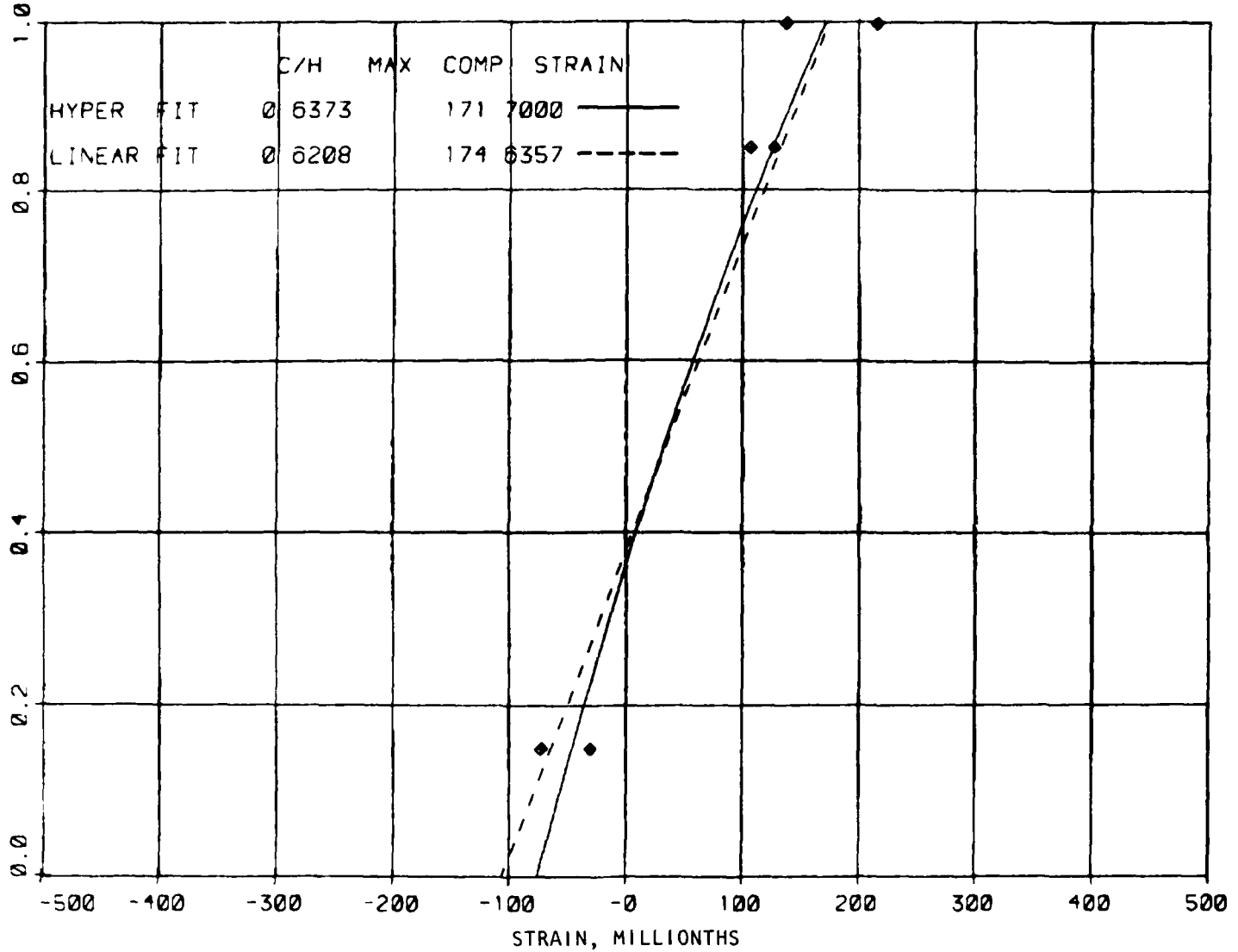

Specimen C3, negative moment, 4-kip load level

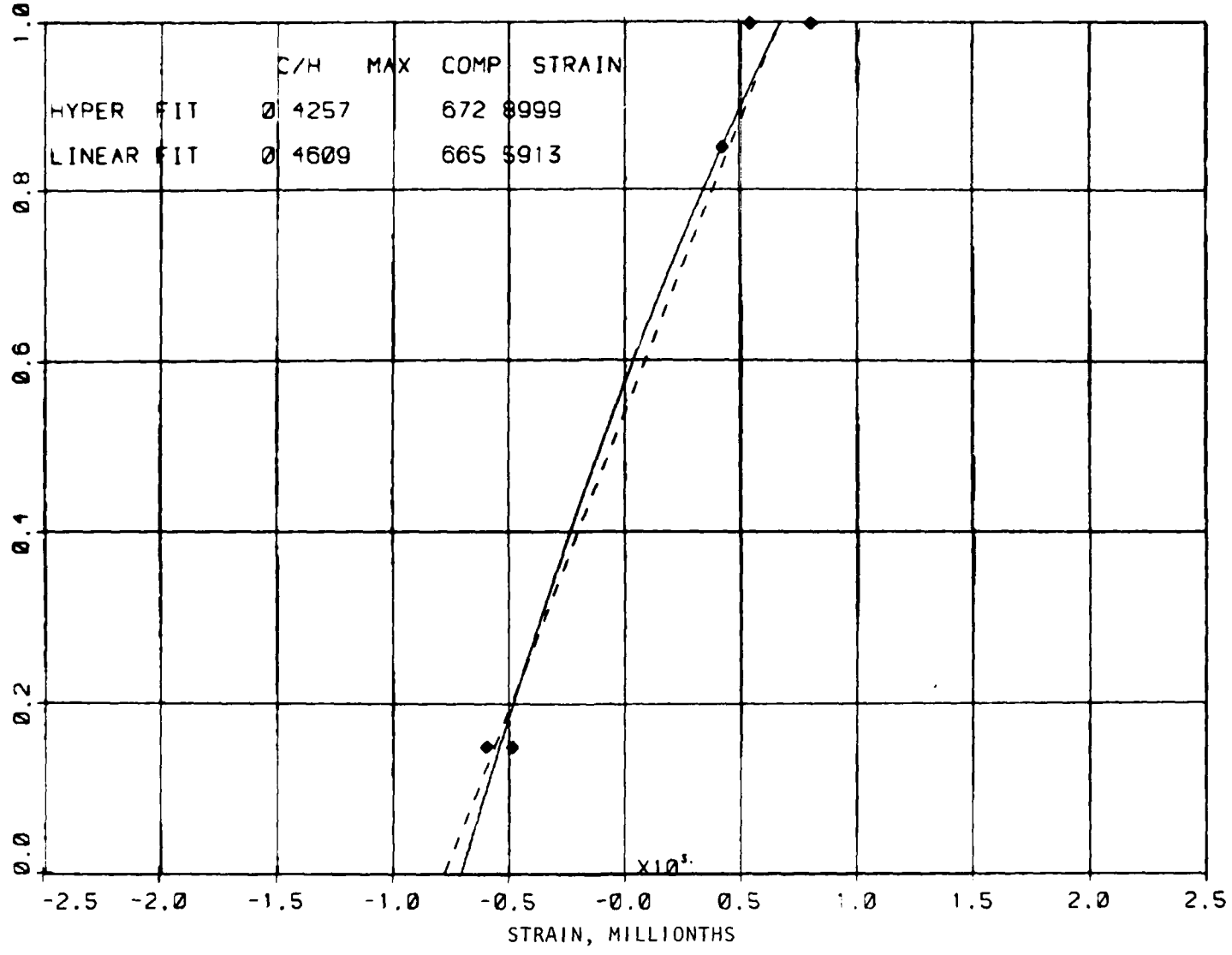

Specimen C3, negative moment, 10-kip load level

APPENDIX D

DERIVATION OF K_1 , K_2 , K_3 *CURVES IN FIGURE 8*

DEPENDENT ON CYLINDER STRENGTH

Assuming $\varepsilon_o = 0.002$ and $\varepsilon_u = 0.004 - \frac{f'_c}{6500}$, where f'_c is ksi units, the following is derived:

Positive Moment Section, Neutral Axis at Inner Radius ($r = R - h/2$)

$$\frac{\varepsilon}{\varepsilon_u} = \frac{\left(\frac{R}{h} + \frac{1}{2}\right)\left(-\frac{y}{h}\right)}{\left(\frac{R}{h} - \frac{1}{2} - \frac{y}{h}\right)}$$

$$= \frac{\left(\frac{R}{h} + \frac{1}{2}\right)\left(1 - \frac{z}{h}\right)}{\left(\frac{R}{h} + \frac{1}{2} - \frac{z}{h}\right)} \quad , \quad \text{where} \quad Z = h + y$$

Negative Moment Section, Neutral Axis at Outer Radius ($r = R + h/2$).

$$\frac{\varepsilon}{\varepsilon_u} = \frac{\left(\frac{R}{h} - \frac{1}{2}\right)\left(\frac{y}{h}\right)}{\left(\frac{R}{h} + \frac{1}{2} - \frac{y}{h}\right)}$$

Derivation of K_1, K_2, K_3 (refer to Figure D1)

K_1 is the ratio of average stress to maximum stress

$$K_1 = \frac{1}{n} \sum_{i=1}^{n} f_i \quad , \quad n = 50$$

where $f_i = \frac{\varepsilon}{\varepsilon_o}\left(2 - \frac{\varepsilon}{\varepsilon_o}\right)$ for $\frac{\varepsilon}{\varepsilon_o} \leq 1$

$$= 1 - \frac{0.15\left(\frac{\varepsilon}{\varepsilon_o} - 1\right)}{\frac{\varepsilon_u}{\varepsilon_o} - 1} \quad \text{for} \quad \frac{\varepsilon}{\varepsilon_o} > 1$$

K_2 is the ratio of depth to resultant at concrete and depth to neutral axis

$$K_2 = \frac{\sum_{i-1}^{n} \frac{z}{h} f_i}{\sum_{i=1}^{n} f_i} \quad \text{for positive moment section}$$

$$= 1 - \frac{\sum_{i=1}^{n} \frac{y}{h} f_i}{\sum_{i=1}^{n} f_i} \quad \text{for negative moment section}$$

K_3 is the ratio of maximum stress to cylinder strength, f'_c (psi)

$$K_3 = \frac{3900 + 0.35 f'_c}{3000 + 0.82 f'_c - \frac{(f'_c)^2}{26000}}$$

(Hognestad, Hanson, and McHenry 1955)

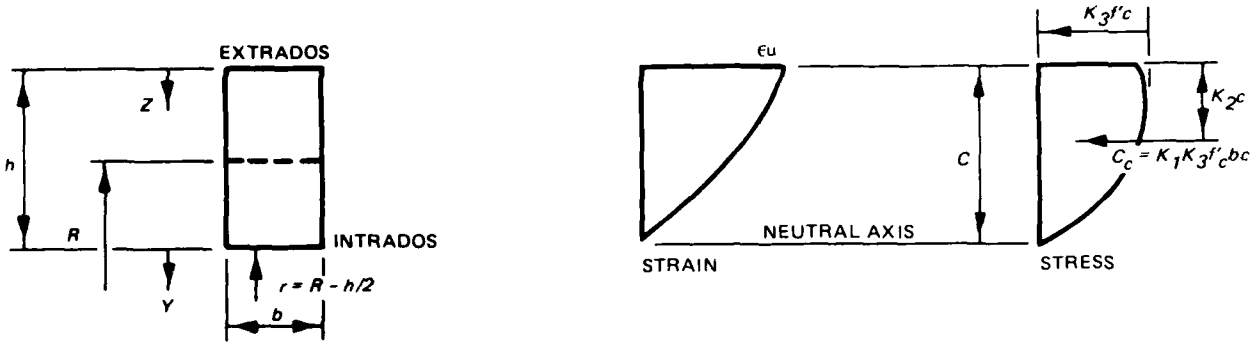

a. POSITIVE-MOMENT SECTION

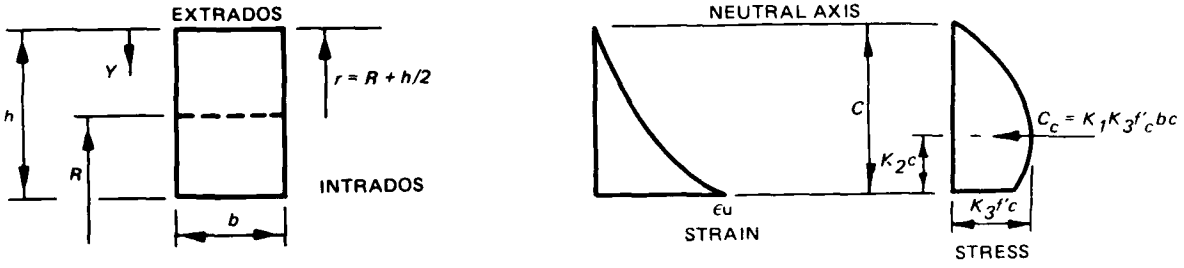

b. NEGATIVE-MOMENT SECTION

Figure D1. Concrete stress distribution at ultimate strength

APPENDIX E

NOTATION

a	Inner radius
b	Width of section: outer radius as defined in Appendix A
c	Depth of section in compression
C_c	Resultant compressive concrete force
C_s	Resultant force in the compressive steel
d	Effective depth of tension steel
d'	Depth to compression steel
$d\phi$	Small angle between two neigboring cross sections
e	Eccentricity (M/P)
E_c	Initial elastic concrete modulus
E_s	Modulus of elasticity of steel (29,000,000 psi)
f_c	Concrete stress
f'_c	28-day compressive strength of standard 6- by 12-in. concrete cylinder
f''_c	Compressive strength of concrete in reinforced concrete members ($0.85\ f'_c$)
f_s	Steel stress
f_u	Uniaxial strength
f_y	Yield strength of reinforcing steel
$-f_y/\epsilon_s$	Tensile yield strain
h	Overall depth of section
K_L	Lateral pressure coefficient
K_V	Vertical pressure coefficient
M	Bending moment
M_c	Crown moment
M_s	Springing line moment
$M(\phi)$	Internal moment
$N(\phi)$	Internal thrust
p	Varying pressure component magnitude
P	Centric thrust
q	Uniform pressure component magnitude
r	Radius of initial curvature to neutral axis of section
R	Radius of initial curvature to middepth of section
R'	$R + \frac{h}{2}$
R_c	Crown thrust
R_o	Outside radius

R_s	Springing line thrust
T_s	Resultant force in the tensile steel
$V(\phi)$	Internal shear
w	Maximum pressure
y	Distance from the neutral axis
$\Delta d\phi$	Small angle of rotation due to moment and thrust
ε	Strain
ε_c	Maximum concrete strain
ε_o	Strain at which the maximum concrete stress f''_c occurs (0.002)
ε_s	Tensile reinforcement strain
ε_u	Limiting useful concrete strain (0.003)
θ	Angle at which P is applied, or angle from springing line of section of interest
ρ_g	Gross tension steel ratio
ρ'_g	Gross compression steel ratio
ϕ	Angle from springing line to section of interest

END

12-86

DTIC